FLEXURAL VIBRATION OF MULTI-LAYER BEAMS WITH VISCOELASTIC DAMPING

by

JAMES ASOCUKWU AGBASIERE

B.Sc.(Eng.) Lond.

Thesis presented for the degree of Doctor of Philosophy of the University of London and Diploma of Imperial College.

Department of Mechanical Engineering,

Imperial College,

London S.W.7.

December 1965.

A B S T R A C T

The one-dimensional differential equations of motion for the flexural vibration of a symmetrical multi-layer damped beam are developed. The viscoelastic damping materials are assumed to obey a general stress - strain law which can be linear or non-linear. Shear and extensional deformations in the viscoelastic layers are included. Rotatory inertia effects, shear in the elastic layers, and thickness-wise deformations in all the layers are neglected.

An experimental method for determining the properties of viscoelastic materials is described, and utilised in the study of some viscoelastic materials with a view to ascertaining their stress - strain law under harmonic loading, their dynamic properties, and the nature of the dependence of these properties on frequency, temperature, and strain.

The information obtained from this study serves as a useful guide in the development of a numerical method of solution of the differential equations for systems subjected to harmonic excitation. The method developed is capable of dealing with all possible boundary conditions, as well as linear and non-linear behaviours of the viscoelastic materials. An experimental verification of the theory is carried out by investigating the displacement responses of

cantilever beams vibrating in the first few modes. Various configurations, combinations of materials, and dimensions of the beams are covered, the experimental results generally showing good agreement with the theory.

Finally, a systematic method for investigating the resonant responses of multi-layer beams is presented. Illustrations are given with a detailed design study of three-layer cantilever beams vibrating in the first mode, and some studies of the five-layer configuration. Various applications of this work are pointed out, including a simple method for obtaining the viscoelastic material properties from tests on symmetrical three-layer beams.

ACKNOWLEDGEMENTS

For suggesting the topic of the research, and for constant encouragement, inspiration, and helpful advice throughout the course, the author is immensely grateful to his supervisor, Dr. P. Grootenhuis.

His thanks are also due to members of the academic and technical staff of Imperial College for their help, and to all his friends, far and near, who assisted in the preparation of the thesis.

Finally, the author wishes to express his gratitude to the University of Ibadan for making these studies possible by providing a scholarship.

TABLE OF CONTENTS

TABLE OF CONTENTS (CONTINUED)

TABLE OF CONTENTS (CONTINUED)

TABLE OF CONTENTS (CONTINUED)

TABLE OF CONTENTS (CONTINUED)

TABLE OF CONTENTS (CONTINUED)

TABLE OF CONTENTS (CONTINUED)

LIST OF SYMBOLS

A list of the essential notations employed is given below. In the text, each symbol is usually defined as soon as it is introduced. In a few cases, the same symbols are used in different sections to denote different quantities. However, these sections are far from each other, so that no confusion is anticipated. Apart from the meanings given below, the following symbols, i, j, k, ℓ, m, p, q, r, s, u, v, F, P, $\mathcal{Q}$, Z, and α, are used in a limited number of places as variable indices for summations, suffices, etc.

A = cross-sectional area of beam; total shear area of shear specimen.

A_i = cross-sectional area of i-th layer of beam.

A_r^i, B_r^i, C_r^i, D_r^i = coefficients of expansions in Chebyshev polynomials of the displacement and shear variables.

$^{+-}A^s$, $^{+-}B^s$, $^{+-}C^s$, $^{+-}D^s$, $^{--}A^s$, $^{--}B^s$, $^{--}C^s$, $^{--}D^s$ = defined in equations 4.3.vi, page 225

a'_o = input motion amplitude

a_o = $\frac{a'_o}{\ell}$

a_T = typical displacement amplitude of beam.

a_r = coefficient of the Chebyshev series expansion of the forcing function.

a_{in} = coefficients of Fourier series expansions of the displacement and shear variables.

b = width of beam.

b_r = coefficient of Fourier series expansion of a_o

C_L = an arbitrary constant.

D = differential operator, $\frac{d}{d\xi}$.

D_1 , D_2 = density ratios.

d_i = distance of the central axis of i-th layer of beam from neutral axis.

E, E^*, E', E'' = effective, complex, in-phase, loss dynamic Young's modulus for viscoelastic material

E_i = Young's modulus of i-th (elastic) layer

E_i' = in-phase dynamic Young's modulus for i-th (viscoelastic) layer.

e = $\frac{E'}{E_2}$, three-layer beam.

e_1 , e_2 , = $\frac{E_1}{E_3}$, $\frac{E_2'}{E_3}$, five-layer beam.

EA = $\sum_i E_i A_i$

EI = $\sum_i E_i I_{Ni}$, dynamic flexural rigidity of a "shear free" sandwich beam.

F_i = longitudinal force acting on the i-th layer.

f = frequency, c.p.s.

f_x = general functional notation.

G, G^*, G', G'' = effective, complex, in-phase, loss dynamic shear modulus of viscoelastic material.

G_r' = reduced in-phase shear modulus with respect to the reference temperature, T_o

G_i' = in-phase dynamic shear modulus of the i-th layer.

g_1 = $\frac{G_1'}{E_2}$, three-layer beam.

g_2 = $\frac{G_2'}{E_3}$, five-layer beam.

H = thickness ratio, $\frac{h_1}{h_2}$, three-layer beam.

H_1, H_2 = thickness ratios, $\frac{h_1}{h_3}$, $\frac{h_2}{h_3}$, five-layer beam.

h = step length for step-wise integration.

h_i = thickness of i-th layer of beam.

I_{Ni} = $A_i(\frac{h_i^2}{12} + d_i^2)$, second moment of area of the i-th layer about the neutral axis.

i = variable index.

J^*, J', J'' = complex, in-phase, loss dynamic shear compliance for a viscoelastic material.

j = $\sqrt{-1}$; variable index.

K = bulk modulus

K_1, K_2, K_g, K_w = constants.

k_T = ratio of $\frac{\text{total viscoelastic layer thickness}}{\text{total elastic layer thickness}}$

k_v = total viscoelastic layer thickness.

k_n^4 = resonant frequency factor for a plain undamped Euler beam.

ℓ = length of beam.

M = total bending moment at any cross-section of beam, total mass of shear specimen.

M_i = bending moment contributed by the i-th layer.

m = mass per unit length of beam; mass of moving parts of the shear test apparatus above the

strain gauge (excluding the specimen layers)

m_s = "equivalent moving mass" of shear specimen

m_c = $m + m_s$, effective moving mass for shear test.

N_p^i, N_q^i = coefficients of the differential equations, defined in equations 2.4.xvii&xL pages 77 & 84

n = variable index.

P = total force measured by strain gauge.

$\hat{P}$ = amplitude of the force, P.

P_e = total tensile force in shear specimen.

p_p^i, p_q^i = coefficients of differential equation, defined in equations 2.4.xxiv & xLv pages 80 & 86

$p(x,t)$ = forcing function.

p_m = $\frac{\ell^3 p(\ell \xi)}{EI}$, modified forcing function.

p_1 ; p_2 = $\frac{\ell}{h_2}$ (three-layer beam); $\frac{\ell}{h_3}$ (five-layer beam)

α_{ps}^i, $\alpha_{q\ell}^i$ = coefficients of the differential equations, defined in equations 2.4.xxvi & xLvi pages 80 & 86

q = spatial rate of loading on the beam.

R_1, R_2 = arbitrary functions

S = strain (shear or direct)

S_o = amplitude of strain, S.

T = temperature, ^oC or Absolute.

$T_r^*(\xi)$ = Chebyshev polynomial of order r for the range ξ = 0 to 1.

T_a = tip displacement amplitude ratio.

t = time variable.

t_o = mean thickness of each layer of shear specimen.

u_i = displacement and shear variables at $\xi = 0$.

u'_o, v'_o = in-phase, quadrature components of displacement

u_o, v_o = $\frac{u'_o}{\ell}$, $\frac{v'_o}{\ell}$, dimensionless displacement components.

X_{o1}, Y_{o1} = in-phase, quadrature components of shear deformation, three-layer beam.

X_{o2}, Y_{o2} = in-phase, quadrature components of shear deformation, five-layer beam.

x = coordinate in the longitudinal direction of beam.

$\underline{x}$ = vertical displacement of centre-piece of the shear test apparatus.

y = vertical displacement at any point on beam; horizontal distance of an element of the shear specimen from the fixed support.

y_i = displacement and shear variables at $\xi = 0$.

z_i = vertical distance of elemental fibre of i-th layer from the central axis of this layer.

A'_1, B'_1, C'_1, D'_1 = integrals for evaluating beam loss factor for a three-layer beam, defined in equations 4.6.ix page 247

A'_2, B'_2, C'_2, D'_2 = integrals for calculating beam loss factor for 5-layer beam, defined in equations 4.7.x page 252

$\alpha_1, \beta_1, \gamma_1, \mu_1, \delta_1, \nu_1, \sigma_1$ = dimensionless coefficients of differential equations for the 3-layer beam, defined in equations 4.1.xvi to xviii page 203

$\alpha_2, \beta_2, \gamma_2, \gamma_3, \mu_2, \delta_2, \delta_3, \nu_2, \sigma_2$ = dimensionless coefficients of differential equations for the 5-layer beam, defined in equations 4.7.vii to 4.7.ix page 250

β_{on} = $\frac{m \omega_{on}^2 l^4}{EI}$, n-th mode resonant frequency factor.

δ = loss angle for viscoelastic material.

ϵ = phase difference between force and displacement - shear test.

ϵ_i = strain in any fibre of i-th layer of beam.

ξ = $\frac{x}{l}$, dimensionless longitudinal coordinate.

K_s = general dynamic modulus (direct or shear)

λ_1, λ_2 = dimensionless quantities, defined in equations 4.6.v and 4.6.x page 246

λ_3, λ_4 = dimensionless quantities, defined in equations 4.7.xi page 252

$\sqcup\!\sqcup(s)$ = some function of the strain in the general stress - strain law of equation 2.1.i page 40

$\sqcup\!\sqcup_{mp}$ = integral defined in equation 2.4.xi page 76

$\sqcup\!\sqcup_{FP}$ = integral defined in equation 2.4.xxii page 78

$\sqcup\!\sqcup_{P}$ = integral defined in equation 2.4.x page 76

ρ = density

ρ_i = density of material of i-th layer of beam.

φ = an arbitrary function.

σ_i = longitudinal stress in i-th layer of beam.

τ, $\hat{\tau}$ = shear stress, shear stress amplitude.

τ_i = shear stress at central axis of i-th (viscoelastic) layer of beam.

ϕ, $\hat{\phi}$ = shear strain, shear strain amplitude.

ϕ_i = shear strain on i-th layer of beam.

η = material constant in general stress - strain law.

$\eta_{ai} \doteq \eta_{ei} \doteq \eta_i$ = shear, extensional material loss factor for the i-th (viscoelastic) layer.

η_{on} = beam loss factor for the n-th mode.

$\frac{\eta_{on}}{\eta_i}$ = damping efficiency for the n-th mode.

π = 3.14.....

Π_i^s = displacement and shear variables at points on beam

ν_c = $\frac{\nu_i}{\beta_{on}^{1/2}}$, the characteristic shear parameter for the 3-layer beam.

ν_k = $\frac{\nu_i}{k_n^2}$, twice Kerwin shear parameter.

ω = forcing circular frequency.

ω_{on} = n-th mode resonant frequency.

$\int$ = a definite integral.

ΔE_D = cyclic energy loss per unit volume of viscoelastic material.

ΔE_S = shear strain energy per unit volume.

$\frac{\Delta R}{R}$ = change in resistance of strain gauge circuit.

C H A P T E R 1

LITERATURE REVIEW AND SCOPE OF WORK

1.1 Introduction

Modern high-speed machines and high-energy power sources give rise to appreciable levels of sound and vibration which extend over a wide frequency range. These may be readily amplified by structural members at resonance, giving rise to large displacements and accelerations, and high stresses at critical points. This fact becomes more evident when it is realised that the present day trend in structural design is towards lighter weight, fewer joints, more integral construction and hence, more "resonant" structures. If resonant vibrations are not controlled, they may result in intolerable noise and human discomfort, structural fatigue and subsequent failure of components.

One way of tackling the problem is by attacking the source of vibrational energy. This can be done by more efficient balancing of rotating machinery, and by the use of vibration isolators [1,2]*. Perfect balance in machinery is, however, not a practical proposition, and at the very high speeds of operation, a very small out of balance will give rise to an appreciable disturbing force (the force is proportional to the square of the speed).

*Numbers in square brackets refer to references at the end of the thesis.

Vibration isolation can cut down the amount of vibration transmitted, but does not eliminate it completely and structural vibrations may still be increased to undesirable levels owing to structural resonances [3].

To tackle the problem satisfactorily it becomes necessary to attempt to control the dynamic response of the structure or its component part. Of the several methods which can be used to eliminate dangerous resonances [3 - 7], by far the most suitable for controling wide frequency-band structural vibration is the use of heavily damped structures.

In the past, considerable attention was focussed on the use of the internal damping in structural materials in combatting resonant vibrations.

Closer study of the mechanisms of internal damping were made and detailed analysis of the dynamic behaviour of systems with internal damping was carried out [8 - 18]. Materials research was also directed to the manufacture of high-strength, high damping alloys. But in spite of the great strides which have been made in this field in recent years, the amount of damping obtainable is still of a very low order. As far as is known, the highest loss factor* reported for any structural material is 0.067 [19].

*For the definition of loss factor as used here, see chapter 4, section 4.6.b.

This falls far short of the requirements of present day high energy sources of vibration.

In the past decade, interest has grown on a new method of approach which involves the application of highly damped viscoelastic materials to the structures as damping treatments. The treatment may be in the form of a layer of the material sprayed or applied on the structural surface. Energy dissipation then occurs when the viscoelastic layer undergoes direct strain due to the bending of the structure. In this form the applied layer is said to be "free" or "unconstrained". Alternatively the material can be built into the structure in the form of sandwich construction. When the structure undergoes flexural vibrations, considerable shear deformation is induced in the material leading to dissipation of energy. Under these conditions, the applied layer is said to be "constrained". A large amount of damping can be achieved by this method. As will be shown in chapter 6 loss factors of 1 or more can be readily obtained by correct choice of material and design.

The incorporation of such damping treatments in structures however involves a basic change in the structural design. An understanding of the dynamic behaviour of such structures is thus necessary in order that efficient design can be carried out. The present work arises out of this need for a clearer insight into the dynamic

behaviour of such systems.

1.2 Review of past work

Past work in this field can be conveniently divided into two groups according to whether it is related to the unconstrained or the constrained damping treatment.

1.2.a The unconstrained damping treatment

This type of damping was introduced first, probably because of the relative ease with which it can be applied. Liénard in France [27], and Oberst and his co-workers in Germany [20 - 23], working independently analysed the case of an infinite beam with a homogeneous layer of a viscoelastic material applied to one face. The damping was assumed to be entirely due to stretching in the attached viscoelastic layer when the beam vibrated in the flexural mode. Expressions were obtained for the beam flexural rigidity. A linear viscoelastic stress - strain law was then assumed, and the Young's modulus of the material was replaced by complex modulus. The damping of the beam was characterised by a loss factor defined as the ratio of the imaginary to the real part of the now complex flexural rigidity. They showed that the beam damping was proportional to the thickness, loss factor, and extensional stiffness of the applied damping layer. These conclusions led Oberst to work towards the development of stiff high damping polymers [23,24].

van Itterbeck and Myncke [25] conducted an

experimental study of the damping of steel plates covered with thin layers of various damping materials. Tests were carried out within the temperature range, $-20^{o}C$ to $80^{o}C$, and their results followed the general trend of Oberst's analysis. An extension of the above analysis to the case of a two-layered structure in which both layers could be viscoelastic was carried out by Schwarzl [26]. His analysis also included coupling between extensional and flexural wave motions.

Other investigators have dealt with special cases. For example, Mead [28 - 30] has carried out a study of the damping and stress distribution in a vibrating stringer-skin combination having an applied layer of Aquaplas. The damping properties of Aquaplas under both random and harmonic excitation were also investigated. Together with Pearce, he has also considered the optimum use of the unconstrained-layer treatment by concentrating the treatment in the regions of highest bending moment [31]. Methods of analysis for such systems are given, and the optimum coverages required for various responses are evaluated. Experimental verification of the analysis is also carried out.

More recently, Hertelendy [32] has considered the displacement and strain energy distributions in a longitudinally vibrating cylindrical rod with a very thin

viscoelastic coating; while Henry and Freudenthal have analysed the forced vibration of a viscoelastic cylinder case-bonded to a thin elastic shell [33].

The analysis of Oberst et al and Schwarzl did not take account of thickness-wise deformation in the viscoelastic layer, this being regarded as negligible. However, experiments on structures with thick viscoelastic layers have shown some behaviours which cannot be explained on the basis of Oberst's theory. Oberst [77] and later Morris [34] and James [35] observed peaks in the damping - frequency response of such structures, and it was suspected that this might be a result of appreciable thickness-wise motion in the applied layer. Quite recently Ungar and Kerwin [36] have tried to explain this behaviour by including thickness-wise deformation in the analysis. The damping is assumed to be small and it is shown that for soft thick applied layers (i.e. weight ratios of base layer to damping layer of up to 4), thickness-wise motion becomes important at frequencies corresponding to standing wave resonances in the damping layer.

1.2.b. Constrained damping treatments or damped sandwich structures

The idea of sandwich construction has for long been employed in design for various reasons, such as the stiffening of structural members and the reduction of stress

levels. As a result, there exists an enormous amount of work in the literature on sandwich structures [e.g. 37,38]. The present work is however solely concerned with sandwich structures with viscoelastic layers built in for the purpose of introducing damping into the structures. Review of past work will therefore be limited to tnis class of structures.

The main attractions of the unconstrained damping treatment are the simplicity with which it can quite often be applied to an existing structure, the relative ease with which its analysis can be carried out, and the fact that the damping is not very sensitive to frequency changes. The damping depends on frequency only because the viscoelastic material properties are frequency-dependent. In most practical applications, however, the constrained damping treatment proves superior. It makes more efficient use of the damping material [39,40,66] and with proper optimisation of the geometry, much greater damping can be achieved with a relatively soft (but cheap) material than can ever be hoped for with stiffer (and invariably more expensive) unconstrained layers. Besides, the sandwich construction is less susceptible to enviromental effects (e.g. humidity, chemically adverse surroundings etc) than the unconstrained layer configuration. The analysis of the sandwich configuration is, however, much more involved; and has only been recently given serious attention.

Three groups of contributors feature prominently in this field, viz :

Kerwin et al

Yu, and

Mead

Their contributions will be dealt with first.

Kerwin et Al.

The first published work on the constrained damping treatment was due to Kerwin [41 - 43] . He considered the flexural vibration of a three - layer beam made up of an elastic base layer, a middle viscoelastic layer and a comparatively thin but stiff top elastic layer - a configuration popularly known as the "damping tape". On assuming that the damping in the beam was due entirely to shear deformation in the viscoelastic layer and that the material loss factor was small enough for its square to be negligible compared to unity, he obtained expressions for the damping of the beam and showed that it was frequency-dependent. A frequency-dependent shear parameter was defined to characterise this dependence.

Ross,Kerwin and Dyer [44, 45] developed a more general analysis of the three - layer beam, imposing no restriction on the thickness of the top layer. They took account of both extensional and shear deformations in the

viscoelastic layer and obtained expressions for the beam damping for various configurations, including the two-layer beam analysed by Oberst, the damping tape treated by Kerwin, and the symmetrical sandwich beam with a very thin layer of viscoelastic material. Expressions were also obtained for the beam geometry for optimum damping in each case. Their analysis was extended to multiple damping tapes by Ungar and Ross [46]. They showed that the damping performance of a multiple tape (made up of identical tapes) approximated that of a single tape having the same thickness of damping material as one of the tapes; but with a constraining layer thickness equal to the sum of the thicknesses of the individual constraining layers.

Ross, Ungar, and Kerwin [47] have also analysed the three-layer beam in which the stiffness of the base plate is much greater than that of the other layers, either or both of which can be dissipative. General expressions are obtained for the damping; and special cases are then treated, including the homogeneous unconstrained layer treatment, and the damping tape. They also deal with the "spaced" damping treatment in which an infinitely shear-stiff spacer separates the damping material from the base layer. This configuration is shown to be advantageous in both constrained and free-layer treatments. The geometry for optimum damping is obtained in each case.

Kerwin [48,49] has further investigated the spaced damping treatment for both free and constrained layers, considering the cases where the spacers have finite stiffness.

A comparison of the effectiveness of constrained and unconstrained damping treatments applied to plates was carried out by Kerwin and Ross [40] . Their study showed that for the stiffest polymer known, the constrained damping treatment(damping tape) is capable of giving a much higher loss factor than the free-layer treatment, for weight ratios of damping treatment to base plate of up to 0.2 for steel and 0.4 for aluminium plates.

The above analysis has been restricted to homogeneous layers. A possible method of extending it to more complex structures has been indicated by Ungar[51]. This involves treating the various layers vibrating in the flexural mode as inter-connected viscoelastic springs in the manner first suggested by Ungar and Kerwin [50] , and then obtaining expressions for the loss factor in terms of energy losses and storages in the spring models.

Several design configurations arising from the above study have been outlined by Ungar [52,53] .

The general method of analysis employed by Kerwin et al has the following feature. No equations of motion are given for the system. The total effective flexural rigidity of the sandwich structure is first obtained.

Then, as in Oberst's analysis, a linear viscoelastic law is assumed, the moduli of the damping layer being replaced by complex moduli; and the damping is characterised by a loss factor defined as the ratio of the imaginary part to the real part of the complex flexural rigidity. When desired, the mode shape for the beam, as well as the shear distribution along the length of the viscoelastic layer, is assumed to be sinusoidal. The analysis is thus only strictly applicable to lightly damped systems vibrating in the higher modes. Ross, Kerwin and Dyer have in fact pointed this out with the remark: "It is assumed that the damping factor of the composite plate is small enough that the basic sine wave shape of the vibrations is still valid" [44] . Besides; the loss factor as defined above is the same as the tangent of the phase difference between the applied bending moment, and the resulting curvature at any given section. The definition is thus unique only for systems where this phase difference does not vary along the beam length.

Attempts have been made to verify some aspects of the above analysis experimentally. Although agreement between theory and experiment has in most cases been regarded as "gratifying", it has by no means been satisfactory. The experimental work reported by Kerwin [41] showed fairly good agreement for the damping-frequency response

of the damping tape within the frequency range 200 cps to 100 kcs. At fairly low frequencies (and also at low temperatures) differences of up to 100 per cent , between calculated and experimental values were recorded. He attributed this to the assumption of small material damping and to uncertainty in the material properties.

Parfitt and Lambeth [54] carried out an experimental study of various configurations of the constrained layer treatment. Their loss factors showed appreciable differences from those calculated from Kerwin's theory (up to 200 per cent in many cases) and this was again attributed to lack of exact information on the material properties.
Ross, Kerwin and Dyer [44] and also Ross, Ungar and Kerwin [47] reported good agreement in trends, but agreement between calculated and experimental values was again poor.

Yu

In a series of articles [55-61], Yu has developed the general equations of motion for the flexural vibrations of an elastic symmetrical three-layer sandwich plate taking account of shear and rotatory inertia effects, but neglecting thickness-wise deformations. Displacement functions are assumed for the various layers in such a manner as to satisfy continuity requirements at the interfaces. The strains and stresses are then obtained

in terms of these functions, and the variational equations of motion are utilised in obtaining the differential equations connecting the above functions. Yu has applied these equations in the analysis of the free vibration of damped infinite and simply supported plates [59] . Like previous investigators, he assumes a linear viscoelastic law and replaces the elastic moduli by complex moduli. Furthermore, on the assumption of small overall damping (in other words, that the natural frequency is unaffected by the damping), he obtains expressions for the frequency and the damping, the latter being characterised by the logarithmic decrement.

The above work has been purely theoretical, and no report has been given of experimental work to check any aspect of the theory.

Mead

Mead has also analysed the symmetrical three-layer plate, confining himself to detailed treatment of the simply supported case [62,63] . He obtains the equations of motion for the plate, neglecting extensional deformation in the core, and thickness-wise deformations in the various layers. These equations are then solved for both harmonic and random excitation, the rotatory inertia terms being ignored. The transverse displacement of the

plate is expressed as an infinite series of sinusoidal transverse displacement modes. Damping is taken account of by replacing the moduli of the core by complex moduli. For each normal mode, the damping of the plate is characterised by a "modal" loss factor which is defined in the same manner as in Oberst's analysis. In addition, a "modal" stiffness ratio is defined as the ratio of the "generalised stiffness" [64] of the damped plate to that of a solid plate vibrating in the same mode, of the same material as, and having a thickness equal to the total thickness of the elastic layers. In a previous work [64] he had pointed out that the loss factor, on its own, does not give a complete assessment of the effectiveness of a damping treatment in the attenuation of a given response. The introduction of a damping treatment modifies, not only the damping, but also the mass and the stiffness of the system and this, by varying amounts. Different criteria for comparison are thus necessary for various responses. He obtains expressions for the criteria for given responses, considering both harmonic and random excitations; and gives the optimum geometry for each response. This is done on the assumption that only one mode is significantly excited, an assumption not likely to hold for highly damped systems.

An experimental check of the above analysis has

been carried out but this was confined to the natural frequencies and the loss factor. The application of some of the results of the above study to design has also been outlined [65,66] .

Other Contributors

Other investigators have tackled various aspects of the problem.

Plass [67] analysed the restricted case of a symmetrical three-layer beam in which the face layers were regarded as very thin membranes. Only two limiting cases of pure shear and pure bending of an infinite beam were considered. The two-dimensional equivalent of this problem, viz., a sandwich plate with thin facings, was also analysed by Yildiz [74] who obtained the equations of motion for the plate but did not attempt to solve them.

Kurtze [89,69] has considered the wave transmission and attenuation in infinite multi-layer plates using impedance techniques. The motions of the various layers are characterised by impedances which are suitably connected to reflect the coupling between them. Kurtze and Watters [70] have also carried out an analysis of the acoustic transmission loss characteristics of layered structures. They show that higher flexural loss factors can be obtained with the sandwich construction although

it is inferior to the unconstrained layer treatment as far as frequency response is concerned.

On the design side, Ruzicka [71] has outlined various configurations in which the shear damping technique can be applied. These include the sandwich construction as well as cell-inserts and strip-damper configurations. No general analysis of such structures is undertaken. Rather, a lumped parameter model is given for studying their damping and frequency characteristics. Some experimental work on cantilever beam models of the various configurations is reported, but this is not related to any theoretical work.

Freudenthal and Bieniek [72,73] have treated the case of flat and curved damped sandwich plates under harmonic excitation. Like Mead, they use the "normal mode" approach, expressing the total response as an infinite series of responses in the various normal modes. The plate core and facings are assumed to be orthotropic and dissipative with linear stress-strain relations, and complex moduli which are frequency-independent.

1.3 Scope of present work

From the above review, it is observed that much of past work has been centred on either simply supported structures or lightly damped structures vibrating in

the higher modes. This is simply because these structures lend themselves more readily to analytical treatment. The lower modes of vibration of systems with other boundary conditions as well as heavily damped structures still remain uninvestigated. At these low modes, the boundary conditions, and hence the mode shapes, are important; and the applicability of some of the generalisations obtained by analysis of the higher modes becomes doubtful (see chapter 6).

Besides, experimental verification of the various theories has not been very systematic. So far only loss factors and natural frequencies have been checked experimentally. The more exacting test of actually checking, say, a predicted displacement or stress response, has not yet been attempted. Lack of good agreement between theory and experiment has often been attributed (sometimes without strict justification) to lack of exact information on the viscoelastic material properties.

Also the viscoelastic material has been assumed to behave like a linear material in the strain ranges encountered in the analyses, although it is well known (see chapter 3) that these materials exhibit a certain amount of "non-linearity" even at very low strains. To what extent is this assumption justified? This question remains unanswered.

The present work is aimed at filling some of the above gaps, by investigating the dynamic behaviour of sandwich

beams vibrating in flexure.

The one-dimensional equations of motion for a symmetrical multi-layer beam with any number of layers are first developed. Shear and extensional deformations in the viscoelastic layers are considered. Rotatory inertia effects, shear deformation in the elastic layers, and thickness-wise deformations in all the layers are neglected. The viscoelastic material is assumed to obey a general (but as yet unprescribed) stress-strain law which could be linear or non-linear.

The solution of the equations requires, amongst other things, a clear knowledge of the dynamic behaviour of viscoelastic materials. Hence, a simple method of determining the dynamic properties of viscoelastic materials is developed; and utilised in the study of a few viscoelastic materials with a view to ascertaining their stress-strain laws under harmonic loading, their dynamic properties and the nature of their dependence on various factors. It is verified that from the point of view of non-linearity, the viscoelastic material can be satisfactorily regarded as a linear material with strain-dependent properties.

In the light of the information obtained from this study, a numerical method of solving the differential equations is developed, the method being capable of dealing with all possible boundary conditions, as well as linear and

non-linear behaviours of the viscoelastic material.

The analysis is then checked experimentally by considering the displacement response of cantilever three-layer and five-layer beams vibrating in the first few modes.

Finally, the application of the analysis to the design study of multi-layer sandwich beams is illustrated with a detailed study of the three-layer configuration vibrating in the first mode, and some studies of the five-layer beam.

C H A P T E R 2

DIFFERENTIAL EQUATIONS FOR MULTI-LAYER VISCOELASTIC SANDWICH BEAMS - DERIVATION.

Introduction

An important step in the analysis of any system is the establishment of the equations governing its behaviour. Accordingly, this chapter sets out to derive the differential equations for a multi-layer beam undergoing flexural vibration.

The general case of an unsymmetrical three-layer beam is first considered. It is shown that, for such a beam, the neutral axis position in general varies from section to section; and at any given section, it varies with the applied load or deflection. The 'symmetrical' beam is shown to be an exception to this, as its neutral axis always coincides with its central axis, no matter the loading.

The one-dimensional differential equations for a symmetrical multi-layer beam are then developed. The viscoelastic materials are assumed to obey a general stress - strain law which can be linear or non-linear. Shear in the elastic layers, and rotatory inertia in all the layers are ignored. Both shear and extensional deformations in the viscoelastic layers are included.

2.1. General assumptions.

The following assumptions are made:

(a) The multi-layer beam is made up of alternate layers of a viscoelastic material and a perfectly elastic material. The viscoelastic layers are always "constrained," that is, there is always an elastic layer above and below any viscoelastic layer. Each layer has uniform thickness.

(b) All the layers partake of the same flexural motion. In other words, at a given cross-section, each layer has the same vertical deflection y, and the same bending angle $\theta \doteq \frac{\partial y}{\partial x}$; x being measured along the length of the beam (fig 2.3). As Ross, Kerwin and Dyer have pointed out [44], this requires that the thicknesses of the layers are small compared with the shortest wavelength of any type of vibration within each layer.

(c) In addition to the bending deformation, each viscoelastic layer has a shear deformation ϕ_i in the plane of bending (figs 2.3.c and 2.3.d). ϕ_i, in general, varies from section to section along the length of the beam; but at a given cross-section, it is assumed constant across the thickness of the layer.

(d) Damping in the entire structure is due to imperfect elasticity in the viscoelastic material which, when subjected to periodic excitation, exhibits a stress - strain loop of

the general form,

$$\sigma = K_s\{S + \eta\,\Psi(S)\} \qquad \text{.....2.1.i}$$

where

S is the applied strain - direct or shear,

σ, the corresponding stress,

K_s, the appropriate dynamic modulus,

η, a 'constant' of the material.

From the above expression for σ, it is clear that $\Psi(S)$ - a yet unprescribed function of the strain, S - represents the departure from a linear stress - strain law.

The stress - strain loop is made up of two branches, the 'forward' or 'loading' branch, and the 'return' or 'unloading' branch. The function $\Psi(S)$ is denoted by $\vec{\Psi}(S)$ for the 'forward' branch, and by $\overleftarrow{\Psi}(S)$ for the 'return' branch. The two branches may both form a continuous curve. An example of this is when the stress - strain law is elliptical (fig 2.1). Then, the loop is a continuous curve with $\Psi(S)$ given by

$$\vec{\Psi}(S) = + (S_o^2 - S^2)^{1/2}$$
$$\overleftarrow{\Psi}(S) = - (S_o^2 - S^2)^{1/2} \qquad \text{..... 2.1.ii}$$

S_o being the maximum value of the strain S in one cycle. However, the loop need not be a continuous curve. The branches may be any two intersecting curves. The law for hysteresis damping in elastic materials affords a simple

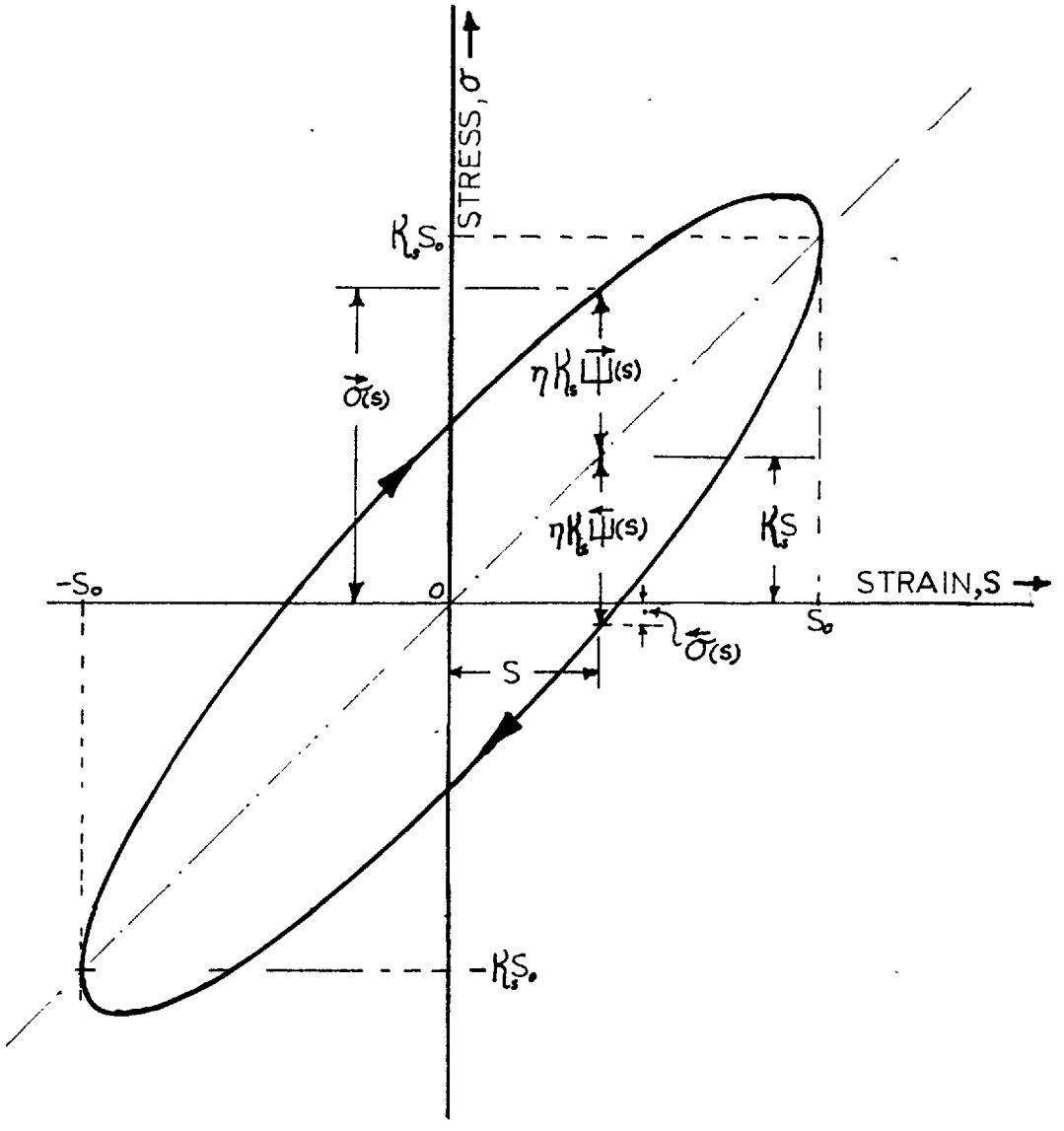

FIG. 2.1 Elliptical Stress–Strain Law. ($\eta = 0.5$)

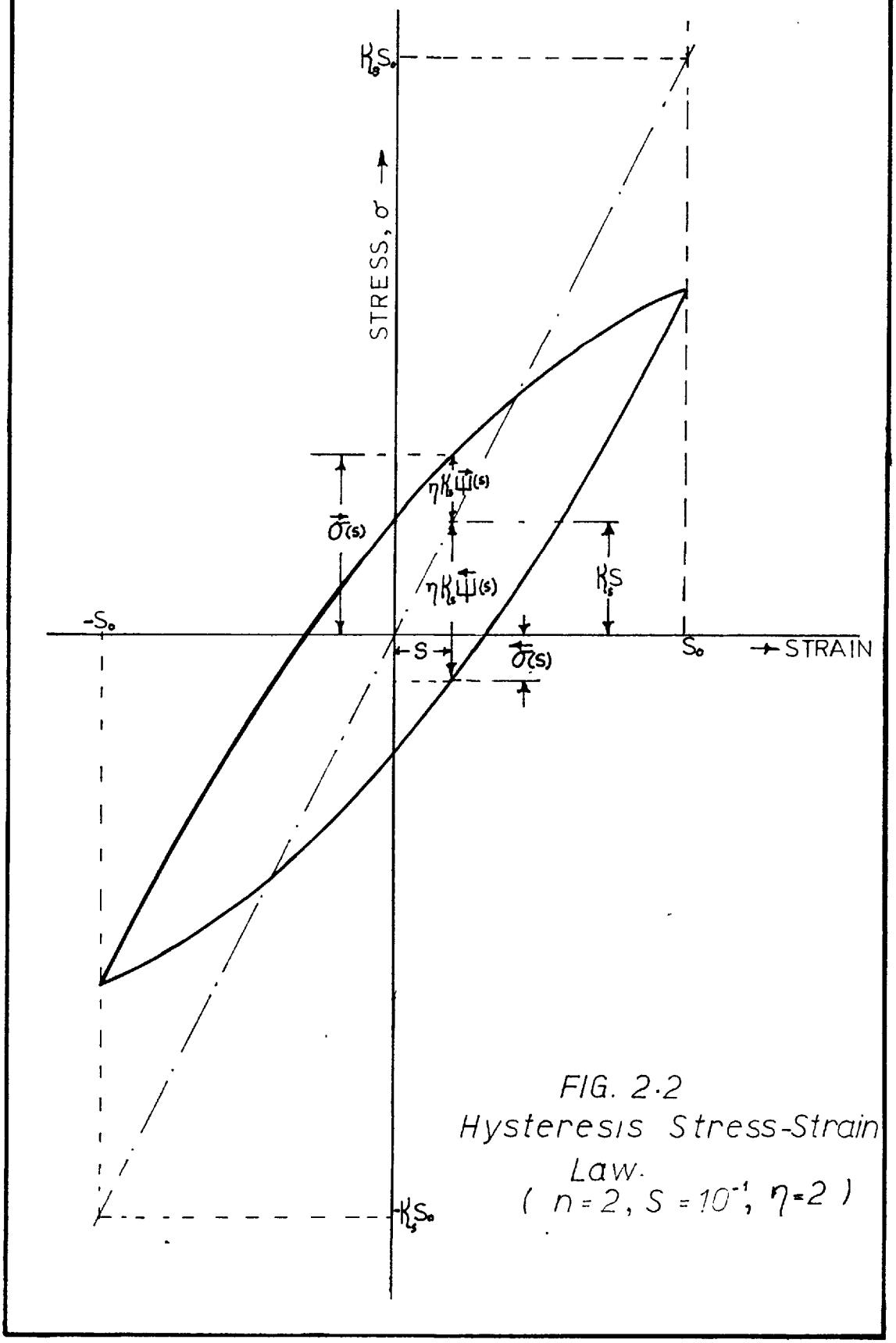

FIG. 2·2
Hysteresis Stress-Strain Law.
($n = 2$, $S = 10^{-1}$, $\eta = 2$)

example of such a case (fig 2.2). For a material obeying such a stress - strain law, Pisarenko has shown [9] that

$$\left.\begin{aligned}\vec{\Psi}(S) &= -\left[(S_o + S)^n - 2^{n-1} S_o^n\right] \\ \overleftarrow{\Psi}(S) &= +\left[(S_o - S)^n - 2^{n-1} S_o^n\right]\end{aligned}\right\} \quad \ldots\ldots\ldots\ldots\ldots 2.1.iii$$

n being a positive constant of the material (n>1).

In the next chapter, the stress - strain law for viscoelastic materials will be prescribed. Until then, however, the analysis will be kept in the general form to show that it is valid for other stress - strain laws. It will only be assumed that the loop has "cyclic symmetry", in the sense that

$$\vec{\Psi}(S) = -\overleftarrow{\Psi}(-S) \quad \ldots\ldots\ldots\ldots 2.1.iv$$

and that $\Psi(S)$ is a homogenous function of the strain S, and the strain amplitude S_o ; and hence is expressible in the form,

$$\Psi(S) = S_o^n \Psi\left(\frac{S}{S_o}\right) \quad \ldots\ldots\ldots\ldots\ldots 2.1.v.$$

Damping in the elastic layers is neglected, consistent with the assumption that these are perfectly elastic.

(e) Shear effects in the elastic layers are neglected, and so is the effect of rotatory inertia.

(f) The elastic layers obey Hooke's law both in tension and in compression.

PART A

THE GENERAL CASE

2.2 The three-layer beam

To illustrate the general method of approach employed, consider the simplest form of a multi-layer beam - the three-layer beam.

2.2.a. Shape of a deformed element.

When the beam of fig. 2.3a is subjected to a bending deformation, owing to assumption (c) above, plane sections no longer remain plane, and the beam might take a shape similar to that shown in fig. 2.3b. In other words, a longitudinal element cccc of fig. 2.3a deforms to c'c'c'c' in fig. 2.3b. An enlarged diagram of the element c'c'c'c' is given in figs 2.3c and 2.3d. Two cases are distinguished:
(i) when the neutral axis is in the viscoelastic layer - fig. 2.3c ; and
(ii) when the neutral axis is in any of the elastic layers - fig. 2.3d.

h_i (i = 1,2,3) is the thickness of the i-th layer, and i - i, represents the central axis of the i-th layer, d_i being the distance of this axis from the neutral axis, N - A , of the beam. z_i is the fibre distance of any longitudinal fibre of the i-th layer from its central axis. The width of the beam, and hence of the element, is b. Its total thickness is $\sum_{i=1}^{3} h_i$ and its length is dx. y is the vertical

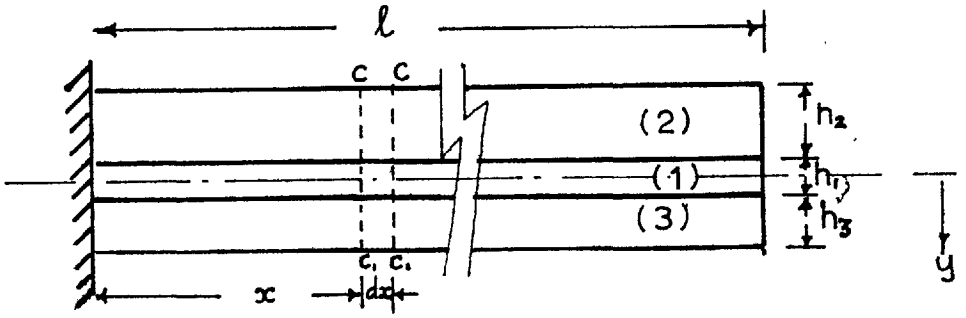

a) Undeformed beam.

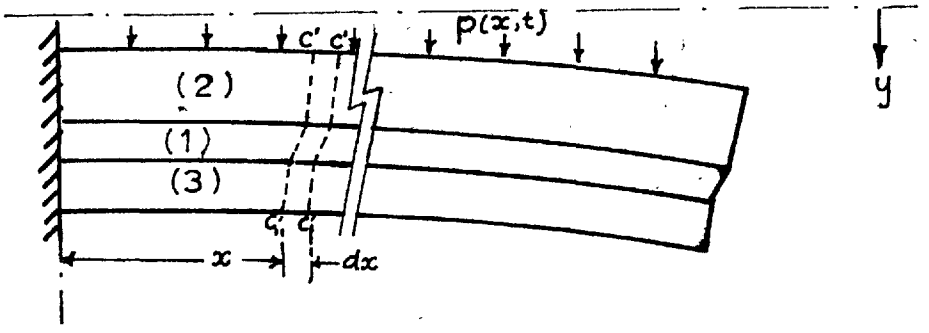

b) Deformed beam.

FIG. 2.3 a) & b) Three-layer Beam.

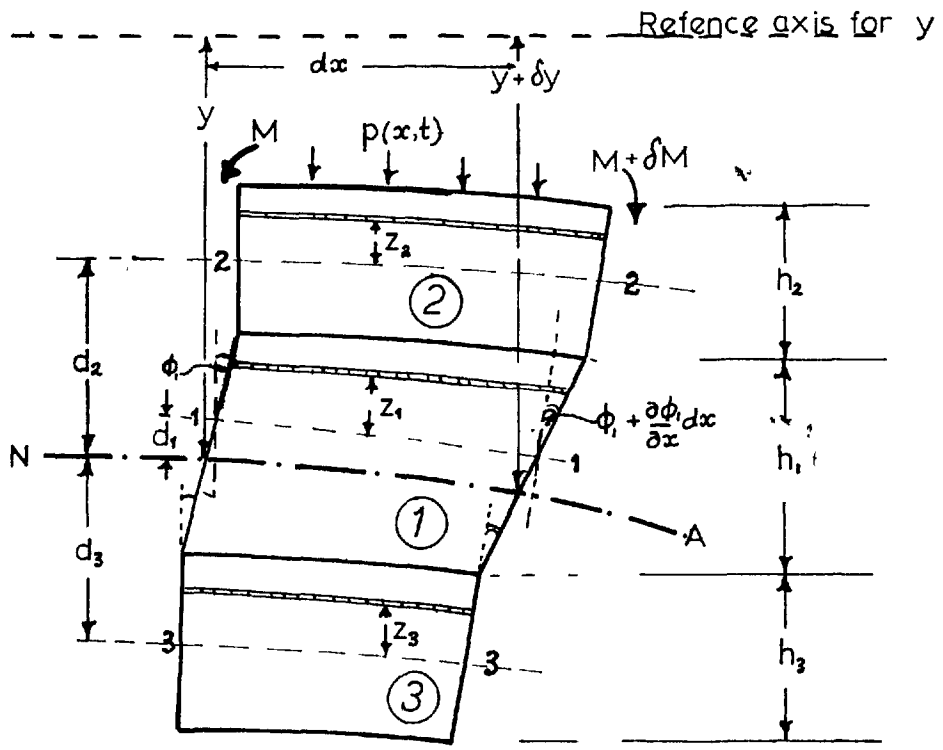

c) Neutral axis in viscoelastic layer.

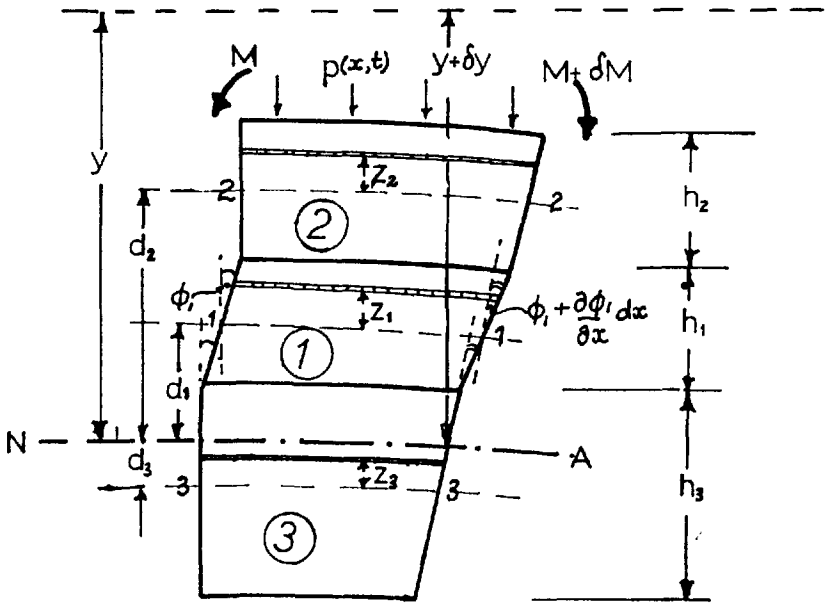

d) Neutral axis in elastic layer.

FIG. 2.3 c) & d) Three layer Beam Deformed element, dx.

displacement of the neutral axis (at a distance x along the beam) measured from its original equilibrium position. ϕ_i is the shear deformation in the i-th (viscoelastic) layer. $A_i (= bh_i)$, is the cross-sectional area of the i-th layer.

2.2.b. Case (i): Neutral axis in the viscoelastic layer.

Consider first the case in which the neutral axis is in the viscoelastic layer.

Longitudinal deformation

LAYER 1.

For any fibre distant z_1 from the axis 1-1, the longitudinal deformation can be thought of as made up of two parts:

(a) Extensional (or compressive) deformation due to bending. The strain due to this is proportional to the curvature and is given by $(z_1 + d_1)\frac{\partial^2 y}{\partial x^2}$

(b) Extensional (or compressive) deformation due to the variation of the shear angle ϕ_1 along the length of the beam. This gives rise to a longitudinal strain of magnitude $(z_1 + d_1)\frac{\partial \phi_1}{\partial x}$. The total longitudinal strain on the fibre is thus

$$\epsilon_1 = (z_1 + d_1)\left\{\frac{\partial^2 y}{\partial x^2} + \frac{\partial \phi_1}{\partial x}\right\} \quad \text{.....2.2.1}$$

LAYER 2.

The entire portion of this layer contained in the element dx suffers an extension (or compression) $(\frac{h_1}{2} + d_1)\frac{\partial \phi_1}{\partial x}dx$ due to the shear in the viscoelastic layer 1. In addition,

each fibre of the layer, distant z_2 from the axis 2-2, experiences a bending strain given by $(z_2 + d_2)\frac{\partial^2 Y}{\partial x^2}$. The total longitudinal strain on this fibre is thus

$$\epsilon_2 = (z_2 + d_2)\frac{\partial^2 Y}{\partial x^2} + (\frac{h_1}{2} + d_1)\frac{\partial \phi_1}{\partial x} \quad \ldots\ldots\ldots\ldots\ldots \quad 2.2.ii.$$

LAYER 3.

Again, owing to the shear in layer 1, the entire portion of layer 3 contained in the element dx, undergoes a compression (or extension) of magnitude $(-\frac{h_1}{2} + d_1)\frac{\partial \phi_1}{\partial x}\,dx$. Also, each fibre of this layer at a distance z_3 from the axis 3-3, experiences an additional bending strain given by $(z_3 - d_3)\frac{\partial^2 Y}{\partial x^2}$. Hence, the total strain in the fibre is

$$\epsilon_3 = (z_3 - d_3)\frac{\partial^2 Y}{\partial x^2} + (-\frac{h_1}{2} + d_1)\frac{\partial \phi_1}{\partial x} \quad \ldots\ldots\ldots\ldots\ldots \quad 2.2.iii$$

<u>Longitudinal stresses and forces.</u>

LAYER 1.

Since the material of this layer is viscoelastic, the appropriate stress - strain law is given in equation 2.1.i. Hence, the longitudinal stress in any fibre of the layer is

$$\sigma_1 = E_1\left\{(z_1 + d_1)(\frac{\partial^2 Y}{\partial x^2} + \frac{\partial \phi_1}{\partial x}) + \eta_{e1}\psi(\epsilon_1)\right\} \quad \ldots\ldots\ldots 2.2.iv,$$

where E_1 and η_{e1} are the material constants in extension (or compression). The total longitudinal force in layer 1 is given by

$$F_1 = \int_{A_1} \sigma_1\, dA_1$$

$$= \int_{-h_1/2}^{+h_1/2} E_1 (z_1 + d_1)(\frac{\partial^2 Y}{\partial x^2} + \frac{\partial \phi_1}{\partial x})b\,dz_1 + \int_{-h_1/2}^{+h_1/2} \eta_{e1} E_1 \psi(\epsilon_1)\, b\,dz_1$$

i.e. $F_1 = E_1 A_1 d_1 \left(\frac{\partial^2 Y}{\partial x^2} + \frac{\partial \phi_1}{\partial x}\right) + \mathcal{J}$ 2.2.v

where $\mathcal{J} = \int_{-h_1/2}^{+h_1/2} \eta_{e1} E_1 \Psi(\epsilon_1) b \, dz_1$.

The integral $\mathcal{J}$ can be conveniently split into

$$\int_{-h_1/2}^{(h_1/2 - 2d_1)} \eta_{e1} E_1 \Psi(\epsilon_1) \, b \, dz_1 + \int_{(h_1/2 - 2d_1)}^{+h_1/2} \eta_{e1} E_1 \Psi(\epsilon_1) \, b \, dz_1 \quad \text{.....2.2.vi.}$$

Fig 2.4 shows the strain distribution in the layer. Consider any two fibres on either side of, and equidistant from the neutral axis. Their strains are equal in magnitude but opposite in sign. Moreover, if the upper fibre is on the 'forward' branch, the lower fibre will be on the 'return' branch of the stress - strain loop. It follows from this and from the assumption in equation 2.1.iv, that

$$\eta_{e1} b E_1 \int_{-h_1/2}^{(h_1/2 - 2d_1)} \Psi(\epsilon_1) \, dz_1 = 0 \quad \text{.....2.2.vii}$$

Since $\epsilon_1 = (z_1 + d_1)\left(\frac{\partial^2 Y}{\partial x^2} + \frac{\partial \phi_1}{\partial x}\right)$, the maximum value of ϵ_1 over a cycle is

$$(\epsilon_1)_{max.} = (z_1 + d_1)\left[\left(\frac{\partial^2 Y}{\partial x^2} + \frac{\partial \phi_1}{\partial x}\right)\right]_{max.} = (z_1 + d_1)\, \varsigma\left(\frac{\partial^2 Y}{\partial x^2}, \frac{\partial \phi_1}{\partial x}\right)$$

.....2.2.viii

where $\varsigma\left(\frac{\partial^2 Y}{\partial x^2}, \frac{\partial \phi}{\partial x}\right)$ is some fuction of $\frac{\partial^2 Y}{\partial x^2}$ and $\frac{\partial \phi_1}{\partial x}$

Hence in view of equation 2.1.v, $\vec{\Psi}(\epsilon_1)$ can be expressed as

$$\vec{\Psi}(\epsilon_1) = (z_1 + d_1)^n \vec{\Psi}\left(\frac{\partial^2 Y}{\partial x^2}, \frac{\partial \phi_1}{\partial x}\right) \quad \text{.....2.2.ix}$$

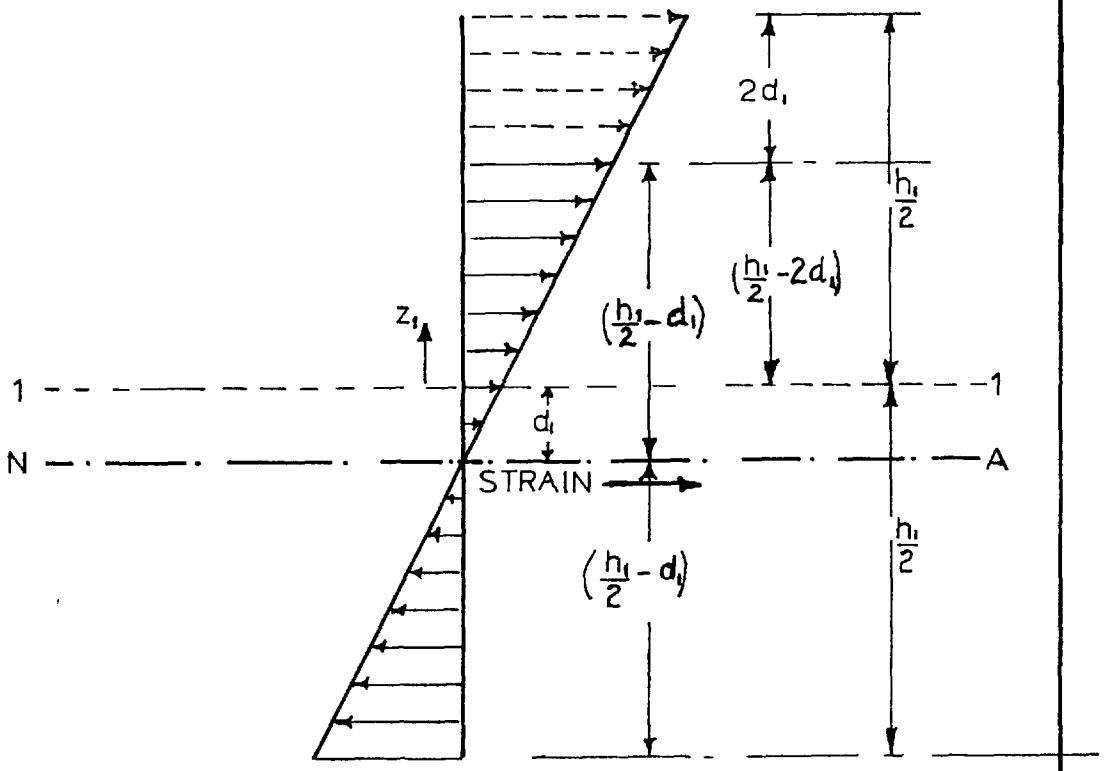

FIG. 2.4 Three layer Beam Longitudinal Strain distribution in Layer 1. Case (i)

It follows from equations 2.2.vi, 2.2.vii and 2.2.ix that

$$\mathcal{J} = \int_{(h_1/2 - 2d_1)}^{+h_1/2} \eta_{e_1} E_1 (z_1 + d_1)^n \vec{\Pi}\left(\frac{\partial^2 y}{\partial x^2}, \frac{\partial \phi_1}{\partial x}\right) b\, dz_1,$$

it being assumed (without any loss of generality) that the portion of the layer **above** the neutral axis is on the 'forward' branch of the stress - strain loop. Hence

$$\mathcal{J} = \frac{\eta_{e_1} E_1 b}{n+1} \vec{\Pi}\left(\frac{\partial^2 y}{\partial x^2}, \frac{\partial \phi_1}{\partial x}\right) \left[\left(\frac{h_1}{2} + d_1\right)^{n+1} - \left(\frac{h_1}{2} - d_1\right)^{n+1}\right]$$

Since d_1 is necessarily less than $\frac{h_1}{2}$, it is easy to show that for all real positive values of n, the expression $\left[\left(\frac{h_1}{2} + d_1\right)^{n+1} - \left(\frac{h_1}{2} - d_1\right)^{n+1}\right]$ can be put in the form $d_1 \varsigma_1(d_1)$, where $\varsigma_1(d_1)$ is an algebraic function of d_1. Thus,

$\mathcal{J} = \frac{\eta_{e_1} b d_1 E_1}{n+1} \vec{\Pi}\left(\frac{\partial^2 y}{\partial x^2}, \frac{\partial \phi_1}{\partial x}\right) \varsigma_1(d_1)$; and putting this in equation 2.2.v,

$$F_1 = E_1 A_1 d_1 \left(\frac{\partial^2 y}{\partial x^2} + \frac{\partial \phi_1}{\partial x}\right) + \frac{\eta_{e_1} b d_1 E_1}{n+1} \vec{\Pi}\left(\frac{\partial^2 y}{\partial x^2}, \frac{\partial \phi_1}{\partial x}\right) \varsigma_1(d_1) \ldots\ldots\ldots 2.2.x$$

LAYER 2.

This is an elastic layer; hence the stress σ_2 in any fibre is given by $\sigma_2 =$ E_2 x strain, where E_2 is the Young's modulus for the material of the layer;

i.e. $\sigma_2 = E_2 \left\{(z_2 + d_2)\frac{\partial^2 y}{\partial x^2} + \left(\frac{h_1}{2} + d_1\right)\frac{\partial \phi_1}{\partial x}\right\} \ldots\ldots\ldots 2.2.xi.$

The longitudinal force F_2, acting on the layer is thus

$$F_2 = \int_{A_2} \sigma_2 dA_2$$

$$= \int_{-h_2/2}^{+h_2/2} E_2 \left\{(z_2 + d_2)\frac{\partial^2 y}{\partial x^2} + \left(\frac{h_1}{2} + d_1\right)\frac{\partial \phi_1}{\partial x}\right\} b\, dz_2$$

i.e. $F_2 = E_2 A_2 d_2 \frac{\partial^2 y}{\partial x^2} + \left(\frac{h_1}{2} + d_1\right) E_2 A_2 \frac{\partial \phi_1}{\partial x}$ 2.2.xii

LAYER 3

This is also an elastic layer, hence the stress σ_3 in any fibre is given by

$$\sigma_3 = E_3\left\{(z_3 - d_3)\frac{\partial^2 y}{\partial x^2} + \left(\frac{h_1}{2} + d_1\right)\frac{\partial \phi_1}{\partial x}\right\} \quad \text{.....2.2.xiii}$$

and the total force in the layer is given by

$$F_3 = \int_{A_3} \sigma_3 \, dA_3$$

or $$F_3 = \int_{-\frac{h_3}{2}}^{+\frac{h_3}{2}} E_3\left\{(z_3 - d_3)\frac{\partial^2 y}{\partial x^2} + \left(\frac{h_1}{2} + d_1\right)\frac{\partial \phi_1}{\partial x}\right\} b \, dz_3$$, giving

$$F_3 = E_3 A_3\left[-d_3 \frac{\partial^2 y}{\partial x^2} + \left(\frac{h_1}{2} + d_1\right)\frac{\partial \phi_1}{\partial x}\right] \quad \text{.....2.2.xiv}$$

E_3 being the Young's modulus for the material of the layer.

2.2.c Case (ii) : Neutral axis in any of the elastic layers:

Next, consider the case when the neutral axis is in an elastic layer. It is clear that it doesn't matter which of the elastic layers contains the neutral axis; the same form of strain distribution will be obtained in each case. Consider, therefore, the case in which the neutral axis is in layer 3 (fig2.3.d).

Longitudinal deformation:

The longitudinal deformation in each layer can be obtaine as in the first case, starting with the layer containing the neutral axis.

LAYER 3: For any fibre distant z_3 from the central axis 3 - 3, the longitudinal strain is entirely due to bending, and is given by

$$\epsilon_3 = (z_3 - d_3)\frac{\partial^2 y}{\partial x^2} \quad \text{.....2.2.iii.a}$$

LAYER 1: Due to bending, any fibre distant z_1 from the axis 1 - 1, has a strain of magnitude $(z_1 + d_1)\frac{\partial^2 y}{\partial x^2}$. There is an additional strain of magnitude $(z_1 + \frac{h_1}{2})\frac{\partial \phi_1}{\partial x}$ due to the variation of ϕ_1 along the beam length. Hence the total strain in the fibre is given by

$$\epsilon_1 = (z_1 + d_1)\frac{\partial^2 y}{\partial x^2} + (z_1 + \frac{h_1}{2})\frac{\partial \phi_1}{\partial x} \quad \text{.....2.2.i.a}$$

LAYER 2: The entire portion of the element contained in this layer suffers a longitudinal strain $h_1\frac{\partial \phi_1}{\partial x}$ due to the shear in the viscoelastic layer. Also any fibre of the layer at a distance z_2 from the axis 2 - 2 experiences a bending strain of magnitude $(z_2 + d_2)\frac{\partial^2 y}{\partial x^2}$. The total strain in the fibr is thus

$$\epsilon_2 = (z_2 + d_2)\frac{\partial^2 y}{\partial x^2} + h_1\frac{\partial \phi_1}{\partial x} \quad \text{.....2.2.ii.a}$$

Longitudinal stresses and forces:

The stresses and forces are obtained in the same manner as in case (i), and are given below.

LAYER 1

$$\sigma_1 = E_1\left\{(z_1 + d_1)\frac{\partial^2 y}{\partial x^2} + (z_1 + \frac{h_1}{2})\frac{\partial \phi_1}{\partial x} + \eta_{e_1}\Psi(\epsilon_1)\right\} \quad \text{.....2.2.iv.a}$$

and $$F_1 = E_1 A_1 d_1\frac{\partial^2 y}{\partial x^2} + E_1 A_1\frac{h_1}{2}\frac{\partial \phi_1}{\partial x} + \rho_2\left(\frac{\partial^2 y}{\partial x^2}, \frac{\partial \phi_1}{\partial x}, d_1\right) \quad \text{.....2.2.x.a}$$

where ρ_2 is some function of $\frac{\partial^2 y}{\partial x^2}$, $\frac{\partial \phi_1}{\partial x}$, and d_1.

LAYER 2

$$\sigma_2 = E_2\left\{(z_2 + d_2)\frac{\partial^2 Y}{\partial x^2} + h_1\frac{\partial \phi_1}{\partial x}\right\} \quad \ldots\ldots\ldots\ldots 2.2.xi.a$$

and $$F_2 = E_2A_2d_2\frac{\partial^2 Y}{\partial x^2} + E_2A_2h_1\frac{\partial \phi_1}{\partial x} \quad \ldots\ldots\ldots\ldots\ldots 2.2.xii.a$$

LAYER 3

$$\sigma_3 = E_3(z_3 - d_3)\frac{\partial^2 Y}{\partial x^2} \quad \ldots\ldots\ldots\ldots 2.2.xiii.a$$

and $$F_3 = -E_3A_3d_3\frac{\partial^2 Y}{\partial x^2} \quad \ldots\ldots\ldots\ldots\ldots 2.2.xiv.a$$

It is seen from equations 2.2.i - iii and 2.2.i.a - iii. that the two cases considered above give rise to different strain distributions in the various layers. This is a consequence of the discontinuities (at the interfaces) in the strain distributions. The fibre stresses and the forces in the layers are also different in each case.

2.2.d. Neutral axis

The equation for the neutral axis is obtained from the condition that the resultant longitudinal force, F, at any cross-section is zero. Consider the case when the neutral axis is in the viscoelastic layer.

Thus $F = \sum_{i=1}^{3} F_i = 0$; which, from equations 2.2.x, 2.2.xii and 2.2.xiv, gives

$$E_1A_1d_1\left(\frac{\partial^2 Y}{\partial x^2} + \frac{\partial \phi_1}{\partial x}\right) + \frac{\eta_{o1}E_1d_1b}{n+1}\rho_1(d_1)\overrightarrow{LH}\left(\frac{\partial^2 Y}{\partial x^2}, \frac{\partial \phi_1}{\partial x}\right) + E_2A_2d_2\frac{\partial^2 Y}{\partial x^2}$$
$$+ E_2A_2\left(\frac{h_1}{2} + d_1\right)\frac{\partial \phi_1}{\partial x} - E_3A_3d_3\frac{\partial^2 Y}{\partial x^2} + \left(-\frac{h_1}{2} + d_1\right)E_3A_3\frac{\partial \phi_1}{\partial x} = 0 \quad \ldots\ldots 2.2.xv$$

Noting that

$d_2 = d_1 + \frac{h_1 + h_2}{2}$ and that $d_3 = -d_1 + \frac{h_1 + h_3}{2}$, it is possible to rearrange equation 2.2.xv to obtain an expression for d_1 in the form,

$$d_1 = \frac{E_3A_3\left(\frac{h_1+h_3}{2}\right) - E_2A_2\left(\frac{h_1+h_2}{2}\right) + \frac{h_1}{2}(E_3A_3 - E_2A_2)R_1\left(\frac{\partial^2 Y}{\partial x^2}, \frac{\partial \phi_1}{\partial x}\right)}{EA\left\{1 + R_1\left(\frac{\partial^2 Y}{\partial x^2}, \frac{\partial \phi_1}{\partial x}\right)\right\} + \frac{\eta_1 b E_1}{n+1}\rho_1(d_1)\, R_2\left(\frac{\partial^2 Y}{\partial x^2}, \frac{\partial \phi_1}{\partial x}\right)} \quad \text{.....2.2.xvi}$$

where the following notations have been employed;

$EA = \sum_{i=1}^{3} E_iA_i$; $R_1\left(\frac{\partial^2 Y}{\partial x^2}, \frac{\partial \phi_1}{\partial x}\right) = \frac{\partial \phi_1}{\partial x} \Big/ \frac{\partial^2 Y}{\partial x^2}$, and

$R_2\left(\frac{\partial^2 Y}{\partial x^2}, \frac{\partial \phi_1}{\partial x}\right) = \prod^{\rightarrow}\left(\frac{\partial^2 Y}{\partial x^2}, \frac{\partial \phi_1}{\partial x}\right) \Big/ \frac{\partial^2 Y}{\partial x^2}$

Equation 2.2.xvi gives d_1 as a function of $\frac{\partial^2 Y}{\partial x^2}$ and $\frac{\partial \phi_1}{\partial x}$ which in turn are functions of x, the position along the beam. But d_1 - the distance of the neutral axis from the central axis of layer 1 - defines the relative position of the neutral axis at any cross-section. It follows, therefore, that in general the neutral axis position varies from section to section along the beam. For any given deflection y - static or dynamic - $\frac{\partial^2 Y}{\partial x^2}$ and $\frac{\partial \phi_1}{\partial x}$ are fixed, and hence the neutral axis is fixed at each section. If y varies, however, the neutral axis position also varies. It is thus possible to think of a case in which for some value of y, the neutral axis no longer remains in the visco-elastic layer for some or all the sections of the beam. The strain distribution, the forces, and hence the neutral axis position obtained for case (i) would no longer hold; and it would be necessary to use the strain distributions etc. for case (ii). The situation becomes rather complicated in a dynamic case where y varies with time.

In such a case, as y varies, it is possible for the neutral axis to oscillate between the elastic and viscoelastic layers, the change from one layer to the other occuring at different points in time in the various sections. Analysis of such a beam by this method would thus be extremely difficult (see chapter 7).

Suppose, however, that $E_2 = E_3$, and $h_2 = h_3$. Then the numerator of the right-hand side of equation 2.2.xvi vanishes. Also, since R_1 and R_2 are arbitrary functions of x, the denominator is not identically zero. Hence d_1 vanishes; that is, the neutral axis coincides with the central axis of the viscoelastic layer. This is the case of the "symmetrical" three-layer beam; and for such a beam, the neutral axis position remains "fixed" at the central axis of the cross-section.

Although this result has been proved here for a symmetrical three-layer beam, it in fact holds true for any symmetrical multi-layer beam. A symmetrical multi-layer beam is characterised by the fact that any two layers equidistant from the central axis (i.e. the neutral axis) of the beam are of the same material and have the same dimensions. Unless otherwise stated, the rest of the work will deal solely with symmetrical multi-layer beams.

PART B

SYMMETRICAL MULTI-LAYER BEAMS

In the last section, a symmetrical multi-layer beam was defined as one in which any two layers equidistant from the central axis of the beam, have the same material properties and dimensions. Because of this symmetry, the neutral axis of such a beam coincides with its central axis, no matter the loading.

Consider the general symmetrical n-layer beam. n is necessarily odd, and can thus be written as $n = 2r + 1$, where r is the number of viscoelastic layers in the beam. The following two cases are distinguished:

(a) when the number of viscoelastic layers is odd. In such a case, r is of the form, $r = 2i - 1$, $i = 1,2,\ldots$.

Owing to symmetry, the shear deformations in any two viscoelastic layers equidistant from the central axis of the beam will be numerically the same at any section; hence, there are i independent shear variables, $\phi_1, \phi_3, \ldots \phi_{(2i-1)}$, associated with the viscoelastic layers. These, together with y, form the unknown variables. The number of differential equations required for such a beam is thus (i+1); and the number of layers, n, is given by $n = 2r + 1 = 4i - 1$.

(b) when the beam has an even number of viscoelastic layers. For such a beam $r = 2i$, $i=1,2,\ldots\ldots$.

Again, there are i independent shear variables, $\phi_2, \phi_4, \ldots \phi_{2i}$;

and hence (i+1) differential equations are needed. The number of layers, n = 4i + 1.

It follows immediately that for all non-zero integral values of i, the (4i-1)-layer beam has the same number of differential equations as the (4i+1)-layer beam. The "proto-type" for each set is obtained by putting i = 1, giving rise to the 3-layer beam for case (a); and the 5-layer for case (b). Before proceeding to obtain the differential equations for the two general cases above, it is intended to first illustrate the method of approach with the simpler cases of the 3-layer and 5-layer beams.

2.2.e. Moments and equation of motion - 3-layer beam.

The expressions for the strains, stresses and forces obtained in section 2.2.b (case(i)) hold good for the symmetrical 3-layer beam, with the additional condition that $d_1 = 0$, $E_2 = E_3$ and $h_2 = h_3$. With these expressions, the bending moments for the various layers can be worked out as follows.

LAYER 1

The bending moment, M_1, about the neutral axis due to the forces in layer 1 is given by

$$M_1 = \int_{A_1} \sigma_1 z_1 dA_1 = \int_{-h_1/2}^{+h_1/2} E_1 z_1^2 \left(\frac{\partial^2 Y}{\partial x^2} + \frac{\partial \phi_1}{\partial x}\right) b\, dz_1 + \int_{-h_1/2}^{+h_1/2} \eta_{le_1} E_1 \text{LLL}(\epsilon_1)\, z_1 b\, dz_1$$

$$\text{or } M_1 = E_1 I_{N1}\left(\frac{\partial^2 Y}{\partial x^2} + \frac{\partial \phi_1}{\partial x}\right) + \tfrac{1}{2} \text{LLL}_{m1} \quad \ldots\ldots\ldots 2.2.\text{xvii},$$

where, in general, $I_{Ni} = A_i\left(\frac{h_i^2}{12} + d_i^2\right)$ ....2.2.xviii is the second moment of area of the i-th layer about the neutral axis and

$$\Psi_{Ni} = 2\int_{-h_i/2}^{+h_i/2} \eta_{ei} E_i b \Psi(\epsilon_i)\,(z_i + d_i)\,dz_i \quad \text{.....2.2.xix.}$$

LAYER 2

The bending moment M_2 contributed by this layer is given by

$$M_2 = \int_{A_2} \sigma_2 (z_2 + d_2) dA_2 = \int_{-h_2/2}^{+h_2/2} E_2\left\{(z_2 + d_2)\frac{\partial^2 y}{\partial x^2} + \frac{h_2}{2}\frac{\partial \phi_2}{\partial x}\right\}(z_2 + d_2)\, b\, dz_2$$

or $M_2 = E_2 I_{N2}\frac{\partial^2 y}{\partial x^2} + E_2 A_2 d_2 \frac{h_2}{2}\frac{\partial \phi_2}{\partial x}$ 2.2.xx

LAYER 3

Similarly the bending moment contributed by layer 3 is

$$M_3 = \int_{A_3} \sigma_3 (z_3 - d_3)\, b\, dz_3 = \int_{-h_3/2}^{+h_3/2} E_3\left\{(z_3 - d_3)\frac{\partial^2 y}{\partial x^2} - \frac{h_3}{2}\frac{\partial \phi_3}{\partial x}\right\}(z_3 - d_3)\, b\, dz_3$$

i.e. $M_3 = E_3 I_{N3}\frac{\partial^2 y}{\partial x^2} + E_3 A_3 d_3 \frac{h_3}{2}\frac{\partial \phi_3}{\partial x}$ 2.2.xxi

$= M_2$, since $E_2 = E_3$ and $h_2 = h_3$.

This result is to be expected from the symmetry of the beam. Also from equations 2.2.xii and 2.2.xiv, on putting $d_i = 0$, it is seen that $F_3 = -F_2$. This means in effect that in dealing with symmetrical multi-layer beams, only the layers of the top half (or the bottom half) of the beam need be considered, since the forces and moments for the layers of the other half can be deduced.

The total bending moment, M, at any cross-section is thus

$M = \sum M_i = M_1 + 2M_2$ or

$$M = EI \frac{\partial^2 y}{\partial x^2} + N_1' \frac{\partial \phi_1}{\partial x} + \tfrac{1}{2} \Psi_{m1} \quad \text{.....2.2.xxii,}$$

where, $EI = \sum_{i=1}^{3} E_i I_{Ni}$, and $N_1' = E_1 I_{N1} + E_2 A_2 h_1 d_2$.

If the spatial rate of loading is q, then

$$\frac{\partial^2 M}{\partial x^2} = q \quad \text{.....2.2.xxiii.}$$

But $$q = p(x,t) - m \frac{\partial^2 y}{\partial t^2} \quad \text{.....2.2.xxiv,}$$

where $m = \sum_{i=1}^{3} \rho_i A_i$, is the mass per unit length of the beam, and p(x,t) is the externally applied load per unit length. ρ_i is the density of the i-th layer. It follows from equations 2.2.xxii, 2.2.xxiii and 2.2.xxiv, that

$$\frac{\partial^2}{\partial x^2} \left\{ EI \frac{\partial^2 y}{\partial x^2} + N_1' \frac{\partial \phi_1}{\partial x} + \tfrac{1}{2} \Psi_{m1} \right\} + m \frac{\partial^2 y}{\partial t^2} = p(x,t) \quad \text{...2.2.xxv.}$$

This is the differential equation of motion for a symmetrical 3-layer beam. However, equation 2.2.xxv contains two unknown variables, y and ϕ_1, so that two differential equations are needed.

2.2.f. <u>Shear deformation - three-layer beam.</u>

The second equation is obtained from consideration of the shear deformation in the viscoelastic layer 1. Fig. 2.5 shows the shape of the element when longitudinal deformation is neglected. ϕ_1 - assumed constant across the thickness of layer 1 - is taken as the shear strain at the central axis of the layer, the shear stress at that axis being τ_1. Thus τ_1 and ϕ_1 are connected by the viscoelastic

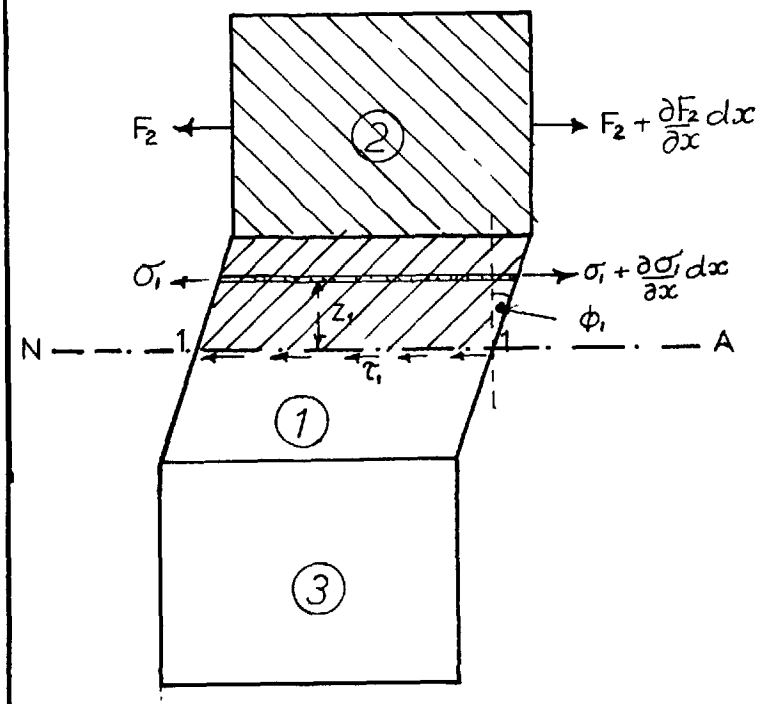

FIG. 2.5. Symmetrical Three-layer Beam. Shear deformation in element.

stress - strain law thus,

$$\tau_1 = G_1\{\phi_1 + \eta_{G_1}\amalg(\dot{\phi}_1)\} \quad \text{.....2.2.xxvi,}$$

G_1 and η_{G_1} being the material constants in shear. It is possible to obtain another expression for τ_1, by considering the equilibrium of the section of the element above (or below) the central axis 1 - 1. Assuming that there is no surface traction (i.e. that free surfaces of the beam are free from shear stress), longitudinal equilibrium of the shaded portion of fig. 2.5 requires that

$$\tau_1 b\,dx = \frac{\partial F_2}{\partial x}dx + \int_0^{+h_1/2}\left(\frac{\partial \sigma_1}{\partial x}dx\right) b\,dz_1 \quad \text{.....2.2.xxvii.}$$

On substituting for σ_1 and F_2 and simplifying, the above equation gives

$$b\tau_1 = \frac{\partial}{\partial x}\left\{\frac{\partial^2 y}{\partial x^2}\left(E_2A_2d_2 + E_1A_1\frac{h_1}{8}\right) + \frac{\partial \phi_1}{\partial x}\left(E_2A_2\frac{h_1}{2} + E_1A_1\frac{h_1}{8}\right) + \amalg_{F_1}\right\} \text{.2.2.xxviii,}$$

where, $$\amalg_{F_1} = \int_0^{+h_1/2} E_1\eta_{e_1}\amalg(\epsilon_1)\,b\,dz_1 \quad \text{.....2.2.xxix.}$$

Finally, equations 2.2.xxvi and 2.2.xxviii are combined to give $\frac{\partial}{\partial x}\left\{P_1'\frac{\partial^2 y}{\partial x^2} + Q_{11}'\frac{\partial \phi_1}{\partial x} + \amalg_{F_1}\right\} - \eta_{G_1}bG_1\amalg(\phi_1) = bG\phi_1$ ..2.2.xxx

where, $P_1' = E_2A_2d_2 + E_1A_1\frac{h_1}{8}$, and $Q_{11}' = E_2A_2\frac{h_1}{2} + E_1A_1\frac{h_1}{8}$.

Thus, equations 2.2.xxx and 2.2.xxv give the differential equations for determining y and ϕ_1.

2.3. The symmetrical 5-layer beam

The method of analysis introduced in section 2.2 will now be extended to beams with more than three-layers. Consider the 5-layer symmetrical beam.

Fig 2.6 shows a deformed longitudinal element, dx, of the beam. The layers are numbered from the centre outwards. Thus, layer 1 is the central layer; the two layers on either side of layer 1 are called layer 2 (upper and lower) and so on. As already pointed out in section 2.2.e, owing to symmetry, only the central and upper layers need be considered in detail. The notations of the previous section are preserved and extended where necessary in the rest of the work.

2.3.a. Longitudinal deformation

The longitudinal strain in any fibre of the various layers can now be worked out as in the previous section starting from the neutral axis - the axis of zero strain - and working outwards.

LAYER 1

This is necessarily an elastic layer (from assumption (a), section 2.1.). Consider any fibre of this layer at a distance z_1 from the central axis 1 - 1 which is coincident with the neutral axis. This fibre experiences only a bending deformation, hence the strain is given by

$$\epsilon_1 = z_1 \frac{\partial^2 y}{\partial x^2} \quad \ldots\ldots\ldots \quad 2.3.i.$$

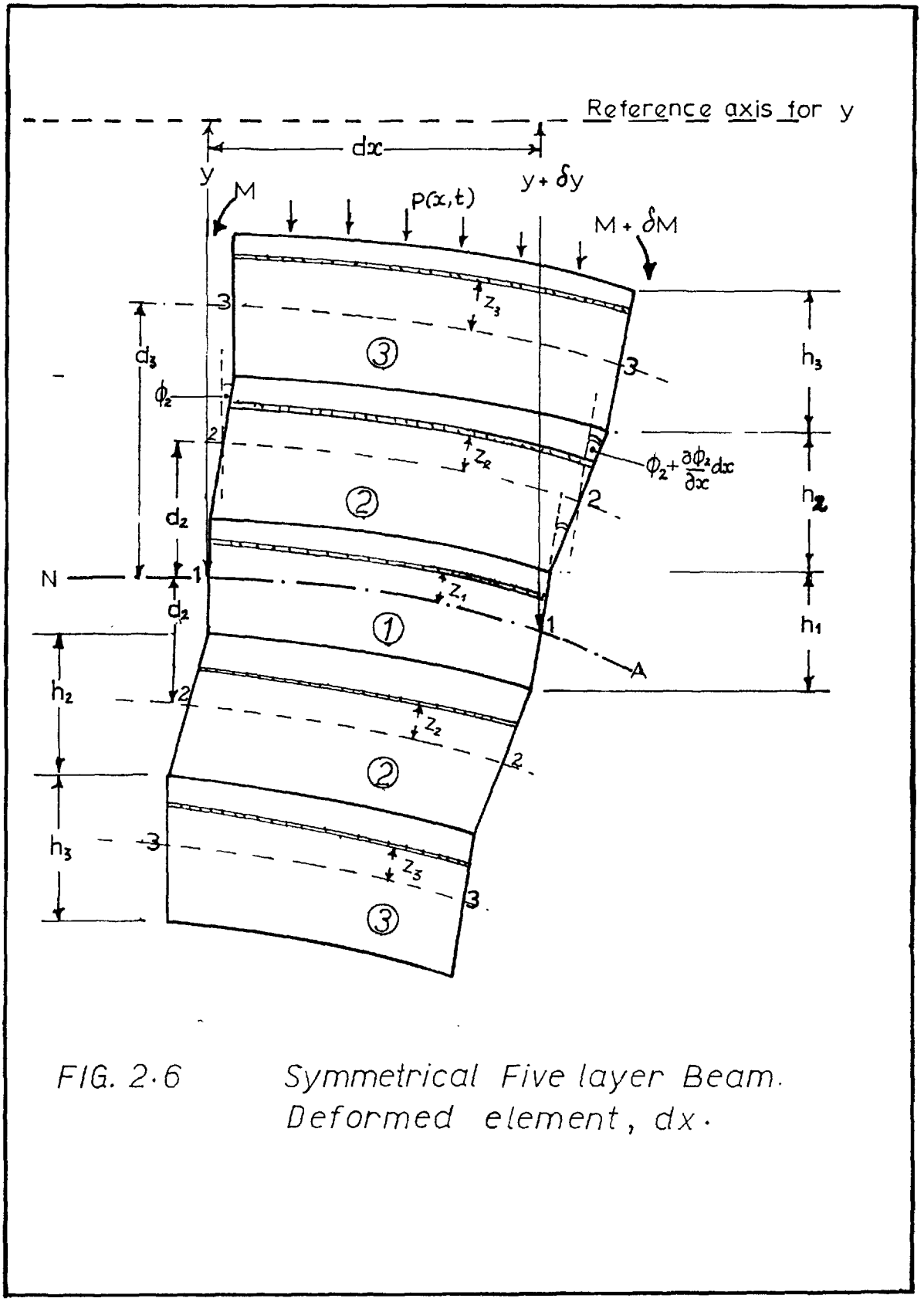

FIG. 2·6 Symmetrical Five layer Beam. Deformed element, dx.

UPPER LAYER 2

Due to bending deformation, any fibre of this layer, z_2 distant from the axis 2 - 2, experiences a strain of magnitude $(z_2 + d_2)\frac{\partial^2 y}{\partial x^2}$. This layer, however, is a viscoelastic layer with an additional shear deformation ϕ_2. This gives rise to a longitudinal strain on this fibre of magnitude $(z_2 + \frac{h_2}{2})\frac{\partial \phi_2}{\partial x}$. Hence the total strain in the fibre is

$$\epsilon_2 = (z_2 + d_2)\frac{\partial^2 y}{\partial x^2} + (z_2 + \frac{h_2}{2})\frac{\partial \phi_2}{\partial x} \quad \ldots\ldots\ldots \text{2.3.ii.}$$

LOWER LAYER 2

The strain in any fibre of this layer is easily deduced from the above result as

$$\epsilon_{2L} = (z_2 - d_2)\frac{\partial^2 y}{\partial x^2} + (z_2 - \frac{h_2}{2})\frac{\partial \phi_2}{\partial x} \quad \ldots\ldots\ldots \text{2.3.iii.}$$

UPPER LAYER 3

Bending deformation gives rise to a strain $(z_3 + d_3)\frac{\partial^2 y}{\partial x^2}$ at a fibre z_3 distant from 3 - 3 and since the whole portion of this layer (forming part of dx) experiences a strain $h_2\frac{\partial \phi_2}{\partial x}$ due to the shear deformation in the viscoelastic layer, the total longitudinal strain ϵ_3 becomes

$$\epsilon_3 = (z_3 + d_3)\frac{\partial^2 y}{\partial x^2} + h_2\frac{\partial \phi_2}{\partial x} \quad \ldots\ldots\ldots \text{2.3.iv.}$$

LOWER LAYER 3

Similarly the strain in any fibre of this layer is

$$\epsilon_{3L} = (z_3 - d_3)\frac{\partial^2 y}{\partial x^2} - h_2\frac{\partial \phi_2}{\partial x} \quad \ldots\ldots\ldots \text{2.3.v.}$$

2.3.b. Stresses, forces, moments, and equation of motion.

LAYER 1

The stress in any fibre of this layer is given by

σ_1 = E_1 x strain,

i.e. $\sigma_1 = E_1 z_1 \frac{\partial^2 y}{\partial x^2}$ ..... 2.3.vi.

Hence the total longitudinal force in the layer is

$$F_1 = \int_{A_1} \sigma_1 dA_1 = \int_{-h_1/2}^{+h_1/2} E_1 z_1 \frac{\partial^2 y}{\partial x^2} b\, dz_1 = 0 \quad \text{..... 2.3.vii}$$

Also the bending moment about the neutral axis contributed by the layer is

$$M_1 = \int_{A_1} \sigma_1 z_1 dA_1 = \int_{-h_1/2}^{+h_1/2} E_1 z_1 \frac{\partial^2 y}{\partial x^2} b\, dz_1 = E_1 I_{11} \frac{\partial^2 y}{\partial x^2} \quad \text{..... 2.3.viii.}$$

UPPER LAYER 2

It will be assumed, for convenience, that each fibre of this layer is on the forward branch of the stress - strain loop, and is in tension. (It follows that every fibre of the lower layer 2 is on the return branch of the loop and in compression). The stress in the fibre is thus

$\sigma_2 = E_2\left\{(z_2 + d_2)\frac{\partial^2 y}{\partial x^2} + (z_2 + \frac{h_2}{2})\frac{\partial \phi_2}{\partial x} + \eta_{e_2} \overrightarrow{\sqcup}(\epsilon_2)\right\}$ 2.3.ix,

(E_2 and η_{e_2} being the material constants in extension).

The longitudinal force, F_2, in the layer is given by

$$F_2 = \int_{A_2} \sigma_2 dA_2$$

$$= \int_{-h_2/2}^{+h_2/2} E_2\left\{(z_2 + d_2)\frac{\partial^2 y}{\partial x^2} + (z_2 + \frac{h_2}{2})\frac{\partial \phi_2}{\partial x} + \eta_{e_2} \overrightarrow{\sqcup}(\epsilon_2)\right\} b\, dz_2$$

$$\text{i.e. } F_2 = E_2 A_2 d_2 \frac{\partial^2 y}{\partial x^2} + E_2 A_2 \frac{h_2}{2} \frac{\partial \phi_2}{\partial x} + \int_{-h_2/2}^{+h_2/2} E_2 \eta_{e_2} \overrightarrow{\Psi}(\epsilon_2)\, b\, dz_2 \quad \ldots\ldots \text{2.3.x.}$$

Also the bending moment M_2 contributed by the layer is given by

$$M_2 = \int_{A_2} \sigma_2 (z_2 + d_2)\, dA_2$$

$$= \int_{-h_2/2}^{+h_2/2} E_2 \left\{ (z_2 + d_2) \frac{\partial^2 y}{\partial x^2} + (z_2 + \frac{h_2}{2}) \frac{\partial \phi_2}{\partial x} \right\} (z_2 + d_2)\, b\, dz_2$$

$$+ \int_{-h_2/2}^{+h_2/2} E_2 \eta_{e_2} \overrightarrow{\Psi}(\epsilon_2)\, (z_2 + d_2)\, b\, dz_2 \quad .$$

$$\text{i.e. } M_2 = E_2 I_{n_2} \frac{\partial^2 y}{\partial x^2} + (E_2 A_2 \frac{h_2^2}{12} + E_2 A_2 d_2 \frac{h_2}{2}) \frac{\partial \phi_2}{\partial x} + \mathcal{J}_1 \quad \ldots\ldots \text{2.3.xi.}$$

$$\text{where } \mathcal{J}_1 = \int_{-h_2/2}^{+h_2/2} E_2 \eta_{e_2} \overrightarrow{\Psi}(\epsilon_2) \left[z_2 + d_2 \right] b\, dz_2 \ldots\ldots \text{2.3.xii.}$$

LOWER LAYER 2

The stress in any fibre of this layer is given by

$$\sigma_{2L} = E_2 \left\{ (z_2 - d_2) \frac{\partial^2 y}{\partial x^2} + (z_2 - \frac{h_2}{2}) \frac{\partial \phi_2}{\partial x} + \eta_{e_2} \overleftarrow{\Psi}(\epsilon_{2L}) \right\} \quad \ldots\ldots \text{2.3.xiii}$$

The force and bending moment are obtained as above to be

$$F_{2L} = -E_2 A_2 d_2 \frac{\partial^2 y}{\partial x^2} - E_2 A_2 \frac{h_2}{2} \frac{\partial \phi_2}{\partial x} + \int_{-h_2/2}^{+h_2/2} E_2 \eta_{e_2} \overleftarrow{\Psi}(\epsilon_{2L})\, b\, dz_2 \ldots\ldots \text{2.3.xiv}$$

and $M_{2L} = E_2 I_{w2} \frac{\partial^2 y}{\partial x^2} + (E_2 A_2 \frac{h_2^2}{12} + E_2 A_2 d_2 \frac{h_2}{2}) \frac{\partial \phi_2}{\partial x} + \mathcal{J}_2$ ..... 2.3.xv.

where $\mathcal{J}_2 = \int_{-h_2/2}^{+h_2/2} E_2 \eta_{e_2} \overleftarrow{\Psi}(\epsilon_{2L}) [z_2 - d_2] b \, dz_2$ 2.3.xvi

It has already been postulated in section 2.2.e that $F_2 = -F_{2L}$, and that $M_2 = M_{2L}$.

Equations 2.3.x, 2.3.xi, 2.3.xiv and 2.3.xv would, therefore, seem to disobey this postulate unless

$$\int_{-h_2/2}^{+h_2/2} E_2 \eta_{e_2} \overleftarrow{\Psi}(\epsilon_{2L}) \, b \, dz_2 = - \int_{-h_2/2}^{+h_2/2} E_2 \eta_{e_2} \overrightarrow{\Psi}(\epsilon_2) \, b \, dz_2 \quad \text{..... 2.3.xviia}$$

and $\mathcal{J}_2 = \mathcal{J}_1$ 2.2.xviib

The above conditions in fact hold; for if the general elemental fibre of lower layer 2 is chosen at $-z_2$ (instead of at z_2), then $\epsilon_{2L} = -\epsilon_2$ (from equations 2.3.iii and 2.3.ii), so that

$$\int_{-h_2/2}^{+h_2/2} E_2 \eta_{e_2} \overleftarrow{\Psi}(\epsilon_{2L}) b \, dz_2 = \int_{-h_2/2}^{+h_2/2} E_2 \eta_{e_2} \overleftarrow{\Psi}(-\epsilon_2) \, b \, dz_2$$

$$= - \int_{-h_2/2}^{+h_2/2} E_2 \eta_{e_2} \overrightarrow{\Psi}(\epsilon_2) \, b \, dz_2 ; \left[\text{since } \overrightarrow{\Psi}(\epsilon_2) = -\overleftarrow{\Psi}(-\epsilon_2)\right]$$

which proves the first condition 2.2.xviia. Similarly

$$\mathcal{J}_2 = \int_{-h_2/2}^{+h_2/2} \eta_{e_2} E_2 \sqcup\!\!\uparrow(\epsilon_2) \left[z_2 - d_2\right] b\, dz_2 = \int_{-h_2/2}^{+h_2/2} -\eta_{e_2} E_2 \sqcup\!\!\uparrow(-\epsilon_2) \left[z_2 + d_2\right] b\, dz_2$$

$$= \int_{-h_2/2}^{+h_2/2} \eta_{e_2} E_2 \sqcup\!\!\downarrow(\epsilon_2) \left[z_2 + d_2\right] b\, dz_2 = \mathcal{J}_1 \text{, proving the second}$$

condition.

UPPER LAYER 3

The stress in any fibre is

$$\sigma_3 = E_3 \times \text{strain} = E_3 \left\{ (z_3 + d_3) \frac{\partial^2 y}{\partial x^2} + h_2 \frac{\partial \phi_2}{\partial x} \right\} \quad \ldots.2.3.\text{xviii}.$$

Hence, the longitudinal force, F_3, on the layer is given by

$$F_3 = \int_{A_3} \sigma_3 \, dA_3 = \int_{-h_3/2}^{+h_3/2} E_3 \left\{ (z_3 + d_3) \frac{\partial^2 y}{\partial x^2} + h_2 \frac{\partial \phi_2}{\partial x} \right\} b\, dz_3$$

$$= E_3 A_3 d_3 \frac{\partial^2 y}{\partial x^2} + E_3 A_3 h_2 \frac{\partial \phi_2}{\partial x} \quad \ldots\ldots\ldots\ldots 2.3.\text{xix}.$$

Also, the moment, M_3, is given by

$$M_3 = \int_{-h_3/2}^{+h_3/2} E_3 \left\{ (z_3 + d_3) \frac{\partial^2 y}{\partial x^2} + h_2 \frac{\partial \phi_2}{\partial x} \right\} (z_3 + d_3)\, b\, dz_3$$

$$\text{i.e.} \quad M_3 = E_3 I_{N3} \frac{\partial^2 y}{\partial x^2} + E_3 A_3 d_3 h_2 \frac{\partial \phi_2}{\partial x} \quad \ldots\ldots 2.3.\text{xx}.$$

LOWER LAYER 3

The expressions for the stress, force, and moment for this layer are given below.

$$\sigma_{3L} = E_3\left\{(z_3 - d_3)\frac{\partial^2 y}{\partial x^2} - h_2\frac{\partial \phi_2}{\partial x}\right\} \quad \text{.....2.3.xxi}$$

$$F_{3L} = -E_3A_3d_3\frac{\partial^2 y}{\partial x^2} - E_3A_3h_2\frac{\partial \phi_2}{\partial x} \quad \text{.....2.3.xxii, and}$$

$$M_{3L} = E_3I_{N3}\frac{\partial^2 y}{\partial x^2} + E_3A_3d_3h_2\frac{\partial \phi_2}{\partial x} \quad \text{.....2.3.xxiii.}$$

The total bending moment at any cross-section is

$$M = \sum M_i = M_1 + 2M_2 + 2M_3 = EI\frac{\partial^2 y}{\partial x^2} + N_2'\frac{\partial \phi_2}{\partial x} + \Psi_{m2} \quad \text{...2.3.xxiv,}$$

where, as previously, $EI = \sum_i E_iI_{Ni}$, and in addition,

$$N_2' = 2\left[E_2A_2\frac{h_2^2}{12} + E_2A_2d_2\frac{h_2}{2} + E_3A_3d_3h_2\right] \quad \text{.....2.3.xxv}$$

and $$\Psi_{m2} = 2\vartheta_1 = 2\int_{-h_2/2}^{+h_2/2} \eta_{e2}E_2\Psi(\epsilon_2)\left[z_2 + d_2\right] b\,dz_2 \quad \text{.....2.3.xxvi.}$$

The differential equation of motion is thus

$$\frac{\partial^2}{\partial x^2}\left[EI\frac{\partial^2 y}{\partial x^2} + N_2'\frac{\partial \phi_2}{\partial x} + \Psi_{m2}\right] + m\frac{\partial^2 y}{\partial t^2} = p(x,t) \quad \text{...2.3.xxvii.}$$

The above differential equation contains two unknown variables, y and ϕ_2. A second equation is thus necessary.

2.3.c. Shear deformation.

As in the case of the three-layer beam, the second differential equation is obtained by considering the shear deformation in the viscoelastic layers.

Fig. 2.7 shows the upper half of the element, dx, of the beam, longitudinal deformation being neglected. Longitudinal equilibrium of the hatched section gives the shear stress, τ_2, at the central axis of layer 2 as

$$b\tau_2 = \frac{\partial F_3}{\partial x} + \int_0^{+h_2/2}\frac{\partial \sigma_2}{\partial x}\,b\,dz_2 \quad \text{.....2.3.xxviii.}$$

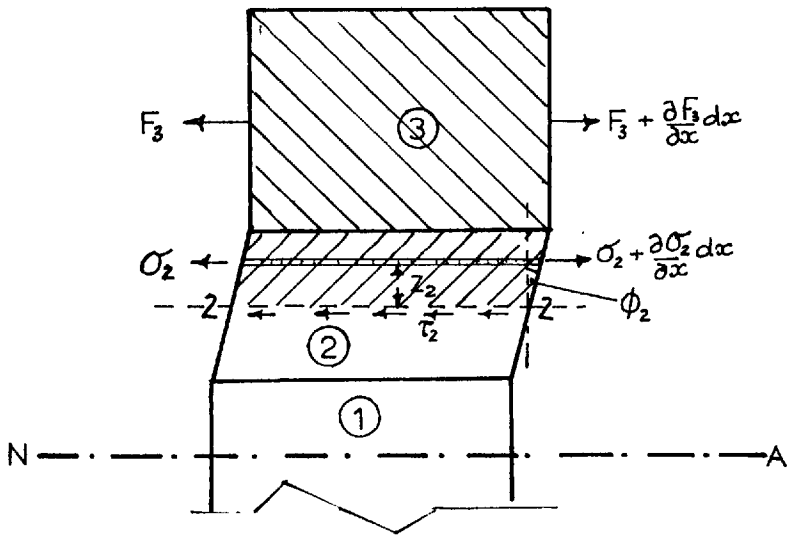

FIG. 2·7 Symmetrical Five-layer Beam. Shear deformation in upper layer 2.

τ_2, however, is related to ϕ_2, the shear strain at the central axis, by the equation,

$$\tau_2 = G_2\{\phi_2 + \eta_{G2}\Psi(\phi_2)\} \quad \ldots\ldots\ldots \quad 2.3.\text{xxix}$$

On putting the appropriate values for F_3, σ_2 and ϕ_2 in the above equations, and eliminating τ_2, the following equation results.

$$\frac{\partial}{\partial x}\left[P_2' \frac{\partial^2 y}{\partial x^2} + Q_{22}' \frac{\partial \phi_2}{\partial x} + \Psi_{F2}\right] - \eta_{G2} G_2 \Psi(\phi_2)\, b = bG_2\phi_2 \quad \ldots\ldots \quad 2.3.\text{xxx}$$

where $P_2' = E_3A_3d_3 + E_2A_2\frac{d_2}{2} + E_2A_2\frac{h_2}{8}$ 2.3.xxxi

$$Q_{22}' = E_3A_3h_2 + \frac{3}{8}E_2A_2h_2 \ldots\ldots\ldots\ldots \quad 2.3.\text{xxxii}$$

$$\Psi_{F2} = \int_0^{+h_2/2} \eta_{e2} E_2 \Psi(\epsilon_2)\, b\, dz_2 \ldots\ldots\ldots \quad 2.3.\text{xxxiii}$$

Equation 2.3.xxx provides the second equation required for determining y and ϕ_2.

A comparison of the differential equations for the five-layer beam with those for the three-layer beam will show that they have the same basic form, differing only in the constants.

It may have been observed that for both beams the bending moment M at any cross-section is <u>not</u> directly proportional to the curvature (as is the case in homogeneous beams). This is a general feature of multi-layer beams.

2.4. The symmetrical n-layer beam.

It is now intended to establish the differential equations for the general case of an n-layer beam. The two cases distinguished at the beginning of this section will be dealt with in turn. Following the convention introduced in section 2.3, the layers are numbered from the centre outwards. The notations of the previous sub-sections are retained, and extended where necessary.

2.4.a Symmetrical n-layer beam with an odd number of viscoelastic layers.

Consider first the case of an n-layer beam with an odd number of viscoelastic layers. The central layer 1 is necessarily viscoelastic. Also any layers p and q are respectively viscoelastic and elastic, where

$p = 2k - 1$; $q = 2k$; for $k = 1, 2, \ldots i \quad \ldots$ 2.4.i

and $n = 4i - 1$

Then, for all valid values of k (i.e. from 1 to i) the longitudinal strain ϵ_p in the elemental fibre of layer p (fig 2.8) is given by

$$\epsilon_p = \underbrace{(z_p + d_p)\frac{\partial^2 y}{\partial x^2}}_{(i)} + \underbrace{\frac{h_1}{2}\frac{\partial \phi_1}{\partial x} + \sum_{\alpha=2}^{k-1} h_s \frac{\partial \phi_s}{\partial x}}_{(ii)} + \underbrace{(z_p + \frac{h_p}{2})\frac{\partial \phi_p}{\partial x}}_{(iii)} \quad k>1 \quad \ldots\ldots 2.4.ii$$

where $s = 2\alpha - 1$, $\alpha = 1,2,3,\ldots$. In equation 2.4.ii, the first term (i) is the strain in the fibre due to bending; the next two terms (ii) are the strains due to the shear deformations in all the viscoelastic layers between

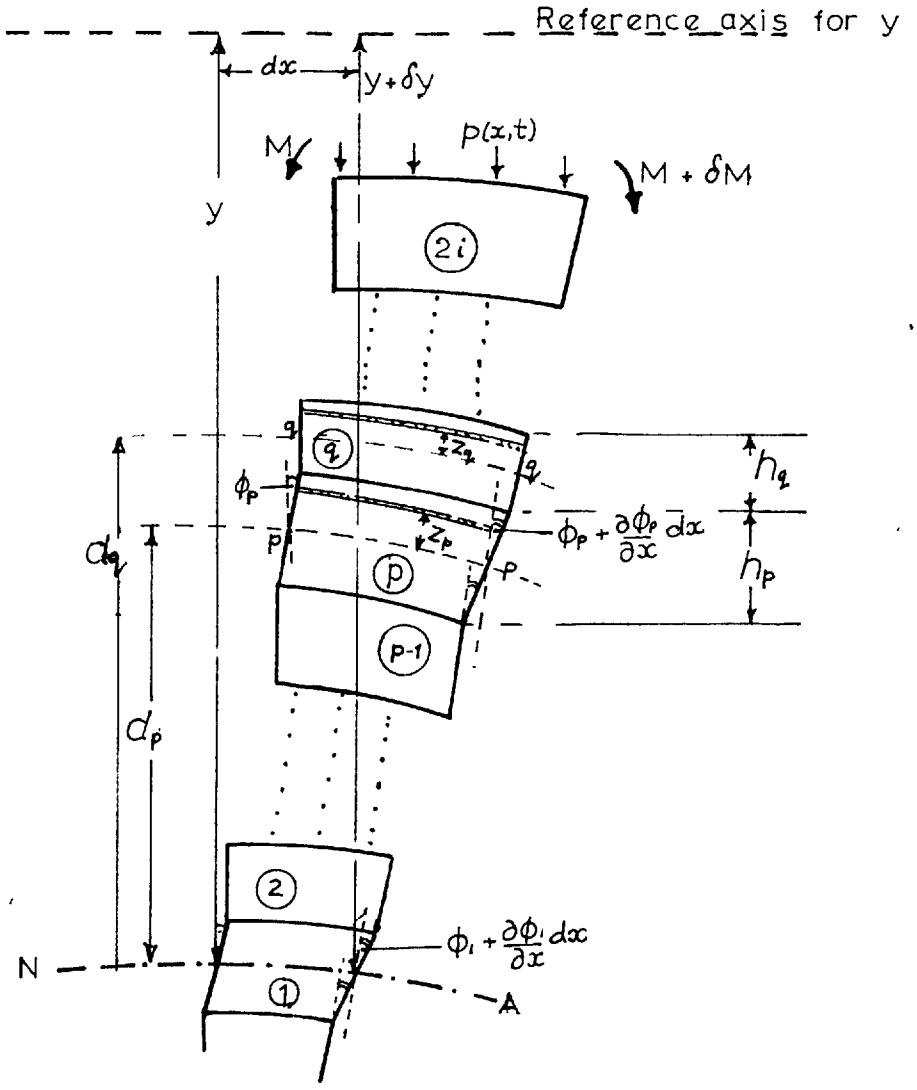

FIG. 2.8 Symmetrical n-layer Beam ($n = 4i-1$)
Upper half of deformed element.

the neutral axis and layer p; and the last term (iii) is the strain due to the shear in layer p itself.

Equation 2.4.ii can be rearranged in a more convenient form thus $\epsilon_p = (z_p + d_p)\frac{\partial^2 y}{\partial x^2} - \frac{h_1}{2}\frac{\partial \phi_1}{\partial x} + \sum_{\alpha=1}^{k} h_s \frac{\partial \phi_s}{\partial x} + (z_p - h_p/2)\frac{\partial \phi_p}{\partial x}$ . . .

$k = 1, 2 \ldots$ 2.4.iii

Similarly, the longitudinal strain in any elastic layer can be expressed as the sum of the fibre strain due to bending, and the strains due to the shear deformations in all the viscoelastic layers between the neutral axis and layer q ; thus

$\epsilon_q = (z_q + d_q)\frac{\partial^2 y}{\partial x^2} + \frac{h_1}{2}\frac{\partial \phi_1}{\partial x} + \sum_{\alpha=2}^{k} h_s \frac{\partial \phi_s}{\partial x}$ 2.4.iv

which can be put in the more convenient form

$\epsilon_q = (z_q + d_q)\frac{\partial^2 y}{\partial x^2} - \frac{h_1}{2}\frac{\partial \phi_1}{\partial x} + \sum_{\alpha=1}^{k} h_s \frac{\partial \phi_s}{\partial x}$ ... 2.4.v; $s = 2\alpha - 1$.

The stresses are thus

$\sigma_p = E_p\left\{(z_p + d_p)\frac{\partial^2 y}{\partial x^2} - \frac{h_1}{2}\frac{\partial \phi_1}{\partial x} + \sum_{\alpha=1}^{k} h_s \frac{\partial \phi_s}{\partial x} + (z_p - h_p/2)\frac{\partial \phi_p}{\partial x} + \eta_{ep} \perp\!\!\!\perp (\epsilon_p)\right\}$ 2.4.vi

and $\sigma_q = E_q\left\{(z_q + d_q)\frac{\partial^2 y}{\partial x^2} - \frac{h_1}{2}\frac{\partial \phi_1}{\partial x} + \sum_{\alpha=1}^{k} h_s \frac{\partial \phi_s}{\partial x}\right\}$ 2.4.vii

where E_p and η_{ep} are the viscoelastic constants (in extension) for layer p; and E_q is the Young's modulus of elasticity of layer q

The forces and bending moments in the layers are obtained in the usual way. Thus, for any viscoelastic layer p;

$$F_p = \int_{A_p} \sigma_p \, dA_p$$

$$\text{i.e. } F_p = E_p A_p d_p \frac{\partial^2 y}{\partial x^2} - E_p A_p \frac{h_1}{2} \frac{\partial \phi_1}{\partial x} + E_p A_p \sum_{\alpha=1}^{k} h_s \frac{\partial \phi_s}{\partial x}$$

$$- \left\{ E_p A_p \, h_p / 2 \right\} \frac{\partial \phi_p}{\partial x} + \Psi_p \quad \ldots\ldots\ldots\ldots \quad 2.4.\text{viii}$$

$$\text{and } M_p = \int_{A_p} (z_p + d_p) \sigma_p \, dA_p$$

$$= E_p I_{Np} \frac{\partial^2 y}{\partial x^2} - E_p A_p d_p \frac{h_1}{2} \frac{\partial \phi_1}{\partial x} + E_p A_p d_p \sum_{\alpha=1}^{k} h_s \frac{\partial \phi_s}{\partial x}$$

$$+ \left(E_p A_p \frac{h_p^2}{12} - E_p A_p d_p h_p / 2 \right) \frac{\partial \phi_p}{\partial x} + \tfrac{1}{2} \Psi_{mp} \quad \ldots\ldots \quad 2.4.\text{ix}$$

$$\text{where } \Psi_p = \int_{-h_p/2}^{+h_p/2} E_p \eta_{ep} \Psi(\epsilon_p) \, b \, dz_p \quad \ldots\ldots\ldots\ldots \quad 2.4.\text{x}$$

$$\text{and } \Psi_{mp} = 2 \int_{-h_p/2}^{+h_p/2} E_p \eta_{ep} \Psi(\epsilon_p) \left\{ z_p + d_p \right\} b \, dz_p \quad \ldots\ldots\ldots \quad 2.4.\text{xi}$$

Similarly, for any elastic layer q,

$$F_q = \int_{A_q} \sigma_q \, dA_q = E_q A_q d_q \frac{\partial^2 y}{\partial x^2} - E_q A_q \frac{h_1}{2} \frac{\partial \phi_1}{\partial x} + E_q A_q \sum_{\alpha=1}^{k} h_s \frac{\partial \phi_s}{\partial x} \quad \ldots 2.4.\text{xii}$$

$$\text{and } M_q = \int_{A_q} (z_q + d_q) \sigma_q \, dA_q$$

$$= E_q I_{Nq} \frac{\partial^2 y}{\partial x^2} - E_q A_q d_q \frac{h_1}{2} \frac{\partial \phi_1}{\partial x} + E_q A_q d_q \sum_{\alpha=1}^{k} h_s \frac{\partial \phi_s}{\partial x} \quad \ldots 2.4.\text{xiii}$$

The total bending moment M at any cross-section is given by $M = M_1 + 2 \sum_{j=2}^{2i} M_j \qquad j = 2,3,4, \ldots$.

$M_1 = E_1 I_{N1} \frac{\partial^2 Y}{\partial x^2} + E_1 I_{N1} \frac{\partial \phi_1}{\partial x} + \frac{1}{2} \Psi_{m1}$, from equation 2.4.ix by putting p=1, and remembering that $d_1 = 0$.

Hence, $M = E_1 I_{N1} \frac{\partial^2 Y}{\partial x^2} + E_1 I_{N1} \frac{\partial \phi_1}{\partial x} + \frac{1}{2} \Psi_{m1} + 2 \sum_{j=2}^{2i} M_j$ ...2.4.xiv.

The expressions for the bending moments, M_j, can be substituted in equation 2.4.xiv to obtain an expression of the form,

$M = EI \frac{\partial^2 Y}{\partial x^2} + \sum_{k=1}^{i} N_p^i \frac{\partial \phi_p}{\partial x} + \frac{1}{2} \Psi_{m1} + \sum_{k=2}^{i} \Psi_{mp}$ 2.4.xv,

where,

$N_1^i = E_1 I_{N1} + h_1 \sum_{j=2}^{2i} E_j A_j d_j$ 2.4.xvi;

$N_p^i = 2E_p A_p h_p^2/12 - 2E_p A_p d_p h_p/2 + 2h_p \sum_{j=P}^{2i} E_j A_j d_j$; $p \neq 1$ 2.4.xvii,

and as before, $EI = E_1 I_{N1} + 2 \sum_{j=2}^{2i} E_j I_{Nj}$ .....2.4.xviii.

It is noted that $j = 2,3,4,....2i$; and

$p = 2k - 1$, $k = 1,2,....i$.

The differential equation of motion for the beam is now given by

$\frac{\partial^2}{\partial x^2} \left\{ EI \frac{\partial^2 Y}{\partial x^2} + \sum_{k=1}^{i} N_p^i \frac{\partial \phi_p}{\partial x} + \frac{1}{2} \Psi_{m1} + \sum_{k=2}^{i} \Psi_{mp} \right\} + m \frac{\partial^2 Y}{\partial t^2} = p(x,t)$ ....
....2.4.xix,

$m = \sum_i \rho_i A_i$ being the mass per unit length of the beam. This is the first of the (i+1) differential equations required.

The other differential equations are obtained, as before, by considering the equilibrium of the portion of the element above the central axis of any viscoelastic

layer. Consider, for instance, the p-th layer (fig. 2.9). Equilibrium of the longitudinal forces acting on the portion of the element above the axis p-p, gives the shear stress τ_p as

$$b\tau_p = \sum_{j=p+1}^{2i} \frac{\partial F_j}{\partial x} + \int_0^{h_p/2} \frac{\partial \sigma_p}{\partial x} \, b\, dz_p$$

$$\text{i.e. } b\tau_p = \frac{\partial}{\partial x}\left\{ \sum_{j=p+1}^{2i} F_j + \int_0^{h_p/2} \sigma_p \, b\, dz_p \right\} \quad \ldots\ldots\ldots 2.4.xx$$

Furthermore, τ_p and the shear strain ϕ_p are related by the equation $\tau_p = G_p\{\phi_p + \eta_{ep} \Psi(\phi_p)\}$ 2.4.xxi

The integral $\mathcal{J} = \int_0^{h_p/2} \sigma_p \, b\, dz_p$ is easily evaluated as

$$\mathcal{J} = (E_p A_p h_p/8 + E_p A_p d_p/2) \frac{\partial^2 y}{\partial x^2} - E_p A_p \frac{h_1}{4} \frac{\partial \phi_1}{\partial x}$$
$$+ E_p A_p \sum_{\alpha=1}^{k} \frac{1}{2} h_s \frac{\partial \phi_s}{\partial x} - \frac{1}{8} E_p A_p h_p \frac{\partial \phi_p}{\partial x} + \Psi_{FP}, \text{ where}$$

$$\Psi_{FP} = \int_0^{h_p/2} E_p \eta_{ep} \Psi(\epsilon_p) \, b\, dz_p \quad \ldots\ldots\ldots 2.4.xxii.$$

On substituting for $\mathcal{J}$ and performing the summation, equation 2.4.xx takes the form

$$b\tau_p = \frac{\partial}{\partial x}\left\{ P_p^i \frac{\partial^2 y}{\partial x^2} + \sum_{\alpha=1}^{i} Q_{ps}^i \frac{\partial \phi_s}{\partial x} + \sum_{\alpha=k+1}^{i} \Psi_s + \Psi_{FP} \right\} \ldots.2.4.xxiii$$

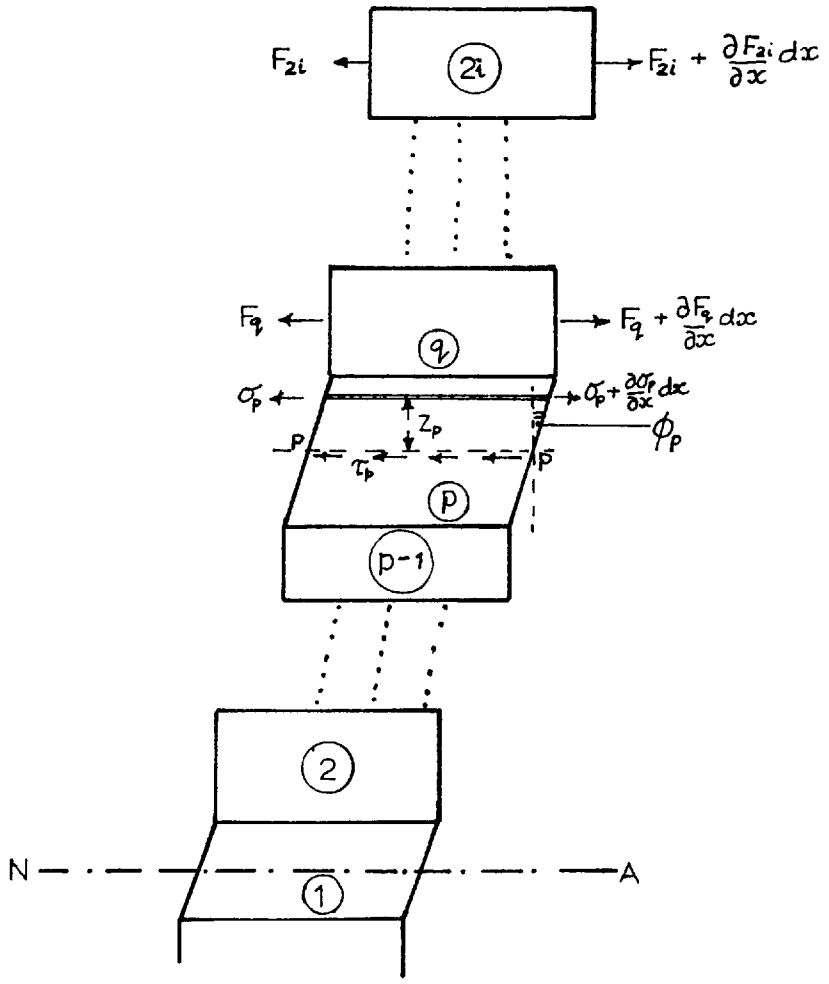

FIG. 2.9 Symmetrical n-layer Beam.
($n = 4i-1$)
Shear deformation in upper half of element.

where $P_p^i = \frac{1}{8} E_p A_p h_p + \frac{1}{2} E_p A_p d_p + \sum_{j=P+1}^{2i} E_j A_j d_j$ 2.4.xxiv

$$\left.\begin{aligned} Q_{p1}^i &= \frac{h_1}{2} \sum_{j=P+1}^{2i} E_j A_j + E_p A_p \frac{h_1}{4}, \text{ for all } p>1 \\ Q_{11}^i &= \frac{h_1}{2} \sum_{j=2}^{2i} E_j A_j + E_1 A_1 \frac{h_1}{8}, \text{ for } p = s = 1 \end{aligned}\right\} \text{....2.4.xxv}$$

$$\left.\begin{aligned} Q_{ps}^i &= h_s \sum_{j=P+1}^{2i} E_j A_j + \frac{1}{2} E_p A_p h_s \quad , \text{ for } s<p \\ &= h_s \sum_{j=S+1}^{2i} E_j A_j + \frac{1}{2} E_s A_s h_s \quad , \text{ for } s>p \\ \text{and } Q_{pp}^i &= h_p \sum_{j=P+1}^{2i} E_j A_j + \frac{3}{8} E_p A_p h_p \quad , \text{ for } s=p \end{aligned}\right\} \text{for } s>1 \text{ .. ..2.4.xxvi}$$

Equation 2.4.xxi can now be combined with equation 2.4.xxiii to obtain

$$\frac{\partial}{\partial x}\left\{P_p^i \frac{\partial^2 y}{\partial x^2} + \sum_{\alpha=1}^{i} Q_{ps}^i \frac{\partial \phi_s}{\partial x} + \sum_{\alpha=K+1}^{i} \amalg_s + \amalg_{FP}\right\} - \eta_{Gp} b G_p \amalg(\phi_p)$$

$$= b G_p \phi_p \quad .....2.4.xxvii.$$

In the summations in equations 2.4.xxiii and 2.4.xxvii, it is important to remember that $p = 2k - 1$, $k = 1,2,..i$; and $s = 2\alpha - 1$, $\alpha = 1,2, \ldots$.

It can thus be seen that as k assumes values from 1 to i , equation 2.4.xxvii gives the remaining i differential equations. Equations 2.4.xix and 2.4.xxvii ,therefore, provide the (i+1) differential equations required for a symmetrical (4i - 1)-layer beam.

As an illustration of how these equations can be applied, consider the 'prototype' for this group of beams, namely, the case i = 1 or the 3-layer beam. The number of differential equations is 1 + 1 = 2. On setting

i = 1, equation 2.4.xix gives

$$\frac{\partial^2}{\partial x^2}\left[EI\,\frac{\partial^2 y}{\partial x^2} + N_1'\,\frac{\partial \phi_1}{\partial x} + \frac{1}{2}\,\Psi_{m1}\right] + m\frac{\partial^2 y}{\partial t^2} = p(x,t) \quad \ldots 2.4.xxviii$$

where $N_1' = \frac{1}{12}E_1A_1h_1^2 + E_2A_2d_2h_1$, from equation 2.4.xxvi.

Also equation 2.4.xxvii yields the single equation

$$\frac{\partial}{\partial x}\left\{P_1'\frac{\partial^2 y}{\partial x^2} + Q_{11}'\frac{\partial \phi_1}{\partial x} + \Psi_{F1}\right\} - \eta_{G1}bG_1\Psi(\phi_1) = bG_1\phi_1 \quad \ldots 2.4.xxix$$

where $P_1' = E_1A_1\frac{h_1}{8} + E_2A_2d_2$, from equation 2.4.xxiv; and

$$Q_{11}' = E_1A_1h_1/8 + E_2A_2h_1/2 \text{ , from equation 2.4.xxv.}$$

The above equations are seen to be exactly the same as equations 2.2.xxv and 2.2.xxx obtained earlier for the 3-layer beam from first principles.

2.4.b Symmetrical n-layer beam with an even number of viscoelastic layers

For the case when the beam has an even number of viscoelastic layers, the central layer 1 is elastic. Also, for

p = 2k - 1 , k = 1, 2,...(i+1);

q = 2k , k = 1,2,...i ; and n = 4i + 1, the q-th layer is viscoelastic whilst the p-th layer is elastic.

With reference to fig 2.10, the strain distributions in the viscoelastic and elastic layers can be summed up, as in the previous case, to obtain for layer q,

$$\epsilon_q = (z_q + d_q)\frac{\partial^2 y}{\partial x^2} + \sum_{\alpha=1}^{k-1} h_{2\alpha}\frac{\partial \phi_{2\alpha}}{\partial x} + (z_q + \frac{1}{2}h_q)\frac{\partial \phi_q}{\partial x} \quad \ldots 2.4.xxx$$

and for layer p, $\epsilon_p = (z_p + d_p)\frac{\partial^2 y}{\partial x^2} + \sum_{\alpha=1}^{k-1} h_{2\alpha}\frac{\partial \phi_{2\alpha}}{\partial x}$ ..2.4.xxxi

where the summation $\sum_{\alpha=u}^{v} h_{2\alpha}\frac{\partial \phi_{2\alpha}}{\partial x} = 0$ for v<u.

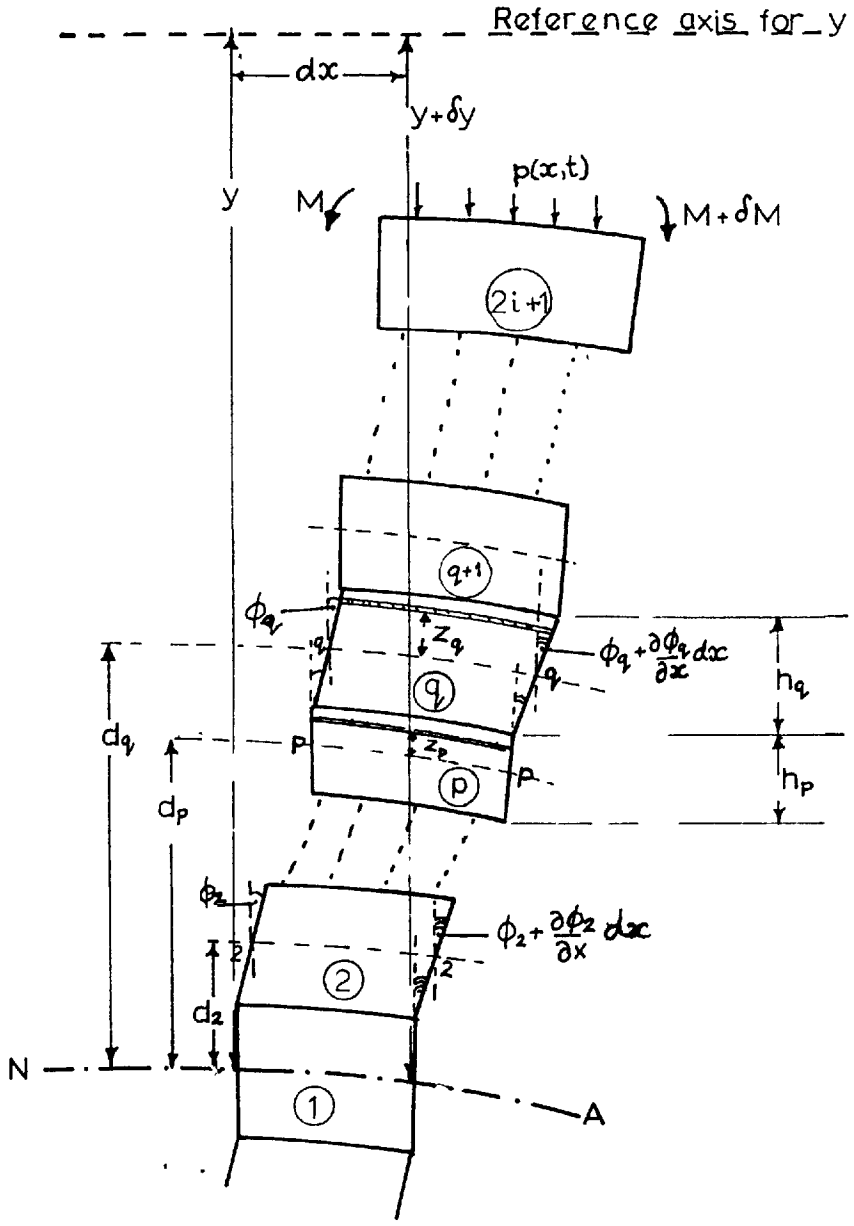

FIG. 2.10 Symmetrical n-layer Beam
$(n = 4i+1)$
Upper half of deformed element.

The fibre stresses are given by

$$\sigma_q = E_q\left\{(z_q + d_q)\frac{\partial^2 Y}{\partial x^2} + \sum_{\alpha=1}^{k-1} h_{2\alpha}\frac{\partial \phi_{2\alpha}}{\partial x} + (z_q + \tfrac{1}{2}h_q)\frac{\partial \phi_q}{\partial x} + \eta_{eq}\Psi(\epsilon_q)\right\} \quad \text{2.4.xxxii, and}$$

$$\sigma_p = E_p\left\{(z_p + d_p)\frac{\partial^2 Y}{\partial x^2} + \sum_{\alpha=1}^{k-1} h_{2\alpha}\frac{\partial \phi_{2\alpha}}{\partial x}\right\} \quad \text{....2.4.xxxiii}$$

The forces and moments in the viscoelastic layers are thus

$$F_q = \int_{A_q} \sigma_q \, dA_q$$

$$= E_q A_q d_q \frac{\partial^2 Y}{\partial x^2} + E_q A_q \sum_{\alpha=1}^{k-1} h_{2\alpha}\frac{\partial \phi_{2\alpha}}{\partial x} + \frac{1}{2} E_q A_q h_q \frac{\partial \phi_q}{\partial x} + \Psi_q \quad \text{..2.4.xxxiv}$$

and

$$M_q = \int_{A_q} (z_q + d_q)\sigma_q \, dA_q$$

$$= E_q I_{Nq}\frac{\partial^2 Y}{\partial x^2} + E_q A_q d_q \sum_{\alpha=1}^{k-1} h_{2\alpha}\frac{\partial \phi_{2\alpha}}{\partial x} + \left(\frac{1}{12}E_q A_q h_q^2 + E_q A_q d_q h_q/2\right)\frac{\partial \phi_q}{\partial x} + \frac{1}{2}\Psi_{mq} \quad \text{..... 2.4.xxxv}$$

where Ψ_q and Ψ_{mq} are as already defined in equations 2.4.x, and 2.4.xi respectively. For the elastic layers, the forces and bending moments are given by

$$F_p = \int_{A_p} \sigma_p \, dA_p = E_p A_p d_p \frac{\partial^2 Y}{\partial x^2} + E_p A_p \sum_{\alpha=1}^{k-1} h_{2\alpha}\frac{\partial \phi_{2\alpha}}{\partial x} \quad \text{....2.4.xxxvi}$$

and $$M_p = \int_{A_p} (z_p + d_p)\sigma_p \, dA_p$$

i.e. $M_p = E_p I_{Np} \frac{\partial^2 y}{\partial x^2} + E_p A_p d_p \sum_{\alpha=1}^{k-1} h_{z\alpha} \frac{\partial \phi_{z\alpha}}{\partial x}$ 2.4.xxxvii

The total bending moment at any cross-section is

$M = M_1 + 2 \sum_{j=2}^{2i+1} M_j$.

$M_1 = E_1 I_{N1} \frac{\partial^2 y}{\partial x^2}$ from equation 2.4.xxxvii, on putting $p = 1$, and noting that $d_1 = 0$.

Hence $M = E_1 I_{N1} \frac{\partial^2 y}{\partial x^2} + 2 \sum_{j=2}^{2i+1} M_j$ 2.4.xxxviii

On substituting for M_j and performing the summation, equation 2.4.xxxviii can be written in the form

$M = EI \frac{\partial^2 y}{\partial x^2} + \sum_{k=1}^{i} N_q^i \frac{\partial \phi_q}{\partial x} + \sum_{K=1}^{i} \mu_{mq}$ 2.4.xxxix

where $N_q^i = 2\left\{E_q A_q h_q^2/12 + E_q A_q d_q h_q/2 + h_q \sum_{j=q+1}^{2i+1} E_j A_j d_j\right\}$ .2.4.xL

and as previously, $EI = E_1 I_{N1} + 2 \sum_{j=2}^{2i+1} E_j I_{Nj}$,

The differential equation of motion is thus

$$\frac{\partial^2}{\partial x^2}\left\{EI\frac{\partial^2 y}{\partial x^2} + \sum_{k=1}^{i} N_q^i \frac{\partial \phi_q}{\partial x} + \sum_{k=1}^{i} \mu_{mq}\right\} + m\frac{\partial^2 y}{\partial t^2} = p(x,t) \quad ..2.4.xLi$$

Once again the remaining i equations are obtained by considering the shear deformation in the viscoelastic layers (fig.2.11).

Consider the equilibrium of the portion of the element dx above the central axis q-q of layer q. The shear stress τ_q at this axis is again given by

$$b\tau_q = \sum_{j=q+1}^{2i+1} \frac{\partial F_j}{\partial x} + \int_0^{h_q/2} \frac{\partial \sigma_q}{\partial x}\, b\, dz_q$$

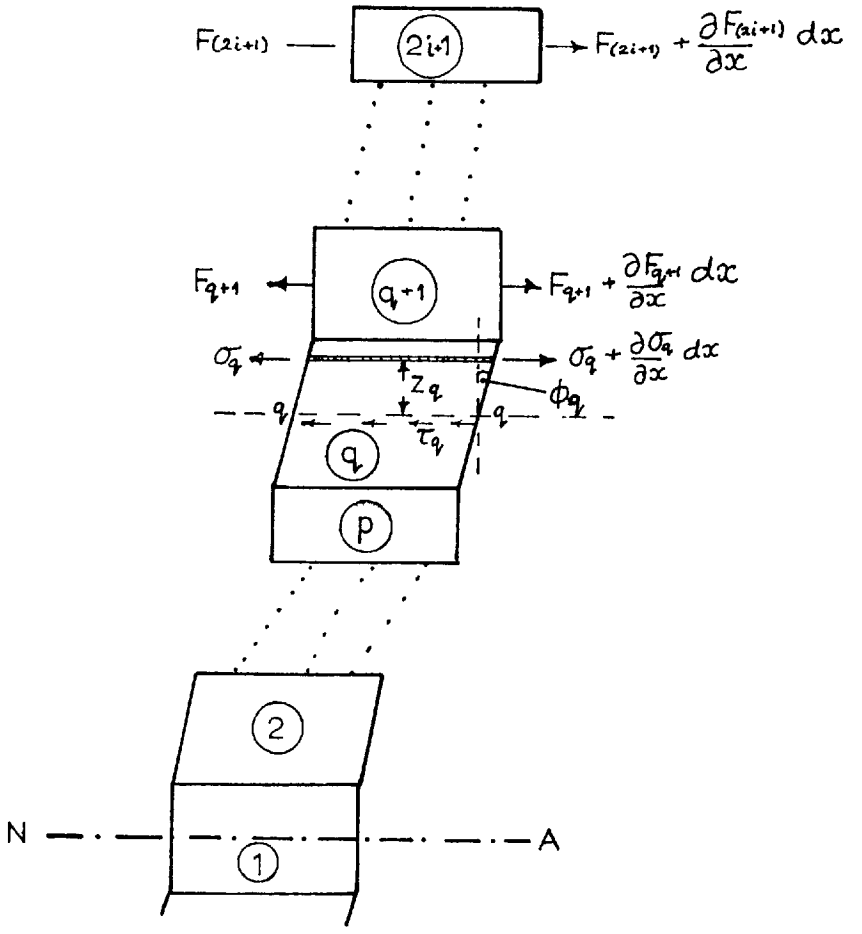

FIG. 2.11 Symmetrical n-layer Beam. ($n = 4i+1$)
Shear deformation in upper half of element.

$$\text{or } b\tau_q = \frac{\partial}{\partial x}\left\{ \sum_{j=q+1}^{2i+1} F_j + \int_0^{h_q/2} \sigma_q \, b\, dz_q \right\} \quad \ldots\ldots \text{2.4.xLii.}$$

The integral $\mathcal{J} = \int_0^{h_q/2} \sigma_q \, b\, dz_q$ is easily evaluated to be

$$\mathcal{J} = \left(\frac{1}{8} E_q A_q h_q + \frac{1}{2} E_q A_q d_q\right) \frac{\partial^2 y}{\partial x^2} + \frac{1}{2} E_q A_q \sum h_{2\alpha} \frac{\partial \phi_{2\alpha}}{\partial x}$$
$$+ \frac{3}{8} E_q A_q h_q \frac{\partial \phi_q}{\partial x} + \Psi_{Fq} \quad \ldots\ldots \text{2.4.xLiii, where}$$

Ψ_{Fq} is as defined in equation 2.4.xxii.

Equation 2.4.xLii can then be expressed in the form

$$b\tau_q = \frac{\partial}{\partial x}\left\{ P_q^i \frac{\partial^2 y}{\partial x^2} + \sum_{\alpha=1}^{i} Q_{q\ell}^i \frac{\partial \phi_\ell}{\partial x} + \sum_{j=k+1}^{i} \Psi_{2j} + \Psi_{Fq} \right\} \ldots\ldots \text{2.4.xLiv}$$

where $\ell = 2\alpha$, and

$$P_q^i = \frac{1}{8} E_q A_q h_q + \frac{1}{2} E_q A_q d_q + \sum_{j=q+1}^{2i+1} E_j A_j d_j \quad \ldots\ldots \text{2.4.xLv}$$

$$\left.\begin{aligned} Q_{q\ell}^i &= h_\ell \sum_{j=\ell+1}^{2i+1} E_j A_j + E_\ell A_\ell \frac{h_\ell}{2} \quad \text{, for } \ell > q \\ &= h_\ell \sum_{j=q+1}^{2i+1} E_j A_j + \frac{1}{2} E_q A_q h_\ell \text{ , for } \ell < q \\ Q_{qq}^i &= h_q \sum_{j=q+1}^{2i+1} E_j A_j + \frac{3}{8} E_q A_q h_q \text{ , for } \ell = q \end{aligned}\right\} \ldots\ldots \text{2.4.xLvi}$$

But τ_q is related to ϕ_q by the viscoelastic stress - strain law thus $\tau_q = G_q\left\{\phi_q + \eta_{Gq} \Psi(\phi_q)\right\}$ $\ldots\ldots$ 2.4.xLvii

Equations 2.4.xLvii and 2.4.xLiv can be combined to give

$$\frac{\partial}{\partial x}\left\{ P_q^i \frac{\partial^2 y}{\partial x^2} + \sum_{\alpha=1}^{i} Q_{q\ell}^i \frac{\partial \phi_\ell}{\partial x} + \sum_{j=k+1}^{i} \Psi_{2j} + \Psi_{Fq} \right\} - b\,\eta_{Gq} G_q \Psi(\phi_q) = b G_q \phi_q \ldots$$
$$\ldots 2.4.\text{xLviii}$$

Noting that $q = 2k$; $k = 1,2,\ldots i$; it is seen that as k varies from 1 to i, equation 2.4.xLviii yields i equations, which together with equation 2.4.xLi, provide the (i+1) equations for the beam.

The case, i = 1, is the five-layer beam - the prototype for this group of beams. It is easily verified that putting i = 1 in equations 2.4.xLi and 2.4.xLviii gives the two equations already obtained earlier for the 5-layer beam.

Comparison of equations 2.4.xLi and 2.4.xLviii with equations 2.4.xix and 2.4.xxvii shows that although each set has the same number of differential equations, no set of equations is derivable from the other by any simple process of rearrangement or interchange of the constants. This is because the strain distributions in the various layers are different in each case.

2.5. Concluding remarks

The differential equations for the general symmetrical n-layer beam have been obtained. To be able to solve these equations some further information is necessary. First, the system must be sufficiently specified. Apart from its 'geometry', the boundary conditions for the beam must be known. Secondly, the method of excitation has to be prescribed. Thirdly, the coefficients of the differential equations must be known. These coefficients are partly

known when the geometry of the system is given. However, they also contain material constants of the beam, and these must be known. For the elastic layers, the material constants that come into the equations are the Young's modulus and the density. These are known to be real physical constants and are easily obtained from existing data or by simple measurements. The properties of the viscoelastic materials, however, are not "constants", as they are known to depend on several factors (such as frequency, temperature and strain) some of which appear in the differential equations. It is thus necessary to understand the nature of these properties, the various factors on which they depend, and the nature of the dependence, before attempting to solve the above equations. Fourthly, the Ψ-functions must be known explicitly. This requires knowing the stress - strain law for the viscoelastic materials.

The first two requirements will be given in chapter 4. Meanwhile, in the next chapter, the properties of viscoelastic materials and their determination will be dealt with.

C H A P T E R 3

DETERMINATION OF THE DYNAMIC PROPERTIES OF VISCOELASTIC MATERIALS

Introduction

In this chapter a study of the dynamic properties of viscoelastic materials subjected to harmonic excitation is carried out. This is chiefly aimed at understanding the nature of these properties and the manner in which they are affected by various factors.

The properties of viscoelastic materials are first defined, and their dependence on the frequency, temperature and strain amplitude are discussed. A simple laboratory method for determining the shear properties is then described. Experimental results obtained for some viscoelastic materials using this test apparatus are presented and discussed. The study of these results helps in selecting materials to be used in the beam tests in chapter 5, and also yields conclusions useful in the solution of the differential equations obtained in chapter 2.

3.1 Dynamic properties - definitions.

An important characteristic of viscoelastic materials is the fact that when they are subjected to a rapidly varying stress (direct or shear), the resulting strain does not occur instantaneously (as would be the case for

perfectly elastic materials). In particular, if the applied stress is sinusoidal and of frequency, ω, observations show that the resulting strain is virtually sinusoidal and of the same frequency, but lags behind the stress by an angle, δ. For any given frequency, the stress - strain curve over one cycle is essentially an ellipse. This characteristic is utilised in the quantitative definition of the dynamic behaviour of viscoelastic materials.

Suppose, for example, that a viscoelastic material is subjected to a sinusoidal shear strain given by $\phi = \hat{\phi} \sin \omega t$ .....3.1.i. Then the corresponding shear stress takes the form, $\tau = \hat{\tau} \sin(\omega t + \delta)$ .....3.1.ii, δ being the angle by which the strain lags behind the stress. Equation 3.1.ii can be put in the form,

$\tau = \hat{\tau} \cos\delta \sin \omega t + \hat{\tau} \sin\delta \cos \omega t$,

i.e. $\tau = \hat{\tau} \cos\delta \sin \omega t + \hat{\tau} \sin\delta \sin(\omega t + \frac{\pi}{2})$ ....3.1.iii.

Equation 3.1.iii shows that the stress can be split into two parts: $\hat{\tau} \cos\delta$ (the 'elastic part') in phase with the applied strain; and $\hat{\tau} \sin\delta$ (the 'viscous part') leading the strain by $\frac{\pi}{2}$. The "elastic" or "in-phase" dynamic shear modulus is defined as $G' = \frac{\hat{\tau} \cos\delta}{\hat{\phi}}$ ....3.1.iv, and the "viscous" or "loss" dynamic shear modulus as

$G'' = \frac{\hat{\tau} \sin\delta}{\hat{\phi}}$ .....3.1.v.

The effective shear modulus* is given by

$G = \frac{\hat{\tau}}{\hat{\phi}} = \left[G'^2 + G''^2\right]^{\frac{1}{2}}$ .....3.1.vi, and the ratio

$\eta_G = \frac{G''}{G'} = \tan\delta$ is called the loss factor, δ itself being often referred to as the loss angle.

The equation of the elliptic stress - strain curve is obtained by eliminating the time variable from equations 3.1.i and 3.1.ii, i.e.

$$\tau = G'\left\{\phi \pm \eta_G(\hat{\phi}^2 - \phi^2)^{\frac{1}{2}}\right\} \quad \text{.....3.1.vii}$$

Fig 3.1 shows a typical stress - strain curve, and how the dynamic properties defined above can be obtained from the ellipse. For example,

G, the effective modulus = $\frac{OE}{OC} = \frac{AA'}{BB'}$;
G', the in-phase shear modulus = $\frac{CD}{OC}$
and G'', the loss shear modulus = $\frac{OA}{OC}$. } ...3.1.viii.

The area of the ellipse gives the energy loss per unit volume of the material during one cycle. This is given numerically by the relation,

Cyclic energy loss per unit volume, $\Delta E_D = \pi G'' \hat{\phi}^2$ .3.1.ix.a

which incidentally explains why G'' is termed the 'loss' modulus.

The shear strain energy per unit volume, ΔE_S, is a

*The qualifying term, "dynamic", is purposely left out from this point onwards as there is no risk of confusion.

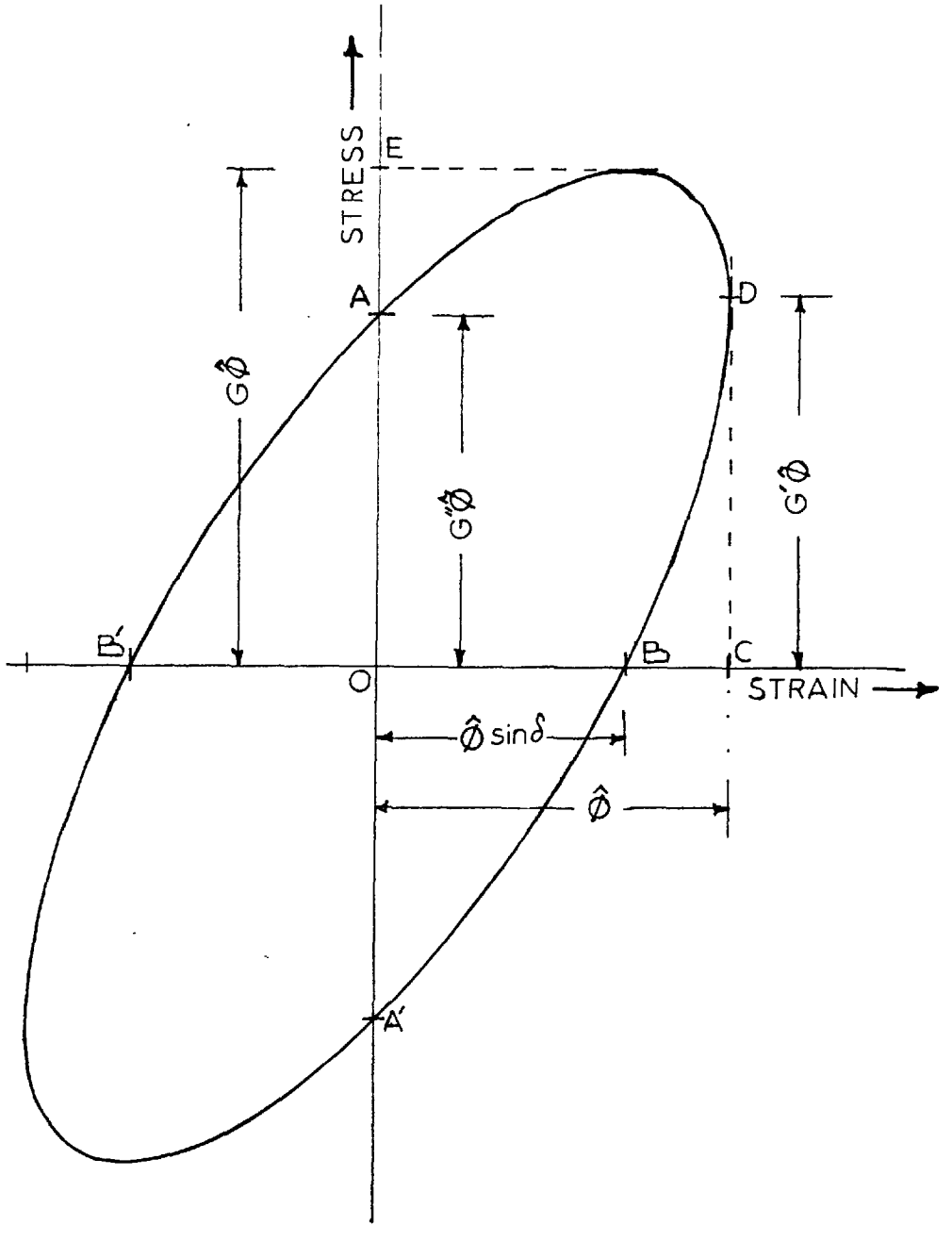

FIG. 3.1 Stress-strain loop for a viscoelastic Material.

half of the product of the applied strain and the in-phase component of the stress. Thus,

$\Delta E_s = \frac{1}{2} G' \phi^2$ .....3.1.ix.b. The maximum shear strain energy per unit volume in one cycle is thus

$(\Delta E_s)_{max} = \frac{1}{2} G' \hat{\phi}^2$ ....3.1.ix.c. From equations 3.1.ix.a and c, it is seen that the shear loss factor, η_G, can be defined as an energy ratio thus

$$\eta_G = \frac{1}{2\pi} \left\{ \frac{\text{shear energy loss in one cycle}}{\text{maximum shear strain energy in a cycle}} \right\} \quad ..3.1.ix.d$$

A mathematical concept, often very convenient in analysis, is that of "complex modulus". If the time axis is replaced by a complex plane so that the applied strain becomes $\phi = \hat{\phi} e^{j\omega t}$; then the corresponding shear strain stress is given by $\tau = \hat{\tau} e^{j(\omega t + \delta)}$ where, $j = \sqrt{-1}$. The shear modulus is now defined as

$$G^* = \frac{\tau}{\phi} = \frac{\hat{\tau} e^{j\delta}}{\hat{\phi}} = \frac{\hat{\tau} \cos\delta}{\hat{\phi}} + j \frac{\hat{\tau} \sin\delta}{\hat{\phi}}$$

or $G^* = G' + jG''$ .....3.1.x. The shear modulus thus defined is seen to be complex, the real part being the elastic modulus, whilst the imaginary part is the loss modulus. A term often used in the literature is the complex shear compliance, J^*, defined as

$J^* = \frac{1}{G^*}$ ..3.1.xi. The real part, J', of this quantity is called the "elastic", "storage" or "in-phase" shear compliance; whilst the imaginary part, J'', is termed the "viscous" or "loss" compliance. J' and J'' are related to

G' and G'' in the manner given below.

$$J' = \frac{G'}{(G'^2 + G''^2)} \quad \ldots\ldots\ldots 3.1.xii$$

$$J'' = \frac{G''}{(G'^2 + G''^2)} \quad \ldots\ldots\ldots 3.1.xiii.$$

The above definitions have been based on shear deformation. Similar terms also exist for direct deformation; viz., an elastic Young's modulus, E'; a loss Young's modulus, E''; an effective Young's modulus, $E = \left[E'^2 + E''^2\right]^{1/2}$; and a complex Young's modulus, $E^* = E' + jE''$. A corresponding complex compliance is also similarly defined.

It may be pointed out that although several quantities have been defined above for a given material, these are not all independent. Any two of them, in fact, are sufficient for specifying the dynamic behaviour of a material (in either shear or direct deformation), the rest being derivable from these two. In the preliminary discussion to follow, the effective modulus and the loss angle (sometimes referred to as the damping) will be regarded as the two fundamental properties of the material. When thought more convenient, however, any other two of the quantities defined above may be used to characterise the dynamic behaviour.

3.2 Factors affecting the dynamic properties.

The dynamic properties defined in section 3.1 depend on several factors such as, stress history, general mean state of stress or strain, humidity, amplitude of applied strain (or stress), frequency of the applied strain, and temperature [96]. Of these factors, the last three are the most significant [93], and will thus be dealt with in some detail here.

3.2.a Temperature and frequency effects

Temperature and frequency effects will be considered together, since they are intimately related.

Fig 3.2 shows the general shape of graphs of the effective modulus (curve 1), the in-phase modulus (curve 2), the loss modulus (curve 3), and the loss factor (curve 4), against temperature (at constant frequency), or against frequency (at constant temperature).

Consider first the graphs against temperature at a given frequency. Both the effective modulus and the in-phase modulus decrease with increase in temperature, the rate of change of the modulus with temperature being small at very low temperatures (in the "glassy" region) and at sufficiently high temperatures (in the "rubbery" region). In between (in the "glass-transition" region), both moduli fall very rapidly with temperature rise. The loss modulus has a similar trend except that it rises sooner

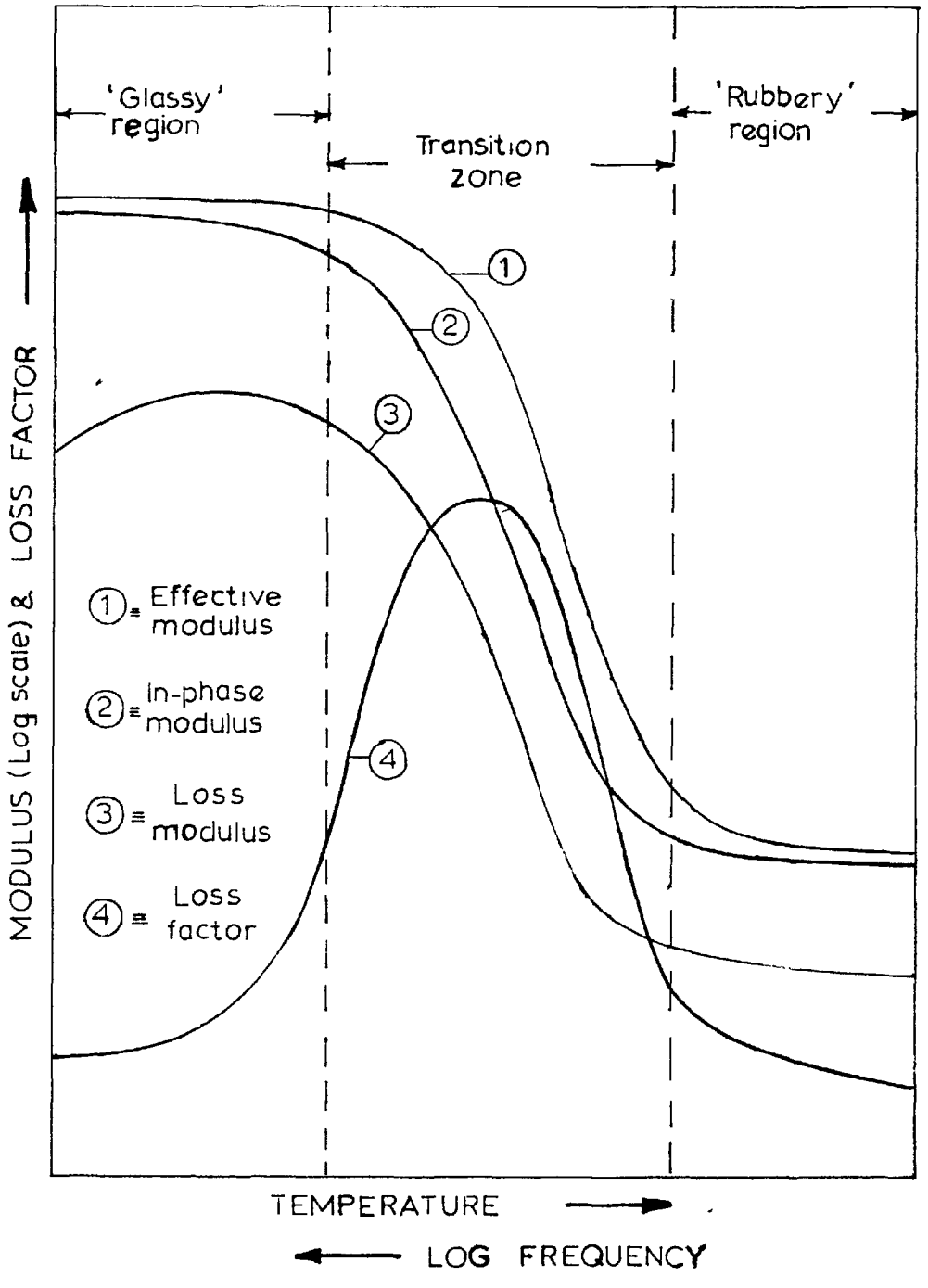

FIG. 3.2 *Variation of Dynamic Properties with Frequency and Temperature for a Viscoelastic Material.*

with decrease in temperature, and falls again at lower temperatures. The loss factor is low at both high and low temperatures, and shows a maximum within the transition region.

If these quantities are plotted against frequency at a given temperature, a similar set of curves is obtained provided that the frequency is plotted backwards (i.e. from right to left) on a log scale, as indicated in fig 3.2. This suggests that there may be some relationship between temperature effects and frequency effects; to be more specific, "temperature differences" may well be related to "frequency ratios". The equivalence between these two quantities will be dealt with later.

3.2.b. Molecular structure and temperature/frequency dependence

The dependence of the dynamic properties of viscoelastic materials on frequency and temperature is very closely tied up with the molecular structure of these materials. A detailed treatment of this does not fall within the scope of this work. (See references 90, 93, 94, 95, 96, 101). It may, however, be mentioned that this field of study has been so developed that, not only is it possible to predict, sometimes quantitatively, the behaviour of these materials under various conditions, but

also it is now possible to literally 'tailor' viscoelastic materials to specification within incredibly close limits [97].

Simply put, the viscoelastic molecular structure is characterised by long flexible chain molecules which are held together here and there by a few cross-links, and which are otherwise free to move readily past one another. Inter-molecular attractions are very small. In the unstrained condition, the atoms in the long chain molecules are subject to random thermal vibrations in all directions, and this results in the molecules taking up an irregular tortuous shape.

When the material is being strained by an externally applied force, the molecules are aligned in a more or less orderly manner in the direction of the strain. To achieve this orderly configuration requires work being done; and when the applied force is removed, the molecules tend to go back to the disorderly configuration. The material is thus said to resist being strained; that is, to be elastic. Owing to the irregular shape of the molecules, it is clear that their alignment in the direction of strain can not possibly occur instantaneously - it takes time. This is why, with a varying stress, the strain lags behind by a time which represents the average time taken by the molecules to respond to the external force.

Consider now what happens when a viscoelastic material is subjected to a sinusoidal stress of a given frequency, and the temperature is being varied. At very low temperatures, intra-molecular motion is almost non-existent; and the entire molecular structure is effectively "frozen-in". Deformation now involves the straining of inter-atomic bonds, similar to that which occurs in perfectly elastic solids. This requires very large forces, and moreover occurs almost instantaneously, so that the effective modulus is high and there is very little damping (small loss factor). At sufficiently high temperatures (i.e. within the 'rubbery' region), almost all the molecules can follow up the applied stress very readily; consequently, the resistance to deformation is small. The damping is also small since the mobile molecules take very little time to respond to the applied stress.

Within the transition zone (i.e. at intermediate temperatures), however, some of the molecules are free to move whilst others are not. Now, under a given deformation, the frozen-in molecules can store much more energy than the moblie ones. The resistance to deformation, or the effective modulus, is thus seen to be intermediate in value between the effective modulus within the glassy region and the effective modulus within the rubbery region. The rate of change of the modulus with temperature within

this zone is high because as the temperature is varied, some of the molecules become either frozen-in or mobile, thus resulting in a change in the effective modulus. This is not the case in the glassy or rubbery region where almost all the molecules have attained the same configuration (either frozen-in or mobile), so that a change in temperature has very little effect on the state of the molecules, and hence, on the effective modulus.

While the effective modulus depends on the relative number of mobile and frozen-in molecules in the structure, the loss angle (or the damping), within the transition zone, depends on the <u>average</u> time taken by all the molecules (mobile and immobile) to respond to the applied stress. As the temperature is increased (starting from the glassy region), this average time increases; and maximum damping is achieved within the temperature interval where a great many of the frozen-in molecules become mobile in a time comparable to the periodic time of the applied stress. Beyond this temperature interval, the damping decreases since the molecules can now follow up the applied stress much better and quicker.

The dependence of the material properties on frequency can also be explained on the basis of the molecular structure. If the temperature is kept constant, then at very low frequencies of the applied

stress, the long chain molecules have ample time to respond to the applied stress. The force required to produce a given deformation is thus small, and so is the average time taken by the molecules to respond to the applied stress (as compared with the periodic time of the stress). Hence the effective modulus and the loss angle are both small. This is clearly similar to the behaviour at high temperatures (constant frequency) already discussed. At very high frequencies, the molecules do not get enough time to follow up the applied stress. They behave effectively as frozen-in molecules, and the situation is exactly similar to that at low temperatures, namely, low damping and very high modulus. At intermediate frequencies some of the molecules can follow up the motion while others cannot. This is comparable to the situation at intermediate temperatures, so that the effective modulus rises very rapidly with increase in frequency, whilst the loss angle or damping passes through a maximum.

3.2.c Temperature - frequency relationship; method of reduced variables

As already indicated above, there is a very close relationship between frequency effects and temperature effects for a given viscoelastic material. Fitzgerald and Ferry [99] , in 1953, established the nature of this relation, and developed a method whereby experimental values

of moduli (and dielectric constant) can be made to fall on a single curve covering a large frequency and temperature range. This method, generally known as the "method of reduced variables", can be found in any standard text on polymer properties (see, for example, [90, 94, 95, 101]).

It is, however, intended to briefly illustrate, by means of a simple example, the significance of the method, and in particular how it can be utilised in checking experimental results. Suppose that there are available, sets of values of a modulus (the elastic shear modulus G', for example) for a limited range of frequency, each set being obtained at a constant temperature. Let the temperatures - expressed on the absolute scale - be T_o, T_1, etc. One of the temperatures, T_o, say, is chosen as the "reference temperature" and the experimental values are "reduced" to values corresponding to this reference temperature using the approximate relation*

$G'_r = G' \frac{T_o \rho_o}{T \rho}$ ..... 3.2.i, where G' is the elastic shear modulus at temperature T; ρ_o and ρ are the densities of the material at temperatures T_o and T respectively; and G'_r is the reduced elastic shear modulus with respect to T_o. The reduced variables are now plotted against frequency,

*This relation would be exact if the effective shear modulus was infinite in the glassy region (see [94]).

resulting in a series of constant temperature plots similar to those shown in fig. 3.3.

Any line of constant modulus will cut the T_o-curve and any other T-curve at frequencies f_o and f respectively,

where $\log(\frac{f}{f_o}) = \frac{-K_1(T - T_o)}{K_2 + (T - T_o)}$ ..... 3.2.ii.

K_1 and K_2 are constants for any given material, and for a given reference temperature. By defining a characteristic temperature, T_s, for each material, Williams, Landel, and Ferry [102] were able to obtain a "master curve" applicable to all materials, in the form

$\log(\frac{f}{f_s}) = \frac{-8.86(T-T_s)}{101.6 + (T-T_s)}$ ..... 3.2.iii.

Equation 3.2.ii shows that, for any two temperatures T_o and T, any line of constant modulus cuts the curves at points having the same frequency ratio. Put in another way, if a plot is made of modulus against log. frequency for various temperatures then each T-curve will run parallel to the T_o-curve in the sense that the intercept made on <u>any</u> line of constant modulus, by the T_o-curve and any other T-curve, has a constant length (see fig. 3.3). This thus provides a very useful way of checking the shapes of experimental curves obtained from tests. It can also be employed in extending experimental curves to frequency ranges which could not be covered experimentally.

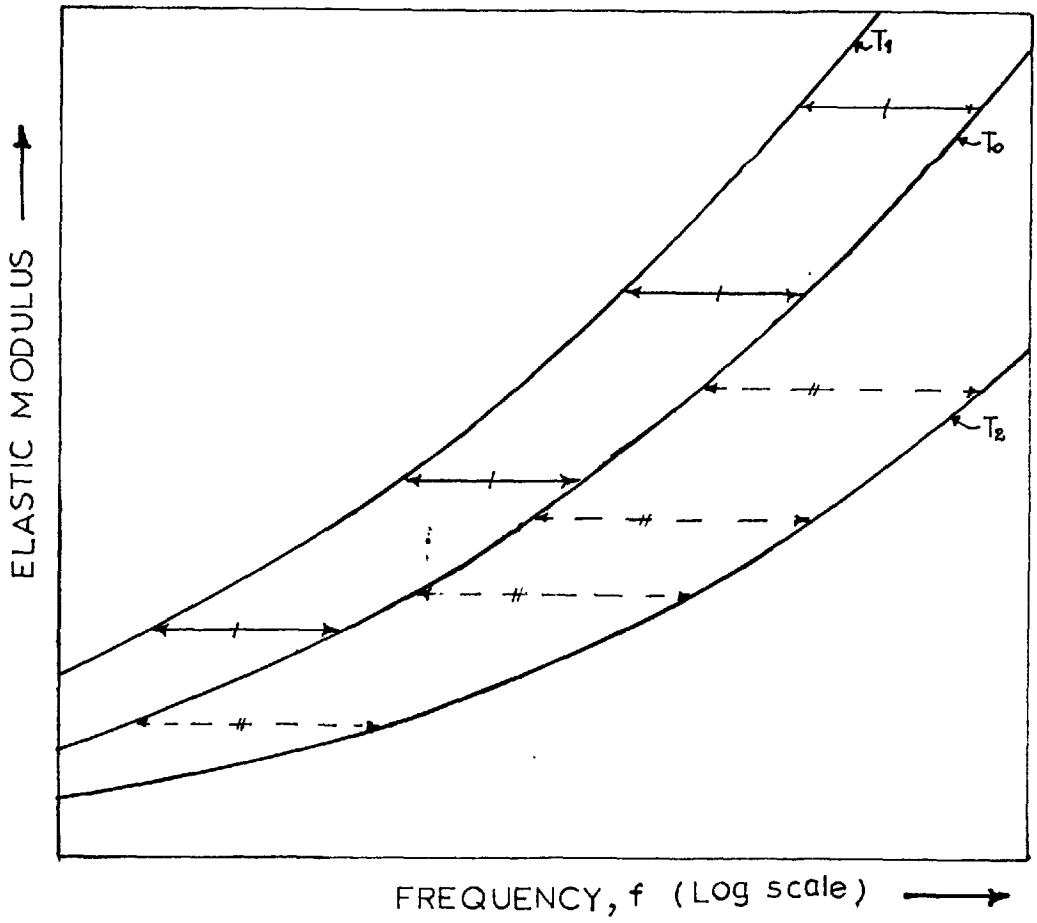

FIG. 3.3 Graphs of Modulus vs Log Frequency for a Typical Viscoelastic Material

It may be necessary to add a word of caution about the use of the above method. Although considerable theoretical evidence is available to back it, the method of reduced variables is essentially an empirical formulation which will hold for most viscoelastic materials subject to some conditions being satisfied. For example, the material must exhibit no structural change with temperature. Furthermore, the method, as it is, will not hold good close to the glassy region; nor is it applicable to highly crystalline polymers. There are also other requirements which involve molecular movements; and it is by no means easy to predetermine these for any given material. Before applying the method in the extension of available data, therefore, it will be wise to first check that these data, by themselves, obey the above temperature - frequency superposition principle. A full treatment of the limitations of the method of reduced variables can be found in [95].

3.2.d Strain amplitude effects

Apart from the dependence of their dynamic properties on frequency and temperature, many viscoelastic materials also show an unusual type of non-linearity. The modulus and the loss factor depend on the amplitude of the applied strain, although at any one amplitude (under conditions of shear) the response to a sinusoidal driving force

is essentially sinusoidal without any detectable evidence of harmonic content such as would be expected if non-linearity was present. The stress - strain curve, at any given amplitude, does not show any appreciable departure from an elliptic shape (see [99], and also the section on results). As soon as the strain amplitude is changed, however, the properties change. All the work reported in the literature (for example, [91, 98, 110, 116 to 119]) shows that the elastic modulus (or the effective modulus) decreases with increase in strain amplitude (e.g. fig.3.4). There is much less agreement as to the nature of the variation of the loss factor with strain amplitude, probably because this variation is much less pronounced.

This topic is still a subject of current study, and its relationship with molecular structure is not yet well established [93]. From a macroscopic standpoint, however, the behaviour described above is equivalent to that of a linear material, whose properties depend on the strain amplitude. The phenomenon will, therefore, be referred to as "strain-amplitude dependence".

3.3. Method of test

3.3.a. Argument for a shear test

In chapter 2, the "shear deformation" assumption of section 2.1 resulted in the differential equations containing viscoelastic material constants in shear, as

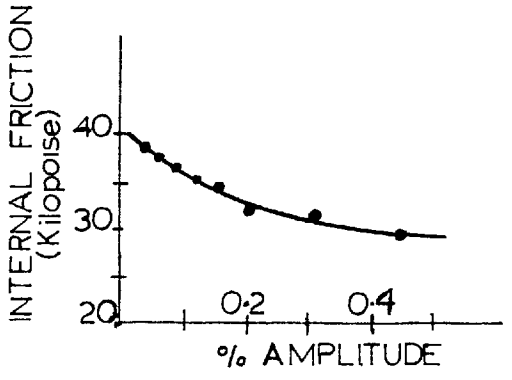

a) Internal Friction at Low Amplitudes for a Hevea-Tread Compound

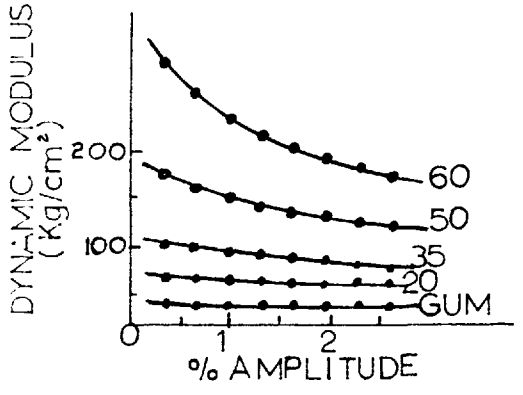

b). Amplitude Effects on Modulus of GR-S Tread with Different Loadings of Carbon Black

FIG. 3.4 As from [91]

well as in extension. In chapter 4, it will be shown that whilst the terms involving the extensional viscoelastic material constants are comparatively insignificant, those containing the shear constants are, in fact, very important.

To be able to test the validity of the above assumption it is thus necessary to know the shear properties of these materials. A considerable amount of data is available in the literature on the shear properties of many viscoelastic materials (for example, [100, 97, 91]), but the information given is always incomplete. Either the materials tested are not properly specified, or the conditions of test - such as temperature, strain amplitude etc. - are not given completely. Moreover, viscoelastic material properties are so much dependent on conditions of manufacture that the same chemical formulation might yield two dynamically dissimilar viscoelastics under different conditions of production. It becomes clear that for the purposes of checking the "shear deformation" theory, it is essential to perform a shear test on the viscoelastic material to obtain its properties within the frequency, temperature, and strain-amplitude ranges in which it may be used.

There is yet another argument in favour of obtaining the properties of viscoelastic materials under conditions of shear. Under static equilibrium conditions, theoretical considerations show, and experiments confirm, that the

deformation of viscoelastic materials in shear is a linear process, the strain being directly proportional to the applied stress. In contrast, however, in direct deformation, the equilibrium stress - strain relationship is distinctly non-linear [94]. Although the deformation characteristics under equilibrium (static) conditions are different from those under dynamic conditions [94], it is natural to expect that dynamic deformation in shear should conform much better to the linear behaviour (described in the previous section) than direct deformation. Experimental evidence tends to confirm this. Many workers (e.g. Payne [98]) have reported some higher harmonics in the response of some materials in direct deformation, as well as considerable distortion of the stress - strain elliptic curves. No such reports have been published for shear deformation, to the knowledge of the writer.

It is, in fact, now usual to regard the shear properties as the more fundamental properties of viscoelastic materials. Once these have been obtained, the material properties in direct deformation are deduced, on making a set of assumptions. One such set of assumptions consists in:

a. regarding the bulk modulus as a real constant, and

b. making use of the elastic isotropic relationship

between the elastic constants, viz.,

$\frac{E}{G} = \frac{9K}{3K + G}$ ..... 3.3.i; E, G, and K being the Young's modulus, the shear modulus and the bulk modulus respectively.

Cramer [92] applied equation 3.3.i to viscoelastic materials, replacing the Young's modulus, E, and the shear modulus, G, by the corresponding complex Young's modulus, E^*, and the complex shear modulus, G^*, to obtain the equations

$$\frac{E'}{G'} = \frac{3 + (\frac{G'}{K})\left\{1 + (\frac{G''}{G'})^2\right\}}{1 + \frac{2G'}{K} + \frac{1}{9}(\frac{G'}{K})^2\left\{1 + (\frac{G''}{G'})^2\right\}} \quad \text{.....3.3.ii,}$$

and $$\frac{\eta_e}{\eta_G} = \frac{1}{1 + \frac{1}{3}(\frac{G'}{K})\left\{1 + (\frac{G''}{G'})^2\right\}} \quad \text{.....3.3.iii}$$

where $\eta_e (= \frac{E''}{E'})$, and $\eta_G (= \frac{G''}{G'})$ are the loss factors in extension (or compression) and in shear repectively. For most viscoelastic materials, the ratio, $\frac{G'}{K}$, is much less than unity within frequency and temperature ranges of interest, so that equations 3.3.ii and 3.3.iii can be approximated to the much simpler relations**

$\frac{E'}{G'} \doteq 3$ ..... 3.3.iv, and $\frac{\eta_e}{\eta_G} \doteq 1$ .....3.3.v.

(It may be mentioned in passing that equation 3.3.iv can be obtained from the usual elastic isotropic relationship between Young's modulus and shear modulus if Poisson's

**Equations 3.3.iv and v would, of course, be exact if the material was incompressible.

ratio is taken as 0.5). Cramer verified the validity of the above approximations experimentally [92].

3.3.b. The mechanical set-up

Having argued in favour of testing the viscoelastic material in shear, it is now intended to show how this can actually be carried out.

Several methods have been developed for determining the dynamic properties of viscoelastic materials in both shear and direct deformation. A general detailed treatment of various test methods can be found in [93, 94, 103]. An exhaustive list of existing methods including their various features have been recently compiled by Praefcke [104]. These methods are conveniently grouped into

a. Free vibration tests
b. Forced resonance tests
c. Forced non-resonance tests
d. Wave propagation tests

The free vibration and forced resonance test methods usually involve a considerable variation in the strain distribution within the test sample in the time interval required to take a reading. They are thus generally inadequate for the investigation of strain-amplitude effects. Moreover, measurement difficulties usually arise if the material damping is high [104]. These methods were thus

considered unsuitable for the tests contemplated. Wave propagation techniques are essentially high-frequency (several kilocycles), low-strain (less than 0.001 per cent in most cases) methods [122 to 125], and are thus not suited for the relatively low frequencies (a few hundred cycles) contemplated.

It follows that forced, non-resonant methods are best for the proposed tests. None of the existing methods, however, seemed to quite satisfy the needs of the test. Either their frequency range is too low (usually not exceeding 50 c.p.s.) as, for instance, the apparatuses of Roelig [105, 106,] Payne [107, 108, 109], Philippoff [110], Fletcher and Gent [111] and Painter [112]; or the apparatus is too complicated to be easily modified for laboratory use, for example, Fitzgerald and Ferry apparatus [99, 113, 114, 115].

For this reason, a simple apparatus was developed for the test. The mechanical set-up is illustrated in fig. 3.5. Two similar layers of the material, (3), constitute the specimen and are glued in between two stationary supports, (5), and a moving centre-piece, (4). The stationary supports are made rigid and identical, and are firmly bolted on to a steel base plate, (8), which is, in turn, rigidly connected to the main body of a Goodman's electro-magnetic vibrator, (10). The centre-piece is a half-inch square

KEY TO FIG. 3.5

(1) Displacement pick-up

(2) Brass piece

(3) Viscoelastic layer under test

(4) Moving centre-piece

(5) Stationary supports

(6) Drive rod

(7) Force measuring strain gauge

(8) Base plate

(9) Output drive of vibrator

(10) Electro-magnetic vibrator

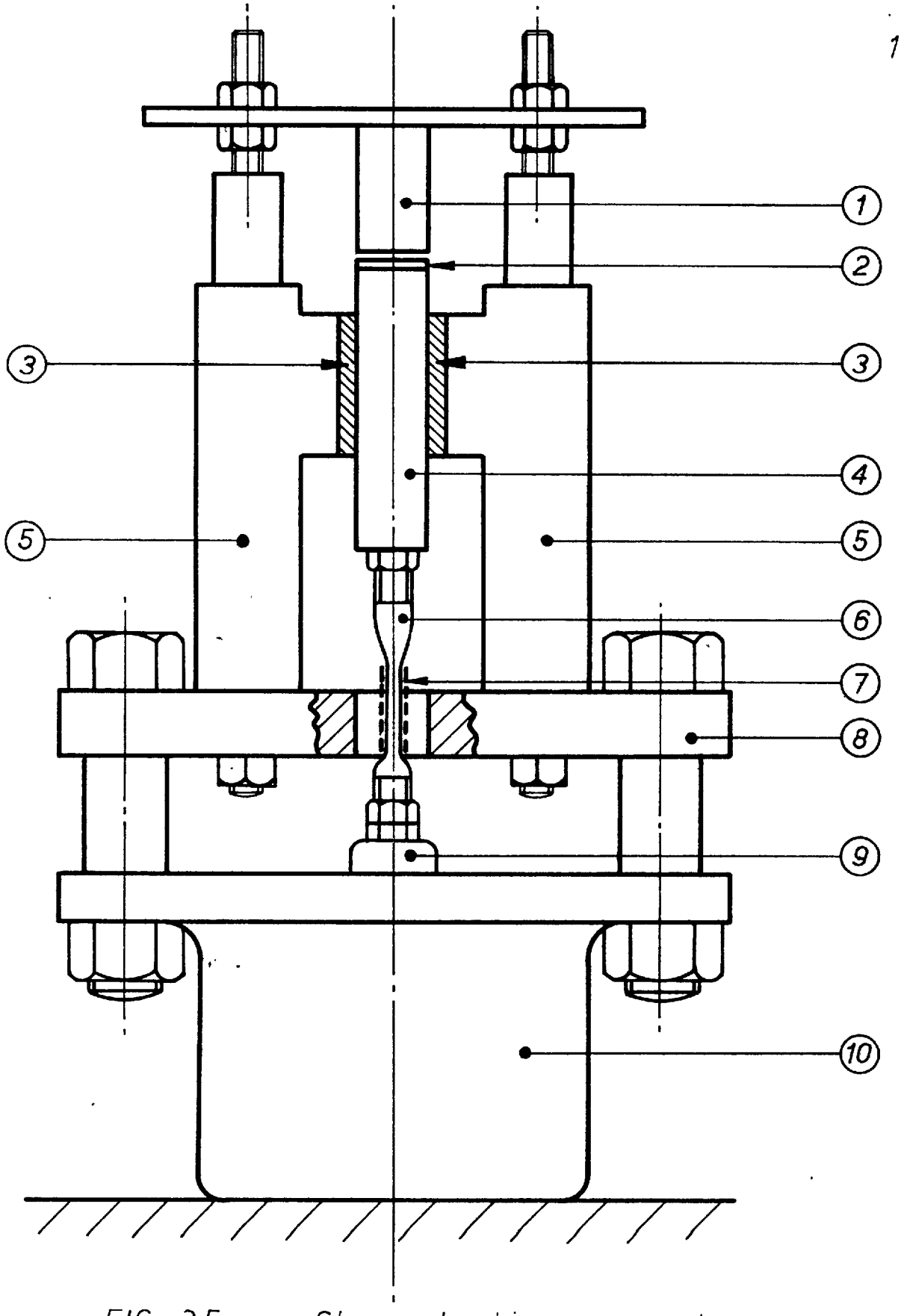

FIG. 3.5 Shear testing apparatus.

aluminium bar about two inches long. To its upper end is glued a half-inch square piece of brass, $\frac{1}{8}$ inch thick, (2). This helps to increase the sensitivity of an inductance proximity gauge, (1), which is rigidly connected to the fixed supports by means of a bridging piece; and which serves as a displacement pick-up to measure the motion of the centre-piece. At the lower end of the centre-piece is attached a short drive rod, (6). This is essentially an aluminium rod, $\frac{1}{4}$ inch in diameter, and two inches long. The central one inch portion is machined down to two flat surfaces with a 0.050 inch thickness of metal between them. Two similar Tinsley strain gauges, (7), each about 100 ohms mean resistance, are stuck at this portion (one on each surface) using durofix cement. These gauges are connected in series to eliminate bending effects, and measure the force transmitted from the vibrator to the moving centre-piece and the specimen. The drive rod is attached at its lower end to the output drive, (9), of the vibrator.

When a sinusoidal signal is fed into the vibrator, the centre-piece is made to move vertically with simple harmonic motion, thus inducing a sinusoidal shear strain in the specimen. A force signal is picked up by the strain gauge whilst the inductance gauge picks up a displacement signal. These can be analysed, in a manner to be indicated shortly,

in order to obtain the shear properties of the material under test.

It is essential that the fixed supports, (5), are vertical on assembly. To ensure this, the bottom faces in contact with the base plate are made exactly at right angles to the vertical faces, and are properly machined so that they are flush with the ground upper surface of the base plate. This surface is initially set in a horizontal position using a spirit level.

3.3.c Theory of method

The force measured by the strain gauge is the force transmitted by the drive rod at the point of attachment of the gauge. This force is the force required:

a. to accelerate the moving centre-piece together with the portion of the drive rod above the strain gauge (neglecting, for the moment, the effective inertia of the specimen); and

b. to cause shear in the viscoelastic material.

Let the moving mass under consideration be m. For a sinusoidal input signal, let the vertical displacement, x, of the centre-piece be $a_o' \sin \omega t$, ω being the frequency of excitation. From fig. 3.6, it is clear that this will induce a shear strain, ϕ, given by

$\phi = \frac{a_o'}{t_o} \sin \omega t$ ...3.3.vi, in the specimens; t_o being the thickness of each layer of specimen. The shear stress in the material will not be in phase with the strain, but will

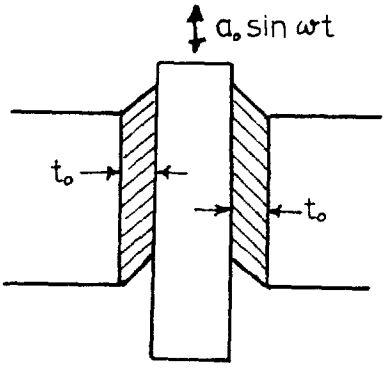

FIG. 3.6 Shear Deformation in the Specimen Layers

lead it by the loss angle, δ, so that the expression for the stress takes the form,

$\tau = \hat{\tau} \sin(\omega t + \delta)$ .....3.3.vii.

The force causing shear equals τA or $\hat{\tau} A \sin(\omega t + \delta)$, where A is the total shear area, that is, the area of both faces of the centre-piece in physical contact with the layers. The force causing acceleration is $m\ddot{x} = -m\omega^2 a'_o \sin \omega t$. Hence, the transmitted force, P, is given by $P = \hat{\tau} A \sin(\omega t + \delta) - m\omega^2 a'_o \sin \omega t$ .....3.3.viii. If the phase difference between the force, P, and the displacement is ϵ, then $P = \hat{P} \sin(\omega t + \epsilon)$ .....3.3.ix, $\hat{P}$ being the amplitude of the transmitted force. Comparing equations 3.3.viii and 3.3.ix, it follows that

$\hat{P} \cos\epsilon = \hat{\tau} A \cos\delta - m\omega^2 a'_o$ .....3.3.x, and

$\hat{P} \sin\epsilon = \hat{\tau} A \sin\delta$ .....3.3.xi.

Hence $\eta_G = \tan\delta = \dfrac{\hat{P} \sin\epsilon}{\hat{P} \cos\epsilon + m\omega^2 a'_o}$ 3.3.xii;

and since $G' = \dfrac{\hat{\tau} \cos\delta}{\hat{\phi}}$ by definition; it follows that

$G' = \dfrac{\hat{P} \cos\epsilon + m\omega^2 a'_o}{A \hat{\phi}} = \dfrac{\hat{P} \cos\epsilon + m\omega^2 a'_o}{A} \left(\dfrac{t_o}{a'_o}\right)$ ...3.3.xiii.

In the above analysis, the inertia of the specimen has been treated as negligible compared with the total moving mass m. When the layers of specimen are reasonably thick, however, the above assumption may no longer hold, and it will then be necessary to take account of this. A simple way of doing this is by adding an "equivalent mass",

m_s, of the specimen on to the moving mass, m, to obtain the corrected inertia mass, $m_c = m + m_s$; which will then replace m in equations 3.3.xii and 3.3.xiii. The equivalent mass m_s of the specimen is obtained as follows.

Referring to fig. 3.7 and assuming perfect bonding of the specimen to the various faces; it is seen that the layer of specimen in direct contact with the stationary support has zero displacement while the layer immediately in contact with the moving centre-piece must have the same displacement as the centre-piece itself i.e. $a'_o \sin \omega t$. It follows, therefore, that under conditions of pure shear which are assumed to hold, any layer at a horizontal distant y from the fixed support has a displacement given by $y(\frac{a'_o}{t_o}) \sin \omega t$. If ρ is the density of the material, then the inertia force of an elemental strip, thickness dy, and distant y from the stationary support, is $-(\rho \frac{A}{2} dy)\omega^2(\frac{a'_o y}{t_o}) \sin \omega t$, remembering that the shear area on one side of the centre-piece is $\frac{A}{2}$. The inertia force for both layers is, therefore,

$2\int_0^{t_o} -(\frac{\rho A a'_o}{2t_o}\omega^2 \sin \omega t)\, y\, dy$; which, when integrated, gives $-(\frac{\rho A t_o}{2})\ a'_o \omega^2 \sin \omega t$. But $\frac{\rho A t_o}{2} = \frac{M}{2}$; M being the mass of both layers of the specimen. Hence the force required to accelerate the specimen is $-\frac{M}{2} a'_o \omega^2 \sin \omega t$, which is the

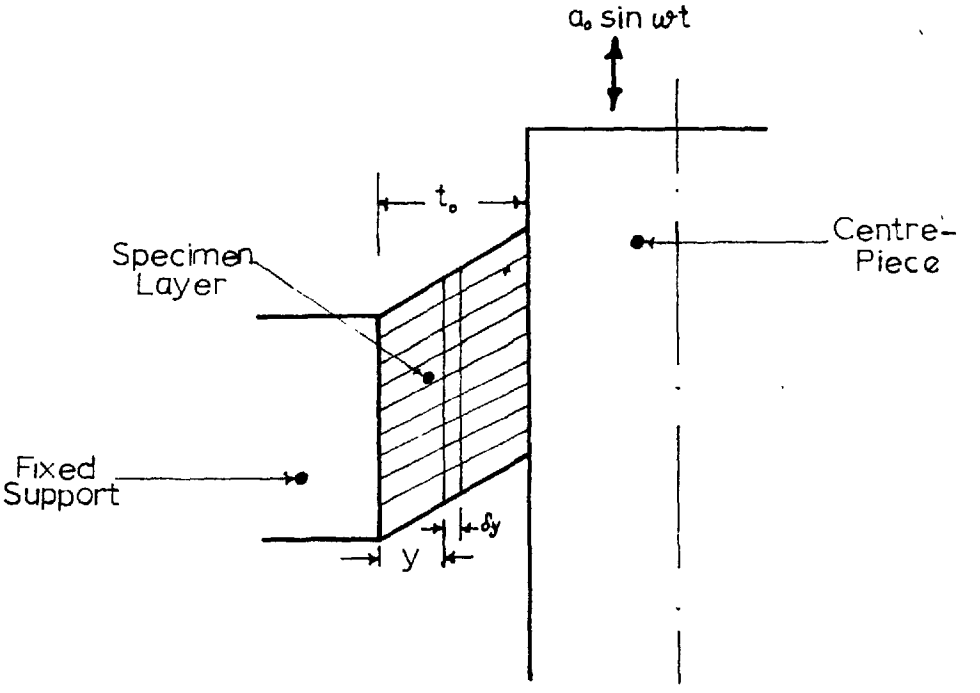

FIG. 3.7 *Determination of the "Equivalent Moving Mass" of the Specimen Layers*

same as the inertia force for a mass, $\frac{M}{2}$, attached to, and moving with the centre-piece. The effective mass, m_s, of the specimen is thus simply half its total physical mass.

3.4. Preparation of the specimens

Before discussing the methods of measurement employed, it is intended to give some further details about the preparation of the test specimens. As already mentioned, the specimen layers were glued to the centre-piece and the stationary supports. In this, it was essential that there was perfect adhesion throughout the areas of contact. Another requirement was that the specimen layers should have the same uniform thickness. This second condition is not very critical, and it can be shown that provided the mean thickness of both layers is used in the calculations, the specimen layers could have as much as 25 per cent difference in thickness without introducing much error in the calculated values of the elastic modulus and the loss factor. How the above requirements were taken care of will become obvious in the following description.

The gluing material used in the preparation of all the specimens was araldite AV 100, together with its hardener HV 100, made by CIBA Ltd. This was chosen because of the relative ease with which it could be applied, and its ability to set at room temperatures. As for its bonding strength, all tests pointed to the fact that there was no

bonding failure. What these tests were will be seen shortly.

Two categories of materials were tested;

(i) "soft" materials - the term, soft, being here loosely applied to materials, samples of which were available in the liquid form.

(ii) "hard" materials or materials available in sheet form.

In either case the surface preparation was as follows. Both faces of the centre-piece as well as the relevant faces of the fixed supports were first degreased by cleaning them with acetone. They were then abraded in dilute sulphuric acid and washed thoroughly in water.

Soft specimens

The faces were allowed to dry and a very thin layer of araldite was applied to the bonding surfaces of the stationary supports. A layer of the liquid material was then applied to each surface using a small fibre brush, and allowed a few hours to set slightly before the next layer was applied. The thickness of the specimen layers was thus gradually built up until about the desired value was obtained. At this stage, a small mould, of height equal to the desired layer thickness, was introduced round each layer and was filled to the brim by pouring in some of the liquid material. This last step was to enable a smooth uniform upper surface to be formed for the bonding of the centre-piece. The layers so formed were now left aside

for about a fortnight to set hard.

The moulds were removed after this time, and the centre-piece was glued to the two faces. A layer of araldite was first smeared on the faces before putting them together. To ensure good bonding, the pieces were held together by means of bolts and nuts tightened against a spring load. This was necessary to keep the layer thicknesses constant during the setting period. The entire set-up was allowed some more time to cure before being connected up for test. The thickness of the specimen layers was determined by taking the difference between the overall width of the set-up when connected up for test and the width of the stationary supports and centre-piece (without the specimen). The thickness of each layer was taken as half this difference. The measurements were made to the accuracy of 0.001 inch using a micrometer screw gauge.

Hard specimens

These were much easier to prepare as the materials were already available in the uniform thickness required for the test. The two specimen layers were first cut out to the desired size from the sheet of material available. They were then degreased with acetone, and thoroughly washed in water. After this, a very thin layer of araldite was applied on all the surfaces to be bonded together. The stationary [illegible]

now appropriately assembled and held together under slight pressure by means of nuts and bolts as above. The set-up was allowed three days (to enable the araldite to harden properly) before being connected up for test. As in the case of the soft specimens, the specimen thickness was determined, not by direct measurement before bonding, but by measuring the overall thickness of the assembly when connected up for test, and taking away from this the corresponding thickness without the layers. This took account of the slight compression of the specimen during bonding, due to the applied pressure.

All the specimens tested (both hard and soft) had about the same dimensions of bonding area - 2 x 0.5 sq.in. Their thicknesses varied from about 0.030 inch to 0.160 inch.

Although care was taken to achieve perfect bonding of the specimen to the metal pieces (by ensuring that a uniform layer of araldite was applied to each of the surfaces bonded together), it would be difficult to check conclusively that perfect bonding existed at every point on the areas of contact. It was, however, much easier to verify that there was no bonding failure when the system had been subjected to large forces, as for example, at high frequencies. One way of doing this is by checking on the repeatability of results obtained before and after such a

process. Since araldite sets to a hard brittle solid, any breaking of the bond would lead to a completely different set of results from that obtained previously, for the same test conditions. This check was applied to each specimen tested, and the good agreement between repeated tests (see section on results) was a clear indication that there was no breaking of the bonds during test. Another method which was mainly applicable to the soft specimens, was to destroy the specimen at the end of the tests, by pulling the stationary supports apart. This resulted in the metal pieces coming apart with each bonding surface having some portion of the specimen on it. Had there been any bonding failure on any of the surfaces, that surface would have come off with the whole or a portion of its area clear of the specimen.

3.5. Measuring techniques and calibration

3.5.a. Quantities to be measured

The different methods of measurement employed in the tests will now be discussed. From equations 3.3.xii and 3.3.xiii, it can be seen that to evaluate the material properties, G' and η_e, the following quantities must be known:

(i) t_o, the thickness of each layer of specimen;

(ii) A, the total shear area.

(iii) m_e, the total (effective) moving mass above the strain gauge,

(iv) ω, the circular frequency of the applied strain,

(v) a_o, the amplitude of the displacement signal,

(vi) $\hat{P}$, the amplitude of the force signal,

(vii) ϵ, the phase difference between the force signal and the displacement signal.

There is yet another quantitiy not expressed directly in the equations but on which the material properties also depend; namely, the temperature, T, of the specimen.

The method of determining t_o has already been explained. The shear area was obtained from measurements of the physical dimensions (length and breadth) of the surfaces concerned. To obtain m_e, the centre-piece and the drive rod were weighed separately on a chemical balance, to the accuracy of 0.01 gm. The mass of the specimen was also obtained by weighing the fixed supports and centre-piece before and after gluing the specimen in position, and then taking the difference. The appropriate inertia mass was then taken as the sum of

(a) the mass of centre-piece,

(b) half the mass of the drive rod (the strain gauges were assumed to be situated at the centre of the symmetrical drive rod), and

(c) half the specimen mass.

How the other quantities were measured are treated in greater detail below.

3.5.b. Frequency measurement

The input signal to the vibrator was derived from a Muirhead D-880 A low-frequency decade oscillator. This has a calibrated frequency scale and a frequency range from 0.01 c.p.s., continuously variable above 0.1 c.p.s., to 11.2 kilocycles per sec. The specified accuracy of the signal frequency is about 0.2 per cent for most of the range. This was checked by means of a Beckman electronic digital counter. Agreement was better than 0.5 per cent. The frequency indicated on the oscillator scale is, of course, the frequency of the driving signal; and should be equal to the frequency of the displacement signal. This was checked using the counter, and found to be so. Also the frequency of the force signal was measured and was found to have the same value as the displacement signal frequency.

A special feature of the above-mentioned oscillator was the fact that it was capable of giving two output signals, both at the same frequency, but differing in phase by about 90°. Use was made of this in the phase measuring set-up to be described later.

3.5.c. Amplitude measurement

Fig. 3.8 is a block diagram showing the train of

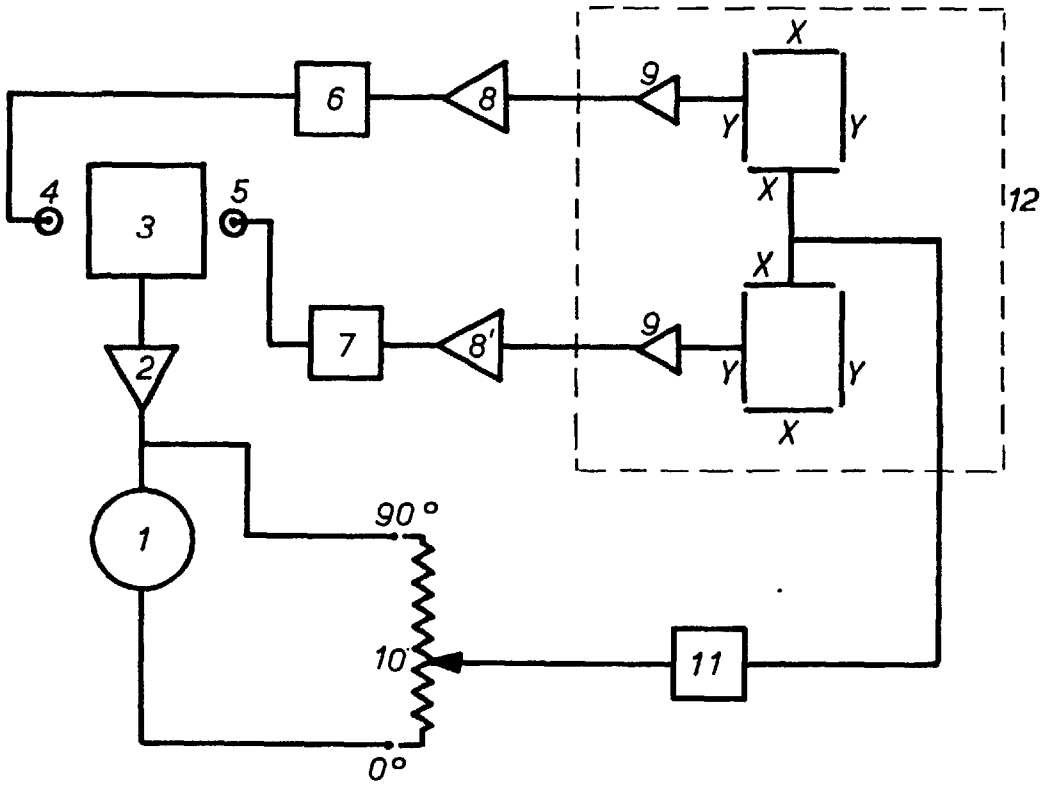

1. DECADE OSCILLATOR - 2 OUTPUTS 90° OUT OF PHASE
2. 250 WATT POWER AMPLIFIER
3. ELECTRO-MAGNETIC VIBRATOR
4. DISPLACEMENT PICK-UP (PROXIMITY GAUGE)
5. FORCE PICK-UP (STRAIN GAUGE)
6. GAUGE OSCILLATOR
7. RESISTANCE BRIDGE
8. FREQUENCY-MODULATED PRE-AMPLIFIER
8'. PRE-AMPLIFIER
9. DRIVER AMPLIFIER
10. VARIABLE PHASE OUTPUT POTENTIOMETER
11. PHASE SHIFTING NETWORK
12. DOUBLE BEAM OSCILLOSCOPE

FIG. 3.8 Block Diagram of Measuring Circuit.

measuring instruments. As mentioned above a signal was first generated at a known frequency by the oscillator, (1), and this was then fed into a Derriton 250 watt low-frequency power amplifier, (2). The amplifier, capable of delivering full power from about 15 c.p.s. to 5 kc/s, had a sinusoidal output wave form with a distortion of less than 2 per cent in this range. The amplified signal was fed into the vibrator, (3), which was capable of taking 4 amps uncooled, and up to 8 amps when air-cooled. As the centre-piece (connected to the output drive of the vibrator through the drive rod) moved up and down in response to the applied signal, the inductance of the proximity gauge, (4), varied proportionately. This caused a gauge oscillator, (6), to send a frequency-modulated signal to a Minirack frequency-modulated pre-amplifier, (8), for demodulation and amplification. The resulting signal then passed through a driver amplifier, (9), on to one channel of a Minirack double beam oscilloscope, (12), The amplitude of the signal could now be measured using the already calibrated scale of the oscilloscope.

This calibration was done optically using a travelling microscope, and also under dynamic conditions. A small piece of very fine emery paper was stuck to the centre-piece and illuminated by an external light source. A signal was then fed into the vibrator, and as the centre-piece moved

up and down, any bright spot on the emery paper lengthened into a vertical line which was then measured using the eye-piece scale of the microscope. It was thus possible to calibrate the scope readings against the microscope eye-piece scale readings. This calibration was done at the beginning and end of each test, and whenever the mean gap between the metal surface and the proximity gauge was changed. Such a calibration graph is shown in fig. 3.9.

It may be pointed out that the above calibration would give the correct calibration for the movement of the centre-piece only if the proximity gauge was perfectly stationary. This was checked during the calibration (for the frequency ranges of interest), and with the highest microscope magnification available, it wasn't possible to detect any measurable motion of the gauge.

The miscroscope eye-piece scale was previously calibrated using a stage micrometer. The stage micrometer contained a standard millimeter length subdivided into 100 parts. Various objectives were calibrated for the same eye-piece and the same working length. Some of the graphs are shown in fig. 3.10. The smallest distance measurable with the microscope - for the combination of eye-piece and objectives used - was 7 microns. The displacement amplitudes actually measured varied from about 200 to 2000 microns.

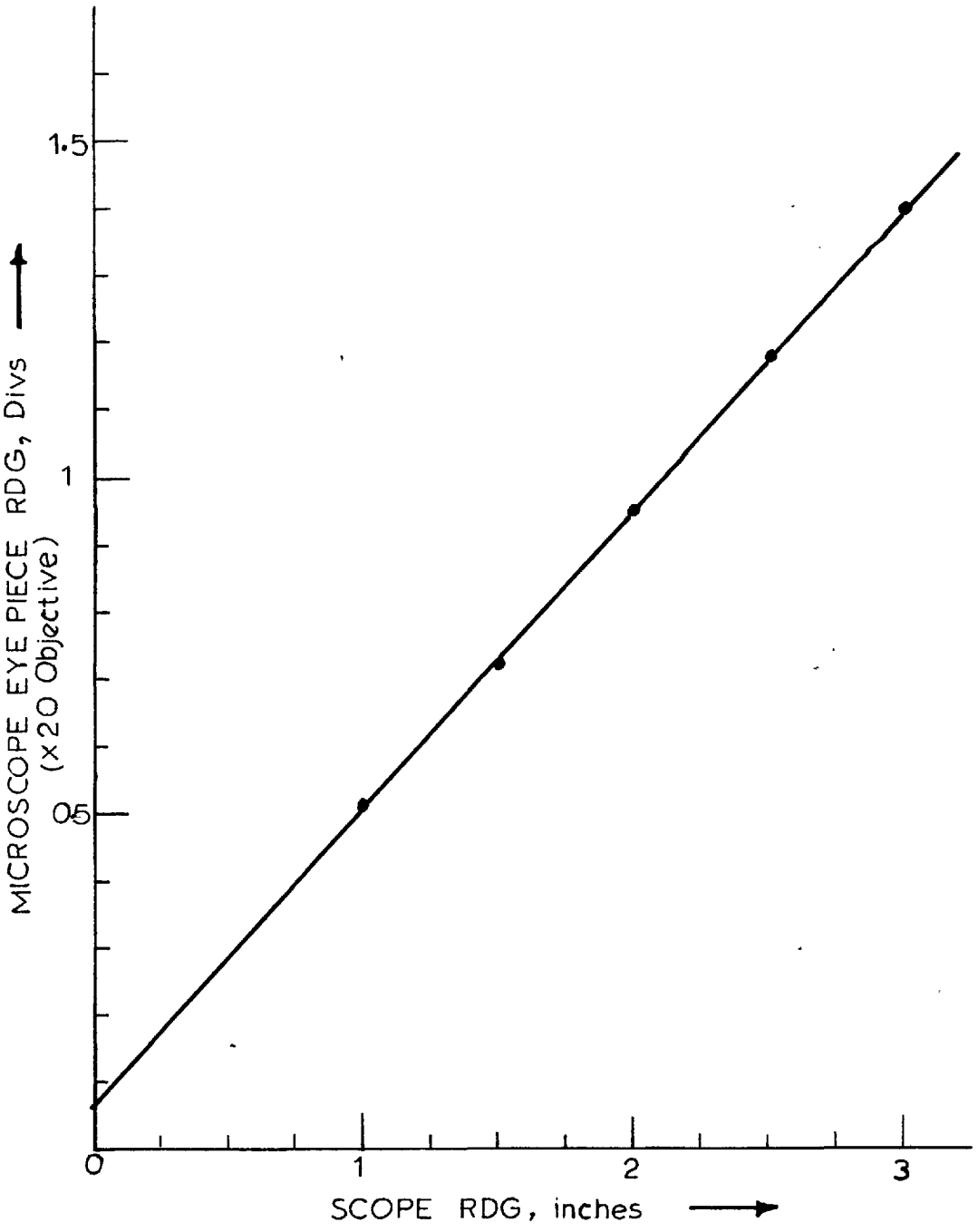

FIG. 3·9 *Typical Calibration Graph for the Displacement Channel of Oscilloscope.*

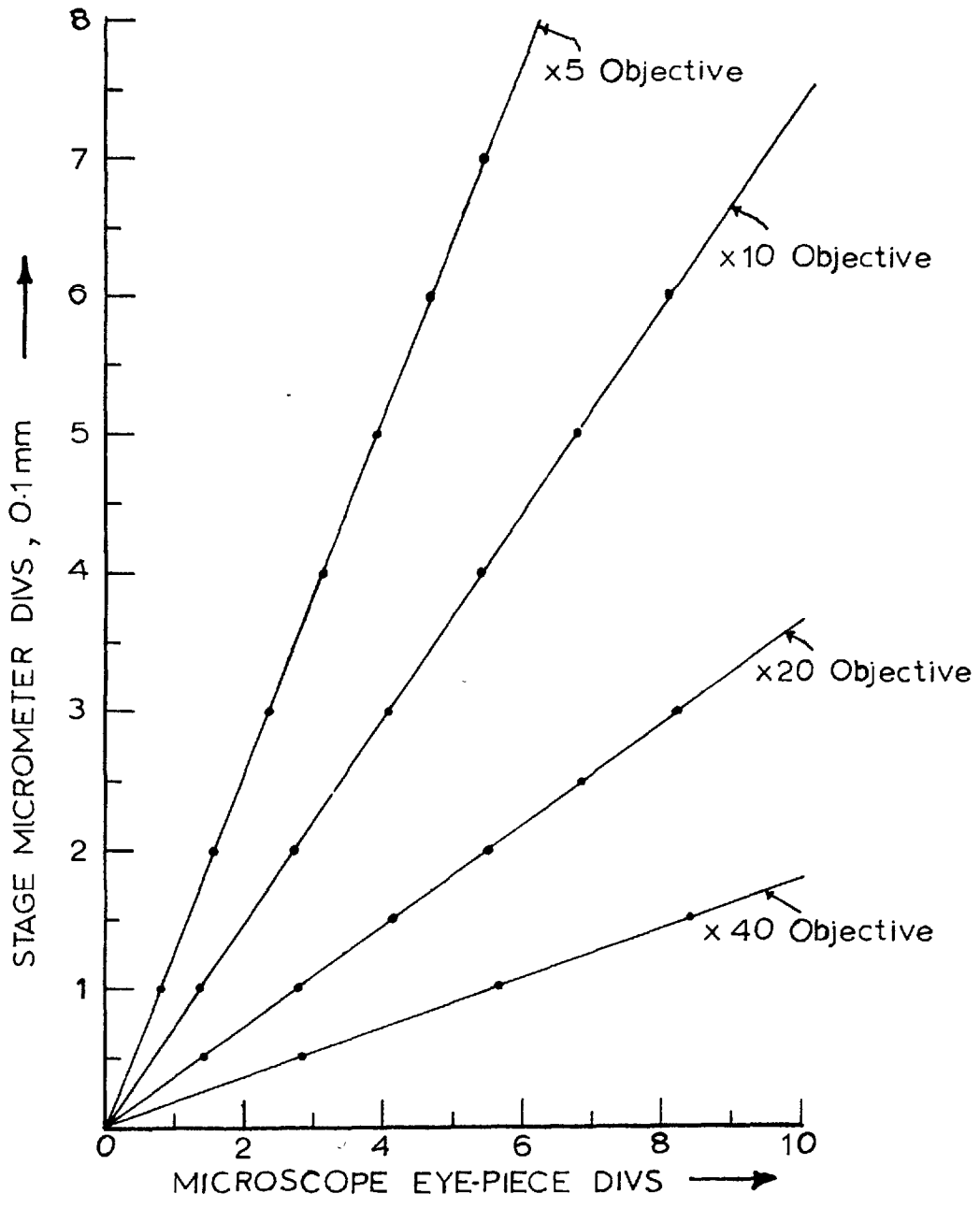

FIG. 3.10 *Calibration of Microscope Objectives using a Stage Micrometer.*

3.5.d. Force measurement

Referring again to the block diagram, fig. 3.8; as the vibrator drove the centre-piece, the transmitted force strained the drive rod causing, in the strain gauge, (5), a change in resistance proportional to the transmitted force. Since the strain gauge formed part of a resistance bridge, (7), a signal proportional to the force was transmitted to a Minirack pre-amplifier, (8), then through a driver amplifier, (9), to the other channel of the double-beam oscilloscope, (12). The amplitude of the force could now be measured on the oscilloscope scale which had been previously calibrated.

To understand the calibration procedure, it is helpful to examine the resistance bridge circuit employed. A simplified sketch of this is given in fig. 3.11. The arm adjacent to the gauge consisted of decade dials covering a range of 11,110 ohms in steps of 1 ohm. Two ratio arms, each of 2K, were provided, separated by a 10-ohm calibrated apex resistor. This was a ten-turn helical potentiometer with a dial subdivided into 100 parts and a counter to indicate complete revolutions. One complete revolution of the dial (i.e. 100 small divisions) corresponded to a change in resistance, $\frac{\Delta R}{R}$, of 10^{-3}, in the resistance of any one arm of the bridge. Each small division was thus equivalent to $\frac{\Delta R}{R} = 10^{-5}$.

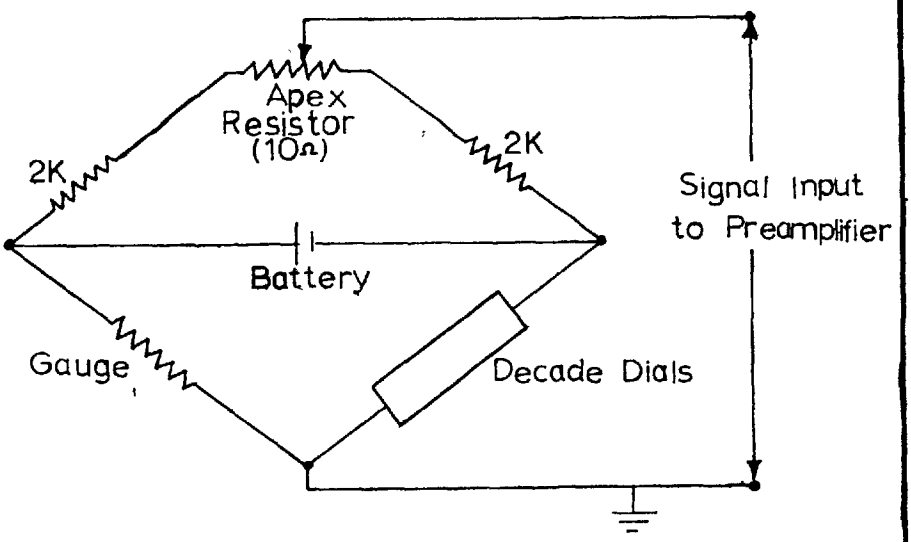

FIG. 3·11 Resistance Bridge Circuit

The apex resistor provided a very convenient medium for calibration in the following way. The scale of the apex resistor was first calibrated statically to measure force. Known weights were hung, in turn, from the drive rod and using the oscilloscope as a null point indicator, balance was effected in each case by suitably varying the apex resistance reading (i.e. the contact point on the apex resistance). A graph of load against $\frac{\Delta R}{R}$ was thus obtained as shown in fig. 3.12. It should be noted that this calibration was independent of the scope sensitivity as well as of the test-battery voltage. It was carried out at the beginning of the tests, and checked when all the tests were completed. The two calibrations agreed to within 2%.

With this calibration, it was now only necessary to calibrate the oscilloscope scale against the change in the apex resistance $\frac{\Delta R}{R}$, for any given amplifier magnification and test-battery voltage. This calibration was done at the beginning and end of each test, and whenever the amplifier settings had to be changed. A typical graph is shown in fig. 3.13.

3.5.e. Phase measurement

The accurate measurement of the phase difference between two signals is usually a very difficult and time-consuming operation. Many of the standard phase meters

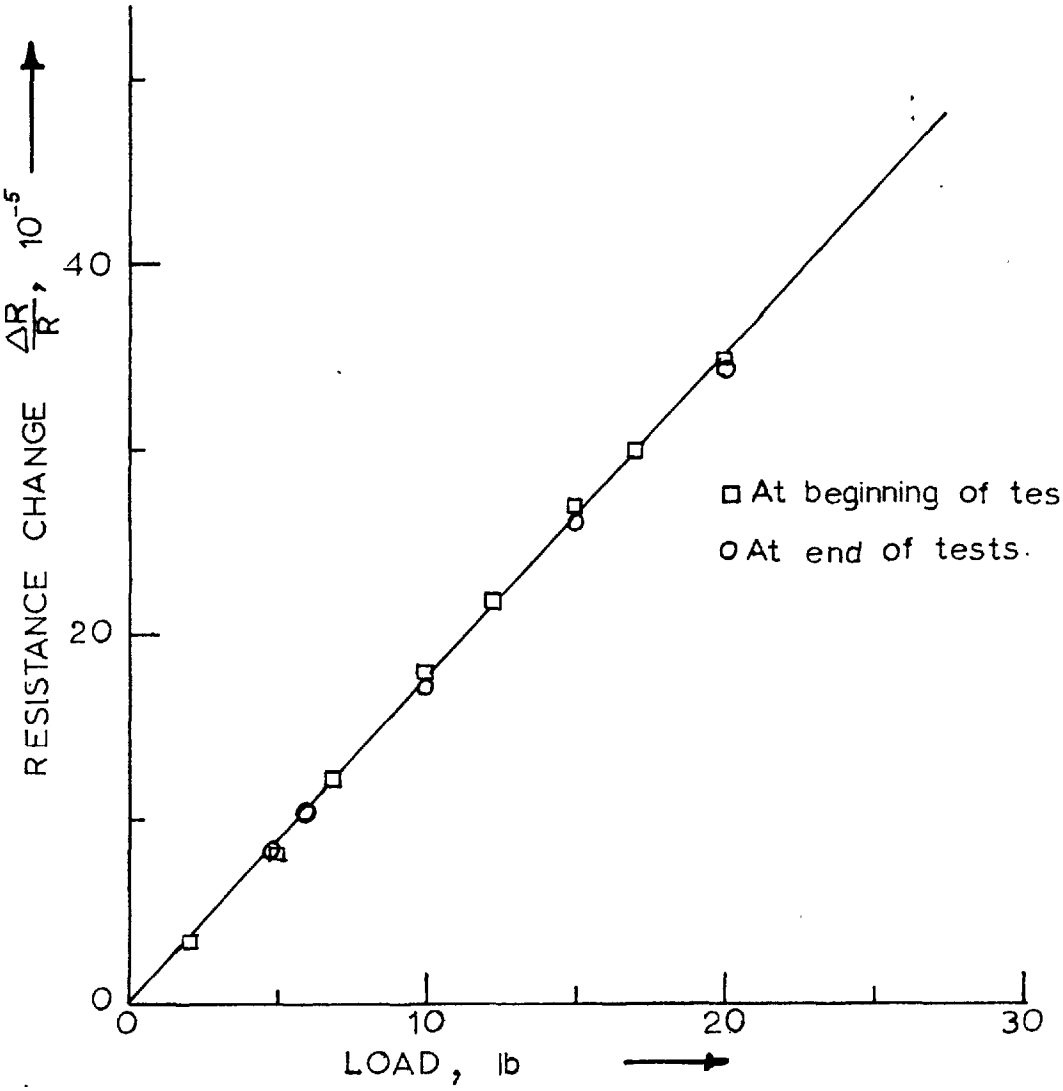

FIG. 3.12 Calibration of Apex Resistor Change in Resistance $\frac{\Delta R}{R}$.

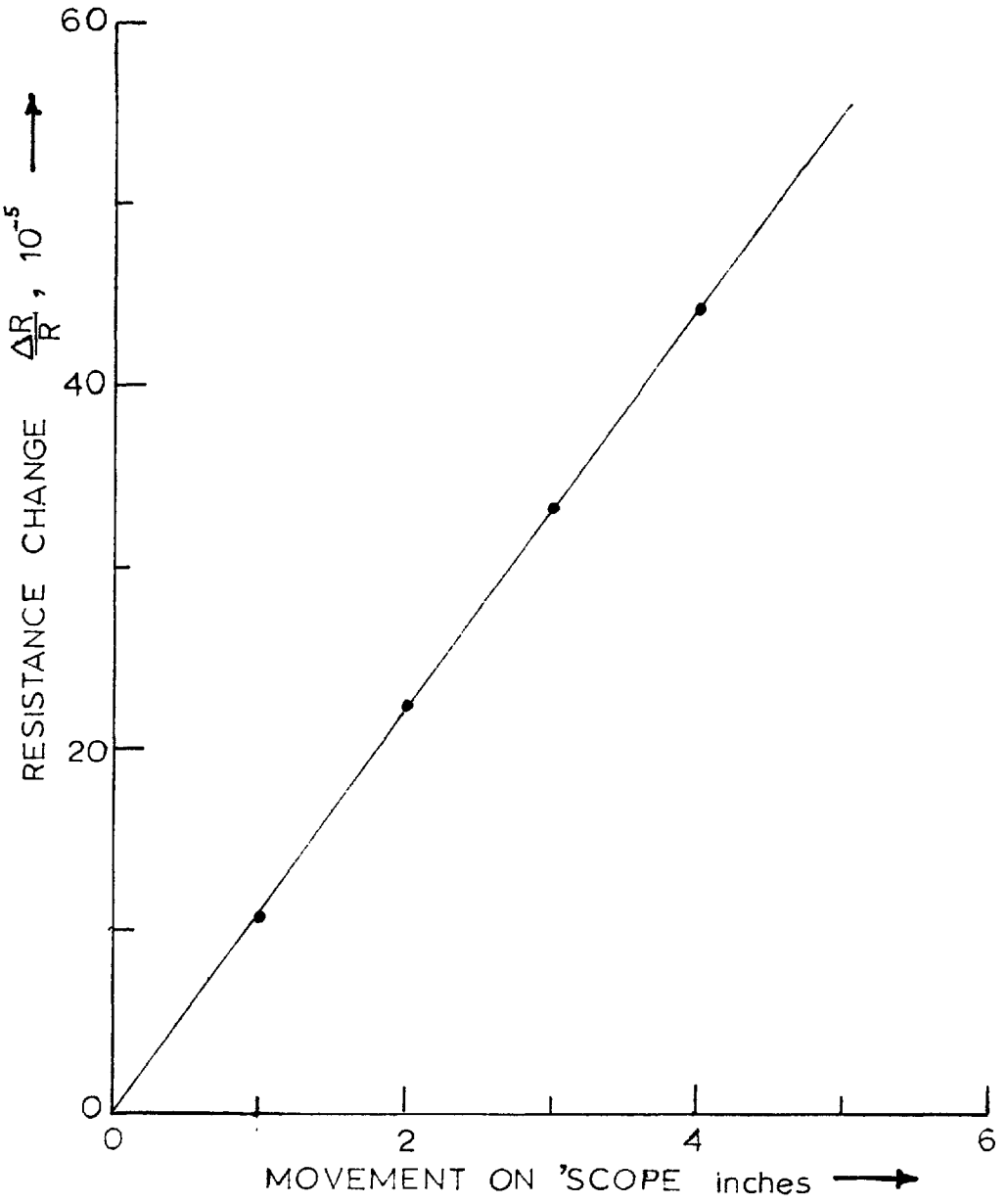

FIG. 3·13 *Typical Calibration Graph for Force Channel of Oscilloscope*

available have an accuracy of the order of ± 2°. This level of accuracy is very inadequate for the measurements contemplated since changes in phase difference of less than 2° would often require to be detected.

The electronic digital counter available could be used to measure the phase difference accurately. Used as a phase meter, the counter basically measured the time interval (in microseconds) between the two signals attaining a certain voltage value. (It is here assumed that both signals have the same continuous periodic form - not necessarily sinusoidal - and are exactly equal). The counter was capable of detecting phase differences as small as 0.02° at 50 c.p.s., the resolution decreasing to 0.2° at 500 c.p.s. In practice, however, this method proved very wieldy and took a considerable amount of time to carry out since the two signals had first to be accurately balanced. Another set-back in the use of the counter was 'noise'. For accurate readings, it required pure waveforms. Any noise in the waveform was easily detectable and could lead to inconsistent sets of results. Owing to the rather high amplification which had to be employed in the force channel, a considerable amount of noise was picked up by the force signal, making measurements with the counter very difficult.

For this reason, another method of measuring the

phase angle was developed. A variable phase potentiometer was obtained by applying the two outputs of the decade oscillator (to be referred to as the 0^{o} and 90^{o} outputs), each to one end of a linear potentiometer. A voltage signal of varying phase (and amplitude) could thus be obtained at the variable terminal of the potentiometer, the phase of the signal being 0^{o} at the zero degree terminal and 90^{o} at the 90^{o} terminal. The phase difference at any point would normally depend on the ratio of the amplitudes of the voltages as well as on the ratio of the resistances on either side of the point. In the set-up used, the voltage signals were of the same amplitude, and under this condition, the phase of the signal at any point depended only on the resistance ratio, the phase being 45^{o} at the "resistance centre" of the potentiometer. The phase at any point could be calculated once the resistance ratio was known.

However, it was thought more reassuring and accurate to actually calibrate the phase potentiometer using the electronic counter. Fig. 3.14 shows the calibrating circuit used. The signals whose phase difference was to be measured were first made equal by displaying them on a double beam scope (both channels of which had been set to the same sensitivity) and monitoring one of the signals appropriately. They were then fed into each channel of the digital counter

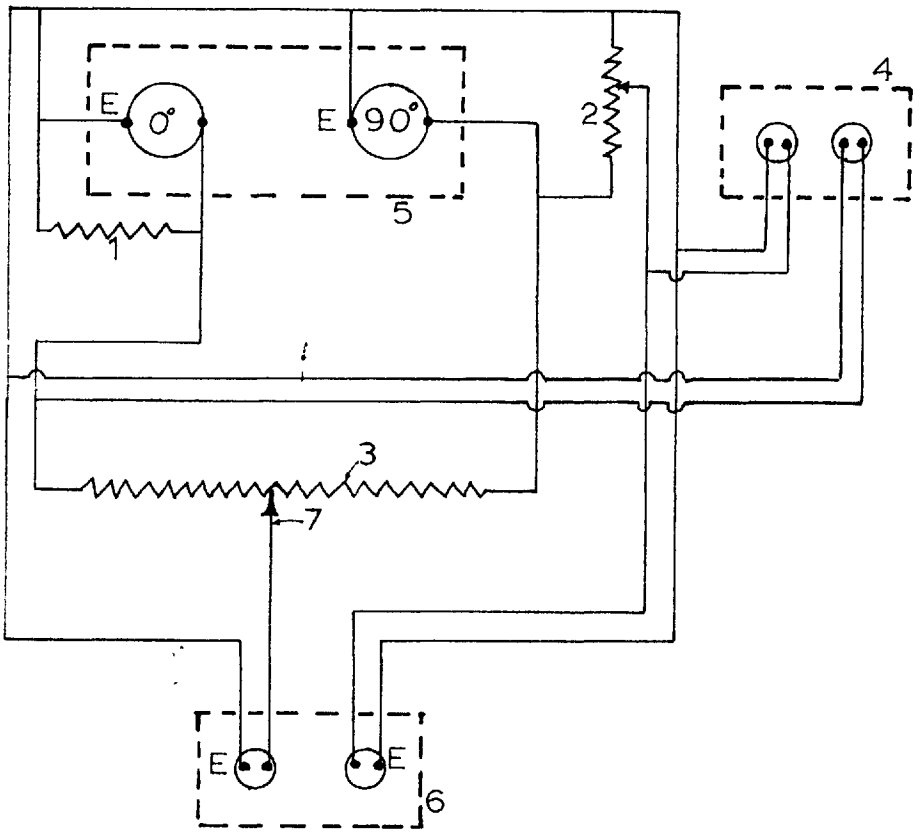

1. 600Ω TERMINATING RESISTANCE.
2. 100K MONITORING RESISTANCE.
3. BANK OF 6 10K POTENTIOMETERS IN SERIES — PHASE POTENTIOMETER.
4. DOUBLE BEAM OSCILLOSCOPE.
5. MUIRHEAD L.F. OSCILLATOR.
6. ELECTRONIC DIGITAL COUNTER.
7. VARIABLE TERMINAL OF PHASE POTENTIOMETER.

FIG. 3.14 *Calibrating Circuit for Phase Potentiometer.*

and the time interval between their attainment of a given voltage level (zero voltage level was aimed at in the settings) was measured. This, together with the periodic time of the signals, also measured with the counter, gave the phase angle as $\frac{\text{TIM}}{\text{Periodic time}} \times 360$ degrees, TIM being the time interval. In this way the settings of the variable tapping were calibrated in degrees, the phase angle specified for each setting being the phase difference between the voltage picked up at that point and the 90° output which served as the driving signal.

The actual setting-up of the phase potentiometer required a careful choice of the potentiometer resistance. A relatively low resistance applied across the terminals of the oscillator might cause the current flowing through the potentiometer to vary appreciably within a small frequency range, resulting in the potentiometer calibration being frequency-dependent. A similar effect would result if a very high resistance was used, a capacitive effect being introduced in the circuit. Various combinations of resistances were tested, and the one giving the best performance, over the frequency range within which measurements took place, was used. The calibration, which was done at 27.78 c.p.s., was found to hold true from 10 to 400 c.p.s. Above this frequency range, it became necessary to make some corrections. The calibrated scale was checked at 500 c.p.s., and also at 1000 c.p.s., and correlating

graphs were obtained to help make the necessary corrections at these frequencies. The graphs are given in fig. 5.15.

The minimum accuracy of calibration is the accuracy of the counter in measuring 1 degree at the calibrating frequency, 27.78 c.p.s. Since the counter accuracy is approximately inversely proportional to the count indication, this accuracy is about 1 per cent. The one degree divisions of the potentiometer were thus located with an accuracy better than 1 per cent.

Having obtained a calibrated phase potentiometer, it is now necessary to show how this was utilised in phase measurement. Referring once more to the block diagram - fig. 5.8; the signal from the potentiometer, (10), was fed through a phase shifting network, (11), to the common X plates of the double beam oscilloscope, (12). The significance of the phase shifting network will be discussed shortly. Already the displacement and force signals had been applied to the two Y plates of the scope. Since all three signals were at the same frequency and were sinusoidal, the resulting Lissajous figures would, in general, be two ellipses. The shapes of the ellipses would vary as the phase of the signal applied to the X plates was varied, and each of the ellipses would degenerate to a straight line when its phase (relative to the 90^{o} output) equalled that of the potentiometer signal. The phase difference between

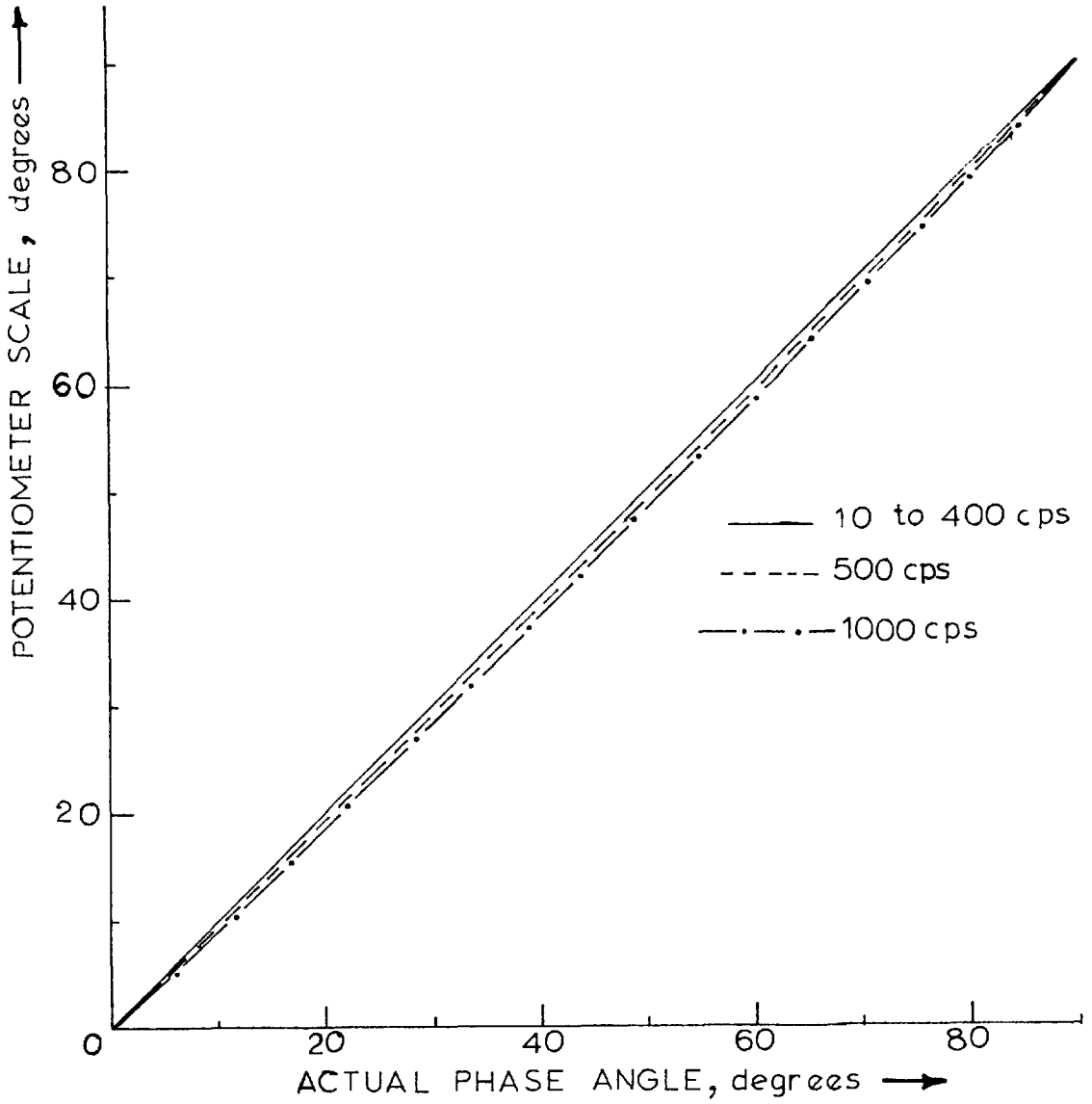

FIG. 3.15 Calibration Graphs for Phase Potentiometer.

the force and the displacement signals was thus obtained by measuring the phase of each of the signals in the way just indicated, and taking the difference.

The phase difference between the force and the displacement signals would normally be less than 90° so that the calibrated range of the potentiometer was basically sufficient for all the phase measurements required. It might happen, however, that one or both of the signals had a phase angle (relative to the 90° output) lying outside the calibrated range. This situation is illustrated in figs 3.16 b and c, where the shaded portion represents the calibrated quadrant. Under this condition, it would no longer be possible to measure the phase of both signals as explained above.

One way of overcoming this difficulty was to change the sign of one of the signals applied to the potentiometer terminals without altering its magnitude. To do this a well-balanced centre-tapped transformer of unity turns ratio was introduced in the 0° channel. This provided two outputs 180° out of phase (one in phase with the 0° signal, and the other of negative sign relative to it) and of equal amplitude. These could then be connected in turn by means of a switch to the 0° end of the phase potentiometer. The range of the calibration was thus effectively extended to cover another quadrant, so that the

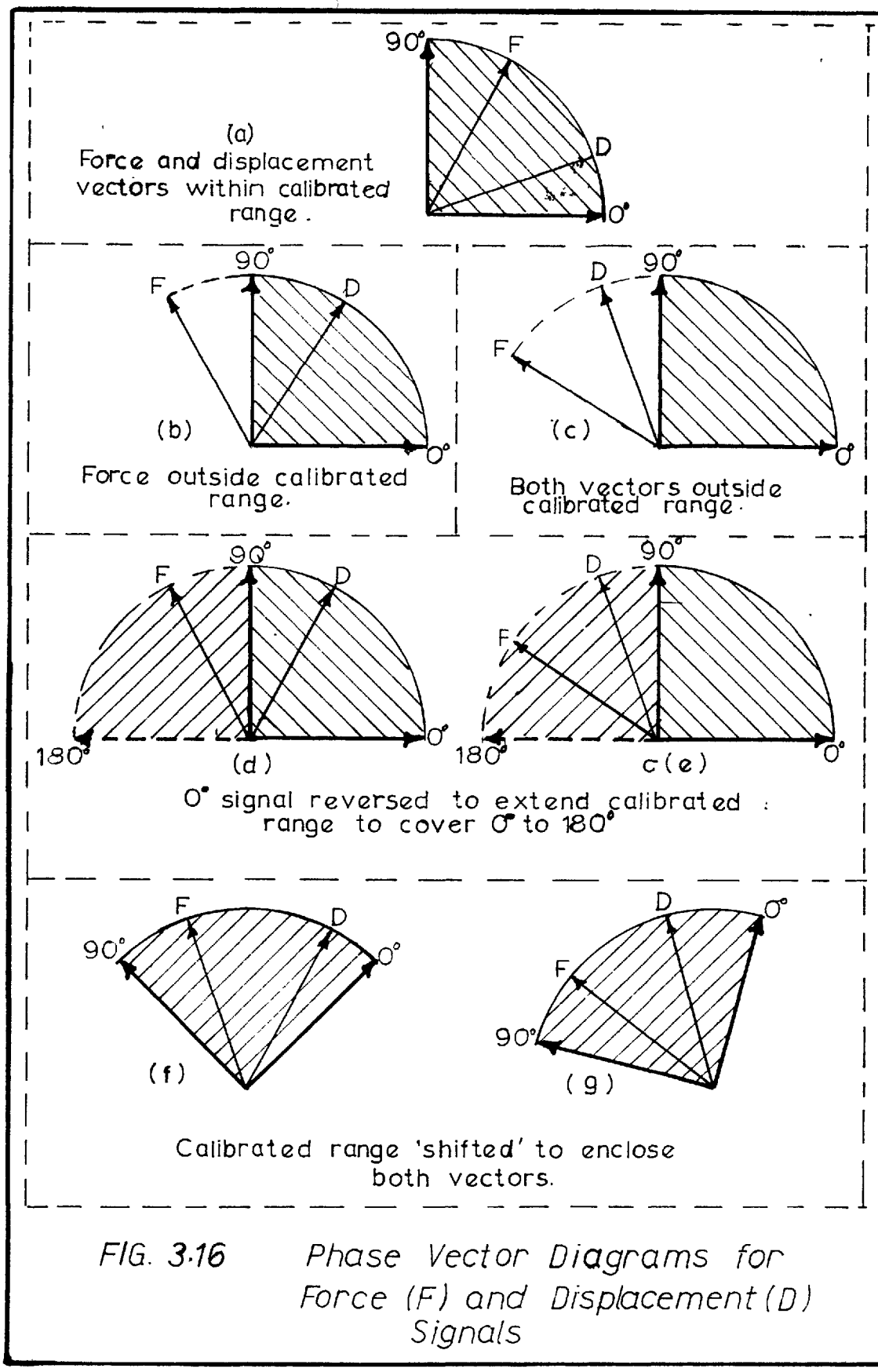

FIG. 3.16 *Phase Vector Diagrams for Force (F) and Displacement (D) Signals*

arrangement could measure any phase between 0° and 180° (and hence between 180° and 360°) - figs 3.16 d and e.

Another solution involved "shifting" the calibrated range appropriately to enclose the two signals - figs 3.16 f and g. This was done using the phase shifting network already mentioned, which was simply a series arrangement of resistances and capacitances so chosen as to produce the required phase shift (see fig. 3.17). In using this method, it was essential that the impedance of the phase shifting network was high compared with that of the potentiometer, so that its introduction did not affect the performance of the oscillator. This second method was employed in the tests reported in this chapter. For the beam tests reported in chapter 5, the first method was found more convenient, and was, therefore, used.

It is interesting to compare the merits and demerits of the two methods of phase measurement - the counter, and the phase potentiometer - in relation to the tests contemplated. As has already been pointed out, the counter was very accurate at low frequencies. Its accuracy, however, was frequency-dependent, and the higher the frequency, the less able it was to detect small phase differences. At about 500 c.p.s., for example, its minimum resolution was about 0.3 of a degree. Moreover, this accuracy was greatly affected by noise levels which could cause as much as

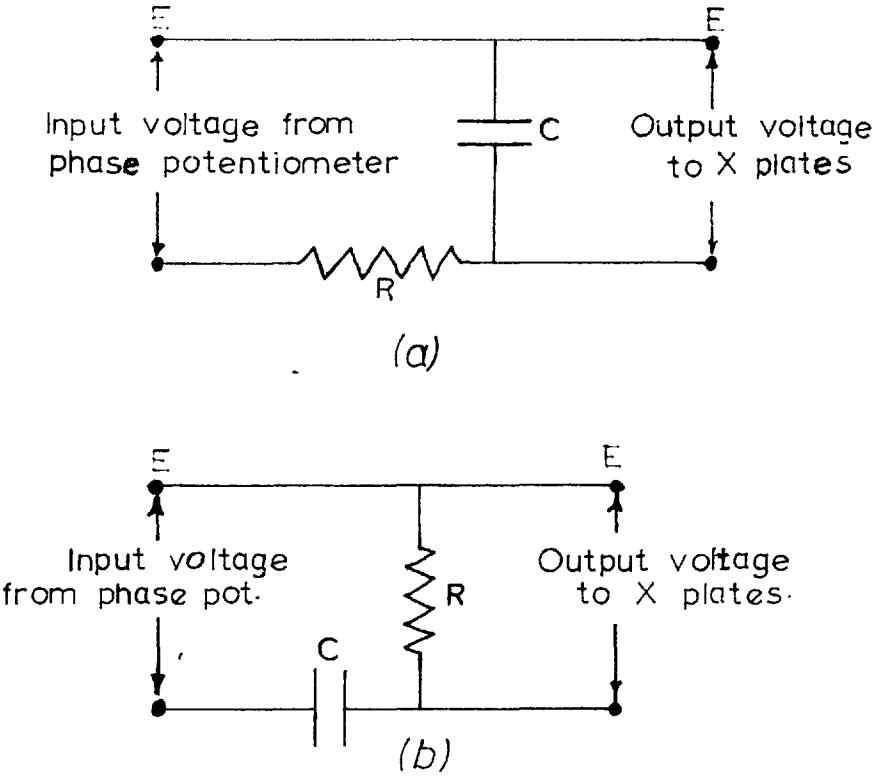

FIG. 3.17 Phase Shifting Circuits.

100 per cent error. The potentiometer accuracy depended on the accuracy of locating the "straight line condition". This depended mainly on the magnitude of the signals applied to the X and Y plates. With reasonably large signals (about two inches peak to peak on the scope), changes in phase difference of less than 0.5 degree, could be easily detected. The accuracy of the measurement was not frequency-dependent (provided the calibrated scale was correct for that frequency). Moreover, small noise levels were easily accomodated and only became a nuisance when they were of comparable magnitude with the signals - it would then be difficult to determine the balance condition accurately.

A more significant fact in the comparison is the time required for taking a measurement in either case. Under the most favourable conditions, counter phase measurement would take about 2 minutes to complete, because of the balancing and setting-up operations involved. On the other hand, phase measurement with the potentiometer was a matter of seconds. This difference in time was particularly important as regards temperature control (to be considered in the next section). For reasonably highly damped materials, the energy loss per cycle was appreciable especially at high strains (energy loss being proportional to the square of the amplitude - equation 3.1.ix.a). If the specimen was subjected to this vibration for a long time,

considerable temperature rise would occur, leading to an observable change in the material properties during the time interval required for a reading.

3.5.f,. Temperature control and measurement

It has already been stated that it was necessary to keep the temperature of the specimen at a definite desired value during any set of tests. The specimen temperature would change if the surrounding temperature changed. Also, owing to internal energy loss, temperature rise would occur in the specimen if it was subjected to vibration for some time. In addition to these, there was an easy 'heat path' from the vibrator out-put drive (via the aluminium drive rod and the aluminium centre-piece) to the specimen, so that any rise in temperature in the vibrator easily affected it.

In view of this, temperature control was effected by controlling the temperature of the room, i.e. heating up the room for high temperature tests, and cooling it down for low temperatures. Also, a constant stream of air was blown against the specimen to help keep it at a constant temperature close to that of the surroundings and the vibrator was kept air-cooled all through the tests.

Next it was necessary to measure this temperature - and hence check that it was really constant. This was done

using a standard copper - constantan thermocouple. For the soft specimens, the thermocouple was easily embedded in the specimens. For the hard specimens, the thermocouples were located in holes drilled on the fixed supports and on the centre-piece, close to the interfaces. The calibration graph for the thermocouple is shown in fig. 3.18.

With the method of temperature control mentioned above, it was possible to limit temperature fluctuation in the specimen to within ± 0.25°C for all the tests performed.

3.6. Test procedure

3.6.a. Materials tested

The following materials were tested:

Velbex P.V.C.

This was available in sheet form of nominal thickness, 0.160 inch. It is a relatively soft polymer obtained by plasticising polyvinyl chloride with 35 to 40 per cent of phthalate type plasticiser. It is of a black texture and is used in industrial applications such as, washers, shot blast cabinets etc. The details of the specimen layers tested are:

mean thickness of each layer, t_o = 0.152 inch,

total shear area, A, = 2 x 0.5 = 1.00 sq. in.,

total effective inertia mass, m_c = 0.0927 lb.

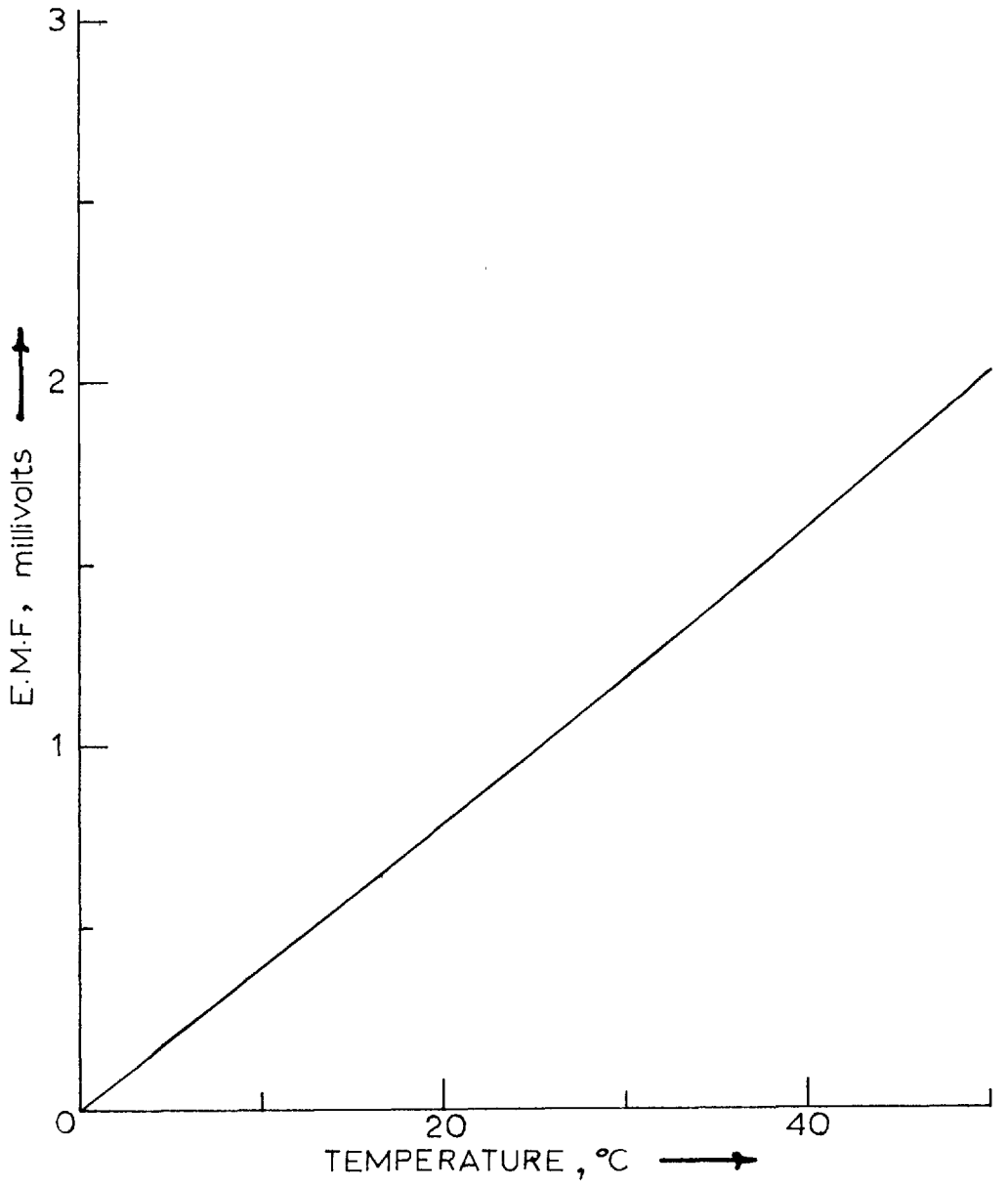

FIG. 3.18 Copper–Constantan Calibration Graph

Hycadamp

This is a mixture of rubber and P.V.C. containing 100 parts of nitrile rubber to 30 parts of P.V.C. It was available in sandwich form, being bonded between two thin backing sheets of aluminium. The material was tested in this form, the aluminium backing layers being glued to the fixed supports and the centre-piece. The mean thickness of each specimen layer was 0.033 inch; and the total shear area was 2 x 0.5 sq. in. The total effective inertia mass, m_c, was 0.0882 lb.

Evoseal 202 and mulseal

These, available in liquid form, are emulsions of rubber latex in a base of liquid bitumen. For evoseal, the mean specimen layer thickness was 0.069 inch, and the total effective inertia mass m_c was 0.0774 lb. The mulseal specimen had a mean layer thickness of 0.168 inch, and the total effective inertia mass was 0.0785 lb. The total shear area in both cases was 2 x 0.479 sq. in.

3.6.b. Detail of tests

The test procedure adopted for each specimen (except mulseal) was as follows.

First, three constant strain, constant temperature tests were carried out. Each test involved keeping the strain amplitude (i.e. the displacement amplitude) constant,

maintaining the specimen temperature at a definite value, varying the forcing frequency in convenient steps, and measuring at each step, the amplitude of the force, and of the displacement, and their phase difference. The three temperatures - the first, a few degrees above the room temperature; the second, room temperature and the third, a few degrees below room temperature - were so chosen as to cover the possible temperature range within which the materials would be used in the subsequent beam tests. All three tests were carried out on the same day, the high temperature test being carried out first, followed by the room temperature test, and then the low temperature test. The value of the strain amplitude was normally the same for all three tests. These constant temperature, constant strain tests will be referred to, in the subsequent sections, simply as "temperature tests".

Next, the frequency and the temperature were both kept constant and the strain amplitude was varied in convenient steps, readings of the force amplitude, displacement amplitude and the phase difference being taken at each step. This was done at two (or more) frequencies, the temperature being maintained constant at about room temperature for each set of readings. This series of tests, also carried out on the same day, will be referred to as 'strain tests'. Finally the room-temperature part of the

temperature tests was carried out again to check for repeatability of results.

Apart from the above tests, it was also thought necessary to check on the shape of the stress - strain curve exhibited by the materials. For this reason the force and the displacement signals were fed to the X and Y plates of one channel of the oscilloscope, and the resulting force - displacement plot was sketched. Fig. 3.39 shows a comparison of one such trace with points on an actual ellipse. The trace was made for an evoseal specimen.

The calibration procedures already outlined were carried out at the beginning and at the end of each set of tests.

The in-phase shear modulus, G', and the loss factor, η_a, were evaluated from the readings using equations 3.3.xii and 3.3.xiii. These two quantities will be utilised in the ensuing discussion as the characterising properties of the materials. To avoid repetition, the in-phase shear modulus, G', will often be called simply the shear modulus (or even, modulus). Also the loss factor may often be referred to as the damping. The material properties have been plotted out against the several variables, as shown in figs 3.19 to 3.39.

Only one temperature test was carried out for mulseal. This was because apart from the fact that it took a

considerable amount of time to set sufficiently hard, it did not show any marked difference in properties from evoseal.

3.7. Discussions

3.7.a. Experimental results.

Velbex P.V.C.

The graphs obtained for P.V.C. are shown in figs 3.19 to 3.23.

Temperature tests

The constant strain, constant temperature graphs are given in figs 3.19 and 3.20. These show that the shear modulus, G', is markedly dependent on frequency, showing a consistent increase with increase in frequency. The rate of increase of modulus with frequency, for each of the curves, decreases as the frequency increases. This suggests that the material is within the portion of the transition zone close to the rubbery region (see fig. 3.2). The damping, on the other hand, shows a much less distinct variation with frequency. The loss factor is seen to increase initially with frequency and then to remain more or less constant at higher frequencies.

Temperature effects can also be easily observed in these graphs. The shear modulus shows a pronounced temperature-dependence, decreasing rather rapidly as the

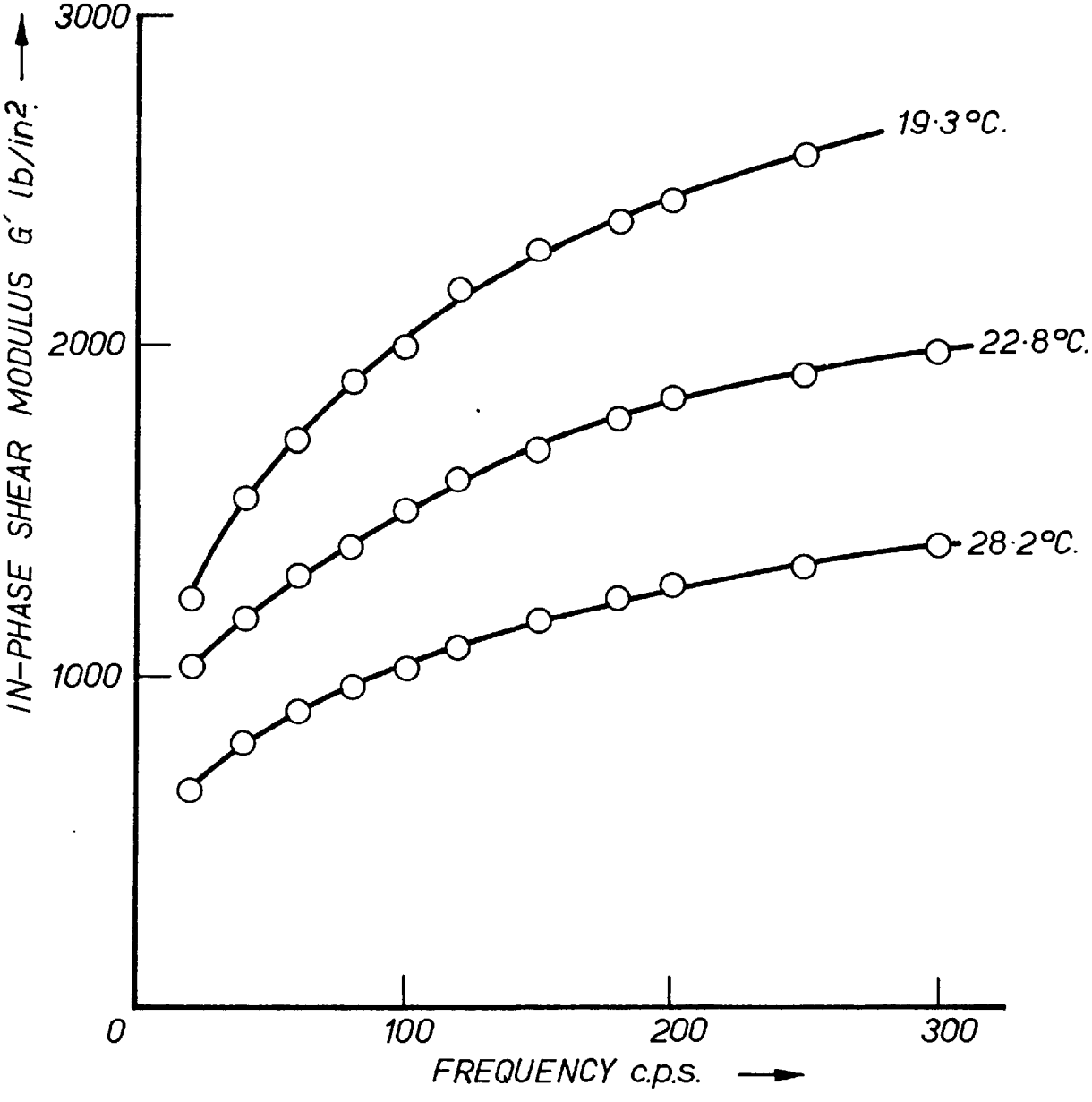

FIG. 3·19 : VELBEX P.V.C. —

Variation of Elastic Shear Modulus with Frequency at a constant strain amplitude of $5{\cdot}27 \times 10^{-3}$

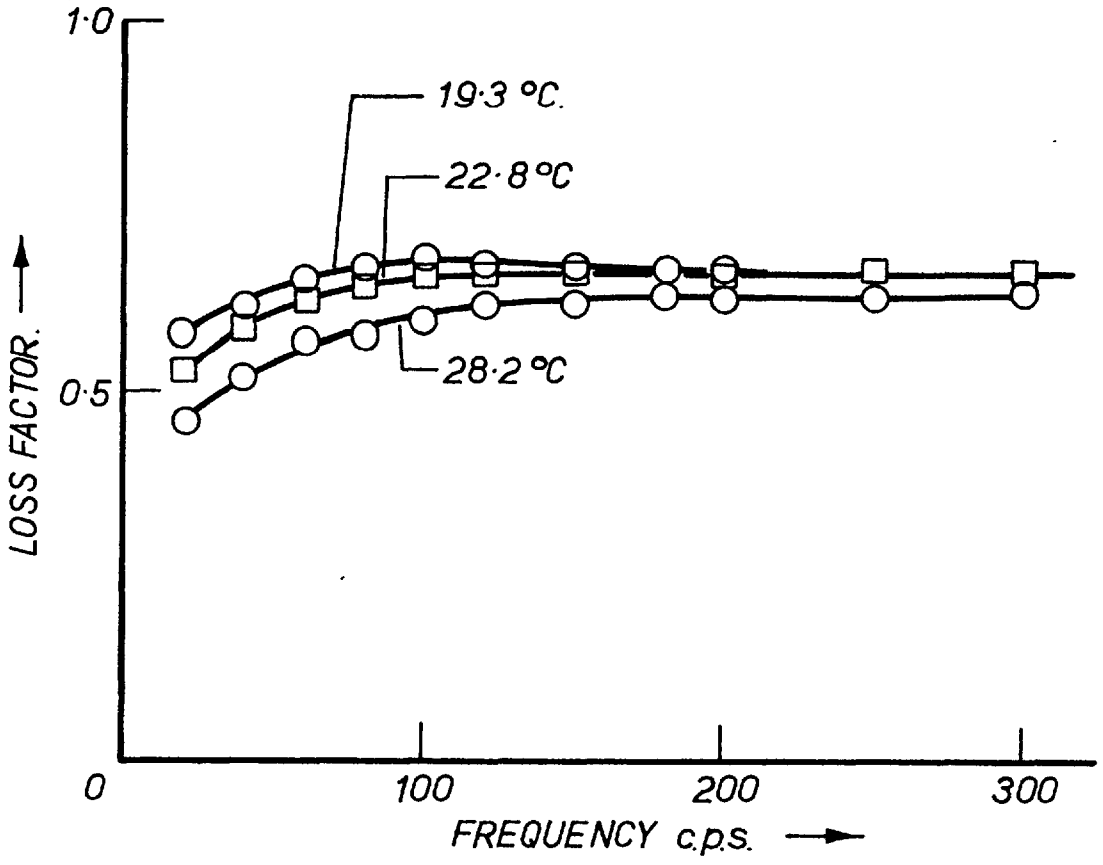

FIG. 3.20 : VELBEX P.V.C. ——

Variation of Loss Factor with Frequency at a constant strain amplitude of $5{\cdot}27 \times 10^{-3}$.

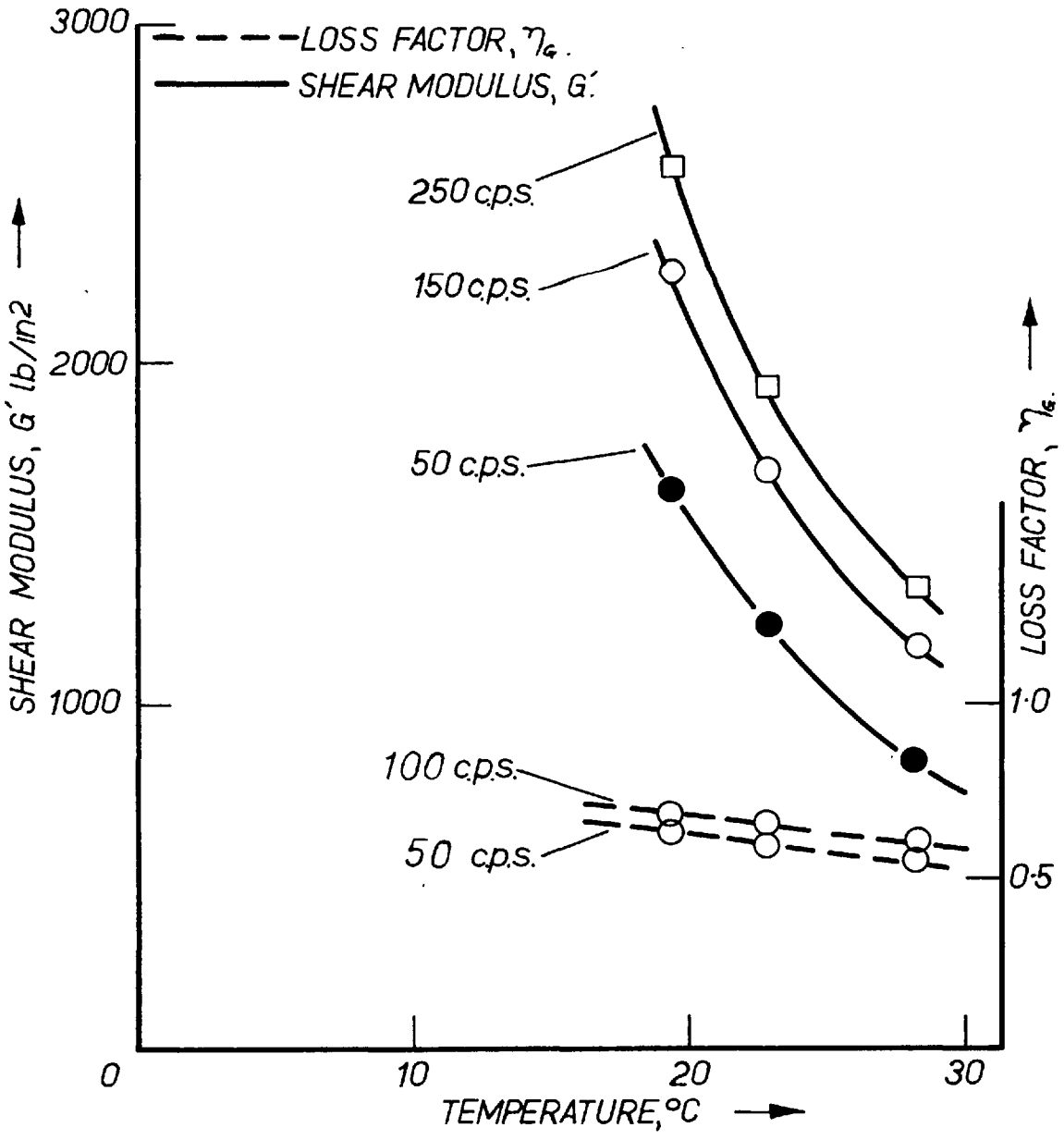

FIG. 3.21 : VELBEX PVC. ——

Variation of Shear Modulus G' and Loss Factor η_G with Temperature.

Shear strain amplitude kept constant at $5{\cdot}27 \times 10^{-3}$.

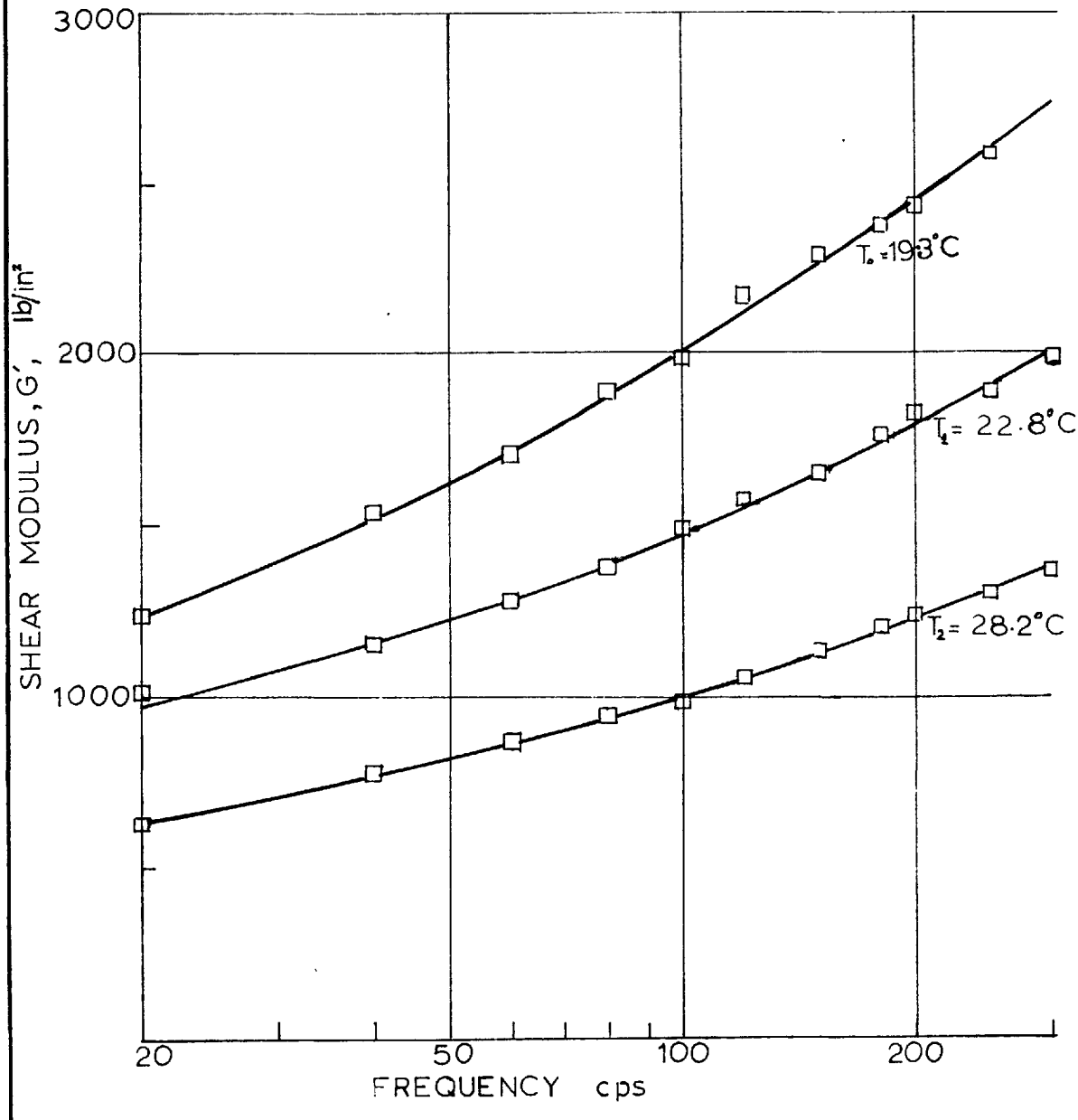

FIG. 3·22 Velbex P.V.C
Variation of In-phase Shear Modulus with Log Frequency at constant Shear strain amplitude of $5{\cdot}27 \times 10^{-3}$.

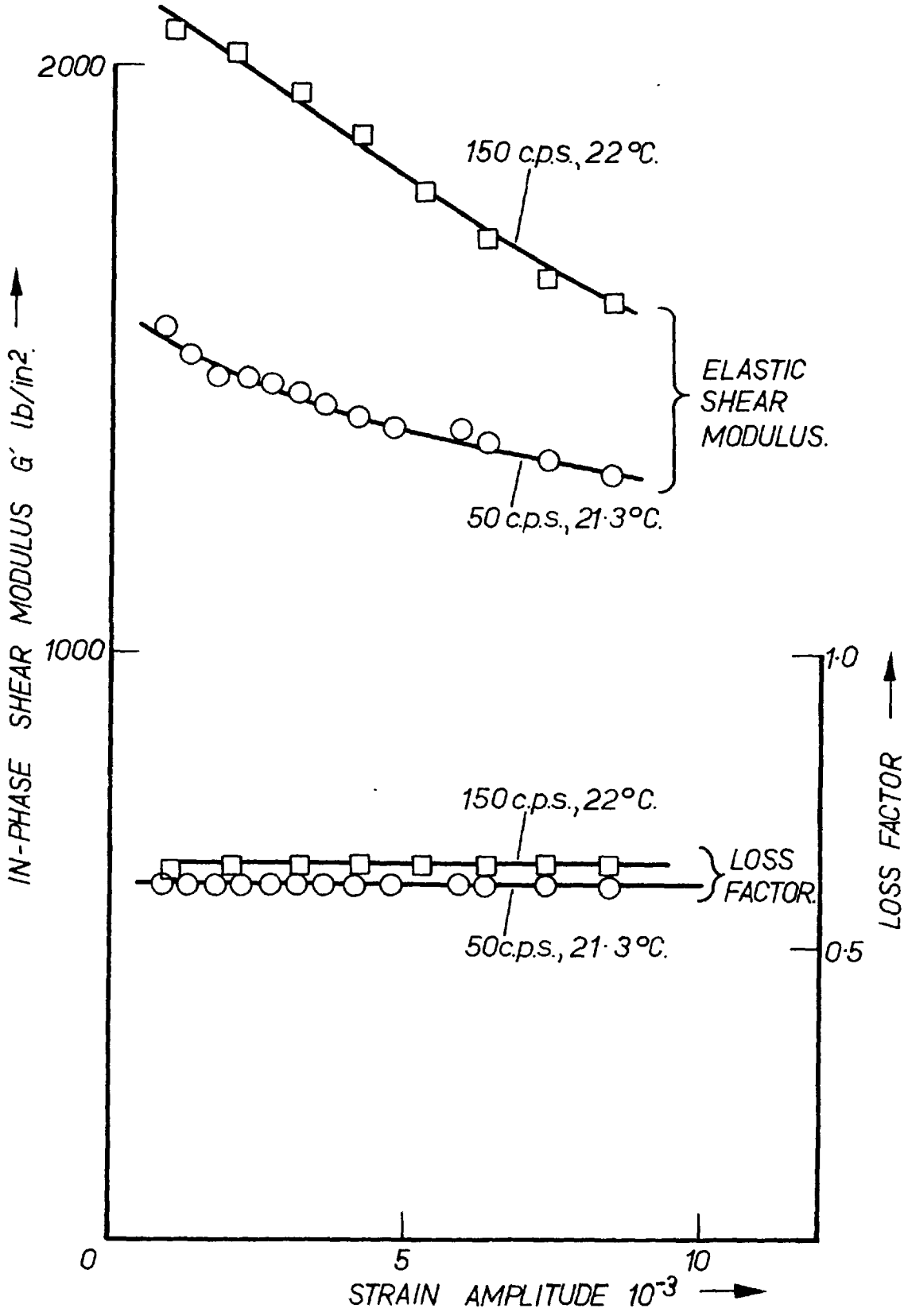

FIG. 3.23 : VELBEX P.V.C. ——
Variation of In-Phase Shear Modulus and Loss Factor with amplitude.

temperature increases. The loss factor also shows a similar trend, confirming the prediction already made, that the material must be on the "rubbery side" of the glass transition zone. The "three-point" graphs of fig. 3.21 may help to give a clearer picture of the dependence on temperature. These are cross-plots from the constant temperature, constant strain graphs, and they show the variation of the shear modulus and the loss factor with temperature, at given frequency and strain amplitude.

The shape of the modulus-versus-frequency graphs was checked using the method of reduced variables explained in section 3.2.c. From the graph of G′ against log. frequency, - fig. 3.22 - the intercepts on lines of constant modulus were measured and laid out in tabular form (table 3.a). Very good agreement is seen to hold, the maximum deviation of any of the intercepts from the mean intercept being about 3 per cent in the frequency range, 20 to 300 c.p.s., covered.

Strain tests

Fig. 3.23 shows the variation of the shear modulus and the loss factor with strain amplitude at constant temperature and frequency. The shear modulus is seen to decrease with increase in strain amplitude, whilst the loss factor is virtually strain-independent. It is, however, seen that the variation of G′ with the strain amplitude is rather slow.

Constant shear modulus, G′ lb/sq. in.	Intercept between T_o and T_1 curves cm	Intercept between T_o and T_2 curves cm
1250	4.7	11.5
1350	4.8	11.6
1500	4.9	11.3
1600	4.9	—
1700	5.0	—
1800	5.0	—
1900	5.1	—
2000	5.1	—
Mean length of intercept	4.94	11.5
Max. percentage deviation from mean	3.2	1.7
Frequency range covered	20 to 300 c/s	20 to 300 c/s

TABLE 3.a

Constant modulus intercepts for P.V.C. (obtained from fig 3.22)

$T_o = 19.3^oC$; $T_1 = 22.8^oC$; $T_2 = 28.2^oC$

For instance, a change in the strain amplitude from 2 per cent to five times this value, causes a drop in G' of less than 20 per cent, at 150 c.p.s., and 22°C.

Within the frequency, and temperature ranges of the tests, the variation of G' with temperature, frequency, and strain can be represented in the single equation;

$$G' = e^{(29.9336 - \frac{T}{12.7143})} \left\{(0.9202\ f^n - 0.3439) + (1.3799\ f^n - 2.2022)\ e^{-\alpha_s \hat{\phi}}\right\}$$

where $n = 0.1621$, $\alpha_s = 184.9$, f = the frequency in c.p.s., $\hat{\phi}$ is the strain amplitude, and T is the temperature in degrees Absolute (Centigrade scale).
This expression was found very convenient for purposes of digital computation (see chapter 4).

After the beam tests of chapter 5, the above shear tests were repeated for a specimen of P.V.C. cut out from the same sheet. This was meant to be a check on the results given above. Fig 3.24 gives a comparison of the results of this test with the results given in figs 3.19 to 3.22 for two temperatures, 18°C and 23.3°C, and a strain amplitude of 3.06×10^{-3}. Good agreement is seen to hold for the shear modulus, G'. The loss factor-versus-frequency curves, however, show a difference of up to 5 per cent. This difference cannot be attributed to calibration errors, as

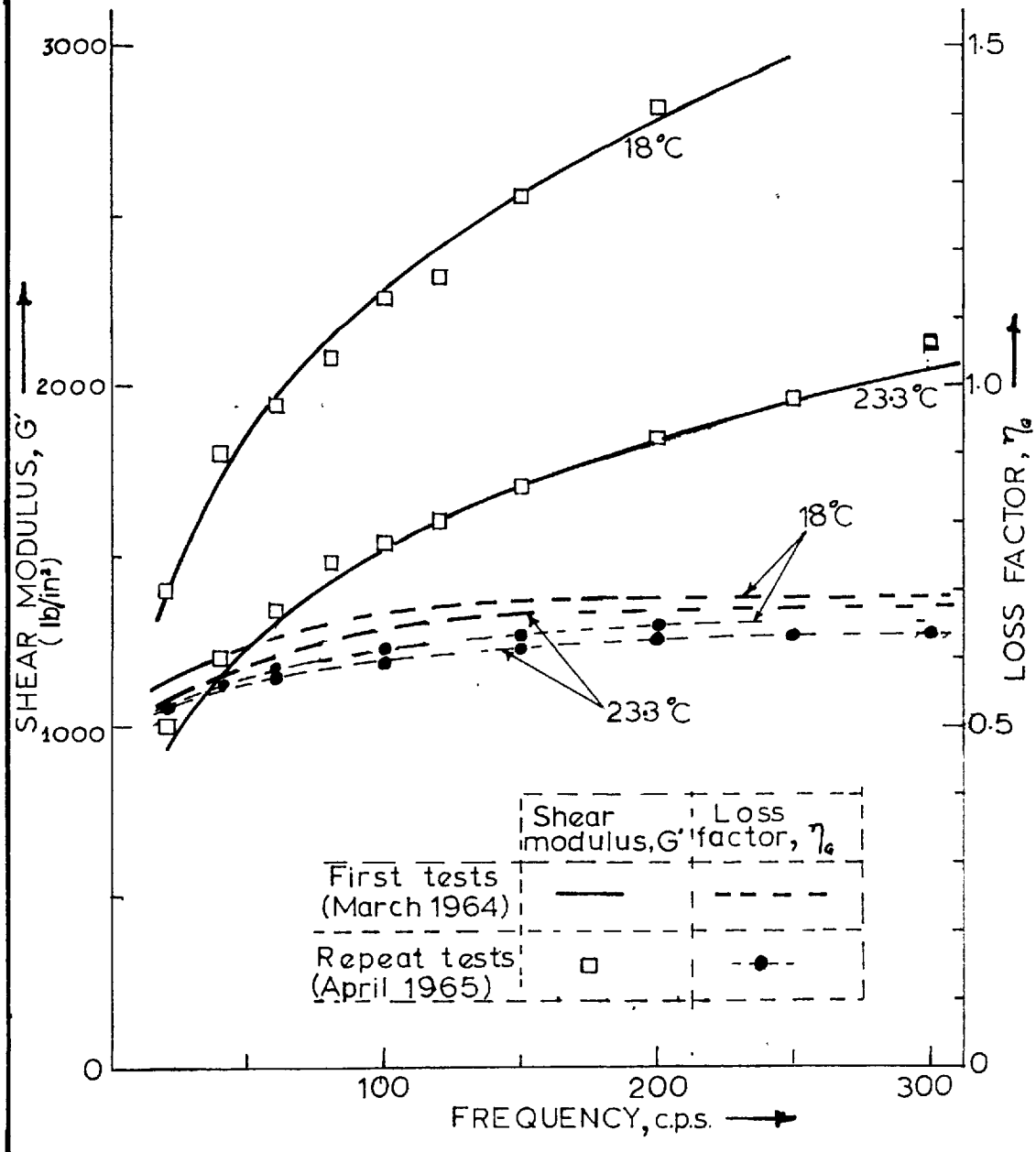

FIG. 3·24 Velbex P.V.C.
Comparison of In-phase Shear Modulus G' and Loss Factor η_6 obtained from two tests. Shear Strain amplitude constant at $3{\cdot}06 \times 10^{-3}$

the calibrations of the first test were checked and found correct. (The same measuring circuit was used in both tests). It is not clear whether the difference was due to a variation in the loss factor with the age of the specimen (the second test was carried out about a year after the first) or to local variation in the properties within the same sheet of material. However, the results implied a possibility of error of up to 5 per cent in the material loss factor. The material properties used in the calculations for the beam tests of chapter 5, were those obtained during the first test (figs 3.19 to 3.23), as these were the only values available at the time.

Evoseal 202

Temperature tests

Figs 3.25 and 3.26 show the variation of the shear modulus, G', and the loss factor, η_a, with frequency for evoseal. The tests were carried out after the evoseal had cured for twelve weeks. The graphs of the shear modulus against the frequency are similar to those for P.V.C. Temperature effects are, however, much more marked as is easily seen from fig. 3.27 which gives the variation of both the shear modulus and the loss factor with temperature at given frequency and strain amplitude. The loss factor is seen to increase with temperature, which seems to suggest

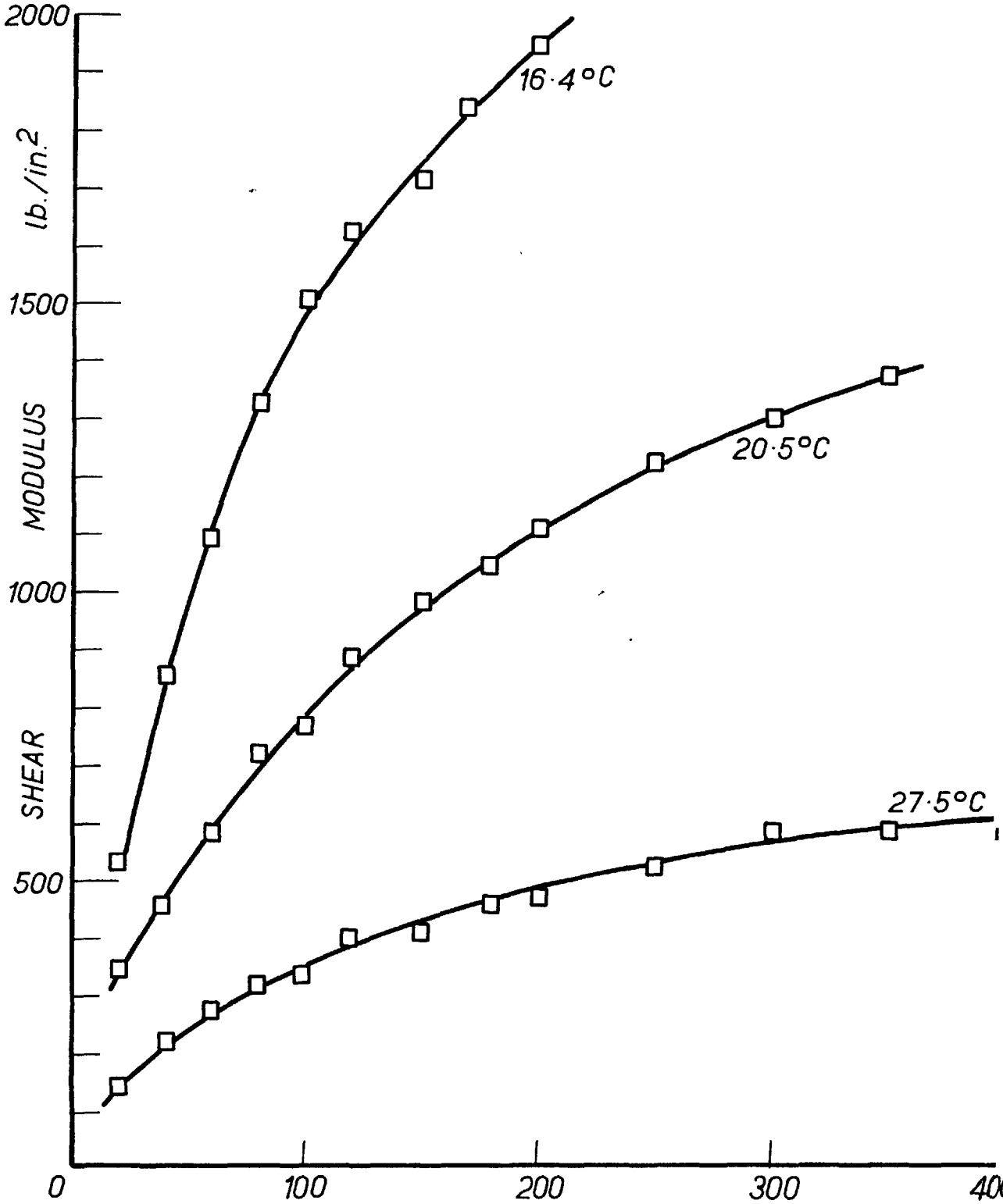

FIG. 3.25

EVOSEAL 202 — Variation of Shear Modulus with Frequency at three temperatures.
Strain constant at $5 \cdot 46 \times 10^{-3}$

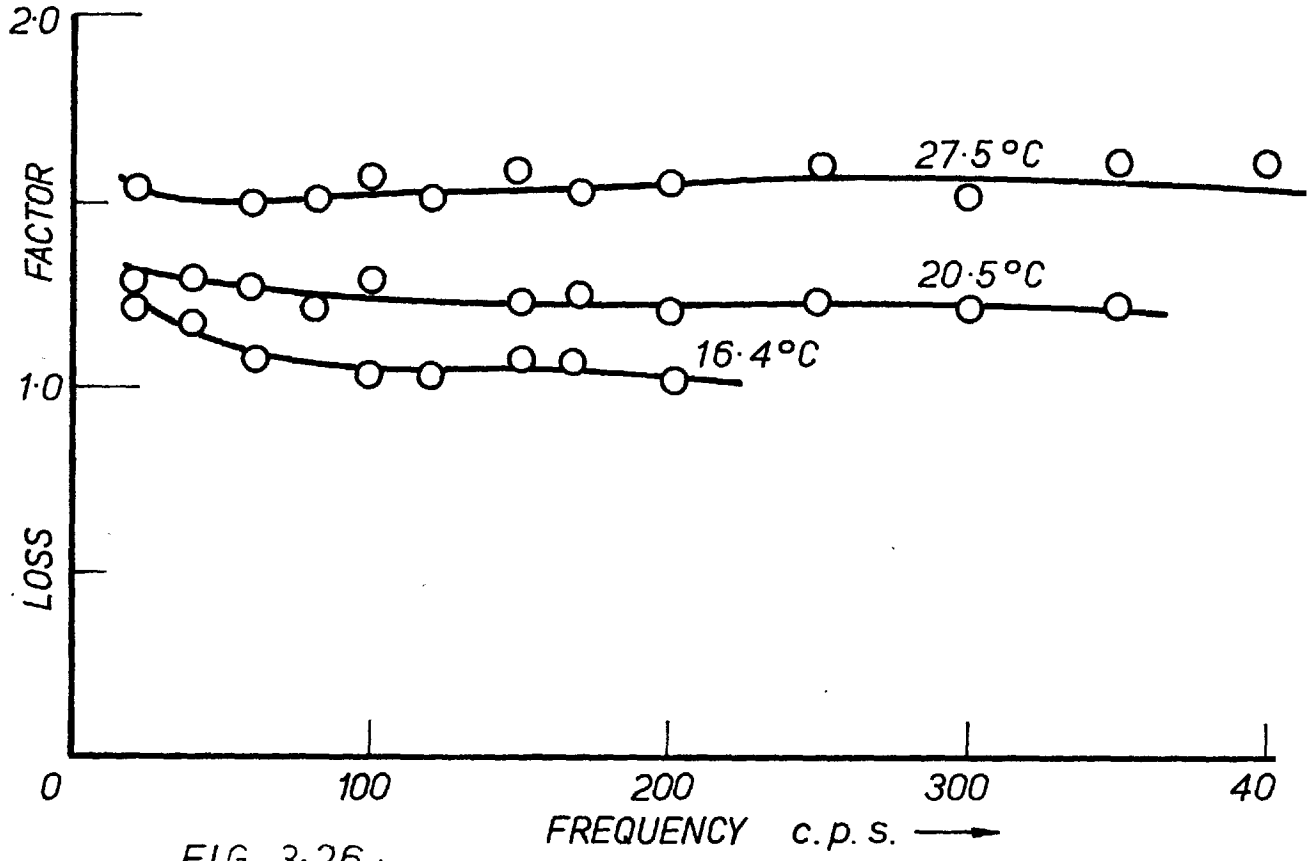

FIG. 3·26 :
EVOSEAL 202 — Variation of Loss Factor with Frequenc at three temperatures.
Shear Strain constant at $5 \cdot 46 \times 10^{-3}$

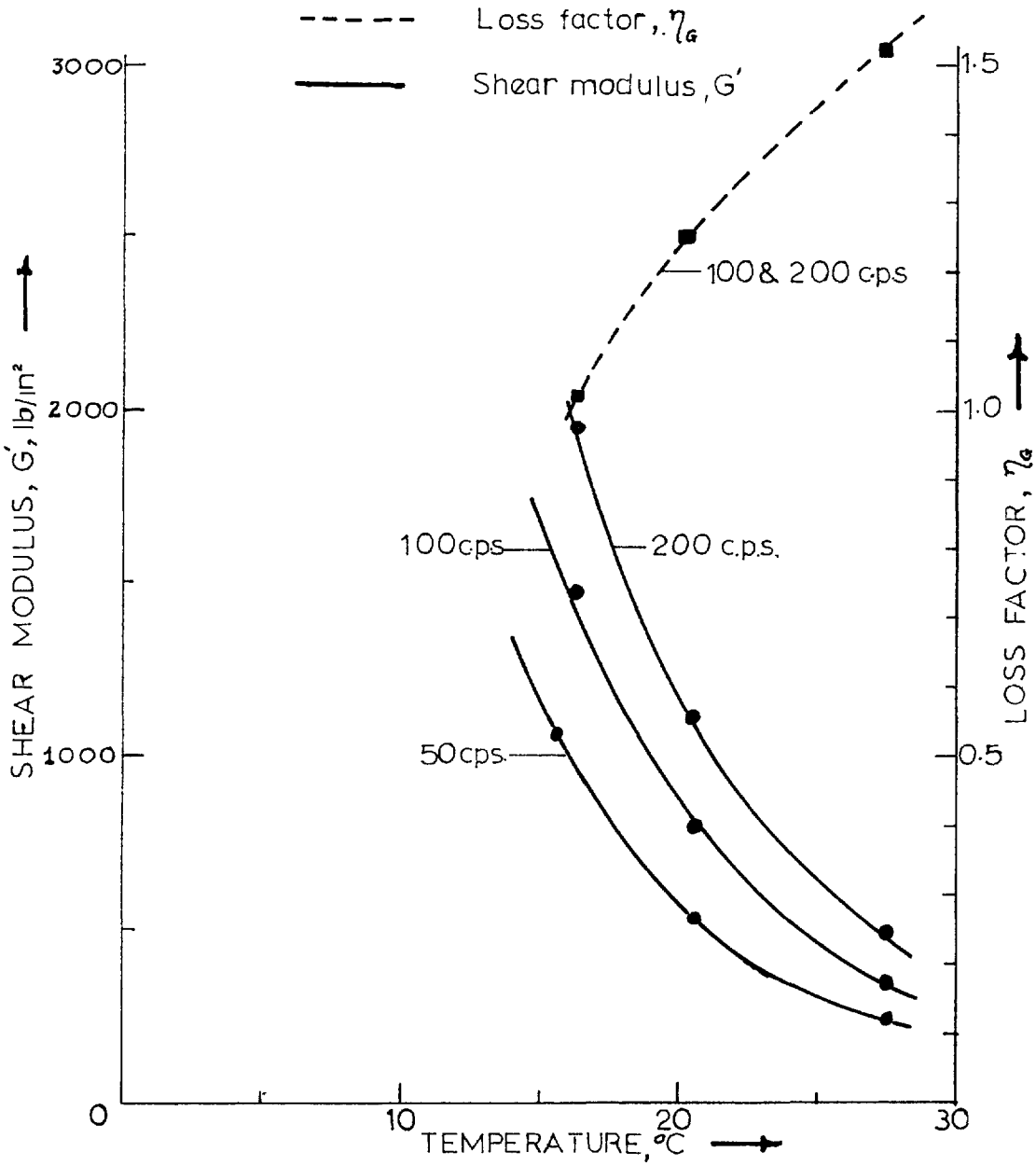

FIG. 3·27 EVOSEAL
Variation of Shear Modulus G' and Loss Factor η_G with Temperature.
Shear strain amplitude const. at $5{\cdot}46 \times 10^{-3}$

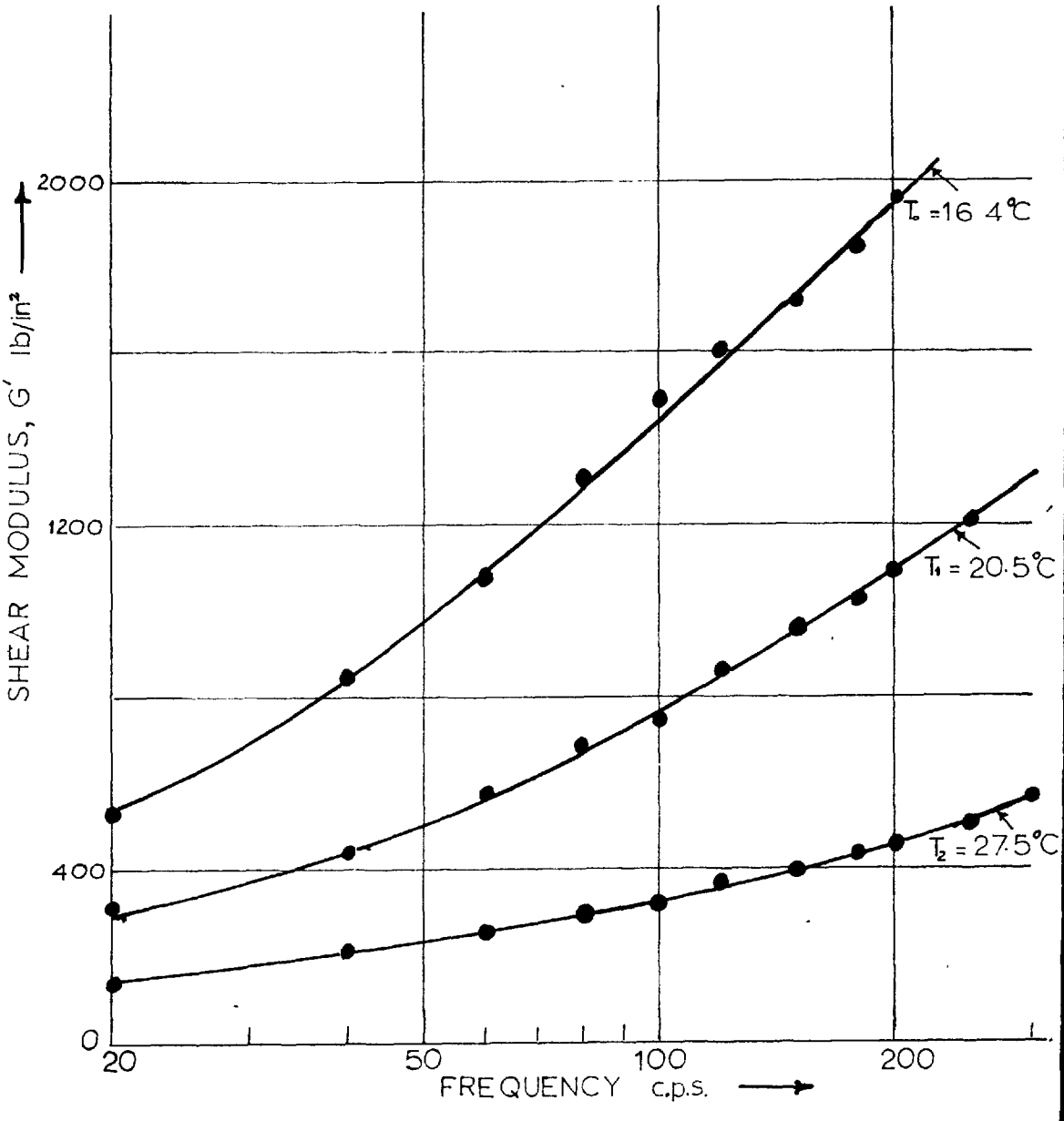

FIG. 3.28 EVOSEAL

Variation of In-phase Shear Modulus G' with Log. Frequency. Shear strain amplitude constant at 5.46×10^{-3}

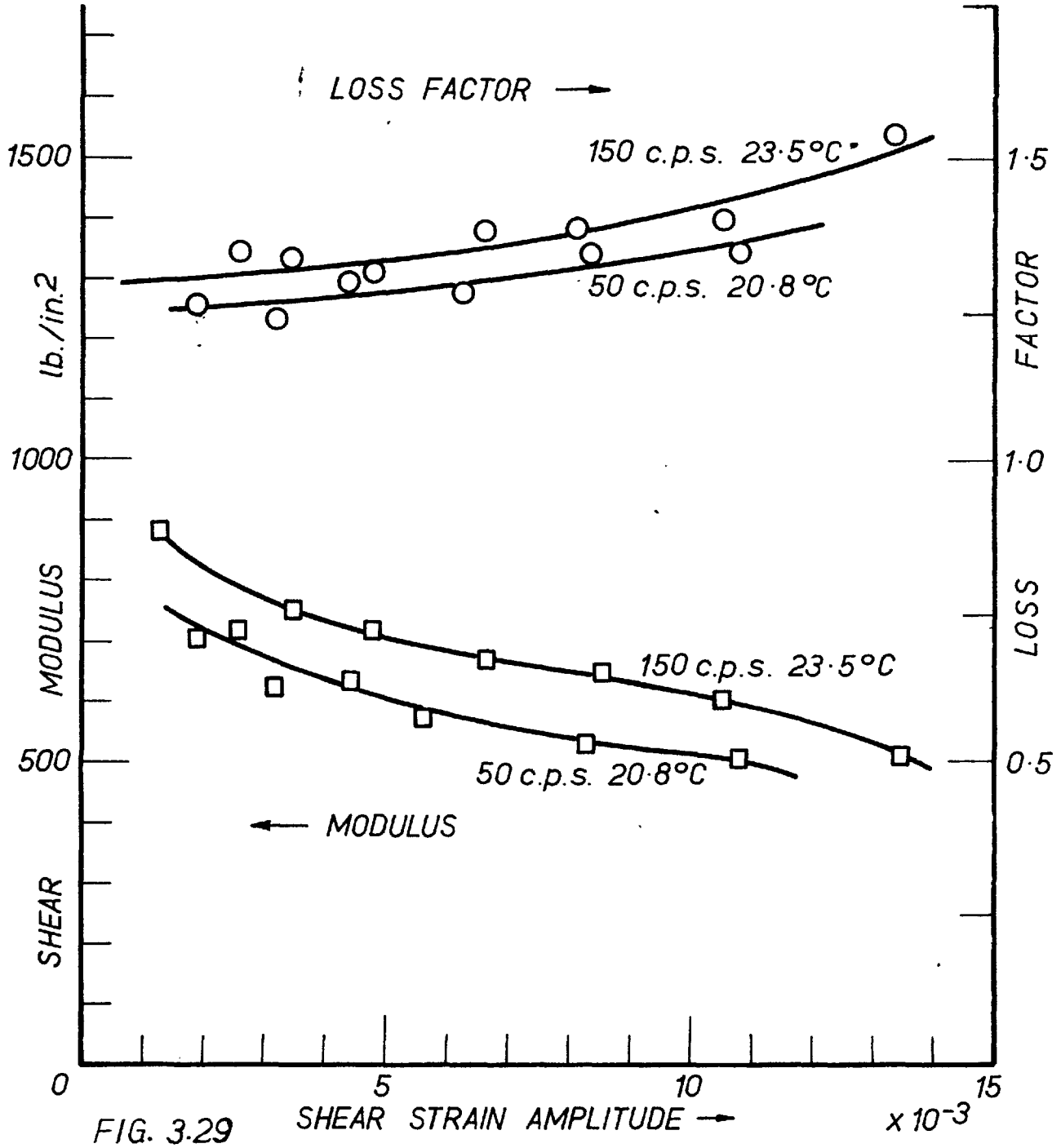

FIG. 3.29 EVOSEAL 202 — Variation of Shear Modulus and Loss Factor with Strain at Constant Temperature & Frequencies.

that the material is still on the rising portion of the damping-versus-temperature curve of fig. 3.2.

Fig. 3.28 gives the graph of the shear modulus against log. frequency. The usual check on the shape of the curves was carried out, and a reasonably good agreement was obtained for most of the range, as can be seen from table 3.b. The maximum deviation from the mean length was about 9 per cent.

It may be pointed out that for this material, the loss factor varies only slightly with the frequency.

Strain tests

Fig. 3.29 shows the dependence of these properties on the strain amplitude. Whilst the shear modulus decreases with the strain amplitude as for P.V.C., the loss factor shows a slight increase with strain. Again, the variation of both the shear modulus and the loss factor with the strain amplitude is seen to be slow.

Dependence of the properties on the time of cure

The properties of evoseal (and mulseal) very much depend on the 'time of cure' of the specimen. This is because the material, originally in liquid form, takes some time to dry out, a process which affects its properties. Fig. 3.30 gives the variation of the shear modulus and the loss factor with time, for a specimen of evoseal prepared during the period when the beam tests (reported in chapter 5)

Constant shear modulus, G′ lb/sq. in.	Intercept between T_o and T_1 curves cm	Intercept between T_o and T_2 curves cm
560	5.1	13.0
640	5.1	13.0
720	5.2	13.1
800	5.3	13.2
880	5.3	-
960	5.5	-
1040	5.7	-
1120	5.9	-
1200	6.0	-
Mean length of intercept	5.5	13.1
Max. percentage deviation from mean	9.1	0.85
Frequency range covered	20 to 300 c/s	20 to 300 c/s

TABLE 3.b

Constant modulus intercepts for evoseal, obtained from fig 3.2

T_o = 16.4°C ; T_1 = 20.5°C ; T_2 = 27.5°C

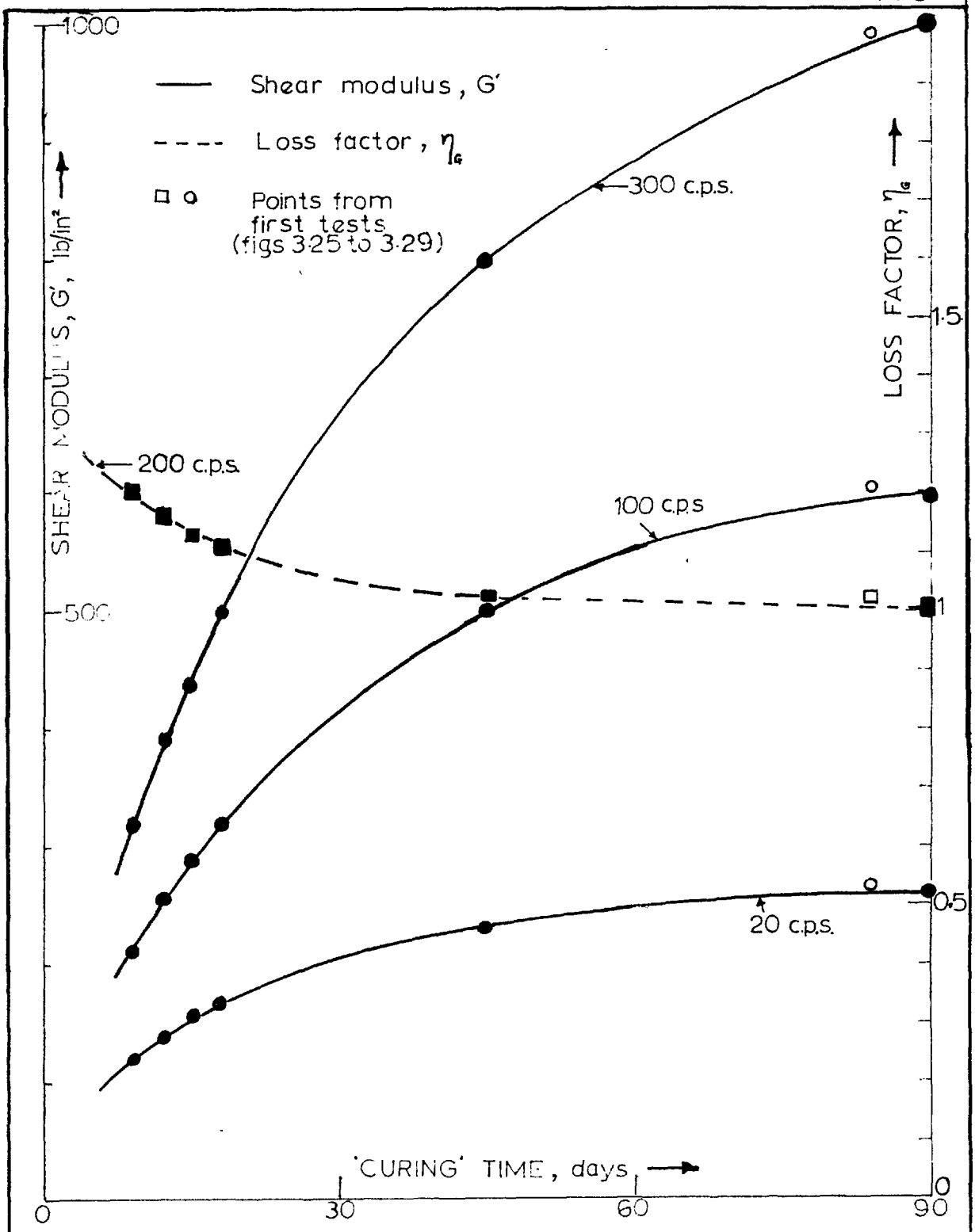

FIG. 3.30 Curing Curve for Evoseal. Graphs of Shear modulus, G', and Loss factor, η_G, against curing time at constant Temp. 22.5°C and strain amplitude of 7.15×10^{-3}

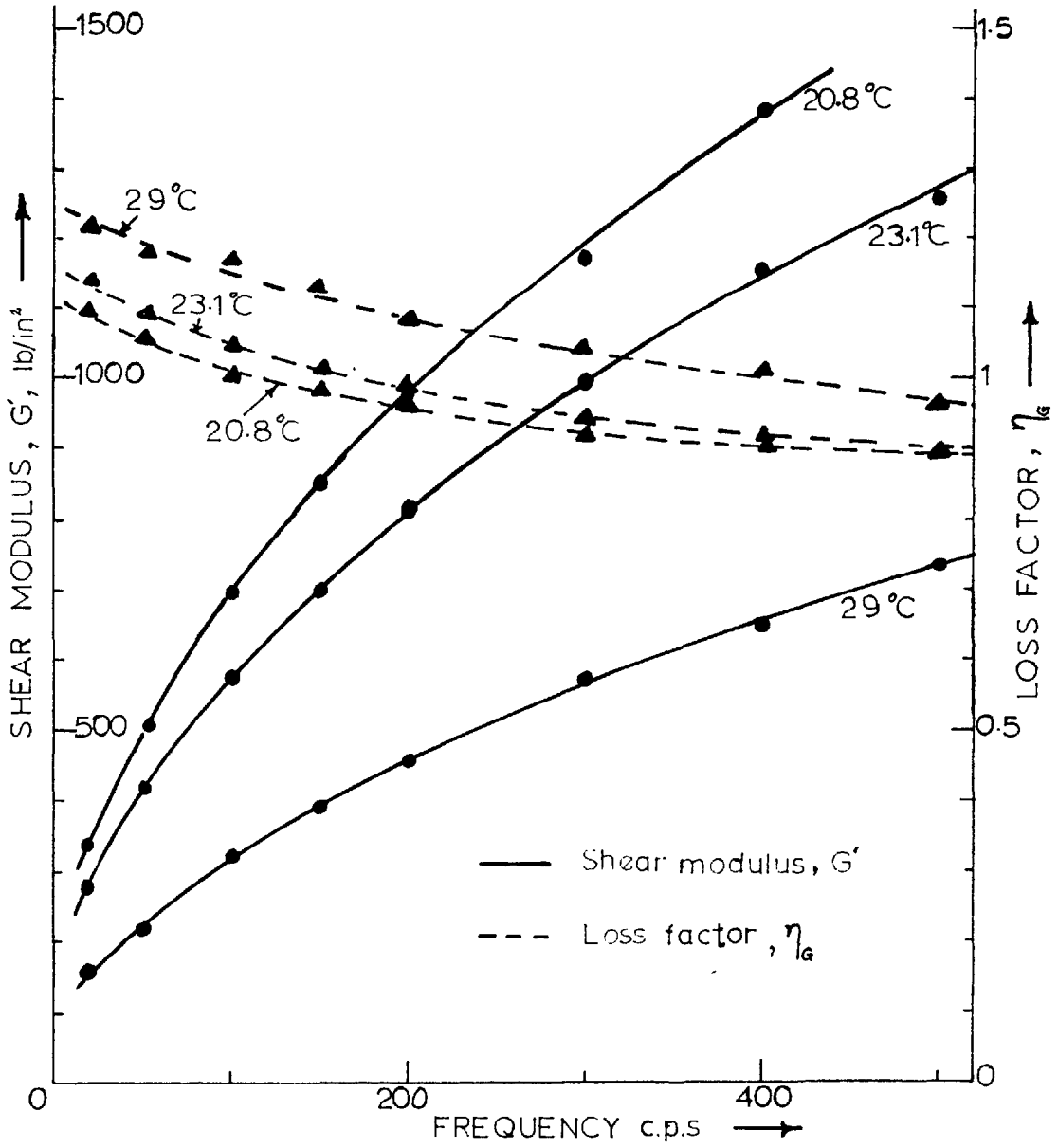

FIG. 3·31 *Evoseal (Tests immediately before the beam tests).*
Variation of Shear modulus, G', and Loss factor, η_G, with Frequency.
Shear strain amplitude constant at $5{\cdot}53 \times 10^{-3}$

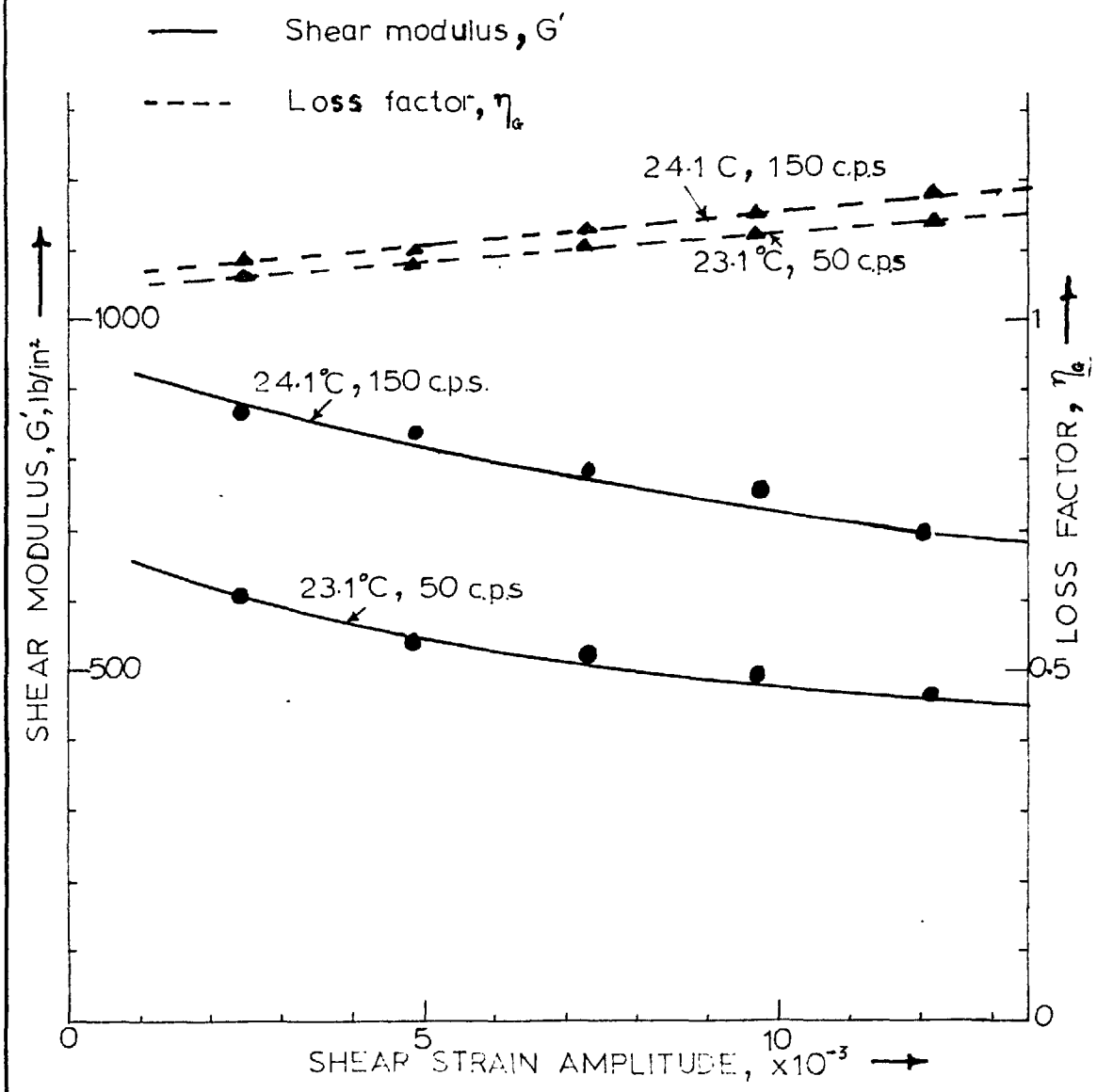

FIG. 3·32 *Evoseal (Tests immediately before the beam tests)*

Variation of Shear modulus, G' and Loss factor, η_G, with Shear strain amplitude.

were being carried out - about a year after the tests reported above. It is seen from the graphs that the shear modulus kept increasing with time for the three months during which the tests were carried out, the approach to steady values being rather slow. The loss factor, however, varied only slightly with time. Also indicated on the graphs, are points corresponding to the test results of figs 3.25 to 3.29. These lie close to the curves, implying that the shear specimens for both tests must have been curing at about the same rate.

Figs 3.31 and 3.32 give the results of the shear tests carried out on the evoseal specimen immediately before the corresponding beam tests were carried out. These were used in the theoretical calculations for predicting the beam responses.

Hycadamp

Temperature tests

The shear modulus-versus-frequency graphs for this material, fig. 3.33, have rather peculiar shapes. Each curve seems to exhibit a point of inflexion, at which the slope passes through a minimum value. For the modulus-versus-log. frequency graphs shown in fig. 3.34, the intercepts on lines of constant modulus show first a distinct region of constant intercept, followed by a kind of 'transition' region where the intercept varies rapidly,

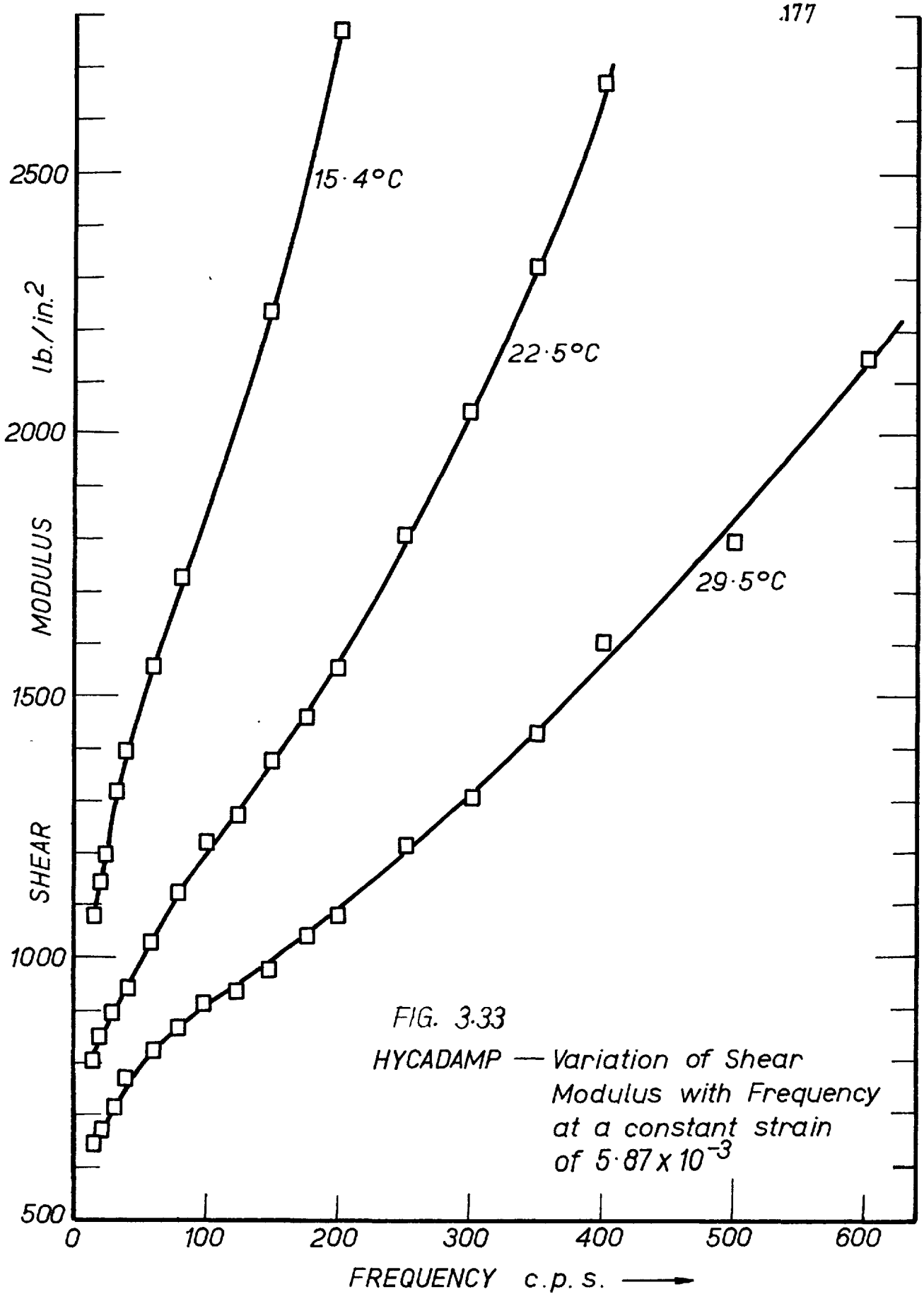

FIG. 3.33

HYCADAMP — Variation of Shear Modulus with Frequency at a constant strain of $5 \cdot 87 \times 10^{-3}$

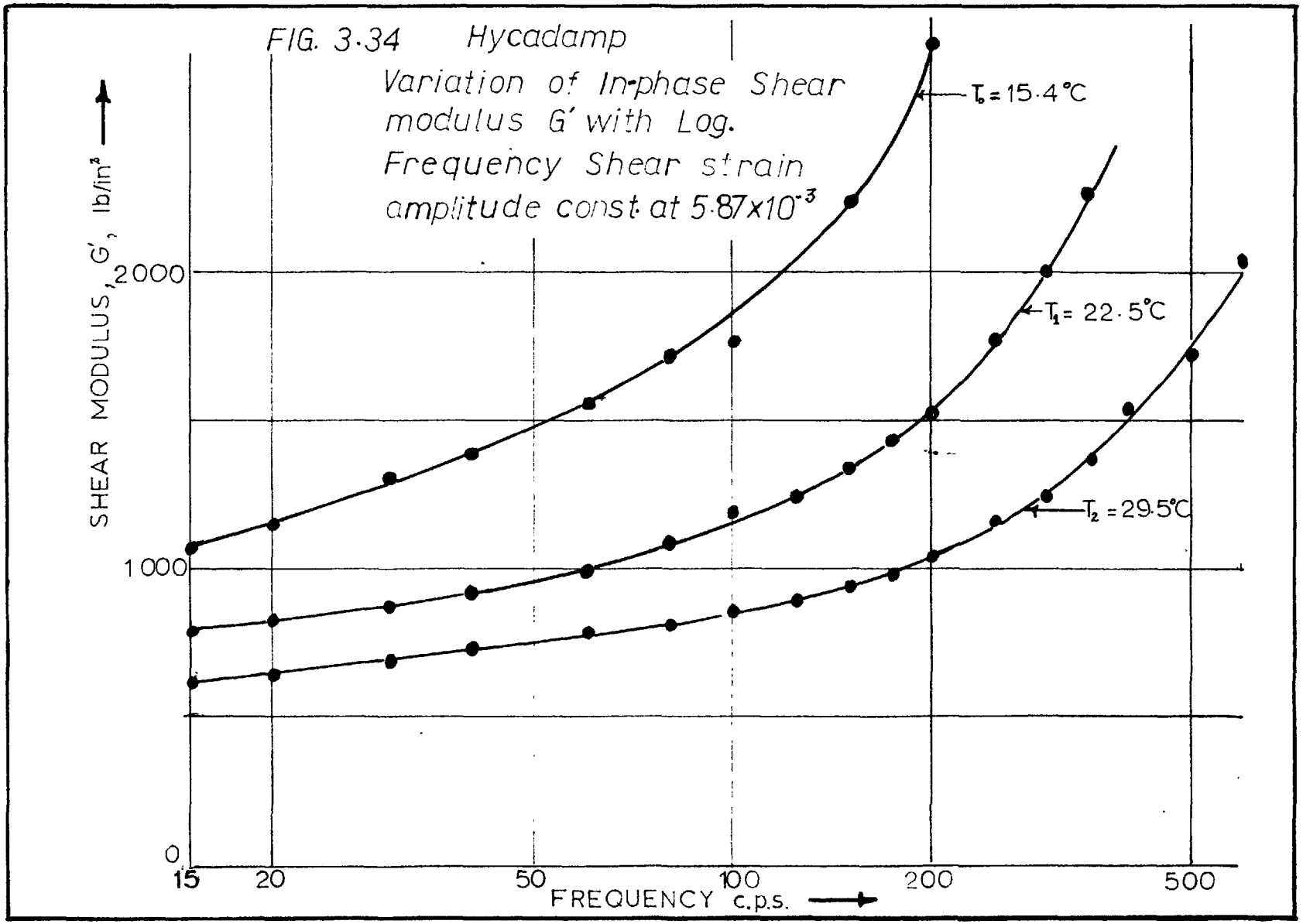
FIG. 3·34 Hycadamp
Variation of In-phase Shear modulus G' with Log. Frequency Shear strain amplitude const. at 5·87x10⁻³
SHEAR MODULUS, G', lb/in²
2000
1000
0
15
20
50
100
200
500
FREQUENCY c.p.s.
T₀ = 15·4°C
T₁ = 22·5°C
T₂ = 29·5°C

Constant modulus, G′ lb/sq. in.	Intercept between T_1 and T_2 curves cm	
800	7.0	First region of constant intercept
850	7.0	
900	6.3	Transition
1000	5.3	
1100	5.0	
1200	4.4	
1400	3.8	
1500	3.5	Second region of constant intercept
1600	3.5	
1700	3.5	
1800	3.5	
2000	3.5	

Frequency range covered 20 and 500 c/s

TABLE 3.c

Constant modulus intercepts for hycadamp, from fig. 3.34

$T_1 = 22.5^{\circ}C$; $T_2 = 29.5^{\circ}C$

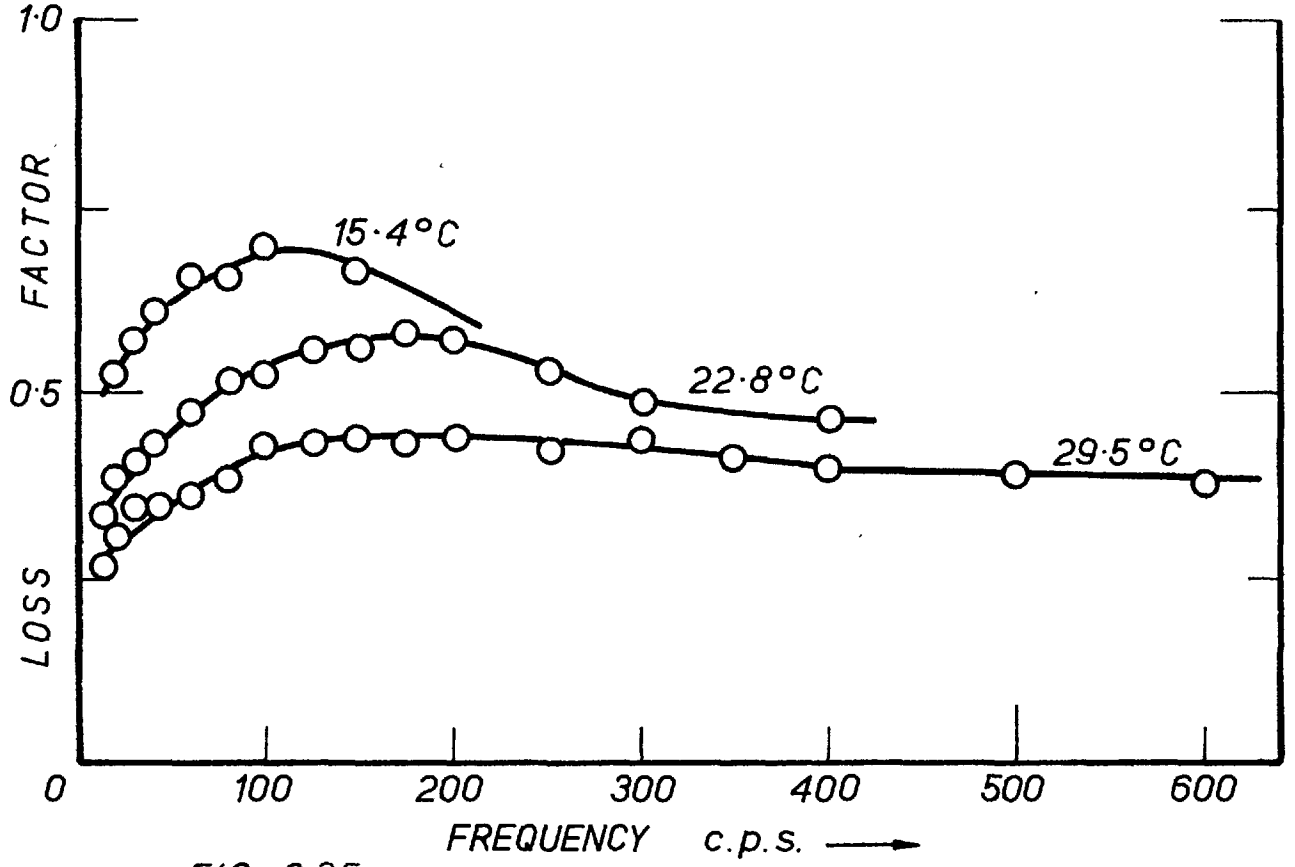

FIG. 3.35
HYCADAMP — Variation of Loss Factor with Frequency at a constant strain of $5 \cdot 87 \times 10^{-3}$

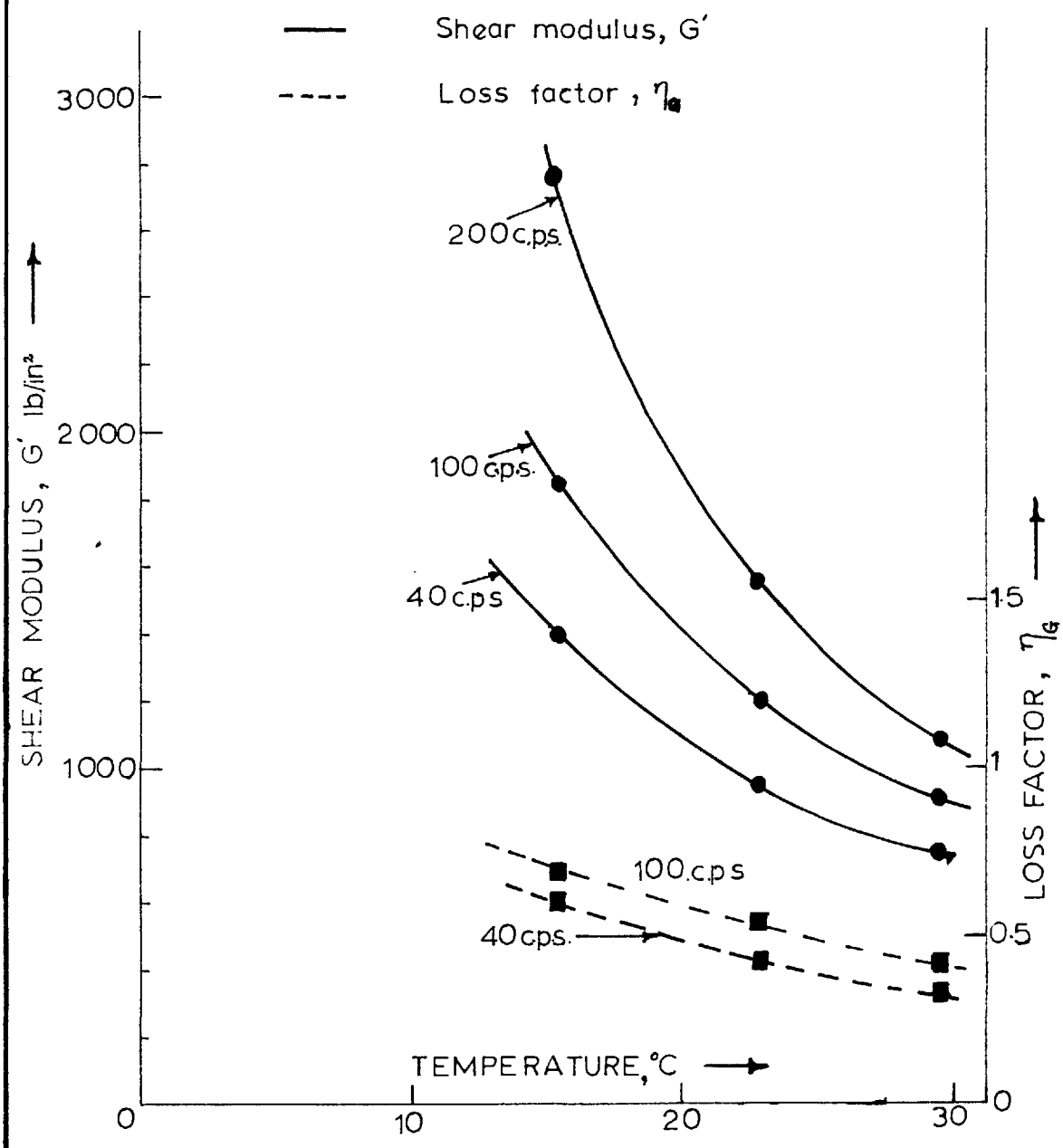

FIG. 3·36 *Hycadamp*

Variation of In-phase Shear Modulus, G', and Loss Factor, η_G, with Temperature. Strain amplitude constant at $5 \cdot 87 \times 10^{-3}$

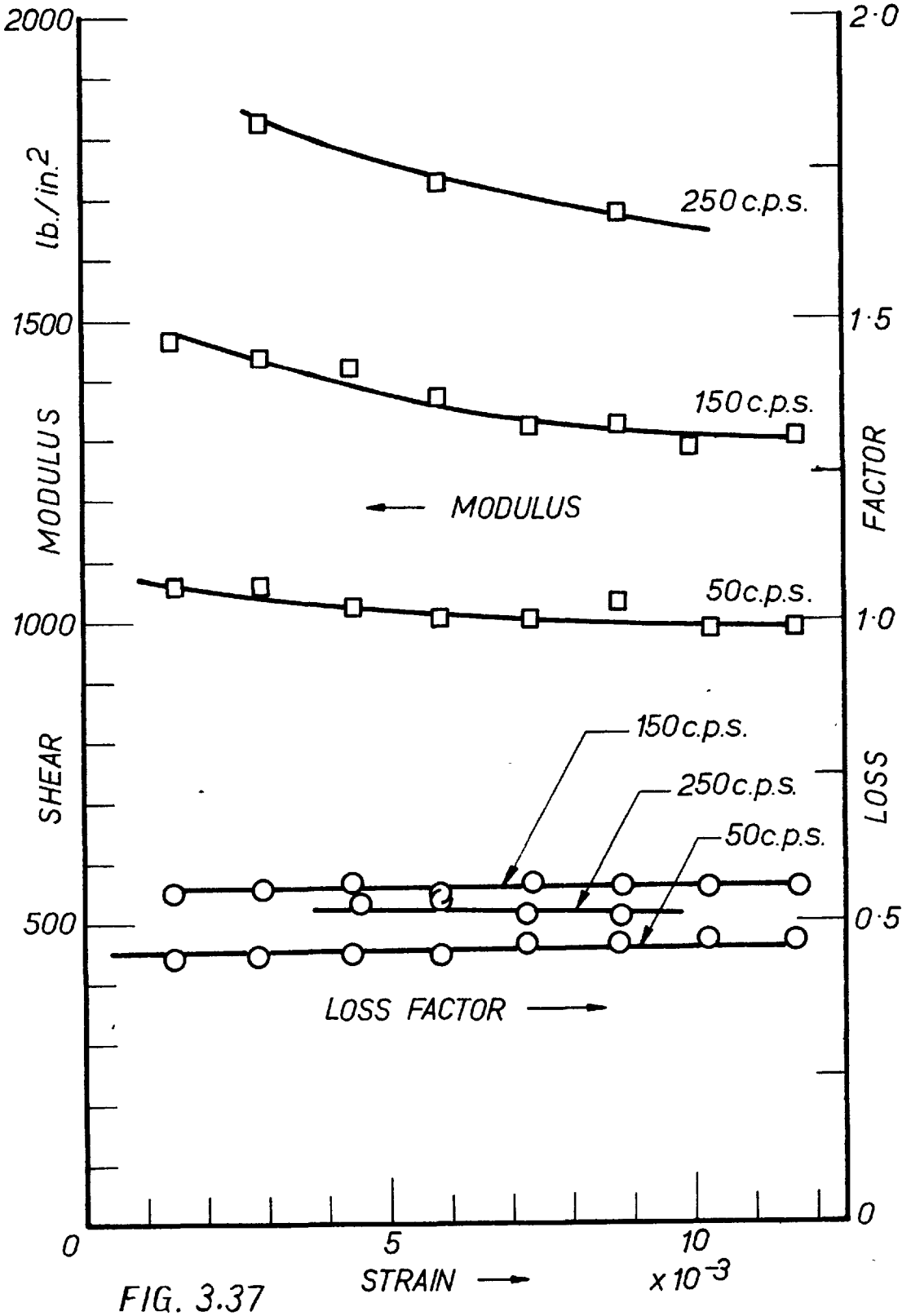

FIG. 3.37

HYCADAMP — Variation of Shear Modulus & Loss Factor with Strain at 3 frequencies. Temp. constant at 22·5°C.

and then finally, another region of constant intercept, the length of the intercept in this region being exactly half that of the first zone (table 3.c).

Also, the graphs of loss factor against frequency (fig. 3.35) have peaks which occur at frequencies close to those at which the corresponding shear modulus-versus-frequency graphs show points of inflexion.

The above observations at first seem to suggest that the material might be in the middle of the glass transition zone (i.e. close to the peak of the damping curve of fig. 3.2). However, if this was the case, one would expect the predictions of the method of reduced variables to hold throughout the range covered, and not just for distinct regions of the range. The observations, on the other hand, are too well-defined and consistent to be dismissed as being merely due to experimental inaccuracies. Secondary transition zones [95] can be ruled out, for although these could affect the shape of the modulus-versus-frequency curves, thus causing a variation in the length of the intercepts within a region of the graphs, they would hardly give rise to two regions of different constant intercepts.

It has been suggested* that the above behaviour could

*This suggestion was made by A.R. Payne in a private correspondence.

be due to the fact that hycadamp is a mixture (and not a chemical compound) of the two polymers, P.V.C. and nitrile rubber. For such a material, it is possible for each component compound to have a dominant influence in the material properties within some frequency (or temperature range) range. This could give rise to two regions of the shear modulus-versus-frequency graph, within which the material would behave like a true viscoelastic material, but would show differing trends. This suggestion seems to explain the observed behaviour satisfactorily.

The dependence of the loss factor and the shear modulus on temperature is shown in fig. 3.36, and has the same features as that for P.V.C., both quantities decreasing with increase in temperature.

Strain tests

The loss factor is virtually independent of the strain, while the shear modulus decreases slowly as the strain amplitude increases, as in the case of P.V.C. These trends can be seen in fig. 3.37.

Mulseal

The mulseal specimen was tested after it had cured for 15 weeks. As already mentioned, only one set of shear modulus and loss factor-versus-frequency curves was obtained (fig. 3.38), since the material had the same order of modulus and damping as evoseal, and was found inferior to

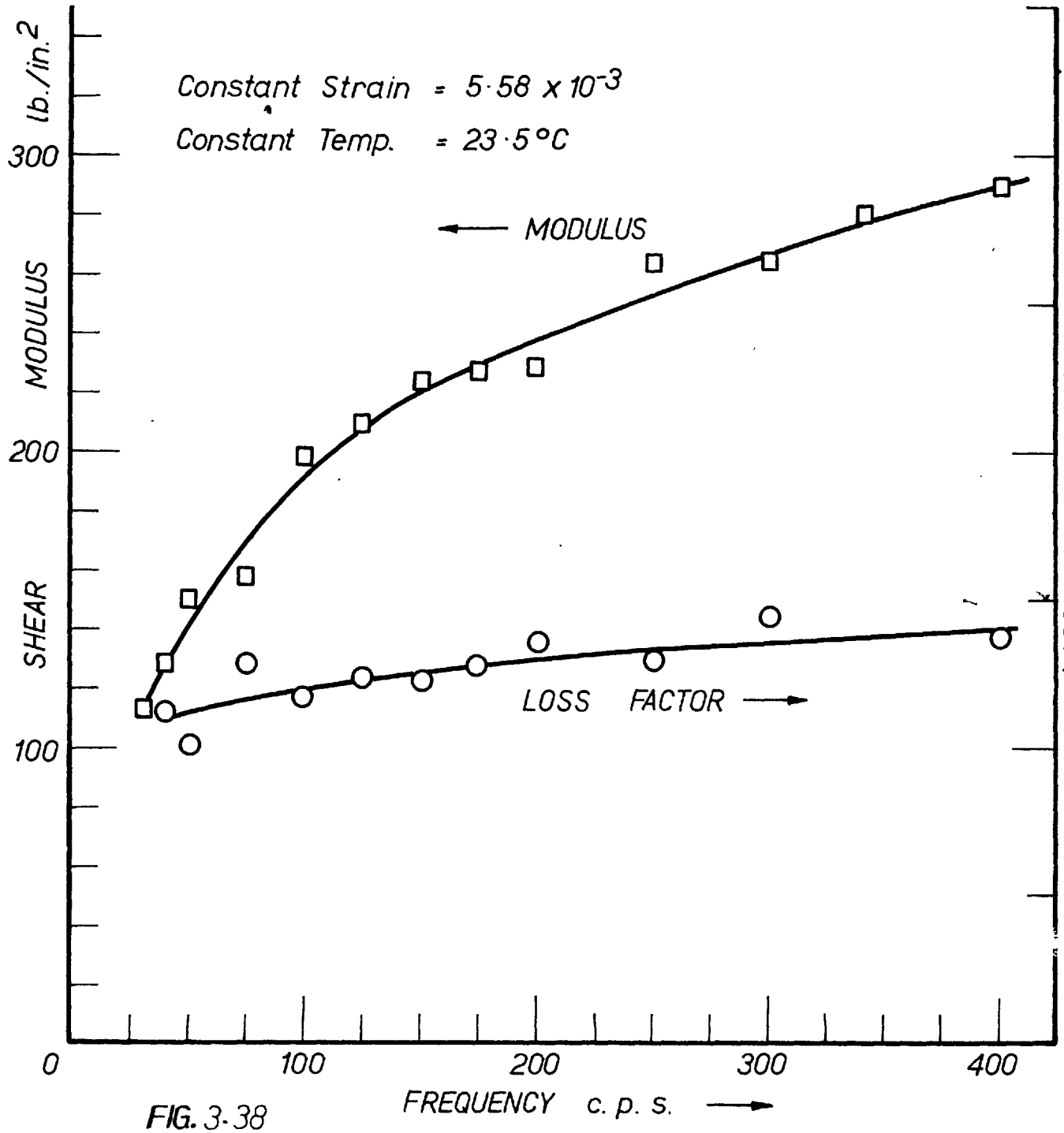

FIG. 3-38
MULSEAL — Variation of Shear Modulus and Loss Factor with Frequency.

evoseal as regards rate of cure. It was thus thought unnecessary to examine its properties in detail.

3.7.b. Shape of the force - displacement curve.

For a linear viscoelastic material, the stress - strain curve over a cycle is, by definition, an ellipse. From the theory given in section 3.3.c, the corresponding force - displacement curve for such a material will also be elliptical. As already mentioned, traces of the force - displacement curves for the specimens were taken during the tests. Such a trace is shown in fig. 3.39, with points on an actual ellipse plotted on it for comparison. A surprisingly high degree of agreement is seen to exist. Since, for all the specimens tested, the inertia forces were much smaller than the shear forces in the frequency range covered (the inertia forces were less than 5 per cent of the total measured forces in most cases), it follows that the stress - strain curves for the materials must be essentially elliptical.

This goes to confirm the observation, already mentioned, that despite the dependence of their properties on the strain amplitude, at any given frequency and strain amplitude, these materials virtually exhibit an elliptical (i.e. linear) stress - strain law.

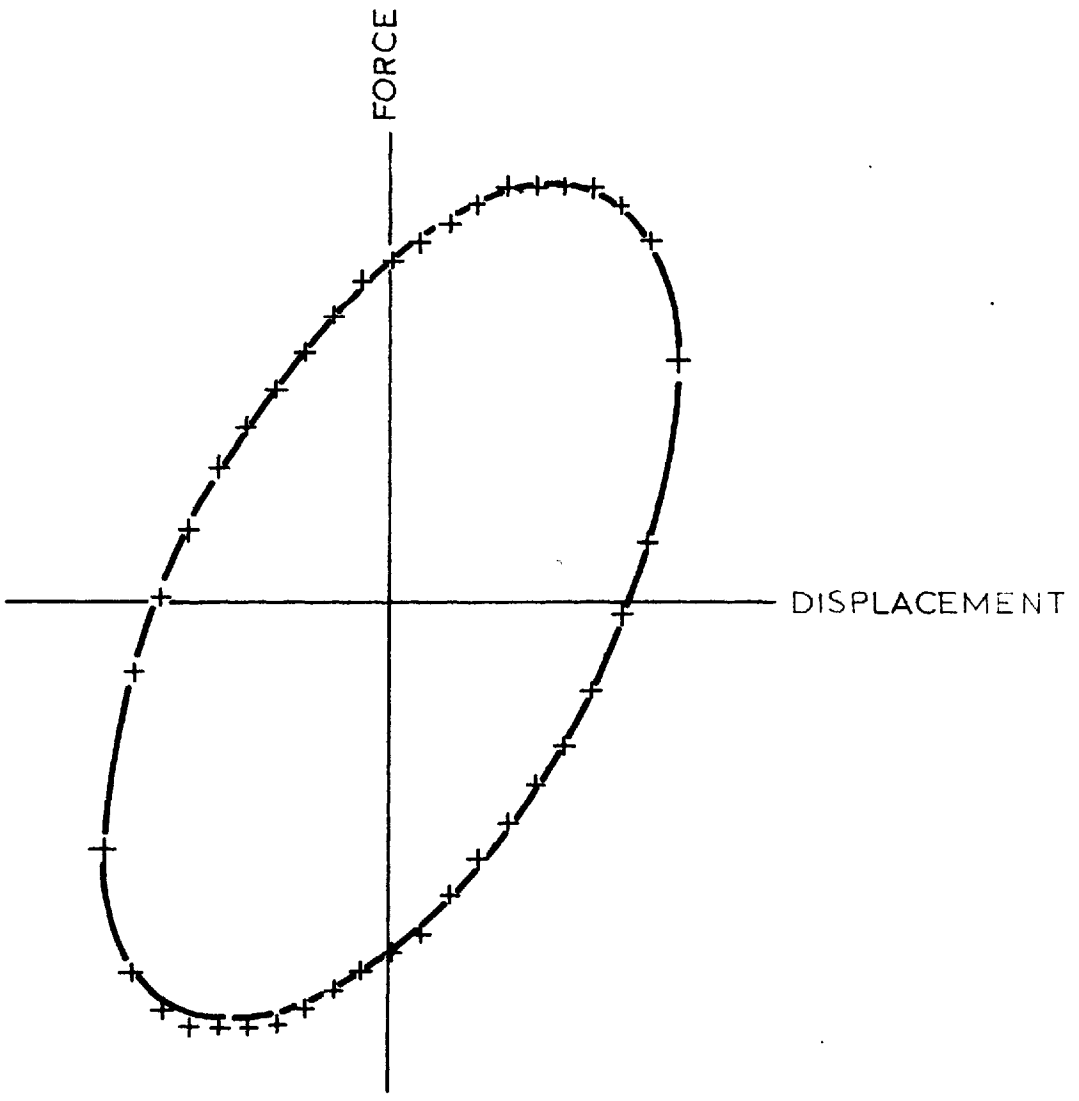

+ = POINT ON AN ACTUAL ELLIPSE.

—— TRACE OBTAINED EXPERIMENTALLY.

FIG. 3.39 Force-Displacement trace for Evoseal specimen

3.7.c. Repeatability of results.

Table 3.d gives an indication of how close readings could be repeated. The table applies to hycadamp. The set of results, A′, was obtained during the temperature tests. The set, B′, was obtained two days afterwards, after the temperature and the strain tests had been completed. The two sets of results agree very well, the disparity between any two corresponding values being less than 2 per cent.

3.7.d. Estimated accuracy of the results.

The accuracy of the values of the shear modulus, G′, and the loss factor, η_G, obtained by the method described in this chapter, will depend on the accuracy of measurement of the various quantities from which G′ and η_G were calculated. The important quantities in the calculation of these properties were $\hat{P}$, a'_o, ϵ, t_o, and A, since the inertia force, $m_c\omega^2 a'_o$, was usually much smaller than the shear force.

It has been mentioned that the smallest length measurable with the microscope available was 7 microns. Since the minimum displacement amplitude measured with it was 200 microns, the maximum error in the displacement measurement was less than ± 2 per cent. This is probably a very 'safe' estimate, since the points for the displacement-channel calibration graphs lay on straight lines with very little scatter.

Frequency c.p.s.	A′		B′	
	Shear modulus G′, lb/sq.in.	Loss factor η_G	Shear modulus G′, lb/sq. in.	Loss factor η_G
30	890	0.405	875	0.404
60	1023	0.475	1030	0.480
100	1217	0.522	1211	0.540
150	1379	0.560	1351	0.562
200	1545	0.574	1558	0.572
250	1810	0.531	1790	0.540
300	2040	0.486	2005	0.490

TABLE 3.d

Repeatability of results for hycadamp

Set A′ - obtained at 22.5°C, during the temperature tests.

Set B′ - obtained two days afterwards, after the temperature and the strain tests; test temperature also 22.5°C.

Both sets were obtained at a constant strain amplitude of 5.87×10^{-3}.

The accuracy of repeatability of the force calibration has been given as better than 3 per cent. The scatter in the force readings taken during a test was within ± 3 per cent, so that the error in the force measurement was unlikely to exceed ± 3 per cent.

The thickness, t_o, was measured to the nearest 0.001 inch. The minimum double thickness measured was 0.066 (for hycadamp); hence, the maximum error anticipated in the measurement of t_o would be less than ± 1 per cent. The error in measuring the shear area, A, would be much less than this, since the dimensions of length (about 1.0 inch) and width (about 0.5 inch) were each measured to an accuracy of 0.001 inch, giving a maximum error of less than ± 0.3 per cent.

For the phase measuring device, it has been stated that the minimum angle detectable was about 0.5°. The range of values measured covered between 20° and 80°, so that the maximum error involved in measuring $\cos\epsilon$ was less than ± 1 per cent, whilst the maximum error in $\tan\epsilon$ was about ± 5 per cent.

From the above analysis, it would appear that the accuracy of the calculated values would be well within ± 7 per cent for G', and ± 5 per cent for η_d. It may be pointed out that this estimate is for the worst possible case. The general level of accuracy in the results obtained

for any given material would be much better than this. For instance, it was stated in section 3.7.c, that the results for hycadamp could be repeated to within 2 per cent ... difference.

3.7.e. Comparison of results

For purposes of comparison, an intensive search was carried out through the literature for published data on the materials tested. As far as is known, there are no published data on evoseal and mulseal. Also, no information could be found on the properties of the brand of P.V.C. tested, although there is published work on other brands of P.V.C. For instance, some data are given in [100], for a formulation of placticised P.V.C. containing some tri-cresyl phosphate as plasticiser. These results are plotted in fig. 3.40, which shows the variation of G' and η_G with the frequency, at a constant temperature of 25°C (the strain amplitude was not specified!). The shear modulus and the loss factor quoted are seen to be much higher than the values obtained here. However, since the two brands of P.V.C. are different, it is doubtful whether further comparison is of any use.

3.7.f. The apparatus - its limitations and possibilities

It is intended to conclude this section with a short discussion on the apparatus..

It will have been observed that the mechanical set-up

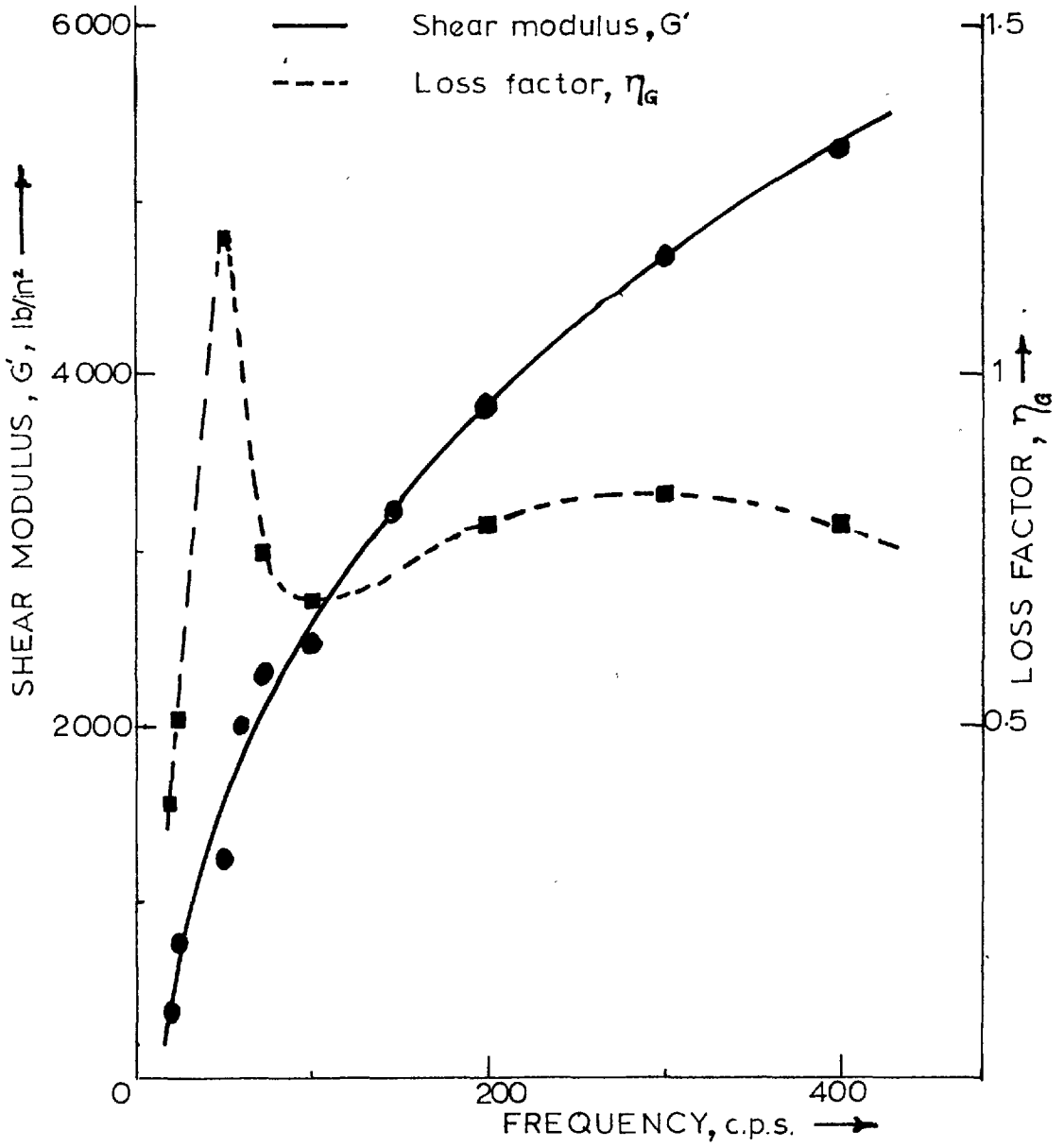

FIG. 3·40. Graphs of Shear Modulus, G', and Loss Factor, η_G, vs Frequency for Plasticised P.V.C at 25 °C. (As from [100])

is very simple. The different components are easy to make, and can be assembled or dismantled in a matter of minutes. The measuring circuit is not very complicated. The displacement measurements can be very accurately made, and the accuracy of the force measurements could be improved upon, if desired, by replacing the strain gauge with a more sensitive force pick-up, as for example, a crystal pick-up.

Although the temperature ranges covered in this work were close to room temperature, temperature ranges of any desirable magnitude can be obtained relatively easily, by providing a small temperature chamber around the specimen.

The set-up is also very suitable for investigating the effect of lateral compression on the shear properties.

One limitation of the apparatus is the fact that it is essentially a low frequency set-up. The frequency limitation arises from the requirement that the test frequency range should be below the fundamental natural frequency of the system (table + fixed supports + bolts etc). By careful design, this frequency can be made reasonably high (up to 5 kc/s), so that a wide frequency range can be covered.

The apparatus, as it is, is not suitable for tests at very high shear strains. Reference to fig. 3.41 will show that when the shear specimen is subjected to a shear deformation, θ; owing to the fact the the supports, (5), are fixed in position, any horizontal element of the specimen

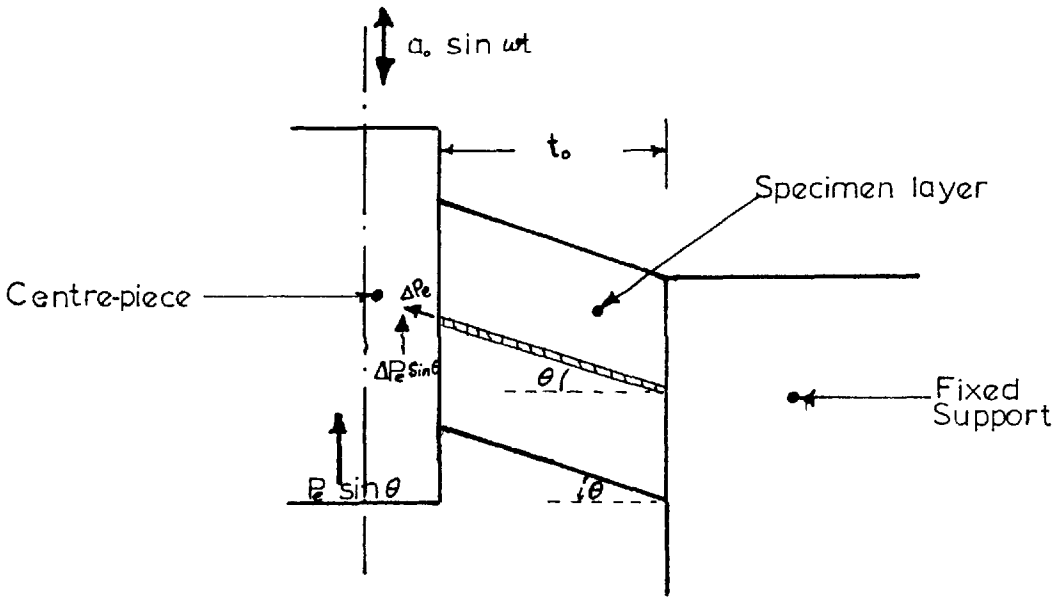

FIG. 3·41 *Effect of extension in the Shear specimen.*

undergoes a tensile strain of magnitude, $(\sec\theta - 1)$. (It is assumed that the element still remains straight after deformation). This gives rise to a tensile force, $\triangle P_e$, in the element. The sum total of all such elemental tensile forces has a vertical component, designated by $P_e \sin\theta$, which must be provided by the drive rod. It follows, therefore, that the total force, P, measured by the strain gauge, not only provides for the shear deformation in the specimen and the inertia of the moving parts, but also has an additional component due to the necessary extension of the specimen. For moderately high values of the strain, the component, $P_e \sin\theta$, is negligibly small. For instance, for a shear strain of 10 per cent (i.e. $\tan\theta = 0.1$), $P_e \sin\theta$ is only 1.5 per cent of the shear force. However, at very high strains (say, 100 per cent or more), $P_e \sin\theta$ becomes very appreciable. Besides, the assumption that the horizontal element deforms to a straight line, and not a curve, becomes less likely to hold. Hence, this method can not be used for tests at such strains.

It may also be added that the results obtained with the apparatus within the frequency range, 20 to 500 c.p.s., do not show any "dispersion resonances" [99] of the type very often experienced using the Fitzgerald - Ferry apparatus (see fig 5.40, for example). Perhaps this is due to the fact that the frequency range covered is low. However, the

apparatus developed can be readily employed in checking on this still uncertain phenomenon. It should then be possible to provide a conclusive evidence as to whether this observation is due to a fault in the Fitzgerald - Ferry apparatus, or is a characteristic peculiar to some viscoelastic materials.

3.8. Concluding remarks

One of the aims of the tests reported in this chapter, was to choose some viscoelastic materials which could be used in the subsequent beam tests. The test results given in section 3.7, show that evoseal and P.V.C. have widely differing properties. Thus, while evoseal has low shear modulus and relatively high loss factor, P.V.C. has fairly high modulus and moderately low loss factor. The properties of hycadamp are close to those of P.V.C., while mulseal has properties similar to those of evoseal. P.V.C. and evoseal were, therefore, chosen as the viscoelastic materials to be employed in the experimental check on the theory on sandwich beams.

Another aim of this chapter was to study the dynamic properties of viscoelastic materials when subjected to harmonic excitation. The experimental results have confirmed that at any given strain amplitude and frequency, their stress - strain loop is practically elliptical. But the results also show that the material properties depend on the

strain amplitude (as well as on frequency and temperature). The dependence of their properties on the strain means that the viscoelastic materials are basically non-linear. It follows, therefore, that the degree of non-linearity exhibited by the materials tested is not strong enough to cause any appreciable distortion of the elliptical stress - strain loop.

In the light of this, these materials will, in the subsequent work, be treated as exhibiting an elliptical stress - strain law at any given strain amplitude, but also having properties which are dependent on the strain amplitude. If this is done, the functions, Ψ and Ψ, (of section 2.1) will take the form given in equation 2.1.ii (for an elliptical stress - strain loop). Also, the material constants, K_s and η, of section 2.1, become the in-phase modulus (Young's or shear) and the material loss factor (in extension or in shear), respectively. It was stated in section 3.3.a (equations 3.3.iv and 3.3.v) that $E' \doteq 3G'$, and $\eta_e \doteq \eta_s$. These approximations will be used as exact relations in the rest of the work. Also, the notations used in chapter 2 for the viscoelastic material properties will, from now on, be replaced with the proper notations introduced in this chapter, thus E_i, G_i (of chapter 2) become E'_i, G'_i.

C H A P T E R 4

SOLUTION OF THE DIFFERENTIAL EQUATIONS

Introduction

The differential equations derived in chapter 2 hold for any symmetrical multi-layer beam subjected to either free or forced vibration. In this chapter, the solution of the equations for forced vibration will be considered. To keep the analysis clear and simple, only three-layer and five-layer beams are treated in detail. Extension of the solution to "higher order" beams will be shown to involve no basic change in the method.

Three important conclusions arrived at in chapter 3 are relevant in the present treatment and are repeated here for emphasis:

(a) The viscoelastic stress-strain loop under harmonic excitation is an ellipse.

(b) The shear modulus (and hence, the Young's modulus) of the viscoelastic material is a function of the strain amplitude (as well as of frequency and temperature).

(c) The rate of change of the shear modulus with the strain amplitude is small for many viscoelastic materials, certainly for those investigated.

From (b), it follows that the coefficients of the differential equations are all functions of the strain

amplitude. The equations are therefore basically non-linear. (c), however, suggests that this non-linearity can be treated as small; that is, as having second order effects. If this is permissible, a first approximate solution could be sought assuming that the coefficients are strain- independent. This solution can then be used as a basis for obtaining improved solutions. It is intended to show first how the equations can be solved for the linear case. The modification of the solutions to deal with strain-dependence will be left to a later stage in the analysis. Finally, conclusion (a) above, apart from specifying the viscoelastic stress-strain law, also implies that in spite of the slight non-linearity in the viscoelastic material, the response of the beam, under sinusoidal excitation, is also sinusoidal and of the same frequency.

4.1 Three-layer beam equations with strain-independent coefficients.

On the assumption of strain-independent coefficients, the equations 2.2.xxv and 2.2.xxx, for the three-layer beam become

$$EI\frac{\partial^4 y}{\partial x^4} + N_1'\frac{\partial^3 \phi_1}{\partial x^3} + \frac{1}{2}\frac{\partial^2}{\partial x^2}\{\psi_{m1}\} + m\frac{\partial^2 y}{\partial t^2} = p(x,t) \quad \ldots\ldots 4.1.i$$

$$P_1'\frac{\partial^3 y}{\partial x^3} + \psi_{11}'\frac{\partial^2 \phi_1}{\partial x^2} + \frac{\partial}{\partial x}(\psi_{F1}) - \eta_1 bG_1'\psi(\phi_1) = bG_1'\phi_1 \ldots 4.1.ii$$

If the forcing function is assumed to be a sinusoidal function time, of frequency ω, thus

$p(x,t) = p(x) \cos \omega t$ 4.1.iii

then from the discussion above, the displacement y, and the shear, ϕ_1, take the forms,

$y = u_o' \cos \omega t + v_o' \sin \omega t$ 4.1.iv

$\phi_1 = X_{o1} \cos \omega t + Y_{o1} \sin \omega t$ 4.1.v

where u_o', v_o', X_{o1}, and Y_{o1} are functions of x.

4.1.a. The Ψ-functions

With the assumed form of y and ϕ_1, it is now possible to determine the Ψ-functions. To illustrate how this can be done, consider $\Psi(\phi_1)$. This is readily obtained from the relation $\Psi(\phi_1) = \pm \sqrt{\hat{\phi}_1^2 - \phi_1^2}$; $\hat{\phi}_1$ being the maximum value of ϕ_1 (see equation 2.1.ii). However, it is beneficial to obtain it from first principles. The shear deformation, ϕ_1, in the viscoelastic material is, from equation 4.1.v, $\phi_1 = X_{o1} \cos \omega t + Y_{o1} \sin \omega t = \hat{\phi}_1 \cos(\omega t - \lambda_s)$ where evidently,

$$\left.\begin{aligned} X_{o1} &= \hat{\phi}_1 \cos\lambda_s \\ \text{and } Y_{o1} &= \hat{\phi}_1 \sin\lambda_s \end{aligned}\right\} \quad \text{.....4.1.vi}$$

Since the resulting shear stress, τ_1, leads ϕ_1 by the loss angle δ (section 3.1.a), it has the form

$\tau_1 = \hat{\tau}_1 \cos(\omega t + \delta - \lambda_s)$ .....4.1.vii.

When expanded, this gives

$\tau_1 = \hat{\tau}_1(\cos\delta \cos\lambda_s + \sin\delta \sin\lambda_s) \cos \omega t$

$- \hat{\tau}_1(\sin\delta \cos\lambda_s - \cos\delta \sin\lambda_s) \sin \omega t$ .....4.1.viii.

But from the definition of the shear modulus of viscoelastic

materials (equations 3.1.iv and v)

$\hat{\tau}_i \cos\delta = G_i' \hat{\phi}_i$ and $\hat{\tau}_i \sin\delta = G'' \hat{\phi}_i = \eta_i G_i' \hat{\phi}_i$.

Using these, and equations 4.1.vi in equation 4.1.viii, the following expression results:

$$\tau_i = G_i' \{ (X_{oi} \cos \omega t + Y_{oi} \sin \omega t) + \eta_i (Y_{oi} \cos \omega t - X_{oi} \sin \omega t) \} . \quad \ldots\ldots 4.1.ix,$$

which is clearly of the form

$\tau_i = G_i' \{ \phi_i + \eta_i \Psi(\phi_i) \}$, whence

$\Psi(\phi_i) = Y_{oi} \cos \omega t - X_{oi} \sin \omega t$ .....4.1.x.a.

The other Ψ- functions can be obtained in a similar manner; and are given below.

$$\Psi_{Fi} = \eta_i E_i' A_i \frac{h_i}{8} \left\{ \frac{d^2 v_o'}{dx^2} \cos \omega t - \frac{d^2 u_o'}{dx^2} \sin \omega t \right\}$$
$$+ \eta_i E_i' A_i \frac{h_i}{8} \left\{ \frac{dY_{oi}}{dx} \cos \omega t - \frac{dX_{oi}}{dx} \sin \omega t \right\} \quad \ldots. 4.1.x.b.$$

$$\frac{1}{2}\Psi_{mi} = \eta_i E_i' I_{mi} \left\{ \frac{d^2 v_o'}{dx^2} \cos \omega t - \frac{d^2 u_o'}{dx^2} \sin \omega t \right\}$$
$$+ \eta_i E_i' I_{mi} \left\{ \frac{dY_{oi}}{dx} \cos \omega t - \frac{dX_{oi}}{dx} \sin \omega t \right\} \quad \ldots. 4.1.x.c.$$

$$\eta_i b G_i' \Psi(\phi_i) = \eta_i b G_i' \{ Y_{oi} \cos \omega t - X_{oi} \sin \omega t \} \quad \ldots. 4.1.x.d.$$

where the distinction between shear and extensional loss factors has been dropped i.e. $\eta_{Gi} = \eta_{Ei} = \eta_i$.

It is noted that all the Ψ-functions appear in the differential equations with the common factor η_i , the loss factor of the viscoelastic material. On account of this, they are called the damping terms of the equations. (When $\eta_i = 0$, these terms disappear from the equations, and the viscoelastic stress-strain law reduces to that of an elastic loss-less material). The damping terms which

contain the dynamic Young's modulus E_i', arise from the extensional deformation in the viscoelastic material, and are therefore referred to as the "extensional damping terms". Similarly those containing the dynamic shear modulus G_i', are called the "shear damping terms".

4.1.b Simplification of the equations

Equations 4.1.iv, 4.1.v, and 4.1.x can now be put into equations 4.1.i and 4.1.ii to obtain the equations

$$EI\left\{\frac{d^4u_o'}{dx^4}\cos\omega t + \frac{d^4v_o'}{dx^4}\sin\omega t\right\} + N_i'\left\{\frac{d^3X_{oi}}{dx^3}\cos\omega t + \frac{d^3Y_{oi}}{dx^3}\sin\omega t\right\}$$
$$+ \eta_i E_i' I_{Ni}\left\{\frac{d^4v_o'}{dx^4}\cos\omega t - \frac{d^4u_o'}{dx^4}\sin\omega t\right\}$$
$$+ \eta_i E_i' I_{Ni}\left\{\frac{d^3Y_{oi}}{dx^3}\cos\omega t - \frac{d^3X_{oi}}{dx^3}\sin\omega t\right\}$$
$$- m\omega^2\left\{u_o'\cos\omega t + v_o'\sin\omega t\right\} = p(x)\cos\omega t \quad \ldots\ldots 4.1.xi,$$

and

$$P_i'\left\{\frac{d^3u_o'}{dx^3}\cos\omega t + \frac{d^3v_o'}{dx^3}\sin\omega t\right\} + Q_{ii}'\left\{\frac{d^2X_{oi}}{dx^2}\cos\omega t + \frac{d^2Y_{oi}}{dx^2}\sin\omega t\right\}$$
$$+ \eta_i E_i' A_i \frac{h_i}{8}\left(\frac{d^3v_o'}{dx^3}\cos\omega t - \frac{d^3u_o'}{dx^3}\sin\omega t\right)$$
$$+ \eta_i E_i' A_i \frac{h_i}{8}\left(\frac{d^2Y_{oi}}{dx^2}\cos\omega t - \frac{d^2X_{oi}}{dx^2}\sin\omega t\right) - \eta_i b G_i'\left(Y_{oi}\cos\omega t - X_{oi}\sin\omega t\right)$$
$$= bG_i'\left(X_{oi}\cos\omega t + Y_{oi}\sin\omega t\right) \quad \ldots\ldots\ldots 4.1.xii.$$

Equations 4.1.xi and 4.1.xii must hold true at any time t. The coefficients of $\sin\omega t$ and $\cos\omega t$ must therefore seperately vanish. This results in the four equations

$$
\left.
\begin{aligned}
&EI\frac{d^4u_o'}{dx^4} + N_1'\frac{d^3X_{o1}}{dx^3} + \eta_1 E_1' I_{N1}\frac{d^4v_o'}{dx^4} + \eta_1 E_1' I_{N1}\frac{d^3Y_{o1}}{dx^3} \\
&- m\omega^2 u_o' = p(x) \\
&EI\frac{d^4v_o'}{dx^4} + N_1'\frac{d^3Y_{o1}}{dx^3} - \eta_1 E_1' I_{N1}\frac{d^4u_o'}{dx^4} - \eta_1 E_1' I_{N1}\frac{d^3X_{o1}}{dx^3} \\
&- m\omega^2 v_o' = o \\
&P_1'\frac{d^3u_o'}{dx^3} + Q_{11}'\frac{d^2X_{o1}}{dx^2} + \eta_1 E_1' A_1\frac{h_1}{8}\frac{d^3v_o'}{dx^3} + \eta_1 E_1' A_1\frac{h_1}{8}\frac{d^2Y_{o1}}{dx^2} \\
&- \eta_1 bG_1' Y_{o1} - bG_1' X_{o1} = o \\
&P_1'\frac{d^3v_o'}{dx^3} + Q_{11}'\frac{d^2Y_{o1}}{dx^2} - \eta_1 E_1' A_1\frac{h_1}{8}\frac{d^3u_o'}{dx^3} - \eta_1 E_1' A_1\frac{h_1}{8}\frac{d^2X_{o1}}{dx^2} \\
&+ \eta_1 bG_1' X_{o1} - bG_1' Y_{o1} = o
\end{aligned}
\right\} \quad \ldots 4.1.\text{xiii}
$$

The above equations can be put into a dimensionless form by introducing the dimensionless variables

$$u_o = \frac{u_o'}{l} \; ; \quad v_o = \frac{v_o'}{l} \; ; \quad \xi = \frac{x}{l} \qquad \ldots\ldots\ldots\ldots\ldots\ldots 4.1.\text{xiv},$$

and simplifying to obtain

$$
\left.
\begin{aligned}
&D^4u_o + \gamma_1 D^4v_o + \alpha_1 D^3X_{o1} + \gamma_1 D^3Y_{o1} - \beta_1 u_o = \frac{l^3}{EI}p(l\xi) \quad ..(a) \\
&-\gamma_1 D^4u_o + D^4v_o - \gamma_1 D^3X_{o1} + \alpha_1 D^3Y_{o1} - \beta_1 v_o = o \quad ..(b) \\
&\mu_1 D^3u_o + \delta_1 D^3v_o + D^2X_{o1} + \delta_1 D^2Y_{o1} - \nu_1 X_{o1} - \sigma_1 Y_{o1} = o \quad ..(c) \\
&-\delta_1 D^3u_o + \mu_1 D^3v_o - \delta_1 D^2X_{o1} + D^2Y_{o1} + \sigma_1 X_{o1} - \nu_1 Y_{o1} = o \quad ..(d)
\end{aligned}
\right\} \ldots 4.1.\text{xv}
$$

where

$$
\left.
\begin{aligned}
&\alpha_1 = \frac{N_1'}{EI} \; ; \quad \beta_1 = \frac{m\omega^2 l^4}{EI} \; ; \quad \gamma_1 = \frac{\eta_1 E_1' I_{N1}}{EI} \; ; \quad \mu = \frac{P_1'}{Q_{11}'} \; ; \\
&\delta_1 = \frac{\eta_1 E_1' A_1}{Q_{11}'}\frac{h_1}{8} \; ; \quad \nu_1 = \frac{l^2 bG_1'}{Q_{11}'} \; ; \quad \sigma_1 = \frac{\eta_1 l^2 bG_1'}{Q_{11}'}
\end{aligned}
\right\} \ldots\ldots 4.1.\text{xvi}
$$

and the operator notation $D \equiv \frac{d}{d\xi}$ has been employed. It is convenient to express the right-hand sides of equations 4.1.xvi in terms of the dimensionless ratios,

$$
\left.
\begin{aligned}
&H = \frac{h_1}{h_2} \; ; \quad P_1 = \frac{l}{h_2} \; ; \quad g_1 = \frac{G_1'}{E_2} \; ; \quad e = \frac{E_1'}{E_2} \; (=3g_1) \; ; \quad D_1 = \frac{\rho_1}{\rho_2}.
\end{aligned}
\right\} 4.1.\text{xvii}
$$

Thus

$$\alpha_1 = \frac{6H + 6H^2 + eH^3}{8 + 12H + 6H^2 + eH^3}$$

$$\beta_1 = \frac{48\pi^2 p_2^2 (2 + D_1 H)}{8 + 12H + 6H^2 + eH^3}\left\{\frac{\ell^2 f^2 \rho_2}{g_o E_2}\right\}$$

$$\gamma_1 = \frac{\eta_1 eH^3}{8 + 12H + 6H^2 + eH^3}$$

$$\delta_1 = \frac{\eta_1 eH}{4 + eH}$$

$$\mu = \frac{4 + 4H + eH^2}{4H + eH^2}$$

$$\nu_1 = \frac{8p_2^2 g_1}{4H + eH^2}$$

$$\sigma_1 = \frac{8\eta_1 p_2^2 g_1}{4H + eH^2}$$

} 4.1.xviii

$f = \frac{\omega}{2\pi}$ is the frequency of excitation in cycles per second; and g_o is the gravitational constant of acceleration.

To give an order of magnitude to these coefficients, consider a symmetrical three-layer beam (beam L1 for short) 20 inches long. The frequency of the exciting force is such that $\beta_1 = 10$, and $G_1' = 1{,}000$ lb/in^2. The other material constants and dimensions are:

$E_2 = 10^7$ lb/sq. in.

$\rho_1 = 0.05$ lb/cu. in.; $\rho_2 = 0.1$ lb/cu. in..

$h_1 = 0.1$ in.; $h_2 = 0.2$ in.

$\eta_1 = \frac{2}{3}$

Then, from equations 4.1.xviii, the coefficients can be evaluated as:

$\alpha_1 = 0.29$; $\beta_1 = 10.00$; $\gamma_1 = 15 \times 10^{-6}$

$\delta_1 = 8 \times 10^{-6}$; $\mu_1 = 3.00$; $\nu_1 = 4.00$; $\sigma_1 = 2.67$

It may be observed that γ_1 and δ_1 - the coefficients of the extensional damping terms - are much smaller than the other coefficients; and in particular, are negligible compared with σ_1, the coefficient of the shear damping term. The relative importance of these terms will be examined in greater detail in section 4.2.f.

The coefficients ν_1 and β_1 will be referred to as the "shear parameter" and the "frequency factor" respectively. Their importance in the design study of multi-layer sandwich beams will become clear in chapter 6.

Equations 4.1.xv can now be compared with those obtained by Mead for a symmetrical three-layer sandwich plate [62, 63]. When his equations are reduced to the case of a sandwich beam, neglecting the lateral inertia terms; they become identical with the above equations with the extensional terms neglected.

Also, when the equations of Yu [55, 78] are reduced to the case of a one-dimensional uniaxially stressed viscoelastic sandwich beam, and the lateral inertia terms are neglected; they agree with the above equations with only a slight difference in the viscoelastic extensional

terms. The slight difference is due to the difference in the methods of obtaining the equations. The equations for shear deformation were obtained in chapter 2 by assuming that the shear in the viscoelastic material is the shear at the central axis of the layer. Yu, however, obtains his equations by applying the variational equations of motion.

4.2. Solution of the linear equations by finite difference approximations - 3-layer beam.

Equations 4.1.xv form a set of simultaneous ordinary differential equations, with constant coefficients and of the twelfth order. It is thus theoretically possible to obtain a closed solution by any of the classical methods available in standard texts on differential equations (see, for instance, [79]). In practice, such a solution would be cumbersome and virtually intractable. Besides, it would not be possible to modify it to apply to the case where the coefficients of the equations are strain-dependent. A numerical method of solution has thus been chosen. Apart from the relative ease with which solutions can be obtained using the fast Atlas digital computer available, the method has the special advantage of being readily adaptable to the 'non-linear' case.

It may be noted that equations 4.1.xv require 12 boundary conditions for their solution. They are, however, not solved in their present form. Equations 4.1.xv.c, and d are differentiated with respect to ξ (to get all the equations into the same homogeneous form), so that they now become

$$
\left.
\begin{aligned}
D^4u_o + \gamma_1 D^4v_o + \alpha_1 D^3X_{o1} + \gamma_1 D^3Y_{o1} - \beta_1 u_o &= \frac{\ell^3}{EI}p(\ell\xi) \quad \ldots\ldots(a)\\
-\gamma_1 D^4u_o + D^4v_o - \gamma_1 D^3X_{o1} + \alpha_1 D^3Y_{o1} - \beta_1 v_o &= 0 \quad \ldots\ldots(b)\\
\mu_1 D^4u_o + \delta_1 D^4v_o + (D^3 - \nu_1 D)X_{o1} + (\delta_1 D^3 - \sigma_1 D)Y_{o1} &= 0 \ldots.(c)\\
-\delta_1 D^4u_o + \mu_1 D^4v_o - (\delta_1 D^3 - \sigma_1 D)X_{o1} + (D^3 - \nu_1 D)Y_{o1} &= 0 \ldots.(d)
\end{aligned}
\right\} \ldots 4.2.i
$$

These equations now form a set of fourteenth order equations requiring fourteen boundary conditions. The two extra boundary conditions are readily obtained by applying equations 4.1.xv.c and d to any point in the system (preferably to either boundary).

4.2.a. Finite-difference equations

For each dependent variable, the highest order derivative is split into a set of first order differential equations as shown below

$$
\left.
\begin{aligned}
&\underline{u_o} \qquad \underline{v_o} \qquad \underline{X_{o1}} \qquad \underline{Y_{o1}}\\
&\pi_2 = D\,u_o \quad \pi_3 = D\,v_o \quad \pi_4 = D\,X_{o1} \quad \pi_5 = D\,Y_{o1}\\
&\text{and the set} \quad \pi_{i+4} = D\pi_i \quad ; \quad i = 2, 3, \ldots 11
\end{aligned}
\right\} \ldots 4.2.ii
$$

where $\pi_{12} = D^3X_{o1}$, $\pi_{13} = D^3Y_{o1}$, $\pi_{14} = D^4u_o$, $\pi_{15} = D^4v_o$.

The beam is now divided into a convenient number of equal steps, the step-length being h. If π_i^s denotes the value of π_i at a point distant sh from the point $\xi = 0$, then the differential equations 4.2.i are exactly equivalent to the following set of 18 simultaneous equations.

$$\left.\begin{aligned}
&\pi_2^s = D\,u_o^s,\quad \pi_3^s = D\,v_o^s,\quad \pi_4^s = D\,X_{o1}^s,\quad \pi_5^s = D\,Y_{o1}^s \quad ..(a)-(d)\\
&\pi_{i+4}^s = D\,\pi_i^s \quad,\ i = 2, 3, \ldots .11 \quad ...(e)-(n)\\
&\pi_{12}^s + \delta_1\pi_{13}^s + \mu_1\pi_{14}^s + \delta_1\pi_{15}^s - \nu_1\pi_4^s - \sigma_1\pi_5^s = 0 \quad ...(p)\\
&-\delta_1\pi_{12}^s + \pi_{13}^s - \delta_1\pi_{14}^s + \mu_1\pi_{15}^s + \sigma_1\pi_4^s - \nu_1\pi_5^s = 0 \quad ..(q)\\
&\alpha_1\pi_{12}^s + \gamma_1\pi_{13}^s + \pi_{14}^s + \gamma_1\pi_{15}^s - \beta_1 u_o^s = \frac{\ell^3}{EI}p(\ell\xi) \quad ..(r)\\
&-\gamma_1\pi_{12}^s + \alpha_1\pi_{13}^s - \gamma_1\pi_{14}^s + \pi_{15}^s - \beta_1 v_o^s = 0 \quad .....(t)
\end{aligned}\right\} \quad ..4.2.iii$$

At this stage, the first order equations (4.2.iii (a) - (n)) are transformed by replacing the derivatives by finite-difference approximations.

The finite-difference equation employed is that due originally to Adams [80, 87] and is of the form

$$\frac{h}{2}(D\,y^s + D\,y^{s-1}) = \left(\bar\delta + \frac{\bar\delta^3}{12} - \frac{\bar\delta^5}{120} + \ldots\right) y^{s-\frac12} \quad .....4.2.iv$$

where the operator $\bar\delta$ is defined in the relation

$$\bar\delta y^{s-\frac12} = y^s - y^{s-1} \quad .....4.2.v$$

and y represents any of the dependent variables.

Equation 4.2.iv is truncated after the first term to yield the approximation*

$$\frac{h}{2}(D\,y^s + D\,y^{s-1}) = y^s - y^{s-1} \quad .....4.2.vi$$

*This relation would be exact if the function y was a parabola. The approximation is thus equivalent to fitting a parabola within the interval h.

This is a "second-order" approximation with a truncation error of the order h^3.

With this approximation, equations 4.2.iii (a) - (n) are changed into the following recurrence relations

$$\left.\begin{aligned}
u_o^s - \tfrac{h}{2}\Pi_2^s &= u_o^{s-1} + \tfrac{h}{2}\Pi_2^{s-1} \quad \text{.....(a)}\\
v_o^s - \tfrac{h}{2}\Pi_3^s &= v_o^{s-1} + \tfrac{h}{2}\Pi_3^{s-1} \quad \text{.....(b)}\\
X_{o1}^s - \tfrac{h}{2}\Pi_4^s &= X_{o1}^{s-1} + \tfrac{h}{2}\Pi_4^{s-1} \quad \text{.....(c)}\\
Y_{o1}^s - \tfrac{h}{2}\Pi_5^s &= Y_{o1}^{s-1} + \tfrac{h}{2}\Pi_5^{s-1} \quad \text{.....(d)}\\
\Pi_i^s - \tfrac{h}{2}\Pi_{i+4}^s &= \Pi_i^{s-1} + \tfrac{h}{2}\Pi_{i+4}^{s-1} \quad , i = 2,3,\ldots 11. \quad \text{...(e) - (n)}
\end{aligned}\right\} \text{..4.2.vii}$$

The above relations 4.2.vii.(a) - (n) along with equations 4.2.iii.(p), (q), (r), (t) form the set of 18 equations which now replace the differential equations.

The recurrence relations relate the variables at any point s with those at the preceding point s-1. Hence if all the variables are known at $\xi = 0$, their values at each successive point can be evaluated. However, this is a "boundary value" problem, and the variables are not all known at any one boundary. A special technique is thus necessary in the above step-by-step process.

4.2.b Boundary condition control

The following method* [81] was used to introduce the correct boundary conditions.

Let the variables be denoted by u_i at one boundary ($\xi = 0$) and y_i at the other boundary ($\xi = nh = 1$); that is,

*This method was suggested by Dr. P. Marcal of Imperial College, London.

$$u_o^o = u_1\ ,\ v_o^o = u_2\ ,\ X_{o1}^o = u_3\ ,\ Y_{o1}^o = u_4$$
$$\pi_i^o = u_{i+3}\ ,\ i = 2,3,\ldots\ldots\ldots\ldots 15 \qquad \ldots\ldots\ldots 4.2.viii.a$$

and

$$u_o^n = y_1\ ,\ v_o^n = y_2\ ,\ X_{o1}^n = y_3\ ,\ Y_{o1}^n = y_4$$
$$\pi_i^n = y_{i+3}\ ,\ i = 2,3,\ldots 15 \qquad \ldots\ldots\ldots 4.2.viii.b$$

$n(=\frac{1}{h})$ being the number of steps. Then, in their most general form, the boundary conditions will comprise P equations of the form

$g_j(u_i) = A_j$ at $\xi = 0$, $s = 0$ .....4.2.ix.a; and Q equations of the form

$f_\ell(y_i) = B_\ell$ at $\xi = 1$, $s = n$ .....4.2.ix.b where

$j = 1,2,\ldots P$; $\ell = 1,2,\ldots Q$; $i = 1,2,\ldots(P+Q)$, and $(P+Q)$ is the order of the differential equations (14, in this case). f_ℓ and g_j are functions of y_i and u_i respectively. Arbitrary (non-zero) values are assumed for Q of the u_i. Let these be u'_k, $k = m,n,\ldots$(to Q values). With these, the other u_i can be calculated using the boundary conditions $g_j(u_i) = A_j$, and the differential equations 4.2.iii p,q,r,t. Since these are not necessarily the correct values, they will be denoted by u'_i. A set of u'_i values are now available with which the step-wise integration process indicated in section 4.2.a can be advanced until the other boundary $\xi = 1$ is reached, yielding a set of variables y'_i at this point. Except by extreme chance the y'_i will not satisfy the boundary conditions $f_\ell(y_i) = B_\ell$. Let $f_\ell(y'_i) = B'_\ell$ .....4.2.x.

Each of the Q assumed u'_k is now increased partially in turn by a small amount and the quantities $\frac{\partial f_\ell}{\partial u'_k}$ are calculated. Finally the corrections $\Delta u'_k$ for the initially assumed u'_k are calculated from the Q simultaneous equations $\sum_k \frac{\partial f_\ell}{\partial u'_k} \Delta u'_k = B_\ell - B'_\ell$ .....4.2.xi, $\ell = 1,2, \ldots Q$. Better assumptions for u'_k are thus $u'_k + \Delta u'_k$. These are now used as starting values and the above process is repeated until the boundary conditions $f_\ell = B_\ell$ are satisfied to a desired accuracy.

In theory, for linear equations, the correct initial values u_i are arrived at by carrying out the above process only once. In practice, however, it may be necessary to repeat the process a few times if the initially assumed values are very poor. For most linear cases, convergence is very rapid and the boundary conditions are adequately satisfied after about two cycles.

4.2.c Systems with displacement forcing

Forcing function

To illustrate how the above general method can be applied to a specific problem, a beam with "displacement forcing" is considered. For such a beam, the supports are subjected to a sinusoidal motion of constant amplitude given by $a = a'_o \cos \omega t$ 4.2.xii

The forcing function p(x) is easily deduced from equations 4.1.xi to be $m\omega^2 a'_i$, where $y = u'_o \cos\omega t + v'_o \sin\omega t$ is, in this case,

the displacement of any point on the beam relative to the supports. Equation 4.2.i.a now becomes

$$D^4u_o + \gamma_1 D^4v_o + \alpha_1 D^3X_{o1} + \gamma_1 D^3Y_{o1} - \beta_1 u_o = \beta_1 a_o \quad \ldots\ldots 4.2.xii.a.$$

where $a_o = \frac{a'_o}{\ell}$. The rest of equations 4.2.i remain unchanged.

Boundary conditions

For a cantilever beam, with the end $\xi = 0$ so clamped as to prevent any shear in the viscoelastic material at that end, the appropriate boundary conditions are

(a) Zero slope, no relative displacement, and no shear deformation at $\xi = 0$.

(b) No longitudinal force in each layer at $\xi = 1$. Also the bending moment and its spatial rate of change must vanish at this point.

Using the notations of 4.2.viii, the above conditions can be put in the form given below.

$$\left.\begin{aligned} &\text{At } \xi = 0;\ u_i = 0,\ i = 1,2,\ldots 6 \quad \ldots.(a) - (f) \\ &\text{At } \xi = 1;\ y_{j+6} = 0,\ j = 1,2,\ldots 4 \quad \ldots.(g) - (j) \\ &\qquad y_{13} + \gamma_1 y_{14} + \alpha_1 y_{11} + \gamma_1 y_{12} = 0 \ldots\ldots(k) \\ &\qquad -\gamma_1 y_{13} + y_{14} - \gamma_1 y_{11} + \alpha_1 y_{12} = 0 \ldots.(l) \end{aligned}\right\} \ldots 4.2.xiii\ (a)-(l)$$

Two other boundary equations are required, and these are obtained by applying equations 4.1.iv at the point $\xi = 0$. This gives

$$\left.\begin{aligned} &\mu_1 u_{13} + \delta_1 u_{14} + u_{11} + \delta_1 u_{12} = 0 \ldots\ldots(m) \\ &-\delta_1 u_{13} + \mu_1 u_{14} - \delta_1 u_{11} + u_{12} = 0 \ldots.(n) \end{aligned}\right\} \quad \ldots.4.2.xiii.(m) - (n)$$

If the beam is simply supported at both ends such that

there is no axial restraint, and the ends are free from longitudinal stress, then the bending moment and the relative displacement vanish at both ends, giving rise to the relations

At $\xi = 0$; $u_1 = 0$, $u_2 = 0$, $u_{i+6} = 0$, $i = 1,2,..4$ ..4.2.xiv.a-f

At $\xi = 1$; $y_1 = 0$, $y_2 = 0$, $y_{i+6} = 0$, $i = 1,2,..4$ ..4.2.xiv.g-l

As above, two other equations are obtained by applying equations 4.1.xv at the boundary $\xi = 0$, giving

$$\left.\begin{aligned} \mu_i u_{13} + \delta_i u_{14} + u_{11} + \delta_i u_{12} - \nu_i u_3 - \sigma_i u_4 = 0 \;..(m) \\ -\delta_i u_{13} + \mu_i u_{14} - \delta_i u_{11} + u_{12} + \sigma_i u_3 - \nu_i u_4 = 0..(n) \end{aligned}\right\} \quad ..4.2.xiv.m\text{-}n.$$

The boundary equations for beams with other end conditions can be readily obtained following the lines illustrated above.

Solution of the equations

Once the boundary equations are known, the process of solution sketched above in sections 4.2.a and b can be applied. Still using the cantilever and the simply supported beams as illustrative cases, it is noted that for each case, six boundary equations are given at $\xi = 1$. Hence any six of the unknown quantities (u_i) at $\xi = 0$ are assumed. With these the remaining unknown u_i are calculated from the boundary equations and the differential equations. A set of 18 starting values are now available at $\xi = 0$. Corresponding values at each successive point are then calculated from the

equations 4.2.vii (a) - (n), 4.2.xii.a, and 4.2.i (b) - (d). This is very conveniently done by matrix inversion, the main matrix of the equations being the 18 x 18 matrix of equation 4.2.xv (see next page). When the boundary $\xi = 1$ is reached, the necessary corrections to the initially assumed values are calculated in the manner indicated in section 4.2.b. The above cycle of operations is then repeated using the corrected values as starting values. The correct solutions are those which satisfy the boundary conditions at $\xi = 1$.

A programme was written for the London University Atlas digital computer for the above process. The boundary equations at $\xi = 1$ were regarded as satisfied when the right-hand sides were less than 10^{-7}. In most cases this involved just one or two cycles.

4.2.d Effect of the step-length n

The accuracy of the results obtained with this method would naturally depend on the step-length, n, used in the step-wise integration process. Table 4.a gives the solutions obtained for the beam L1 (of section 4.1.b) for various step-lengths. The beam is solved as a cantilever with displacement forcing, and the forcing frequency is such that $\beta_1 = 10$. The percentage error relative to the "corrected" value is given underneath each figure. The "corrected" values are obtained by the method of interpolation suggested by

u_0^s	v_0^s	X_{01}^s	Y_{01}^s	π_2^s	π_3^s	π_4^s	π_5^s	π_6^s	π_7^s	π_8^s	π_9^s	π_{10}^s	π_{11}^s	π_{12}^s	π_{13}^s	π_{14}^s	π_{15}^s
1	·	·	·	$-\frac{h}{2}$	·	·	·	·	·	·	·	·	·	·	·	·	·
·	1	·	·	·	$-\frac{h}{2}$	·	·	·	·	·	·	·	·	·	·	·	·
·	·	1	·	·	·	$-\frac{h}{2}$	·	·	·	·	·	·	·	·	·	·	·
·	·	·	1	·	·	·	$-\frac{h}{2}$	·	·	·	·	·	·	·	·	·	·
·	·	·	·	1	·	·	·	$-\frac{h}{2}$	·	·	·	·	·	·	·	·	·
·	·	·	·	·	1	·	·	·	$-\frac{h}{2}$	·	·	·	·	·	·	·	·
·	·	·	·	·	·	1	·	·	·	$-\frac{h}{2}$	·	·	·	·	·	·	·
·	·	·	·	·	·	·	1	·	·	·	$-\frac{h}{2}$	·	·	·	·	·	·
·	·	·	·	·	·	·	·	1	·	·	·	$-\frac{h}{2}$	·	·	·	·	·
·	·	·	·	·	·	·	·	·	1	·	·	·	$-\frac{h}{2}$	·	·	·	·
·	·	·	·	·	·	·	·	·	·	1	·	·	·	$-\frac{h}{2}$	·	·	·
·	·	·	·	·	·	·	·	·	·	·	1	·	·	·	$-\frac{h}{2}$	·	·
·	·	·	·	·	·	·	·	·	·	·	·	1	·	·	·	$-\frac{h}{2}$	·
·	·	·	·	·	·	·	·	·	·	·	·	·	1	·	·	·	$-\frac{h}{2}$
·	·	·	·	·	·	$-V_1$	$-\sigma_1$	·	·	·	·	·	·	1	δ_1	μ_1	δ_1
·	·	·	·	·	·	σ_1	$-V_1$	·	·	·	·	·	·	$-\delta_1$	1	$-\delta_1$	μ_1
$-\beta_1$	·	·	·	·	·	·	·	·	·	·	·	·	·	α_1	γ_1	1	γ_1
·	$-\beta_1$	·	·	·	·	·	·	·	·	·	·	·	·	$-\gamma_1$	α_1	$-\gamma_1$	1

(Dots indicate zero terms)

Equation 4·2·xv — Main matrix for step-wise integration — linear case.

No.of steps	$\frac{u_o}{a_o}$	$\frac{V_o}{a_o}$	$\frac{X_{o1}}{a_o}$	$\frac{Y_{o1}}{a_o}$
5	-5.013465 (5.77)	3.500559 (16.0)	4.386566 (8.60)	0.232360 (-36.2)
10	-4.852005 (1.15)	3.129886 (3.76)	4.054024 (2.70)	0.335027 (-8.08)
20	-4.810786 (0.28)	3.044429 (0.93)	3.973944 (0.67)	0.357310 (-1.91)
40	-4.800445 (0.07)	3.023488 (0.23)	3.954126 (0.17)	0.362682 (-0.49)
"CORRECTED" VALUE	-4.796998	3.016508	3.947520	0.364473

TABLE 4.a.

Displacement and Shear Components at $\xi_o = 1$ for Cantilever Beam L1.

Richardson [82,83].

The table shows that as the number of steps is increased (i.e. the step-length is decreased) the accuracy of the solution increases. This is a consequence of the fact that the error in the finite-difference approximation becomes less and less as the step-length decreases. There is, however, a practical limit to the number of steps. Apart from the fact that the computation time increases with the number of steps; when the step-length becomes very small, there is the danger that rounding-off errors and other random errors may build up to substantial proportions, thereby nullifying the accuracy sought [84].

Twenty to forty steps were found sufficiently accurate for most of the computations made. No attempt was made to correct for the higher order terms of the finite difference expressions 4.2.iv which were dropped in the approximation 4.2.v. The solutions obtained proved sufficiently accurate; and when better accuracy was desired, this was achieved by increasing the number of steps and by interpolation.

4.2.e. Effect of the finite-difference approximation.

To check how the solutions were affected by the finite-difference approximation used, another finite-difference formula of a higher order truncation error was used, viz

$$\frac{1}{2}(y^{s} - y^{s-2}) = \frac{h}{6}(D y^{s-2} + 4D y^{s-1} + D y^{s}) \quad \ldots\ldots 4.2.xvi$$

with an error of the order h^5. This formula given by Crandall [84] is simply the application of Simpson's rule to the integration of differential equations. Unlike the previous one, it connects values at 3 successive points (instead of two). It is thus necessary to start it off using the finite-difference approximation of equation 4.2.v. Once this is done, the step-wise integration process can be carried out as above.

Table 4.b shows the solutions obtained for beam LI using the above finite-difference formula and various step-lengths. The displacement and shear components at $\xi = 1$ are given as well as their percentage differences relative to the "corrected" values.

Compared with the results of table 4.a, it is seen that for a given number of steps, the higher order difference formula gives more accurate results in the displacements but less accurate results in the shear components. As the number of steps increases, both solutions agree more closely. The "corrected" values (which are meant to be better approximations to the limiting case in which the number of steps becomes infinitely large) are seen to agree very well. It is observed, however, that the agreement in Y_{61}/a_0 is not very good. This is most likely due to the fact that for small values, errors (other than those due to the truncation of the difference equations) become of comparable

No. of steps	$\frac{u_o}{a_o}$	$\frac{v_o}{a_o}$	$\frac{X_{o1}}{a_o}$	$\frac{Y_{o1}}{a_o}$
10	-4.796226 (-0.012)	3.118992 (3.31)	3.976619 (0.68)	1.223462 (225.0)
20	-4.795455 (-0.028)	3.032301 (0.48)	3.964226 (0.37)	0.501335 (33.41)
40	-4.796696 (-0.002)	3.018711 (0.03)	3.950589 (0.02)	0.383528 (2.09)
"CORRECTED" VALUE	-4.796779	3.017805	3.949679	0.375673

TABLE 4.b.

Displacement and Shear Components at $\xi = 1$ for Cantilever Beam L1. "Higher order" Difference Formula.

magnitude and accurate results are difficult to obtain.

The above consideration shows that there is very little to suggest the second difference-formula in preference to the first which, in practice, is much easier to handle.

4.2.f. Extensional damping effects

From equations 4.1.xviii, the extensional damping coefficients γ_i, and δ_i, are seen to depend on the ratios H and $\eta_i e$ (or $\eta_i g_i$). It has already been pointed out that the coefficients γ_i, δ_i and σ_i control the damping in the system. The relative contribution of γ_i and δ_i to the overall damping would therefore depend on their magnitude compared with σ_i, which as well as depending on H and $\eta_i g_i$, also varies with P_i. As H increases, γ_i and δ_i increase, while σ_i decreases. Also σ_i is proportional to the square of P_i. It follows therefore that the extensional damping terms are more significant in short beams rather than long ones, and in beams with relatively thick and/or stiff viscoelastic layers.

Within frequency and temperature ranges of practical interest, the in-phase shear modulus of most viscoelastic materials lie between 10^5 and 10^2 lb/in^2 [44]. Hence for most engineering materials $\eta_i g_i$ is not likely to exceed 10^{-2}.

Tables 4.c & 4.d give the solutions of the 3-layer differential equations with and without extensional damping, for various values of g_i. Table 4.c is for a relatively

$g_1 = \frac{G_1'}{E_2}$	Forcing Frequency c.p.s.	Beam with Extensional Damping		Beam without Extensional Damping	
		$T_a = \frac{u_a}{a_o}$	$\frac{\hat{\Phi}_1}{a_o}$	$T_a = \frac{u_a}{a_o}$	$\frac{\hat{\Phi}_1}{a_o}$
10^{-5}	36.7	7.21213	15.25305	7.21235 (0.003)	15.25354 (0.003)
10^{-4}	66.0	6.88703	4.78205	6.88746 (0.006)	4.78244 (0.008)
10^{-3}	95.2	24.16341	1.25914	24.16946 (0.025)	1.25945 (0.024)

TABLE 4.c.

3-layer Beam with and without Extensional Damping.

Beam Dimensions and Material Properties:

$h_1 = 0.1$ in. ; $h_2 = 0.1$ in. ; $\ell = 10.0$ in. ;

$\rho_1 = 0.05$ lb/cu.in. ; $\rho_2 = 0.1$ lb/cu.in. ;

$E_2 = 10^7$ lb/sq.in. ; $\eta_1 = 1.0$

$g_1 = \frac{G_1'}{E_2}$	Forcing Frequency c.p.s.	Beam with Extensional Damping		Beam without Extensional Damping	
		$T_a = \frac{u_a}{a_o}$	$\frac{\hat{\Phi}_1}{a_o}$	$T_a = \frac{u_a}{a_o}$	$\frac{\hat{\Phi}_1}{a_o}$
10^{-5}	536.0	10.61996	16.37173	10.62139 (0.014)	16.37397 (0.014)
10^{-4}	656.0	7.27186	10.50375	7.29977 (0.26)	10.53208 (0.27)
10^{-3}	1248.0	4.249338	3.52930	4.27634 (0.64)	3.55709 (0.79)
10^{-2}	2980.0	5.03785	1.04092	5.08329 (0.91)	1.04997 (0.87)

TABLE 4.d.

3-layer Beam with and without Extensional Damping.

Beam Dimensions and Material Properties:

$h_1 = 0.4$ in. ; $h_2 = 0.1$ in. ; $\ell = 2.0$ in. ;
$\rho_1 = 0.05$ lb/cu.in. ; $\rho_2 = 0.1$ lb/cu.in. ;
$E_2 = 10^7$ lb/sq.in. ; $\eta_1 = 1.0$

long beam, while table 4.d is for a short beam with a thick viscoelastic layer. The figures given are the absolute displacement amplitude ratios (T_a) and the shear amplitude ratios ($\frac{\hat{\phi}}{a_o}$) at the free end of a cantilever beam with displacement forcing at the root. The percentage error in neglecting extensional damping is given below the figures where relevant. The forcing frequency in each case is so chosen as to be close to the first natural frequency of the beam.

It is seen from the tables that the error in neglecting extensional damping increases with g_1. This error is, however, still very small even at high values of g_1 and for most practical cases can be regarded as insignificant.

4.3. Solution of the linear differential equations by Chebyshev series

As a check on the accuracy of the solutions obtained by the finite-difference method of section 4.2., other methods of solution were employed. One such method is by expansion in Chebyshev polynomials. The procedure adopted is that due to Clenshaw [85,86] .

It is assumed that each variable and its derivatives can be expressed in infinite Chebyshev series in the form

$$\left.\begin{aligned} F &= \tfrac{1}{2}Z_o + \sum_{r=1}^{\infty} Z_r T^*_r(\xi) \\ DF &= \tfrac{1}{2}Z_o + \sum_{r=1}^{\infty} Z'_r T^*_r(\xi) \\ &\vdots \qquad\quad \vdots \\ D^i F &= \tfrac{1}{2}Z^i_o + \sum_{r=1}^{\infty} Z^i_r T^*_r(\xi) \end{aligned}\right\} \qquad \ldots\ldots 4.3.i.$$

where F and Z_r are "dummy variables". Z_r represents the coefficients A_r, B_r, C_r, or D_r according as F takes the values u_o, v_o, X_{o1} and Y_{o1} respectively. In equation 4.3.i, following the notation of Lanczos [86], $T^*_r(\xi)$ represents the Chebyshev polynomial of order r for the range $\xi = 0$ to 1.

The coefficients of the polynomials obey the recurrence relations

$$\left.\begin{aligned} 4rA'''_r &= A^{IV}_{r-1} - A^{IV}_{r+1} \\ 4rA''_r &= A'''_{r-1} - A'''_{r+1} \\ 4rA'_r &= A''_{r-1} - A''_{r+1} \\ 4rA_r &= A'_{r-1} - A'_{r+1} \end{aligned}\right\} \qquad \ldots\ldots 4.3.iia$$

with similar expressions for the B_r-coefficients, and

$$\left.\begin{aligned} 4rC''_r &= C'''_{r-1} - C'''_{r+1} \\ 4rC'_r &= C''_{r-1} - C''_{r+1} \\ 4rC_r &= C'_{r-1} - C'_{r+1} \end{aligned}\right\} \qquad \ldots\ldots 4.3.iib$$

with similar expressions for the D_r-coefficients. Also the assumed series of equations 4.3.i must satisfy the differential equations 4.2.i. This gives rise to the following relations:

$$\left.\begin{aligned}
&A^{IV}_r + \gamma_1 B^{IV}_r + \alpha_1 C'''_r + \gamma_1 D'''_r = a_r + \beta_1 A_r \\
&-\gamma_1 A^{IV}_r + B^{IV}_r - \gamma_1 C'''_r + \alpha_1 D'''_r = \beta_1 B_r \\
&\mu_1 A^{IV}_r + \delta_1 B^{IV}_r + C'''_r + \delta_1 D'''_r = \nu_1 C'_r + \sigma_1 D'_r \\
&-\delta_1 A^{IV}_r + \mu_1 B^{IV}_r - \delta_1 C'''_r + D'''_r = -\sigma_1 C'_r + \nu_1 D'_r
\end{aligned}\right\} \quad \ldots\ldots 4.3.iii,$$

where a_r is the r-th coefficient of the expansion in Chebyshev series of the forcing function. For a system with "displacement forcing",

$$\left.\begin{aligned}
a_r &= 2\beta_1 a_o, \quad \text{for } r = 0 \\
&= 0 \qquad \text{for } r \neq 0
\end{aligned}\right\} \quad \ldots\ldots\ldots 4.3.iv$$

Equations 4.3.i must also satisfy the boundary conditions at $\xi = 0$ and $\xi = 1$.

Using the relations

$$T^*_r(0) = (-1)^r \text{ and } T^*_r(1) = 1 \quad \ldots\ldots\ldots 4.3.iv,$$

the boundary equations 4.2.xiii for a cantilever beam with displacement forcing give rise to the equations

$$\left.\begin{aligned}
&A_o = {}^{+-}A \;,\; A'_o = {}^{+-}A' \;,\; B_o = {}^{+-}B \;,\; B'_o = {}^{+-}B' \\
&C_o = {}^{+-}C \;,\; D_o = {}^{+-}D \;,\; A''_o = {}^{--}A'' \;,\; B''_o = {}^{--}B'' \\
&C'_o = {}^{--}C' \;,\; D'_o = {}^{--}D' \\
&A'''_o + \gamma_1 B'''_o + \alpha_1 C''_o + \gamma_1 D''_o = {}^{--}A''' + \gamma_1 {}^{--}B''' + \alpha_1 {}^{--}C'' + \gamma_1 {}^{--}D'' \\
&-\gamma_1 A'''_o + B'''_o - \gamma_1 C''_o + \alpha_1 D''_o = -\gamma_1 {}^{--}A''' + {}^{--}B''' - \gamma_1 {}^{--}C'' + \alpha_1 {}^{--}D'' \\
&\mu_1 A'''_o + \delta_1 B'''_o + C''_o + \delta_1 D''_o = \mu_1 {}^{+-}A''' + \delta_1 {}^{+-}B''' + {}^{+-}C'' + \delta_1 {}^{+-}D'' \\
&-\delta_1 A'''_o + \mu_1 B'''_o - \delta_1 C''_o + D''_o = -\delta_1 {}^{+-}A''' + \mu_1 {}^{+-}B''' - \delta_1 {}^{+-}C'' + {}^{+-}D''
\end{aligned}\right\} \quad \ldots 4.3.v$$

where the notations

$${}^{+-}A^s = 2\sum_{r=1}^{\infty}(-1)^{r-1} A^s_r \;;\; {}^{--}A^s = -2\sum_{r=1}^{\infty} A^s_r \;, \text{ etc.} \quad \ldots 4.3.vi$$

have been employed. Similarly the equations in the case of a simply-supported beam are easily obtained from equations 4.2.xiv.

To solve the above equations for the coefficients, the infinite series are curtailed after a suitable number of terms, say at r = N. Thus $A^s_r = B^s_r = C^s_r = D^s_r = 0$ for $r > N$. The rest of the solution is then carried out in the following sequence:

(a) Assume trial values for A^s_N, B^s_N, C^s_N, and D^s_N such that they satisfy the differential equations i.e. equations 4.3.iii.

(b) Use the recurrence relations 4.3.ii and the equations 4.3.iii to obtain

A^{iv}_{N-1}, A^{iii}_{N-1}, A^{ii}_{N-1}, A^{i}_{N-1}, A_{N-1}

B^{iv}_{N-1}, B^{iii}_{N-1}, B^{ii}_{N-1}, B^{i}_{N-1}, B_{N-1}

C^{iii}_{N-1}, C^{ii}_{N-1}; C^{i}_{N-1}, C_{N-1}

D^{iii}_{N-1}, D^{ii}_{N-1}, D^{i}_{N-1}, D_{N-1}

The step for r = N-1 is thus complete.

(c) Continue operation (b) for r = N-2, N-3, etc. until the step r = 0 is reached.

(d) Having obtained

A^{iv}_o , A^{iii}_o , A^{ii}_o , A^{i}_o ; B^{iv}_o , B^{iii}_o , B^{ii}_o , B^{i}_o

C^{iii}_o , C^{ii}_o , C^{i}_o ; D^{iii}_o , D^{ii}_o , D^{i}_o

from the recurrence relations, determine A_o, B_o, C_o, D_o this time using four of the boundary equations 4.3.v. This leaves the four equations 4.3.iii at r = 0 and 10 other boundary equations unsatisfied.

(e) Go back to step (a), and assume a new set of values for the coefficients. Then repeat the cycle of operations to obtain a second set of trial solutions. Continue this process until 14 such sets of solutions are obtained.

A linear combination of these solutions, so chosen as to satisfy the 14 outstanding equations of step (d), gives the correct solution.

It may be pointed out that, owing to the convergence of the Chebyshev series, the coefficients A_r^s, B_r^s, etc. increase in magnitude as r decreases. Hence in dealing with high-order equations such as these, it may be necessary to keep the initially assumed values small, so as to avoid the lower coefficients becoming exceedingly large. This would be disadvantageous (especially in digital computation) since the solution sought is a linear combination of the various solutions and would therefore suffer from serious rounding-off errors if the individual quantities are large numbers.

Once the coefficients have been calculated, the displacement and shear components (as well as their derivatives) are obtained from equations 4.3.i. A table of the Chebyshev polynomials T_r^* can be found in [86].

A programme for calculating the coefficients in the manner outlined above was written for the Atlas computer.

Tables 4.e and 4.f give the solutions obtained for a cantilever beam and a simply-supported beam by both Chebyshev series and the finite-difference method. The dimensions given above for beam L1 are used in each case. The Chebyshev series expansions were terminated after the 10th term.

Agreement between the two methods of solution is seen to be good.

4.4. Solution of the differential equations by Fourier series expansions - 3-layer simply-supported beam without extensional damping.

When the extensional damping terms are neglected, the differential equations 4.1.xv take the form

$$\left.\begin{aligned} (D^4 - \beta_1)u_o + \alpha_1 D^3 X_{o1} &= a_o \beta_1 \\ (D^4 - \beta_1)v_o + D^3 Y_{o1} &= 0 \\ \mu_1 D^3 u_o + (D^2 - \nu_1)X_{o1} - \sigma_1 Y_{o1} &= 0 \\ \mu_1 D^3 v_o + (D - \nu_1)Y_{o1} + \sigma_1 X_{o1} &= 0 \end{aligned}\right\} \quad \ldots\ldots\ldots 4.4.i$$

for a beam with displacement forcing.

For a simply-supported beam, the variables u_o, v_o, X_{o1}, and Y_{o1} may be assumed to take the forms

	Chebyshev Series Solution	Finite-difference Solution (40 steps)
$\frac{u_o}{a_o}$ at $\xi = 1$	-4.789991	-4.796998
$\frac{v_o}{a_o}$ at $\xi = 1$	3.032033	3.016508
$\frac{X_{o1}}{a_o}$ at $\xi = 1$	3.941305	3.94752
$\frac{Y_{o1}}{a_o}$ at $\xi = 1$	0.344629	0.364473

TABLE 4.e

Cantilever Beam L1. $\beta_1 = 10$
Comparison of solutions by Chebyshev series and by Finite difference.

	Chebyshev Series Solution	Finite-difference Solution (40 steps)
$\frac{u_o}{a_o}$ at $\xi = \frac{1}{2}$	-0.339883	-0.339758
$\frac{v_o}{a_o}$ at $\xi = \frac{1}{2}$	4.524041	4.524703
$\frac{X_{o1}}{a_o}$ at $\xi = 1$	-7.303103	-7.31135
$\frac{Y_{o1}}{a_o}$ at $\xi = 1$	28.92389	28.92982

TABLE 4.f

Simply-supported Beam L1. $\beta_1 = 40$
Comparison of solutions by Chebyshev series and by Finite difference.

$$u_o = \sum_{n=1}^{\infty} a_{1n} \sin k_n\xi \quad ; \quad v_o = \sum_{n=1}^{\infty} a_{2n} \sin k_n\xi$$
$$X_{o1} = \sum_{n=1}^{\infty} a_{3n} \cos k_n\xi \quad ; \quad Y_{o1} = \sum_{n=1}^{\infty} a_{4n} \cos k_n\xi \qquad \text{.....4.4.ii}$$

where $k_n = n\pi$, $n = 1,2,\ldots$.

It is noted that the assumed functions satisfy the boundary conditions. a_o can also be expanded in an infinite sine series, thus $a_o = \sum_{n=1}^{\infty} b_n \sin k_n\xi$ .....4.4.iii ,

where $b_n = \frac{2a_o}{K_n}\{1 - (-1)^n\}$, or

$$b_{2r+1} = \frac{4a_o}{k_{2r+1}} \quad , \quad r = 0,1,2,\ldots \qquad \ldots 4.4.iv.$$

On substituting in the differential equations 4.4.i, the following algebraic equations relating the coefficients are obtained.

$$\left.\begin{aligned}
(k_n^4 - \beta_1)a_{1n} + \alpha_1 k_n^3 a_{3n} &= \beta_1 b_n \\
(k_n^4 - \beta_1)a_{2n} + \alpha_1 k_n^3 a_{4n} &= 0 \\
\mu_1 k_n^3 a_{1n} + (k_n^2 + \nu_1)a_{3n} + \sigma_1 a_{4n} &= 0 \\
\mu_1 k_n^3 a_{2n} + (k_n^2 + \nu_1)a_{4n} - \sigma_1 a_{3n} &= 0
\end{aligned}\right\} \qquad \text{.....4.4.v}$$

Equations 4.4.v are readily solved to obtain the following expressions:

$$a_{1n} = \frac{-\beta_1 b_n}{k_n^3}\left[\frac{(k_n^2 + \nu_1)\left\{\alpha_1\mu_1 k_n^3 - (k_n^2 + \nu_1)(k_n - \frac{\beta_1}{k_n^3})\right\} - \sigma_1^2(k_n - \frac{\beta_1}{k_n^3})}{D_n}\right]$$

$$a_{2n} = \frac{\mu_1\alpha_1\sigma_1\beta_1 b_n}{D_n}$$

$$a_{3n} = \frac{\mu_1\beta_1 b_n\left\{\alpha_1\mu_1 k_n^3 - (k_n^2 + \nu_1)(k_n - \frac{\beta_1}{k_n^3})\right\}}{D_n}$$

$$a_{4n} = \frac{-\mu_1\beta_1 b_n\left\{\sigma_1(k_n - \frac{\beta_1}{k_n^3})\right\}}{D_n} \qquad \text{.....4.4.vi}$$

where

$$D_n = \left\{\alpha_1\mu_1 k_n^3 - (k_n^2 + \nu_1)(k_n - \frac{\beta_1}{k_n^3})\right\}^2 + \left\{\sigma_1(k_n - \frac{\beta_1}{k_n^3})\right\}^2 .$$

The above coefficients can now be calculated using a desk machine or a digital computer.

Table 4.3 gives the first six non-zero coefficients of the Fourier series expansion for u_o , v_o , X_{o1}, and Y_{o1}. The same beam L1 is considered, and the forcing frequency is such that $\beta_1 = 40$. It can be seen that the rate of convergence is fairly rapid for the beam considered.

Table 4.4 gives a comparison of the solutions obtained by the Fourier series expansions and the finite-difference method. The close agreement between the two solutions further checks on the accuracy of the numerical method.

n	a_{1n}	a_{2n}	a_{3n}	a_{4n}
1	-3.27728×10^{-1}	4.52624	7.74774	-2.88659×10^{1}
3	1.29830×10^{-2}	1.91479×10^{-3}	-3.49483×10^{-1}	-6.18445×10^{-2}
5	1.17027×10^{-3}	7.49050×10^{-5}	-5.42232×10^{-2}	-4.05007×10^{-3}
7	2.28381×10^{-4}	7.92945×10^{-6}	-1.49398×10^{-2}	-6.00529×10^{-4}
9	6.63768×10^{-5}	1.43185×10^{-6}	-5.60165×10^{-3}	-1.39438×10^{-4}
11	2.46012×10^{-5}	3.60207×10^{-7}	-2.54180×10^{-3}	-4.28746×10^{-5}

TABLE 4.g

Beam L1. $\beta_1 = 40$ Fourier Series Coefficients.

	Fourier series Solution	Finite-difference Solution(40 steps)
$\frac{u_o}{a_o}$ at $\xi = \frac{1}{2}$	-0.33972	-0.33986
$\frac{v_o}{a_o}$ at $\xi = \frac{1}{2}$	4.52439	4.52493
$\frac{X_{o1}}{a_o}$ at $\xi = 0$	7.31844	7.31244
$\frac{Y_{o1}}{a_o}$ at $\xi = 0$	-28.93263	-28.90142

TABLE 4.h

Simply-supported Beam L1. $\beta_1 = 40$

Comparison of solutions by Fourier series and by Finite difference.

4.5. Solution of the equations taking account of strain-dependence.

It has been pointed out that when the shear modulus G_1' is strain-dependent, each of the coefficients of the differential equations is strain-dependent. The methods of solution so far discussed cannot be directly applied in this case.

It will be assumed, for simplicity of illustration, that the only coefficients that are significantly affected by the strain-amplitude dependence of G_1' are ν_1 and σ_1. This is equivalent to assuming that the viscoelastic extensional terms make very little contribution to the coefficients, so that any small variations in these terms (due to the strain-dependence) have negligible effect.

On this assumption, the differential equations 4.1.xv remain valid. To get them into a homogeneous form, equations 4.1.xv (c) and (d) are differentiated with respect to ξ, to obtain

$$\left.\begin{aligned} &\mu_1 D^4 u_0 + \delta_1 D^4 v_0 + D^3 X_{01} + \delta_1 D^3 Y_{01} - \nu_1 D X_{01} - \sigma_1 D Y_{01} - \nu_1' X_{01} - \sigma_1' Y_{01} = 0 \\ &-\delta_1 D^4 u_0 + \mu_1 D^4 v_0 - \delta_1 D^3 X_{01} + D^3 Y_{01} + \sigma_1 D X_{01} - \nu_1 D Y_{01} + \sigma_1' X_{01} - \nu_1' Y_{01} = 0 \end{aligned}\right\} \quad \ldots\ldots 4.5.i$$

where $\sigma_1' = \dfrac{d\sigma_1}{d\xi}$, and $\nu_1' = \dfrac{d\nu_1}{d\xi}$ $\quad \ldots\ldots\ldots 4.5.ii.$

It is noted that

$$\frac{d\sigma_1}{d\xi} = \frac{\ell^2 b}{Q_{11}'} \frac{d}{d\xi}(\eta_1 G_1') \quad , \quad \text{and} \quad \frac{d\nu_1}{d\xi} = \frac{\ell^2 b}{Q_{11}'} \frac{dG_1'}{d\xi} \quad .$$

Since G_1' and $\eta_1 G_1'$ are functions of the strain amplitude $\hat{\phi}_1$,

it follows that

$$\frac{dG_1'}{d\xi} = \frac{dG_1'}{d\hat{\phi}_1}\frac{d\hat{\phi}_1}{d\xi}, \quad \text{and} \quad \frac{d(\eta_1 G_1')}{d\hat{\phi}_1}\frac{d\hat{\phi}_1}{d\xi} = \frac{d(\eta_1 G_1')}{d\xi} \qquad \text{.....4.5.iii.}$$

Both $\frac{dG_1'}{d\hat{\phi}_1}$ and $\frac{d(\eta_1 G_1')}{d\hat{\phi}_1}$ are obtained from the law of strain-amplitude dependence for η_1 and G_1'. To obtain $\frac{d\hat{\phi}_1}{d\xi}$, it is noted that $\hat{\phi}_1 = (X_{o1}^2 + Y_{o1}^2)^{1/2}$, so that

$$\frac{d\hat{\phi}_1}{d\xi} = \frac{X_{o1}DX_{o1} + Y_{o1}DY_{o1}}{\{X_{o1}^2 + Y_{o1}^2\}^{1/2}} \qquad \text{.....4.5.iv.}$$

To solve the equations, an iterative method is employed, the numerical method of solution developed in section 4.2. being used. A convenient shear-strain distribution is assumed for the viscoelastic layer. With this, the coefficients ν_1, σ_1, ν_1', and σ_1' are calculated for each point on the beam. Using these values of the coefficients, the differential equations can now be solved by the finite-difference method. The process of solution is basically the same as described in section 4.2. The only difference is that the main matrix (for the step-wise integration process) which now takes the form given in equation 4.5.v (see next page) varies from point to point. The boundary condition control is the same. The solution of the equations will yield a new shear-strain distribution which will in general be different from that initially assumed. With this new shear distribution, ν_1, σ_1, ν_1', and σ_1' are again calculated for each point, and the equations

u_o^s	v_o^s	X_{o1}^s	Y_{o1}^s	π_2^s	π_3^s	π_4^s	π_5^s	π_6^s	π_7^s	π_8^s	π_9^s	π_{10}^s	π_{11}^s	π_{12}^s	π_{13}^s	π_{14}^s	π_{15}^s
1	•	•	•	$-\frac{h}{2}$	•	•	•	•	•	•	•	•	•	•	•	•	•
•	1	•	•	•	$-\frac{h}{2}$	•	•	•	•	•	•	•	•	•	•	•	•
•	•	1	•	•	•	$-\frac{h}{2}$	•	•	•	•	•	•	•	•	•	•	•
•	•	•	1	•	•	•	$-\frac{h}{2}$	•	•	•	•	•	•	•	•	•	•
•	•	•	•	1	•	•	•	$-\frac{h}{2}$	•	•	•	•	•	•	•	•	•
•	•	•	•	•	1	•	•	•	$-\frac{h}{2}$	•	•	•	•	•	•	•	•
•	•	•	•	•	•	1	•	•	•	$-\frac{h}{2}$	•	•	•	•	•	•	•
•	•	•	•	•	•	•	1	•	•	•	$-\frac{h}{2}$	•	•	•	•	•	•
•	•	•	•	•	•	•	•	1	•	•	•	$-\frac{h}{2}$	•	•	•	•	•
•	•	•	•	•	•	•	•	•	1	•	•	•	$-\frac{h}{2}$	•	•	•	•
•	•	•	•	•	•	•	•	•	•	1	•	•	•	$-\frac{h}{2}$	•	•	•
•	•	•	•	•	•	•	•	•	•	•	1	•	•	•	$-\frac{h}{2}$	•	•
•	•	•	•	•	•	•	•	•	•	•	•	1	•	•	•	$-\frac{h}{2}$	•
•	•	•	•	•	•	•	•	•	•	•	•	•	1	•	•	•	$-\frac{h}{2}$
•	•	$-\gamma_1'$	$-\sigma_1'$	•	•	$-\gamma_1$	$-\sigma_1$	•	•	•	•	•	•	1	δ_1	μ_1	δ_1
•	•	σ_1'	$-\gamma_1'$	•	•	σ_1	$-\gamma_1$	•	•	•	•	•	•	$-\delta_1$	1	$-\delta_1$	μ_1
$-\beta_1$	•	•	•	•	•	•	•	•	•	•	•	•	•	α_1	γ_1	1	γ_1
•	$-\beta_1$	•	•	•	•	•	•	•	•	•	•	•	•	$-\gamma_1$	α_1	$-\gamma_1$	1

(Dots indicate zero terms)

Equation 4.5.v — Main matrix for step-wise integration – strain-dependence case.

solved again. This cycle of operations is repeated until convergence is achieved, that is, two successive strain distributions agree to a specified accuracy.

A programme for solving in the above manner the equations for a beam with displacement forcing was developed for the Atlas computer*.

It was assumed initially that only ν_i and σ_i were affected by strain-dependence. This assumption does not, however, determine the validity of the above method of solution. Consideration of the strain-dependence of the other coefficients merely involves introducing further terms similar to ν_i', and σ_i' in the equations. The iterative procedure remains valid.

Tables 4.i to 4.ℓ give the solutions obtained by the above method for various cantilever beams. Solutions obtained by assuming a constant strain distribution are also shown alongside for purposes of comparison. The laws of strain-amplitude dependence used are as embodied in the graphs of shear modulus G_i' and loss factor η_i against strain amplitude for the materials, as given in chapter 3. In the tables, T_a is the absolute displacement amplitude ratio at the tip, already defined in section 4.2.f, and

*This and all the other programmes mentioned in this chapter are available in the Imperial College (Mech. Eng.) programme library.

FREQ. c.p.s.	"Strain-dependence" solution Input motion ampl. = 0.00055 in.		"Constant-strain" solution Assumed strain ampl. = 0.0001		"Constant-strain" solution Assumed strain ampl. = 0.001	
	$T_a = \frac{u_a}{a_o}$	$\frac{\hat{\phi}_1}{a_o}$	$T_a = \frac{u_a}{a_o}$	$\frac{\hat{\phi}_1}{a_o}$	$T_a = \frac{u_a}{a_o}$	$\frac{\hat{\phi}_1}{a_o}$
20	1.67820	0.95944	1.67856 (0.02)	0.96066 (0.13)	1.68046 (0.13)	0.96694 (0.78)
37	7.92228	9.52738	7.93556 (0.17)	9.46961 (-0.61)	7.88784 (-0.43)	9.70440 (1.86)
37.5	7.87429	9.61608	7.90663 (0.41)	9.57881 (-0.39)	7.80223 (-0.91)	9.74936 (1.38)
38	7.70183	9.54664	7.75014 (0.69)	9.53606 (-0.10)	7.59733 (-1.36)	9.63946 (0.97)
40	6.34319	8.31517	6.40123 (0.92)	8.33460 (0.23)	6.18676 (-2.47)	8.32405 (0.11)

TABLE 4.i

Aluminium - P.V.C. 3-layer beam. Solutions in the region of the first resonant frequency (37 c.p.s.).
h_1 = 0.135 in. ; h_2 = 0.25 in. ; ℓ = 20 in. ; T = 27°C
$E_2 = 1.0 \times 10^7$ lb/in² ; ρ_2 = 0.1 lb/cu.in. ; ρ_1 = 0.048 lb/in³
for the properties of P.V.C., see figs 3.19 to 3.23.

Forcing Frequency	"Strain-dependence" Solution Input motion ampl. = 0.00034 in.		"Constant-strain" Solution Assumed constant-strain ampl. = 10^{-4}	
c.p.s.	$T_a = \frac{u_a}{a_o}$	$\frac{\hat{\phi}_1}{a_o}$	$T_a = \frac{u_a}{a_o}$	$\frac{\hat{\phi}_1}{a_o}$
150	1.51368	9.81636	1.50994 (-0.25)	9.75641 (-0.61)
195	4.23649	33.88405	4.07727 (-3.76)	32.03876 (-2.49)
205	4.79761	39.96995	4.70980 (-1.87)	38.43920 (-3.82)
220	3.61738	31.63785	3.69162 (2.21)	31.79417 (0.50)
250	1.89948	18.16827	1.91650 (0.90)	18.19771 (0.16)

TABLE 4.j

Steel - P.V.C. 3-layer beam. Solutions in the region of the second resonant frequency (206 c.p.s).

h_2 = 0.187 in. ; h_1 = 0.137 in. ; ℓ = 15 in. ; T = 26.7 °C

E_2 = 3.0 x 10^7 lb/in^2; ρ_2 = 0.283 lb/cu.in. ; ρ_1 = 0.048 lb/in^3.

For the properties of P.V.C., see figs 3.19 to 3.23.

Forcing frequency	"Strain-dependence" solution Input motion ampl. = 0.000226 in.		"Constant-strain" solution Assumed strain ampl. = 0.0001	
c.p.s.	$T_a = \frac{u_a}{a_o}$	$\frac{\hat{\phi}_1}{a_o}$	$T_a = \frac{u_a}{a_o}$	$\frac{\hat{\phi}_1}{a_o}$
480	2.27396	32.30699	2.22425 (-2.23)	31.38506 (-2.87)
520	3.75240	56.25050	3.59180 (-4.27)	53.18631 (-5.45)
528	3.77443	57.09430	3.66527 (-2.90)	54.76321 (-4.08)

TABLE 4.k

Steel - P.V.C. 3-layer beam. Solutions in the region of the third resonant frequency (527 c.p.s.).
h_1 = 0.137 in. ; h_2 = 0.187 in. ; ℓ = 15 in. ; T = 23.8 °C
E_2 = 3.0 x 10^7 lb/sq.in. ; ρ_2 = 0.283 lb/cu.in. ; ρ_1 = 0.048 lb/in^3.
for the properties of P.V.C., see figs 3.19 to 3.23.

Forcing frequency	"Strain-dependence" solution Input motion ampl. = 0.000681 in.		"Constant-strain" solution Assumed strain ampl. = 0.001	
c.p.s.	$T_a = \frac{u_a}{a_o}$	$\frac{\hat{\phi}_1}{a_o}$	$T_a = \frac{u_a}{a_o}$	$\frac{\hat{\phi}_1}{a_o}$
25	2.06390	1.82247	2.09394 (1.46)	1.95800 (7.42)
36	4.393373	5.97061	4.39791 (0.10)	6.25083 (4.70)
38	4.57243	6.60001	4.52635 (-1.02)	6.81744 (3.29)
40	4.38430	6.67925	4.29945 (-1.97)	6.83503 (2.33)
50	2.43571	4.69133	2.37005 (-2.70)	4.71293 (2.64)

TABLE 4.ℓ

Aluminium - Evoseal 3-layer beam. Solutions in the region of the first resonant frequency (37.8 c.p.s)

h_1 = 0.057 in. ; h_2 = 0.125 in. ; ℓ = 14.02 in. ; T = 22.1°C

E_2 = 1.0 x 10^7 lb/in^2. ; ρ_2 = 0.1 lb/cu.in. ; ρ_1 = 0.041 lb/in^3.

for the properties of Evoseal, see figs 3.31 & 3.32.

$\hat{\phi}_1$ is the shear-strain amplitude at the free end. The percentage error in the "constant strain" solutions (relative to the "strain-dependence" solutions) is given underneath each figure.

In general, the tables show that strain-dependence has comparatively little effect on the displacement amplitude. The error in the solutions which assume a constant shear-strain distribution would naturally depend on the actual value of the shear strain assumed. For example, in table 4.i, it is seen that an assumed constant shear-strain amplitude of 0.0001 gives a better approximation to the exact solution than a value of 0.001. Tables 4.j and 4.k show that the negligence of strain-dependence leads to worse results at the higher modes of vibration of the beam. This is clearly due to the fact that the variation of the shear strain ϕ_1 along the beam becomes much greater at these modes.

It has been tacitly assumed that the above method will always converge to a unique solution no matter the nature of the initially assumed strain distribution. The establishment of an "Existence theorem" for the method is evidently a difficult mathematical problem, and is not attempted here. It is, however, believed that provided the degree of strain-dependence is sufficiently small for a unique solution to exist, the above method will always

converge to this solution.

In all the cases in which the method was applied, a constant shear-strain distribution was initially assumed. It was found that (for the viscoelastic material properties available) no matter the value of the initially assumed strain amplitude, the solutions converged to the same final result. Convergence to an accuracy of better than 0.01 per cent was usually obtained within three cycles.

4.6. Application of the solutions.

4.6.a. Resonance curves.

It will now be shown how the solutions developed can be employed in predicting the dynamic behaviour of actual beams.

Suppose, for instance, that it is desired to obtain the displacement response of a 3-layer beam subjected to displacement forcing, within a frequency range close to any of its "resonant frequencies" (that is, its "displacement resonance curve"). Then, for the given temperature, a suitable frequency is chosen. The viscoelastic material properties can now be obtained from the appropriate graphs of the properties (or from any general equations satisfying these graphs), on the assumption of a convenient shear-strain amplitude. From the dimensions of the beam and the material properties, the coefficients of the

differential equations are evaluated. The equations are then solved by the finite-difference method. They are solved again by the "iterative method" of section 4.5 to check that the above "constant-strain" solution gives reasonably accurate results for the displacements. Various values of the frequency are now chosen in turn, the equations being solved in each case as above. The process is stopped when the desired frequency range has been satisfactorily covered.

The absolute displacement-amplitude ratio, T_a , at a typical point on the beam (for instance, the free end, for a cantilever beam), together with its phase relative to the input motion, is plotted against the forcing frequency. The frequency at which this amplitude ratio is a maximum is referred to here as a "resonant frequency" of the beam*, and in the immediate neighbourhood of this frequency, the graphs of the amplitude ratio, T_a, and its phase, against the frequency, are called "displacement-resonance curves". At the resonant frequency, the locus of the absolute displacement amplitudes at each point on the beam will be referred to (rather loosely) as the "mode shape" at that frequency. In plotting this locus, the following convention

*Close to the resonant frequency, frequency steps of 0.5 per cent (or less) difference were taken in the calculations, in order to locate the peak of the resonance curve accurately.

has been adopted: If the phase difference between the absolute displacement at a given point and the input motion is positive (i.e. between 0° and 180° , with the input motion leading), the displacement amplitude at that point (or its ratio relative to the input motion) is plotted below the axis; otherwise, it is plotted above the axis. It is emphasized that this locus does not represent the true shape of the beam at the resonant frequency. The true beam-shape would require a three-dimensional polar plot to indicate the variation, along the beam length, of the displacement amplitude as well as its phase relative to the input motion. The locus described here is only a convenient way of representing the displacement amplitudes at various points along the beam, for comparison with experimentally measured values (see chapter 5).

For examples of the above-mentioned graphs, see figs 5.6 to 5.15.

4.6.b. Overall loss factor - 3-layer beam.

One way of specifying the damping in the beam is by the "loss factor". The definition of "loss factor" employed by Kerwin et al [41,44,47], and by Mead [62,63] are strictly applicable to systems whose dynamic flexural rigidity (i.e. the ratio of the resisting moment to the curvature) is independent of the position along the beam. A typical example of such a system would be a beam whose displacement

and shear amplitudes, at a resonant frequency, are sinusoidally distributed along the length (for instance, a lightly-damped simply-supported beam). For most damped sandwich beams, however, the dynamic flexural rigidity varies from point to point along the beam. Hence, a loss factor defined as the ratio of the quadrature component to the in-phase component of the dynamic flexural rigidity, would vary from point to point along the beam, and would therefore not have a unique value for the system.

In the present work, the energy definition of "loss factor" (applicable to all damped systems [8]) is used in the form

$$\eta_{on} = \frac{1}{2\pi}\left\{\frac{\text{Total energy dissipated per cycle}}{\text{Maximum strain energy in a cycle}}\right\} \quad \ldots\ldots\ldots 4.6.i,$$

η_{on} being used to designate the "overall loss factor" or the "beam loss factor". It is noted that this definition has the same form as the energy definition of the material loss factor given in equation 3.1.ix.d. η_{on} is evaluated at a resonant frequency, and is termed the beam loss factor for the mode, n, of flexural vibration corresponding to this frequency. The expressions for evaluating it are developed below for a 3-layer beam.

From equation 3.1.ix.a, the energy dissipated per cycle in an elemental volume dV_i of the viscoelastic material

is given by $\Delta E_D = \pi\eta_1\left\{G_1'\hat{\phi}_1^2 + E_1'\hat{\epsilon}_1^2\right\}dV_1$ 4.6.ii,

where $\hat{\phi}_1$ and $\hat{\epsilon}_1$ represent the shear and extensional strain amplitudes in the element. The total cyclic energy loss in the viscoelastic material - and hence in the beam - is thus

$$E_D = \pi\eta_1\int_{V_1}\left[G_1'\hat{\phi}_1^2 + E_1'\hat{\epsilon}_1^2\right]dV_1 \quad \text{.....4.6.iii.}$$

Noting that $\hat{\phi}_1^2 = X_{o1}^2 + Y_{o1}^2$, and

$\hat{\epsilon}_1^2 = \frac{z^2}{\ell^2}\left\{\left(\frac{d^2u_o}{d\xi^2} + \frac{dX_{o1}}{d\xi}\right)^2 + \left(\frac{d^2v_o}{d\xi^2} + \frac{dY_{o1}}{d\xi}\right)^2\right\}$, equation 4.6.iii can be reduced to the form

$$E_D = 2\pi\left(\frac{EI}{2\ell}\right)\left\{\int_0^1 \gamma_1\left[\left(D^2u_o + DX_{o1}\right)^2 + \left(D^2v_o + DY_{o1}\right)^2\right] + \eta_1\lambda_1\left[X_{o1}^2 + Y_{o1}^2\right]d\xi\right\} \quad \text{.4.6.i}$$

where $\lambda_1 = \frac{\ell^2 b G_1' h_1}{EI} = \frac{12p^2 g_1 H}{8 + 12H + 6H^2 + eH^3}$ 4.6.v;

and γ_1 is as defined in equations 4.1.xviii. The operator $D = \frac{d}{d\xi}$ has again been employed.

The strain energy in an element dV of any layer of the beam is given by $\Delta(S.E.) = \frac{1}{2}K_s S^2 dV$, where S is the strain in the element, and K_s is the appropriate modulus. The elastic top and bottom layers suffer only extensional (or compressive) deformation, while the central viscoelastic layer undergoes both shear and extensional deformation. Hence the total strain energy in the viscoelastic layer 1 at any time t is given by

$S.E._1 = \frac{1}{2}\int_{V_1}\left[E_1'\epsilon_1^2 + G_1'\phi_1^2\right]dV_1$ .....4.6.vi; and the

strain energy in each of the elastic layers is

$$S.E._2 = \frac{1}{2}\int_{V_2} E_2 \epsilon_2^2 \, dV_2 \quad \ldots\ldots\ldots\ldots 4.6.vii.$$

When the expressions for the various strains are substituted into equations 4.6.vi and 4.6.vii, and the integrals are simplified, the total strain energy in the beam, at any time t, can be put into the form

$$S.E. = \frac{EI}{2\ell}\left\{A_1' \cos^2 \omega t + B_1' \sin^2 \omega t + 2C_1' \sin \omega t \cos \omega t\right\} \quad \ldots 4.6.viii$$

where

$$A_1' = \int_0^1 \left[(D^2 u_o)^2 + 2\alpha_1 D^2 u_o DX_{o1} + \lambda_2 (DX_{o1})^2 + \lambda_1 X_{o1}^2\right] d\xi \quad \ldots\ldots 4.6.ix.a$$

$$B_1' = \int_0^1 \left[(D^2 v_o)^2 + 2\alpha_1 D^2 v_o DY_{o1} + \lambda_2 (DY_{o1})^2 + \lambda_1 Y_{o1}\right] d\xi \quad \ldots\ldots\ldots 4.6.ix.b$$

$$C_1' = \int_0^1 \left[D^2 u_o D^2 v_o + \alpha_1 D^2 u_o DY_{o1} + \alpha_1 D^2 v_o DX_{o1} + \lambda_2 DX_{o1} DY_{o1} + \lambda_1 X_{o1} Y_{o1}\right] d\xi \ldots$$
$$\ldots\ldots 4.6.ix.c.$$

In equations 4.6.ix a to c ,

$$\lambda_2 = \frac{E_2 A_2 \frac{h_1^2}{2} + E_1 I_{N1}}{EI} = \frac{6H^2 + eH^3}{8 + 12H + 6H^2 + eH^3} \quad \ldots 4.6.x.$$

The maximum value of the expression 4.6.viii, as time varies, is given by

$$[S.E.]_{max} = \frac{EI}{2\ell}\left\{\frac{1}{2}\left[A_1' + B_1'\right] + \frac{1}{2}\left[(A_1' - B_1')^2 + 4C_1'^2\right]^{\frac{1}{2}}\right\} \quad \ldots\ldots 4.6.xi.$$

On denoting $\int_0^1 \left[Y_1\left\{(D^2 u_o + DX_{o1})^2 + (D^2 v_o + DY_{o1})^2\right\} + \eta_1 \lambda_1 (X_{o1}^2 + Y_{o1}^2)\right] d\xi$

by D_1' .....4.6.ix.d , the beam loss factor is given by

$$\eta_{on} = \frac{D_1'}{\frac{1}{2}\left[A_1' + B_1' + \left\{(A_1' - B_1')^2 + 4C_1'^2\right\}^{1/2}\right]} \quad .....4.6.xii.$$

Once the differential equations have been solved, η_{on} can be calculated. The integrations involved in the evaluation of A_1', B_1', C_1', and D_1' are carried out numerically using Simpson's rule.

A programme for calculating the beam loss factor in the manner indicated above was written for the Atlas Computer.

It may be remarked that for systems whose dynamic flexural rigidity is independent of the position along the beam, the beam loss factor defined here is not the same as the ratio of the imaginary to the real part of the complex dynamic flexural rigidity. This is a consequence of the fact that the strains in the various fibres are not all in phase with one another. Both definitions of the loss factor will tend to the same value at small values of the system damping when the fibre-strains become in phase with one another.

4.7. Five-layer beam - Solution of the differential equations.

As in the case of the 3-layer beam, it is first assumed that the coefficients of the differential equations are strain-independent. Equations 2.3.xxvii

and 2.3.xxx thus become

$$\left.\begin{aligned} EI\frac{\partial^4 y}{\partial x^4} + N_2'\frac{\partial^3 \phi_2}{\partial x^3} + \frac{\partial^2}{\partial x^2}(\amalg_{m2}) + m\frac{\partial^2 y}{\partial t^2} &= p(x,t) \\ P_2'\frac{\partial^3 y}{\partial x^3} + Q_{22}'\frac{\partial^2 \phi_2}{\partial x^2} + \frac{\partial}{\partial x}(\amalg_{F2}) - \eta_2 b G_2' \amalg(\phi_2) &= bG_2'\phi_2 \end{aligned}\right\} \ldots 4.7.i .$$

On assuming a sinusoidal forcing function, of frequency ω, viz., $p(x,t) = p(x)\cos\omega t$ .....4.7.ii, the variables, y and ϕ_2, take the forms

$y = u_o'\cos\omega t + v_o'\sin\omega t$; $\phi_2 = X_{o2}\cos\omega t + Y_{o2}\sin\omega t$ ..4.7.ii

With these, the $\amalg$-functions can be determined in the manner illustrated in section 4.1.a. They are quoted below.

$$\left.\begin{aligned} \amalg_{m2} &= 2\eta_2 E_2' I_{w2}\left\{\frac{d^2 v_o'}{dx^2}\cos\omega t - \frac{d^2 u_o'}{dx^2}\sin\omega t\right\} \\ &\quad + 2\eta_2\left(E_2'A_2\frac{h_2^2}{12} + E_2'A_2\frac{d_2}{2}h_2\right)\left\{\frac{dY_{o2}}{dx}\cos\omega t - \frac{dX_{o2}}{dx}\sin\omega t\right\} \quad \ldots(a) \\ \amalg_{F2} &= \eta_2\left(E_2'A_2\frac{h_2}{8} + E_2'A_2\frac{d_2}{2}\right)\left\{\frac{d^2 v_o'}{dx^2}\cos\omega t - \frac{d^2 u_o'}{dx^2}\sin\omega t\right\} \\ &\quad + \left(\frac{3}{8}E_2'A_2 h_2\right)\left\{\frac{dY_{o2}}{dx}\cos\omega t - \frac{dX_{o2}}{dx}\sin\omega t\right\} \quad \ldots\ldots(b) \\ \eta_2 G_2' b \amalg(\phi_2) &= \eta_2 b G_2'\left\{Y_{o2}\cos\omega t - X_{o2}\sin\omega t\right\} \quad \ldots\ldots(c) \end{aligned}\right\} \ldots\ldots 4.7.iv.$$

The distinction between the extensional and shear loss factors has been dropped in the above expressions, i.e., $\eta_{G2} = \eta_{e2} = \eta_2$.

Equations 4.7.ii, iii, and iv can be substituted into the differential equations, and the coefficients of $\sin\omega t$ and $\cos\omega t$ equated to zero. The resulting equations are then put into a dimensionless form, employing the

dimensionless variables $u_o = \frac{u'_o}{l}$, $v_o = \frac{v'_o}{l}$, $\xi = \frac{x}{l}$ ...4.7.v,

and simplifying to obtain

$$\left.\begin{aligned} &D^4u_o + \gamma_2 D^4v_o + \alpha_2 D^3X_{o2} + \gamma_3 D^3Y_{o2} - \beta_2 u_o = \frac{l^3}{EI}p(l\xi) \\ &-\gamma_2 D^4u_o + D^4v_o - \gamma_3 D^3X_{o2} + \alpha_2 D^3Y_{o2} - \beta_2 v_o = 0 \\ &\mu_2 D^3u_o + \delta_2 D^3v_o + D^2X_{o2} + \delta_3 D^2Y_{o2} - \nu_2 X_{o2} - \sigma_2 Y_{o2} = 0 \\ &-\delta_2 D^3u_o + \mu_2 D^3v_o - \delta_3 D^2X_{o2} + D^2Y_{o2} + \sigma_2 X_{o2} - \nu_2 Y_{o2} = 0 \end{aligned}\right\} \text{...4.7.vi,}$$

where,

$$\left.\begin{aligned} &\alpha_2 = \frac{N'_2}{EI}, \quad \beta_2 = \frac{m\omega^2 l^4}{EI}, \quad \gamma_2 = \frac{2\eta_2 E'_2 I_{N2}}{EI}, \quad \mu_2 = \frac{P'_2}{Q'_{22}} \\ &\gamma_3 = \frac{2\eta_2\left(E'_2A_2\frac{h_2^2}{12} + E'_2A_2d_2\frac{h_2}{2}\right)}{EI}, \quad \delta_2 = \frac{\left(E'_2A_2\frac{h_2}{8} + E'_2A_2\frac{d_2}{2}\right)}{Q'_{22}} \\ &\delta_3 = \frac{3}{8}\frac{\eta_2 E'_2A_2h_2}{Q'_{22}}, \quad \nu_2 = \frac{l^2bG'_2}{Q'_{22}}, \quad \sigma_2 = \frac{\eta_2 l^2bG'_2}{Q'_{22}}. \end{aligned}\right\} \text{..4.7.vii}$$

The right-hand sides of equations 4.7.vii can also be expressed in terms of the dimensionless ratios

$$\left.\begin{aligned} &H_1 = \frac{h_1}{h_3}, \quad H_2 = \frac{h_2}{h_3}, \quad P_2 = \frac{l}{h_3}, \quad g_2 = \frac{G'_2}{E_3}, \\ &e_1 = \frac{E_1}{E_3}, \quad e_2 = \frac{E'_2}{E_3}(= 3g_2), \quad D_1 = \frac{\rho_1}{\rho_3}, \quad D_2 = \frac{\rho_2}{\rho_3}. \end{aligned}\right\} \text{..4.7.viii}$$

Thus,

$$\alpha_2 = \frac{12H_2(1 + H_1 + 2H_2) + 6e_2H_2^2(H_1 + H_2) + 2e_2H_2^3}{2 + e_1H_1^3 + 2e_2H_2^3 + 6e_2H_2(H_1 + H_2)^2 + 6(1 + 2H_2 + H_1)^2} \text{..4.7.ix.a}$$

$$\beta_2 = \frac{48\pi^2 P_2^2(2 + D_1H_1 + 2D_2H_2)}{2 + e_1H_1^3 + 2e_2H_2^3 + 6e_2H_2(H_1 + H_2)^2 + 6(1 + 2H_2 + H_1)^2}\left(\frac{f^2l^2\rho_3}{g_oE_3}\right) \text{...}$$

..4.7.ix.b

$$\gamma_2 = \frac{2\eta_2\left[e_2H_2^3 + 3e_2H_2(H_1 + H_2)^2\right]}{2 + e_1H_1^3 + 2e_2H_2^3 + 6e_2H_2(H_1 + H_2)^2 + 6(1 + 2H_2 + H_1)^2} \text{..4.7.ix.c}$$

$$\gamma_3 = \frac{2\eta_2\left[e_2H_2^3 + 3e_2H_2^2(H_1 + H_2)\right]}{2 + e_1H_1^3 + 2e_2H_2^3 + 6e_2H_2(H_1 + H_2)^2 + 6(1 + 2H_2 + H_1)^2} \text{....4.7.ix.d}$$

$$\mu_2 = \frac{4(1 + H_1 + 2H_2) + 2e_2H_2(H_1 + H_2) + e_2H_2^2}{8H_2 + 3e_2H_2^2} \quad \text{.....4.7.ix.e}$$

$$\nu_2 = \frac{8p_2^2 g_2}{8H_2 + 3e_2H_2^2} \quad \text{.....4.7.ix.f}$$

$$\sigma_2 = \frac{8\eta_2 p_2^2 g_2}{8H_2 + 3e_2H_2^2} \quad \text{.....4.7.ix.g}$$

$$\delta_2 = \frac{\eta_2 e_2(3H_2 + 2H_1)}{8 + 3e_2H_2} \quad \text{.....4.7.ix.h}$$

$$\delta_3 = \frac{3\eta_2 e_2 H_2}{8 + 3e_2H_2} \quad \text{.....4.7.ix.i .}$$

As in equations 4.1.xviii, $f = \frac{\omega}{2\pi}$, is the frequency of excitation in cycles per second, and g_o is the gravitational constant of acceleration.

Equations 4.7.vi are seen to be similar to equations 4.1.xv for the three-layer beam. Hence the method of solution developed for the 3-layer beam is applicable without any modification. When the coefficients of the differential equations are strain-dependent, the method of section 4.5 is employed.

The expression for the overall loss factor is also similar to that for the 3-layer beam. Thus,

$$\eta_{on} \doteq \frac{D_2'}{\frac{1}{2}\left\{A_2' + B_2' + \left[(A_2' - B_2')^2 + 4C_2'^2\right]^{1/2}\right\}}$$

where,

$$D_2' = \int_0^1 \Big[\gamma_2 (D^2 u_o)^2 + \gamma_2 (D^2 v_o)^2 + \lambda_3 (DX_{o2})^2 + \lambda_3 (DY_{o2})^2 + 2\gamma_3 (DX_{o2} D^2 u_o + D^2 v_o DY_{o2}) + \eta_2 \lambda_4 (X_{o2}^2 + Y_{o2}^2) \Big] d\xi$$

$$A_2' = \int_0^1 \Big[(D^2 u_o)^2 + \lambda_2 (DX_{o2})^2 + 2\alpha_2 D^2 u_o DX_{o2} + \lambda_4 X_{o2}^2 \Big] d\xi$$

$$B_2' = \int_0^1 \Big[(D^2 v_o)^2 + \lambda_2 (DY_{o2})^2 + 2\alpha_2 D^2 v_o DY_{o2} + \lambda_4 Y_{o2}^2 \Big] d\xi \qquad \text{.....4.7.x}$$

$$C_2' = \int_0^1 \Big[D^2 v_o D^2 u_o + \lambda_2 DY_{o2} DX_{o2} + \alpha_2 \{ DY_{o2} D^2 u_o + DX_{o2} D^2 v_o \} + \lambda_4 X_{o2} Y_{o2} \Big] d\xi$$

and the following additional notations have been employed:

$$\lambda_3 = \frac{2\eta_2}{EI} \left\{ E_2' b \frac{h_2^3}{12} + E_2 b \frac{h_2^3}{4} \right\}$$

$$= \frac{8\eta_2 e_2 H_2^3}{2 + 6(1 + 2H_2 + H_1)^2 + e_1 H_1^3 + 2e_2 H_2^3 + 6e_2 H_2 (H_1 + H_2)^2} \qquad \text{.....4.7.xi.}$$

$$\lambda_4 = \frac{2\ell^2 G_2' A_2}{EI}$$

$$= \frac{8 p_2^2 e_2 H_2}{2 + 6(1 + 2H_2 + H_1)^2 + e_1 H_1^3 + 2e_2 H_2^3 + 6e_2 H_2 (H_1 + H_2)^2}$$

4.8. Solution of the equations for any multi-layer beam

The order of the differential equations for a multi-layer beam increases with the number of layers. In the method of solution developed above for the 3-layer and 5-layer beams, the differential equations are solved as a set of simultaneous equations of the 14-th order. The method can be readily extended to the solution of the equations for the general n-layer beam, where n = 4i - 1,

or $4i + 1$; $i = 1,2,3$, etc. For such a beam, the differential equations are solved as a set, of the $(8 + 6i)$-th order. The number of boundary equations required is thus $(8 + 6i)$. The procedure for the numerical method of solution of these equations is the same, the main matrix for the step-wise integration process being a square matrix of order $(8i + 10)$. Systems with strain-dependent coefficients can also be solved, employing the method of section 4.5.

C H A P T E R 5

EXPERIMENTAL VERIFICATION OF THE THEORY

Introduction

To check the theory developed in chapters 2 and 4, the displacement responses of 3-layer and 5-layer beams were investigated experimentally. The beams were tested as double cantilever beams with displacement forcing at the root. Various lengths, as well as combinations of elastic and viscoelastic materials, were dealt with. For each specimen, the tip displacement amplitude and phase responses were determined over a frequency range covering the first two or three resonant frequencies. At each resonant frequency, the displacement amplitudes at various points along the beam were also measured. These were then compared with theoretically calculated values.

The details of the test procedure, as well as the results, are reported in this chapter.

5.1. Details of the apparatus.

5.1.a. The mechanical set-up

Fig. 5.1 shows a diagrammatic sketch of the mechanical set-up of the test apparatus. The specimen, (1), was clamped at its central 2¼-inch portion (details of the clamping arrangement, (2), are given shortly), and then

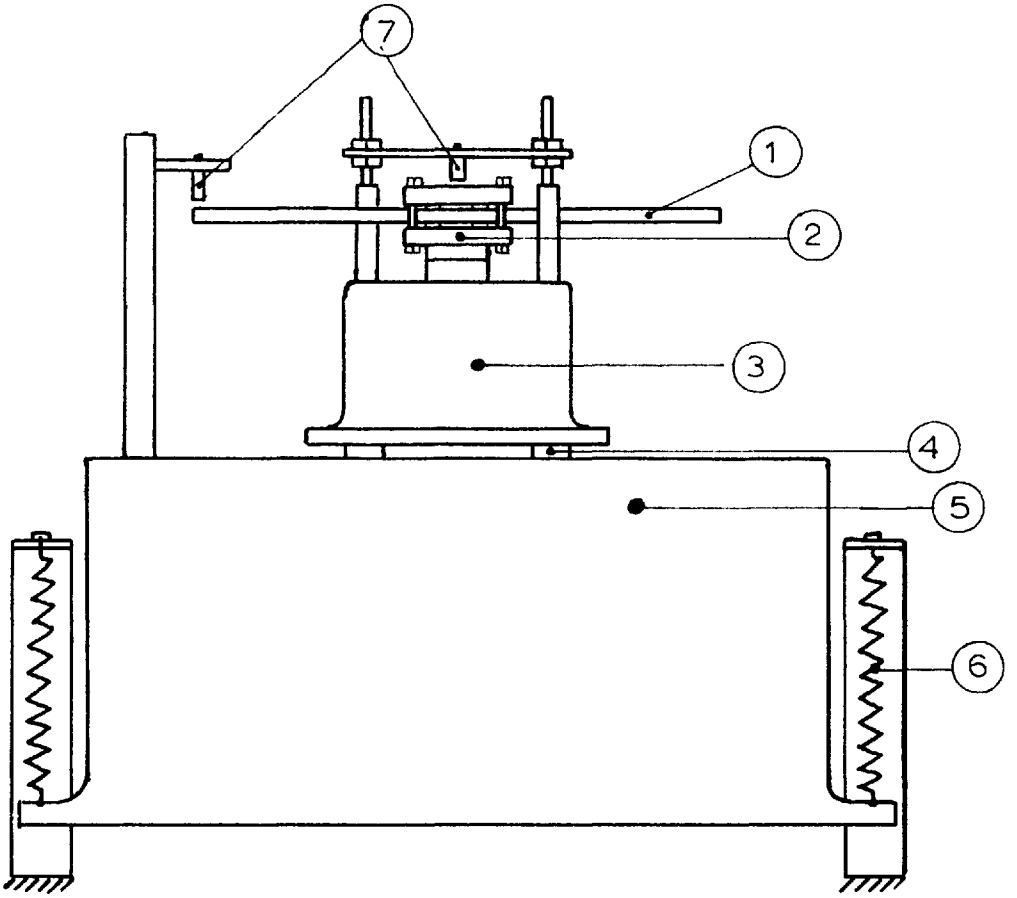

1. BEAM SPECIMEN.
2. CLAMPING DEVICE.
3. ELECTROMAGNETIC VIBRATOR.
4. FLAT PIECES.
5. MASSIVE TABLE.
6. SOFT COIL SPRINGS.
7. DISPLACEMENT PICKUPS (PROXIMITY GAUGES).

FIG 5.1 Diagrammatic Sketch of Test Apparatus.

mounted, by means of six 2 B.A. Allen screws, on the table of a Derritron V.P.5 electro-magnetic vibrator, (3). The vibrator was powered by the Derritron 250 watt power amplifier, details of which have already been given in section 3.5.c. This amplifier also energised the d.c. coils of the vibrator field, and supplied a fan which provided suction cooling for the vibrator moving coils and field energising coils. The vibrator was capable of giving up to 70 pounds thrust, and had a working frequency range of between 5 cycles per second and 12 kilocycles per second. It sat on two carefully machined flat pieces, (4), on top of a massive table, (5), which was isolated from the surroundings by means of four soft coil springs, (6), in tension. The highest natural frequency of the table and its attachments on the springs was in vertical translation, and was about 0.5 c.p.s.. A travelling microscope (not shown in the sketch) was rigidly mounted on the table. With it, the displacement amplitudes at various points on the beam could be measured. Two electro-dynamic inductance proximity gauges were suitably mounted at the beam support and tip, for picking up the motions at these points.

5.1.b. The clamping device

Two essential requirements were borne in mind in the design of the clamping device. The first was the necessity for ensuring proper clamping in which there was negligible

movement at the root. The second had to do with temperature control. Inspite of the cooling, the vibrator table (which was made of a magnesium alloy, a good conductor of heat) would normally get relatively warm during a test period. It was thus necessary to insulate the specimen from possible heat from the vibrator table.

Fig 5.2 gives some details of the clamp. Two identical strips of compressed asbestos, (a), $\frac{3}{8}$ inch wide, were bonded to each half of the clamp, (b), in such a way that their outer edges were 2¼ inches apart. The free surfaces of these strips were carefully ground so that they were flush with each other when the two halves of the clamp were assembled. The specimen, (c), was clamped between these surfaces. This arrangement apart from providing the required insulation also helped to reduce the number of "high spots" which would be detrimental to the good clamping sought. To prevent the squashing of the viscoelastic layer, the central 2¼-inch section, (h), of the specimen (at which the clamp was located) was made of metal - see the section on the preparation of the specimens. Four ¼-inch B.S.F. bolts, (d) held the specimen between the camping surfaces. These were further assisted by the six 2 B.A. screws, (e), which held the clamp on to the vibrator table, (f). These screws passed very close to the outer edges of the strips thus ensuring good clamping

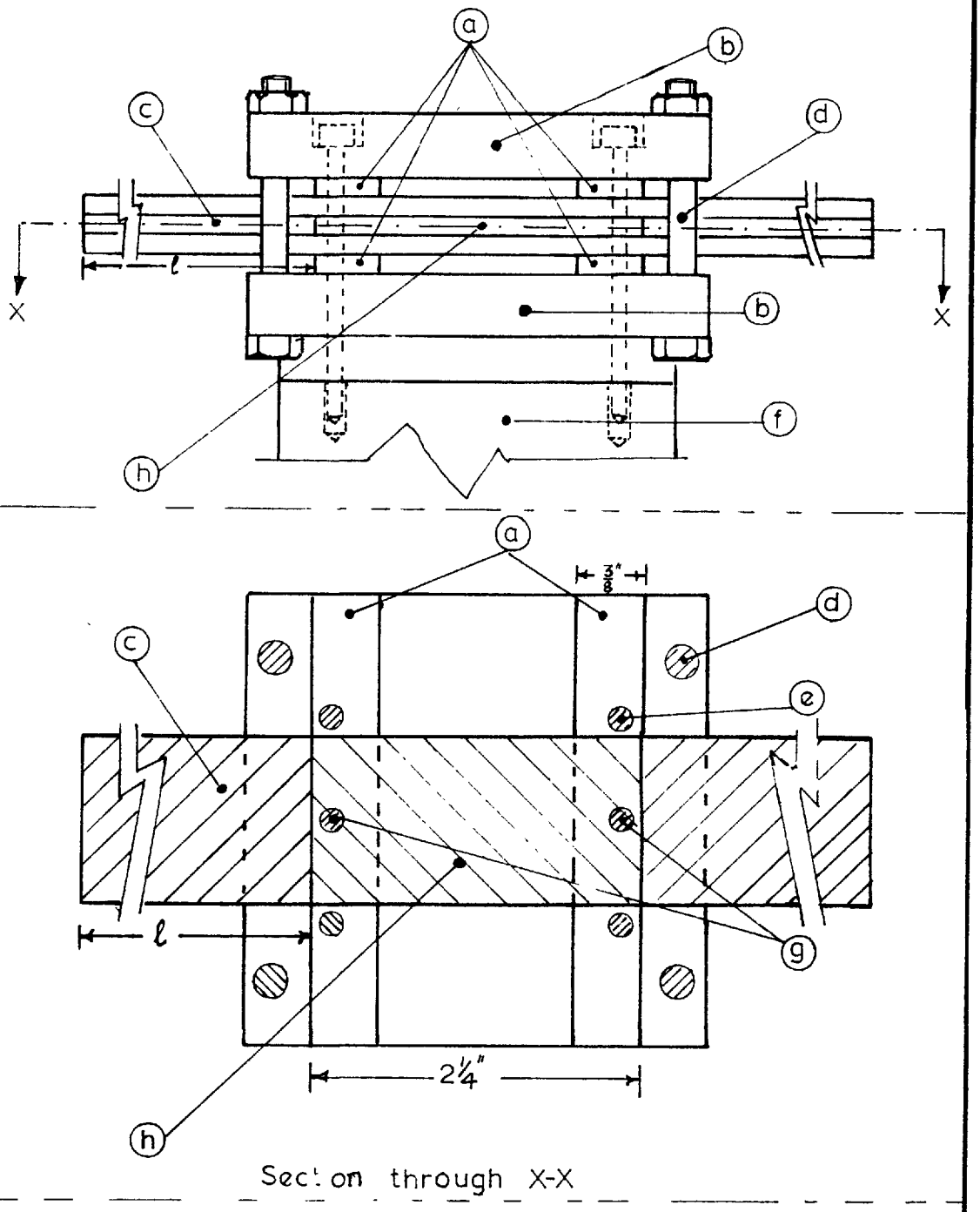

FIG. 5.2 Details of Clamping Device.

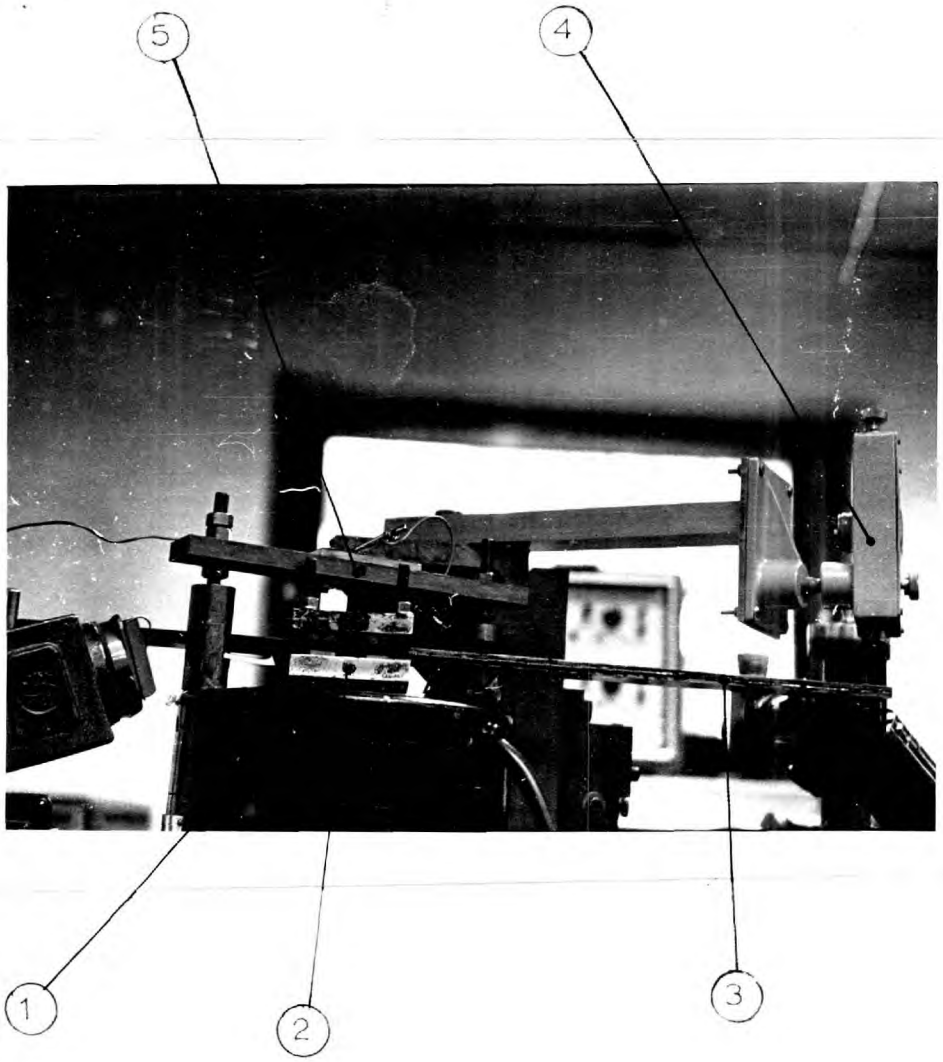

1. VIBRATOR
2. CLAMPING DEVICE
3. SPECIMEN
4. TIP DISPLACEMENT GAUGE
5. SUPPORT DISPLACEMENT GAUGE

FIG. 5.2a Photograph of the clamp mounted on the vibrator.

at these edges. Besides, the two central screws, (g), passed through the specimen, the clearance holes being fairly large to avoid any heat transmission through the screws. In this way, possible motion at the clamping surfaces was reduced to the barest minimum. The effective length, ℓ, of the beam was measured from each outer edge of the strips, as shown on the sketch.

A photograph of the clamp mounted on the vibrator is shown in fig 5.2a.

5.1.c. The electrical circuit.

A block diagram of the electrical circuitry is given in fig 5.3. The only difference between this and the circuit employed in the shear tests (fig 3.8) is that the force measuring (strain-gauge) channel is here replaced by another f.m. displacement-gauge channel. Also for phase measurement, instead of the phase shifting device, the other alternative - a phase-inverter in the form of a centre-tapped transformer - was employed. Details of these have already been given in section 3.5.

5.2. Specimen preparation

Two viscoelastic materials, namely, Velbex P.V.C., and Evoseal 202, were used in the tests. The method of preparation of the specimens was slightly different in each case.

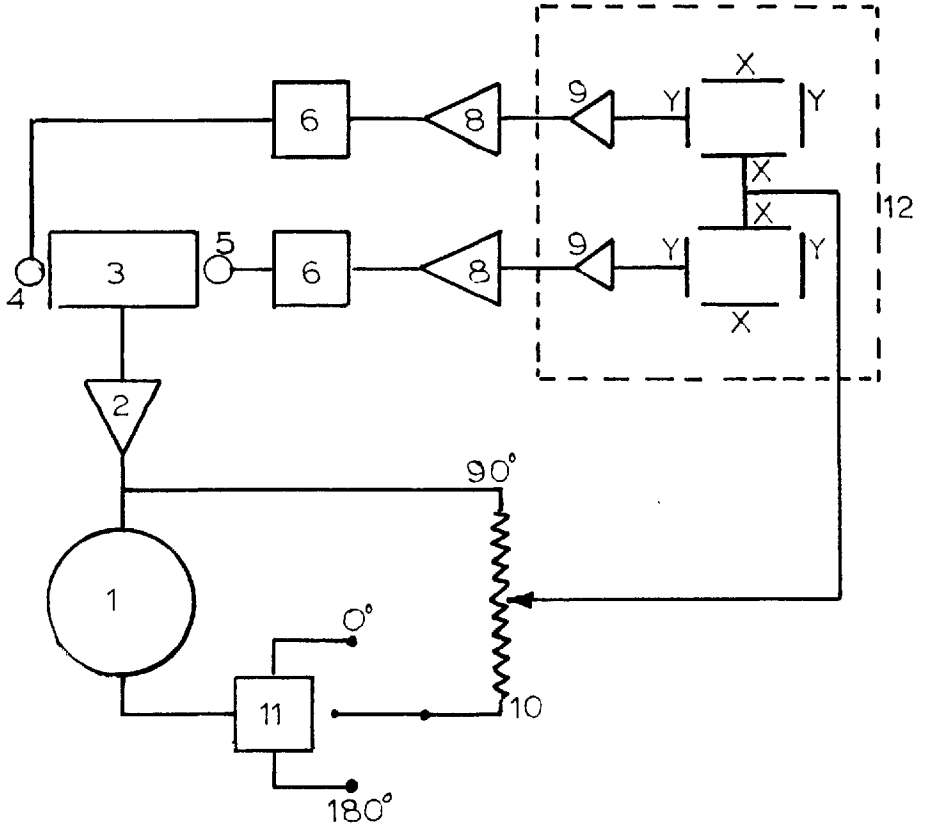

1. DECADE OSCILLATOR - 2 OUTPUTS 90 OUT OF PHASE.
2. 250 WATT POWER AMPLIFIER.
3. ELECTROMAGNETIC VIBRATOR.
4,5. DISPLACEMENT PICKUPS (PROXIMITY GAUGES).
6. GAUGE OSCILLATOR.
8. FREQUENCY-MODULATED PRE-AMPLIFIER.
9. DRIVER AMPLIFIER.
10. PHASE POTENTIOMETER.
11. PHASE-INVERTING TRANSFORMER.
12. DOUBLE BEAM OSCILLOSCOPE.

FIG. 5.3 Block Diagram of Measuring Circuit.

5.2.a. Beams with P.V.C. layers.

The P.V.C. was available as a sheet - the same sheet from which the shear test specimens (chapter 3) were cut off. As the thickness of the sheet varied slightly over its area, a strip of about the required width was first cut out. The thickness was then measured at one inch intervals and the most uniform portion of the strip was cut out for use. Two such identical strips were required for a 3-layer beam, and four for the 5-layer beam.

The surfaces to be bonded together were degreased by cleaning thoroughly with carbon tetrachloride, and then with acetone, and finally washing with plenty of water. The metal surfaces were then abraded with the appropriate reagent. Dilute sulphuric acid was used for steel surfaces, and 2 per cent hydrofluoric acid for aluminium surfaces. After abrasion, the surfaces were finally cleaned with acetone and thoroughly washed in water.

For a three-layer specimen, a steel piece 2¼ inches long, of the same width as the specimen layers, and of thickness equal to the mean thickness of the viscoelastic strips, was glued with araldite to the central portion of one of the metal layers. The araldite used was the same cold-setting type used in the shear tests of chapter 3. In the case of a five-layer beam, two such pieces were bonded (one to each face) at the central portion of the

central layer. Also, for both three-layer and five-layer beams, small copper - constantan thermo-couple wires, 0.020 inch thick, were planted with araldite in small grooves cut at suitable intervals in the metal faces. The "hot" junctions were raised slightly so that they projected by about 0.005 inch above the metal surface. This was to ensure that the actual temperature being measured was that of the viscoelastic layer (which would be bonded to this surface). The araldite was allowed a day to set.

Next, a very thin layer of araldite was evenly applied, by means of a small roller, on all the faces to be bonded together, including the inner edges of the viscoelastic strips which were to bear on the central steel pieces. The layers were now assembled, care being taken that the inner edges of the viscoelastic layers were pressing firmly against the edges of the central metal pieces. (This was essential in order to satisfy the assumed condition of zero shear in the viscoelastic layers at the clamped end - see section 4.2.c.). The assembly was carefully loaded, between two flat surfaces, on a Denison testing machine. The applied load, which was released after twelve hours, was such as to give a setting pressure of about 10 lb/sq.in. The specimen was left for a few days to allow the araldite to reach its optimum bonding strength. Any excess araldite was scraped off the edges, and the specimen was now ready

for test. If it was required to test a shorter length of the specimen, the excess bits were cut off from each end using a band saw. For specimens with steel facing layers, a thin strip of brass or aluminium (½"x ½"x 0.020") was glued to the top surface close to each free end. This helped to increase the sensitivity of the inductance pick-up.

5.2.b. Specimens with Evoseal layers

The surface preparation was the same as for the P.V.C. sandwich specimens. The central steel piece was also bonded to one of the metal layers as in the first case. In addition, two metal pieces , of the same thickness as the central piece, were glued (with araldite) one to each end surface of the metal layer.

A thin layer of araldite was now evenly applied to the surface of the metal layer (in the space between the bonded metal pieces); and the first layer of the evoseal was painted on, using a small fibre brush. This was allowed about six hours to harden slightly. Subsequent layers were then applied, at six hour intervals, until it was felt that the desired thickness had been approached. It would evidently be difficult to obtain uniform thickness no matter how carefully the evoseal layers were applied. To take care of this, the evoseal layer thickness was built up to a slightly higher value than desired. The top facing

layer was then glued on with araldite, and the assembly was allowed to set under load, as in the previous case. Enough load was applied to enable the viscoelastic layer to attain a fairly uniform thickness, the metal pieces at the centre and the ends acting as "stops" to determine this thickness. The excess evoseal spread out to the edges of the beam. The load was taken off after 24 hours, and the specimen was left to cure gradually. A shear specimen was prepared at the same time as the evoseal sandwich beams.

Before testing the specimen, the ends containing the metal pieces were cut off, and the excess viscoelastic material at the edges was also trimmed off. Small copper - constantan thermo-couple wires were stuck into the visco-elastic layer at convenient intervals for measuring the temperature of the layer.

5.2.c. Beam geometry and material properties

The overall thickness of each specimen was measured at one inch intervals using a micrometer screw gauge; and the mean value was taken as the correct thickness. The thicknesses of the metal layers were measured before bonding, and the viscoelastic layer thicknesses were found by difference. No allowance was made for the thickness of the bonding material, this being assumed negligible.

All thicknesses were measured to the nearest 0.001 inch. After each specimen had been mounted for test, its effective length (see section 5.2.b.) was measured to the nearest 0.01 inch using a suitably graduated scale.

The elastic layers were either steel or aluminium. The steel layers were chosen from a stock of "bright mild steel" bars, 1½ inches wide, available in various thicknesses. The properties of the material were taken as $E = 3 \times 10^7$ lb/sq.in. ; $\rho = 0.283$ lb/cu.in. The aluminium layers were chosen from a similar batch of bars of an aluminium alloy, SIC ½H, whose composition is specified in B.S. 1470. The material properties were taken as $E = 10^7$ lb/sq.in. ; $\rho = 0.1$ lb/cu.in.

As the P.V.C. layers were cut out from the same sheet as the shear specimens of chapter 3, the properties are as given in that chapter (figs 3.19 to 3.23). For the properties of evoseal, the shear specimen prepared at the same time as the beam specimens were first tested before the beam tests, and the properties obtained were used in the theoretical calculations (see comments on this, in sections 5.4.b and 5.5.c). These have already been given in figs 3.31 and 3.32.

To obtain the densities of P.V.C. and evoseal, portions cut off from the beam specimens were weighed. From the weights and dimensions of these portions, and using the

known densities of the metal layers, the densities of the viscoelastic materials were calculated to be 0.041 lb/cu.in. for evoseal, and 0.048 lb/cu.in. for P.V.C.

5.3. Measuring techniques and calibration

But for the modifications mentioned in section 5.1.c, the measuring techniques and calibration are the same as already described in section 3.5.

5.4. Test procedure

5.4.a. Check on the clamping device

To check that the clamping device gave the correct boundary conditions, a test was carried out initially on a plain aluminium beam. The displacement amplitude responses in the region of the first three resonant frequencies were measured, as well as the corresponding mode shapes. The resonant frequencies, and the amplitude ratios of $\frac{\text{motion at any point on the beam}}{\text{motion at tip}}$ at resonance, were compared with those calculated from the classical beam equation. The results are given in fig 5.4 and table 5.a. Also the graphs of the tip amplitude ratio against frequency are given in 5.5. The damping was estimated from the bandwidth of these curves, and the values are given as well in table 5.a.

5.4.b. Beam tests

A total of ten specimens were tested. Details of these are given in table 5.b.

The P.V.C. sandwich specimens

The tests on each specimen involved obtaining (a) the tip amplitude and phase responses in the frequency range covering the first two or three resonant frequencies, and (b) the 'mode shapes'* at each resonant frequency.

For (a), the input motion was kept constant. The forcing frequency was varied in convenient steps, and at each step the temperature of the viscoelastic layer, the tip displacement amplitude, the input motion at the root, and the phase difference between the tip motion and the input motion, were measured. This was continued until the particular resonant frequency was fully covered. Temperature changes during a test interval were kept to a minimum by carrying out the test when the ambient temperature was fairly steady.

For the mode shapes, the appropriate resonant frequency was first quickly determined. The phase potentiometer proved very useful in this, since the rate of change of the phase difference with frequency was maximum close to the resonant frequencies. The displacement amplitudes

*For the method of plotting this locus here, see section 4.6.a.

along the beam were then measured at one inch intervals, using the travelling microscope. The input motion and the temperature of the viscoelastic layer were also measured.

The tip amplitude ratios, phase differences, and mode shapes corresponding to each of the tests were calculated theoretically and compared with the experimental values. These are given in figs 5.6 to 5.13.

The above tests were usually carried out on one side of the double cantilever beam. Although care was taken (during the preparation of the specimens) to make both sides of the beam identical, it was thought necessary to check, for each specimen, that the motion of both sides of the cantilever beam was the same. For the specimens tested, the resonant frequencies and the tip amplitudes at resonance were checked for both sides. No change could be detected in the resonant frequencies within the frequency steps usually taken in the measurements (steps of about one per cent difference were usually taken close to the resonant frequencies). The amplitudes were also found to be the same.

The evoseal sandwich specimens

The specimens with evoseal viscoelastic layers presented some extra experimental problems. Since the evoseal was originally in liquid form, its properties would be expected to depend on the "state of cure" of the

layer. This fact motivated the preparation of a shear specimen alongside the beam specimens. It was, however, recognised that the state of the material was determined, not only by the method of preparation of the specimen, but also by its rate of cure. This rate would depend on several factors, such as, local humidity and temperature conditions. An even more significant factor is the "effective curing thickness" of the layer, which may be defined as the ratio, $\frac{\text{volume of material}}{\text{exposed surface area}}$ of the layer. Clearly, the smaller this ratio, the quicker would be the rate of cure. The shear specimen had an effective curing thickness of 1/6 inch while that of the beam specimens was about 3/4 inch. Hence, assuming the same initial conditions of cure and the same local atmospheric conditions, it is clear that the small shear specimen would cure much faster than the beams. If the exact dependence of the cure rate on the effective thickness were known, then the properties corresponding to the state of the material of the beam could be deduced from observation of the curing rate of the shear specimen (since both specimens were prepared at the same time, and cured under the same environment).

It was thought necessary, at any rate, to obtain the "curing curve" for the shear specimen. If the rate proved to be fairly rapid, then the problem could be solved by allowing a considerable amount of time to elapse to enable

both specimens to reach the flat portions of their curing curves. Accordingly, tests were carried out on the shear specimen at regular intervals. From the results, the in-phase shear modulus and the loss factor at a constant temperature, strain amplitude, and frequency were plotted against the time of cure. The graphs have already been given in chapter 3 - fig 3.30.

When it was realised that the rate of cure was not as rapid as was desired, tests were carried out on the beam specimens after a time of cure of three months. The test procedure was the same as for the P.V.C. specimens. The experimental results are compared with theoretical values in figs 5.14 and 5.15, and discussions on these follow in the next section.

The temperatures and input motions for all the tests are given in tables 5.d and 5.e of appendix II

5.5. Discussion of the experimental results

5.5.a. The plain aluminium beam

Fig 5.5 gives the displacement resonance curves, for the plain aluminium beam, in the regions of the first three resonant frequencies. In the graphs, the tip displacement amplitude ratio, T_a, already defined as

$$\frac{\text{absolute displacement amplitude at tip}}{\text{input motion amplitude}},$$

is plotted against the frequency. The corresponding mode

FIG. 5.4.

PLAIN ALUMINIUM BEAM.

MODE SHAPES.

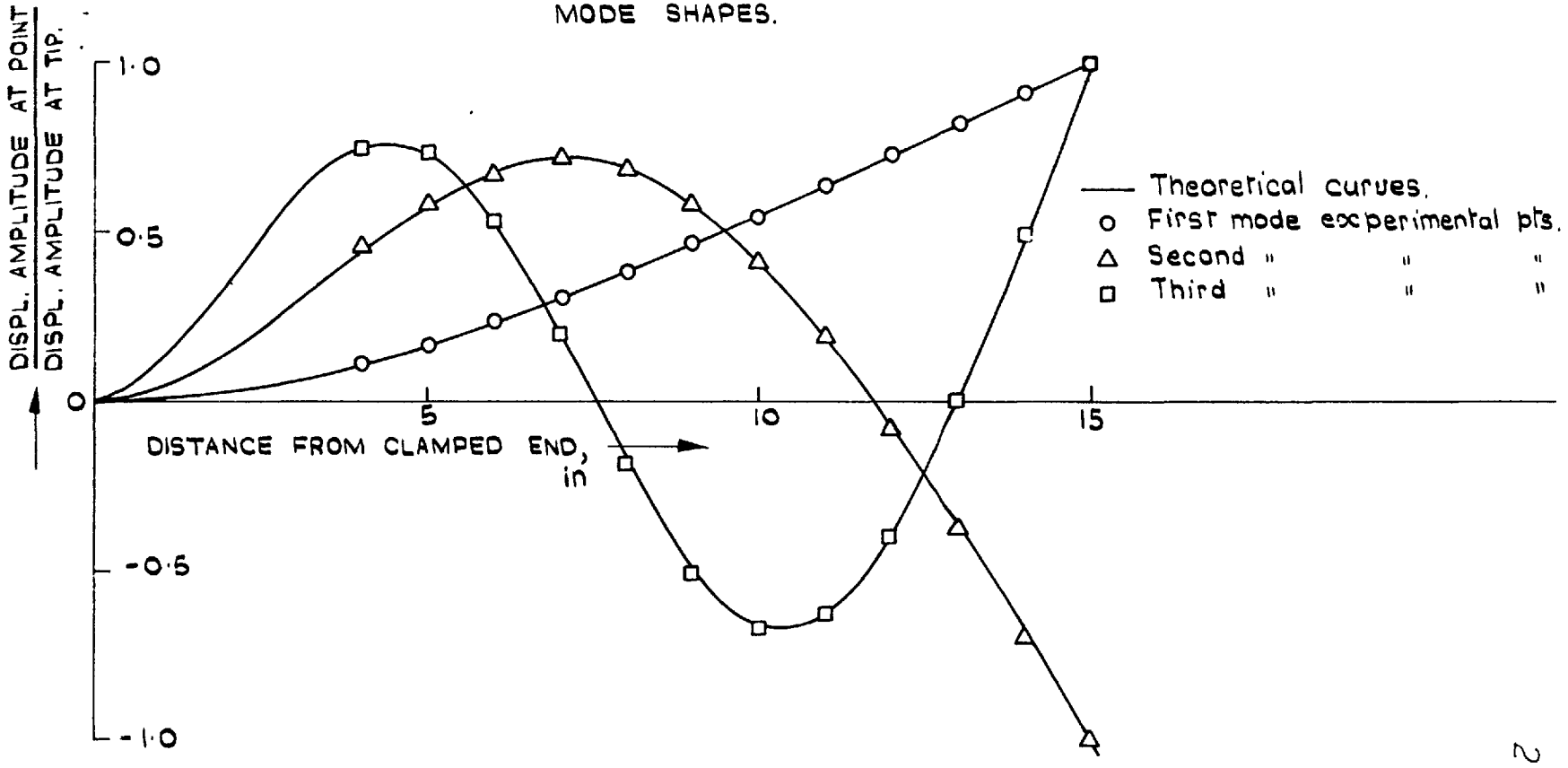

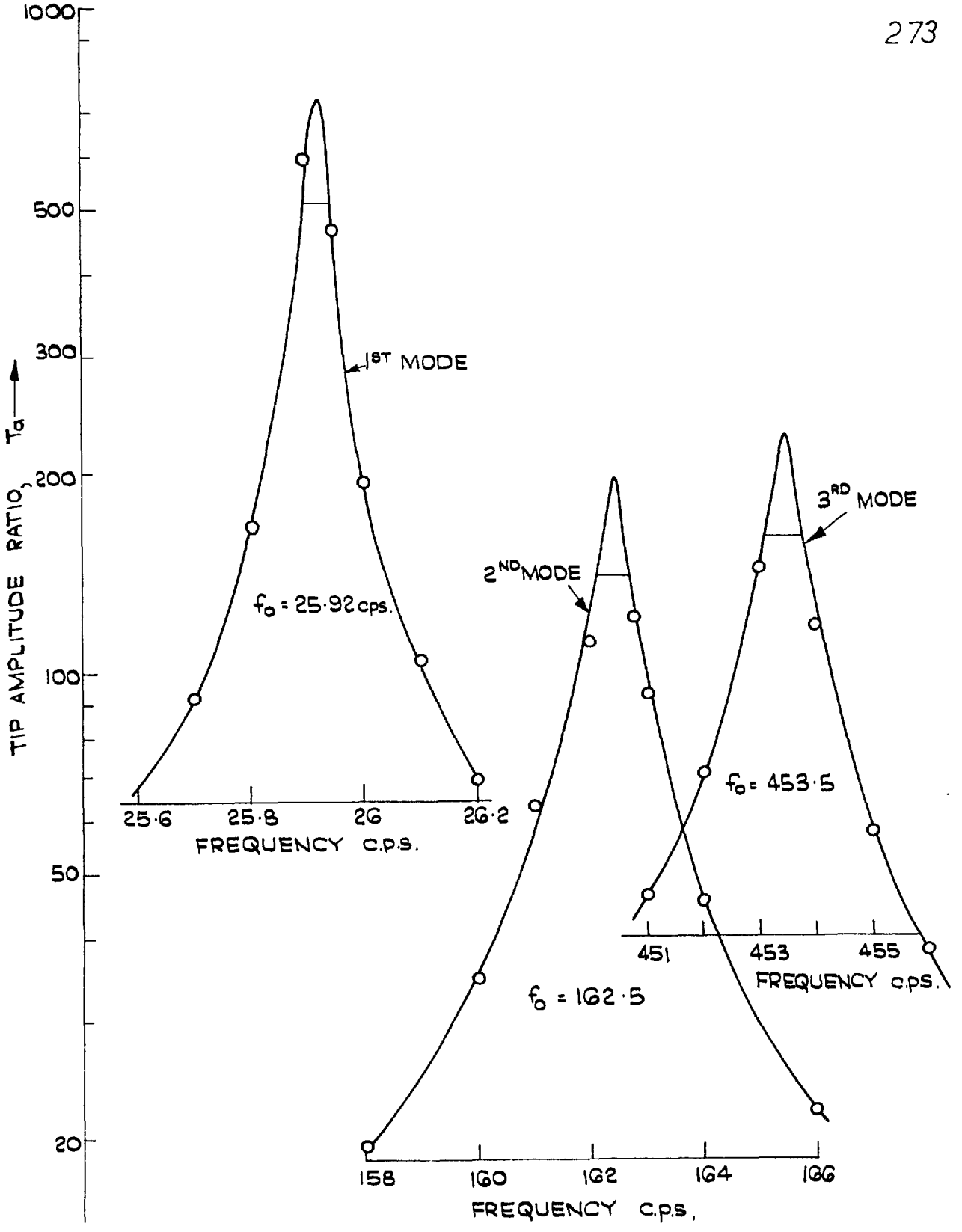

FIG. 5.5 RESONANCE CURVES FOR PLAIN ALUMINIUM BEAM.

MODE NO.	RESONANT FREQUENCY, c.p.s.		LOSS FACTOR
	Calculated	Measured	η_{on}, (measured)
1	26.10	25.92 (0.69)	0.00193
2	163.6	162.5 (0.67)	0.00338
3	457.5	453.5 (0.87)	0.00155

TABLE 5.a

Test results for the plain aluminium beam

Details of beam dimensions: length = 15.07 in.
Thickness = 0.187 in.

shapes are also shown in fig 5.4, in comparison with theoretically calculated values. Since theoretically the absolute amplitude at each point on the undamped beam becomes infinite at resonance, the quantity plotted in fig 5.4 is the ratio of the displacement amplitude at any point to the tip displacement amplitude. This ratio has a finite value for any given mode. The graphs show very close agreement between the experimental and theoretical mode shapes. Table 5.a gives the theoretical and experimental resonant frequencies, the percentage difference between any two corresponding values being given underneath each experimental figure. Agreement is seen to be better than 1 per cent.

The good agreement in the frequencies and mode shapes confirms that movement at the cantilever root must have been negligibly small, and hence checks on the adequacy of the clamping device.

The loss factors* for the beam, as estimated from the bandwidth of the resonance curves of fig 5.5, are also given in table 5.a. It is seen that the system damping (the clamp and the plain metal beam) is of a small order and can thus be justifiably ignored in the analysis.

*For the relation between the loss factor (energy definition) and the bandwidth of the resonance curve, for a lightly damped system with one degree of freedom, see, for instance, [3].

5.5.b. Specimens with P.V.C. layers

The experimental results for the three-layer and five-layer beams with P.V.C. viscoelastic layers are compared with theoretical values in figs 5.6 to 5.13.

Figs 5.6a to 5.13a give the variation of the tip displacement amplitude ratio, T_a, and the phase difference (between the input motion and the tip motion), with frequency for the first two or three modes. The graphs show good agreement in the resonant frequencies, the maximum percentage difference between the measured and the theoretical values being less than 3 in all the cases. Agreement is much better for the three-layer than for the five-layer beams. It is, in fact, thought that in the case of the three-layer beams, the slight disparities could be due mainly to slight temperature variations along the beam length during a test interval. The temperature used in the theoretical calculations was the mean of the temperatures at two points along the beam. The difference between these two temperatures could be as high as 0.5 °C especially at the higher modes.

The five-layer beams show consistently higher resonant frequencies than theoretically calculated. This is thought to be due to the effect of the araldite bonding layers. In the calculations, these were assumed to be part of the viscoelastic layers, since the thickness of the viscoelastic

BEAM NO.	ELASTIC LAYERS		VISCOELASTIC LAYERS		BEAM LENGTH
	Material	Thickness h_2, in.	Material	Thickness h_1, in.	ℓ, in.
3	Aluminium	0.250	P.V.C.	0.135	20.00
3A	"	0.250	"	0.135	18.00
3B	"	0.250	"	0.135	12.00
4	Steel	0.187	"	0.137	15.00
4A	"	0.187	"	0.137	12.00
7	Aluminium	0.124	Evoseal	0.063	14.04
8	Steel	0.187	"	0.077	15.07

(i) Three-layer Beams.

BEAM NO.	ELASTIC LAYERS				VISCOELASTIC LAYERS		BEAM LENGTH
	CENTRAL LAYER		FACING LAYERS				
	Material	Thickness h_1, in.	Material	Thickness h_3, in.	Material	Thickness h_2, in	ℓ, in.
5	Steel	0.123	Alum.	0.124	P.V.C.	0.161	17.93
5A	"	0.123	"	0.124	"	0.161	12.00
6	Alum.	0.250	Steel	0.123	"	0.155	15.00

(ii) Five-layer beams.

TABLE 5.b Details of the beam specimens.

KEY TO FIGS 5.6 TO 5.15

FIGS (a)

—— Theoretical curves (Tip amplitude ratio and phase difference)

Experimental points

	Tip amplitude ratio, T_a	Phase difference
First mode	○	●
Second mode	△	▲
Third mode	□	■

FIGS (b)

—— Theoretical curves (Amplitude ratio at point)

Experimental points

○ First mode

△ Second mode

□ Third mode

ξ = $\frac{\text{distance from clamped end}}{\text{length of beam}}$

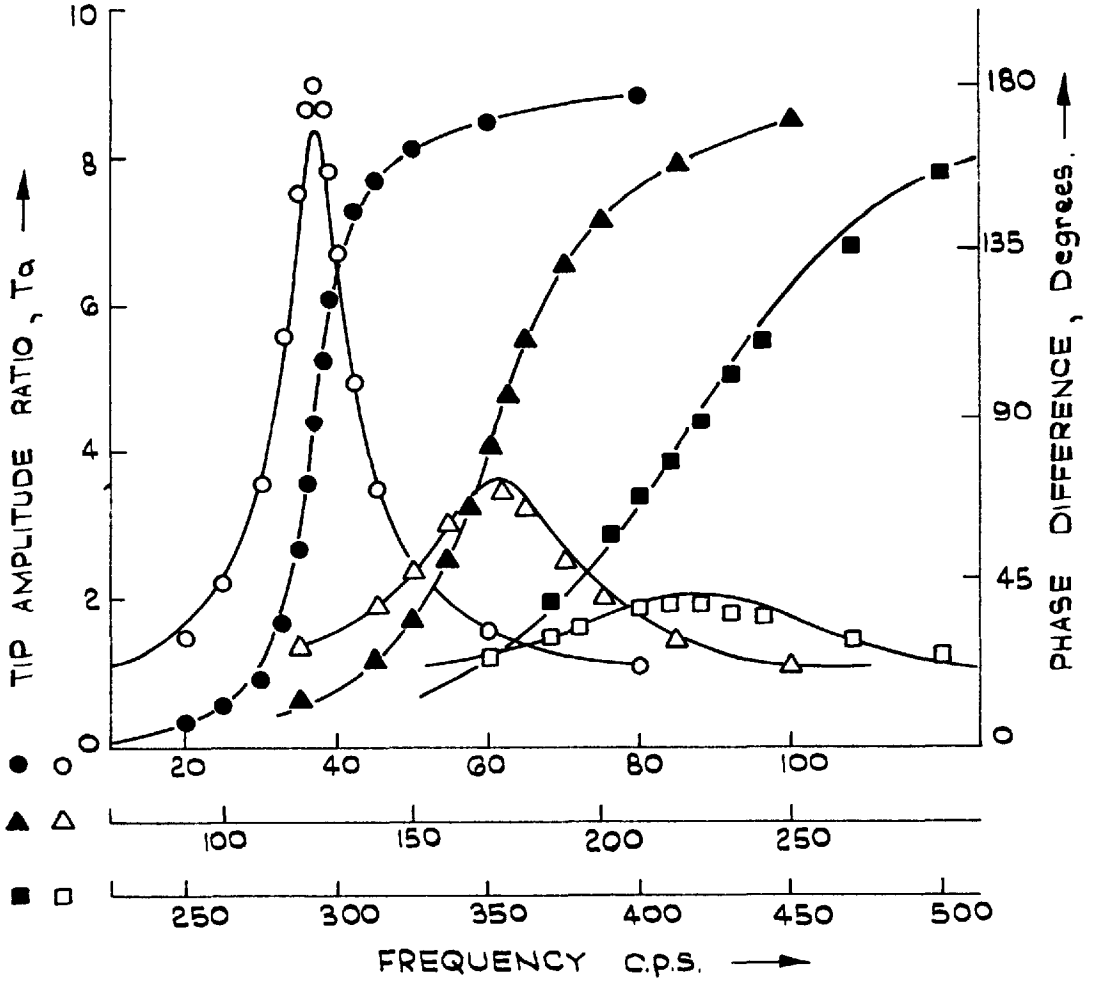

a) RESONANCE CURVES.

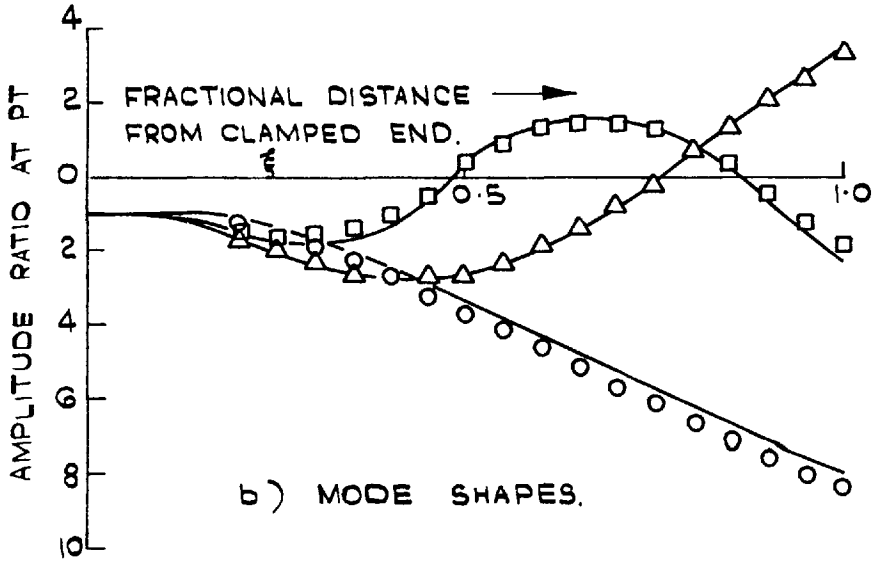

b) MODE SHAPES.

FIG. 5.6. THREE-LAYER BEAM. 3.

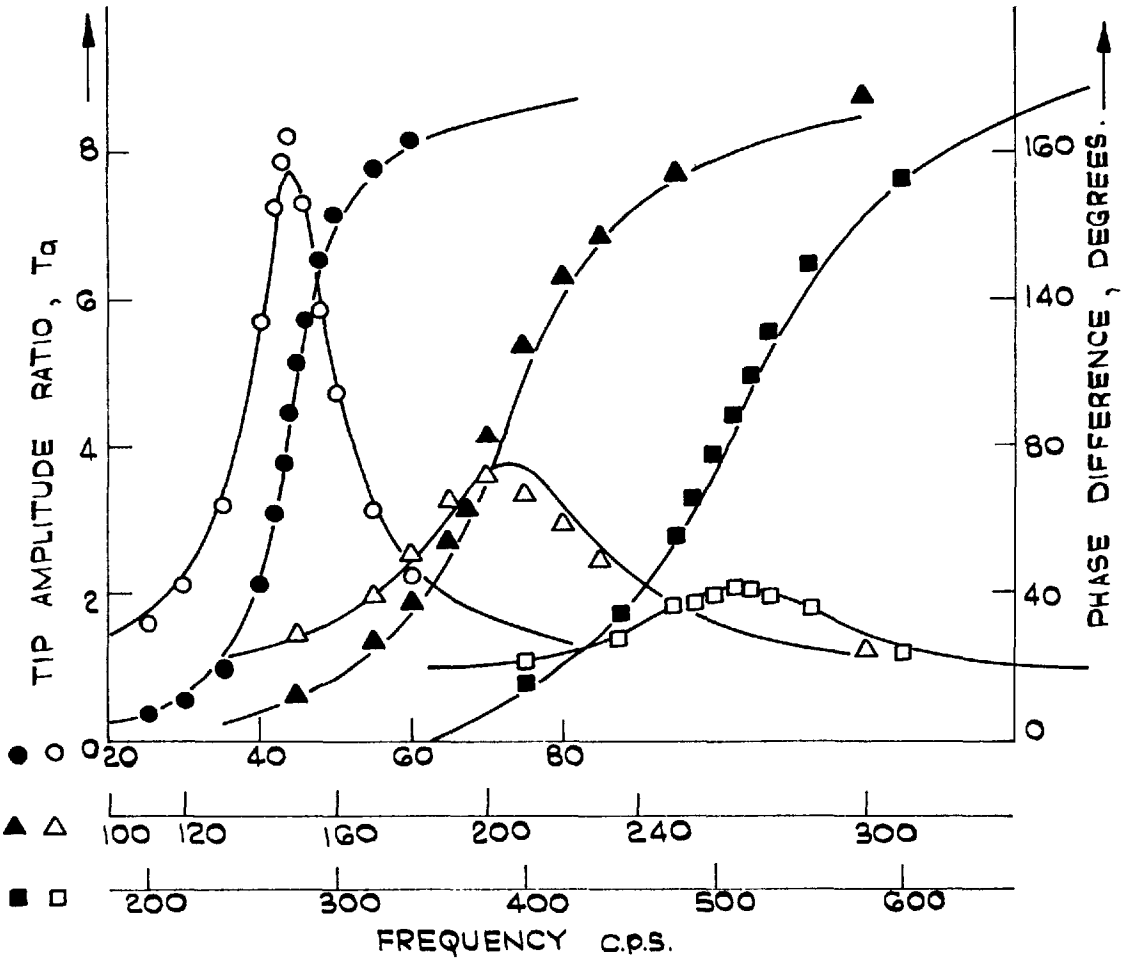

FIG. 5.7. THREE - LAYER BEAM. 3A.

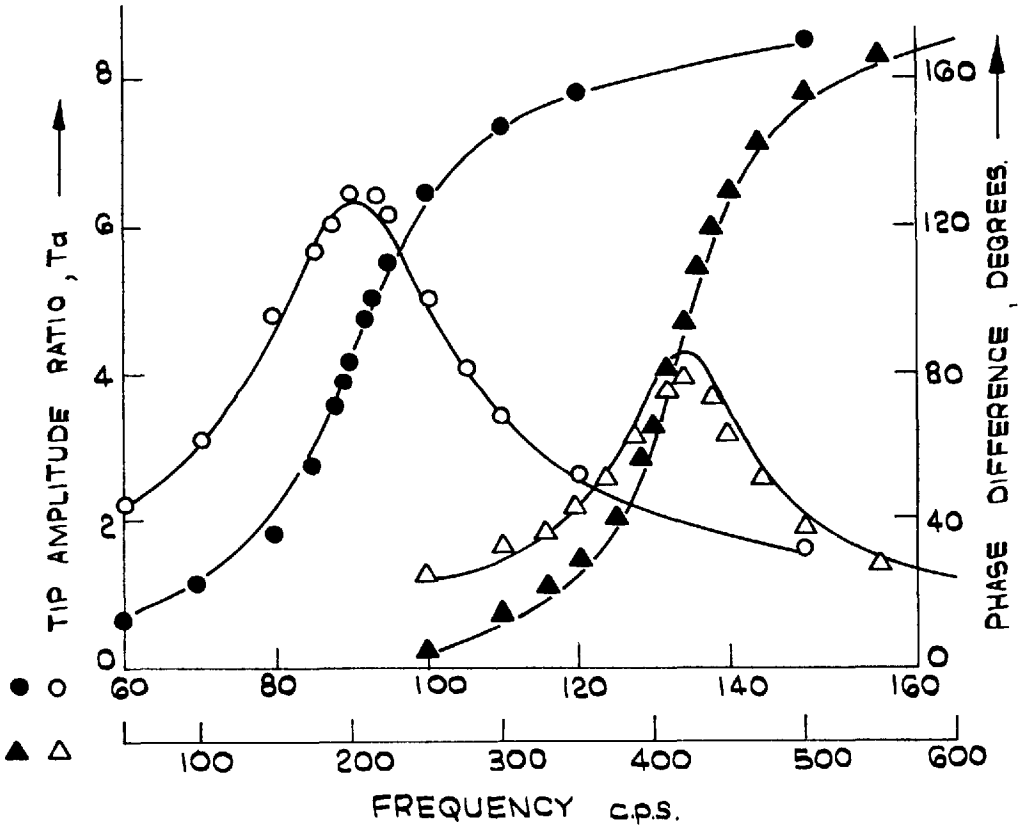

RESONANCE CURVES.

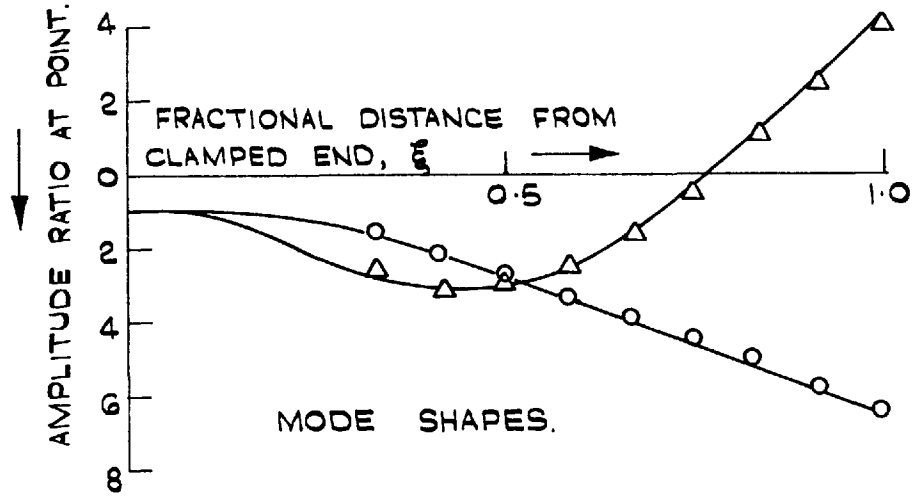

FIG. 5.8. THREE-LAYER BEAM. 3B.

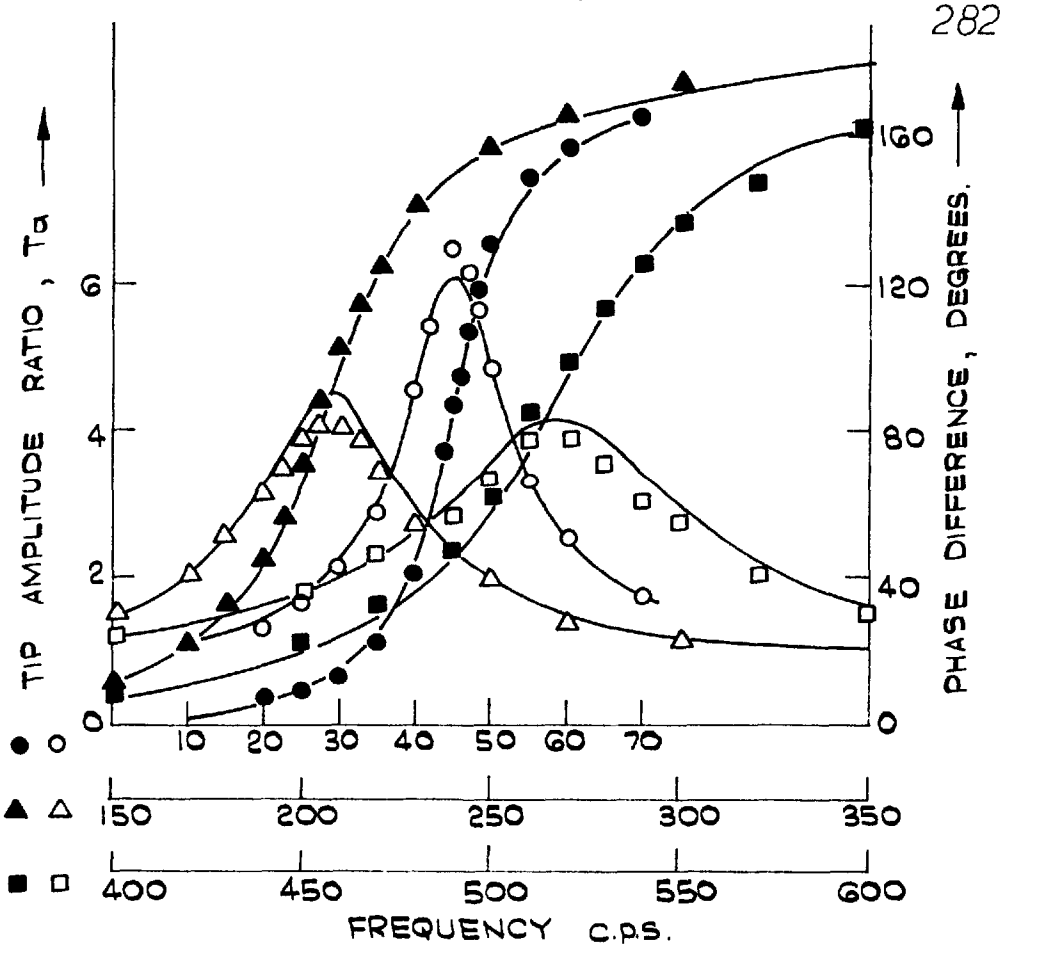

a) RESONANCE CURVES.

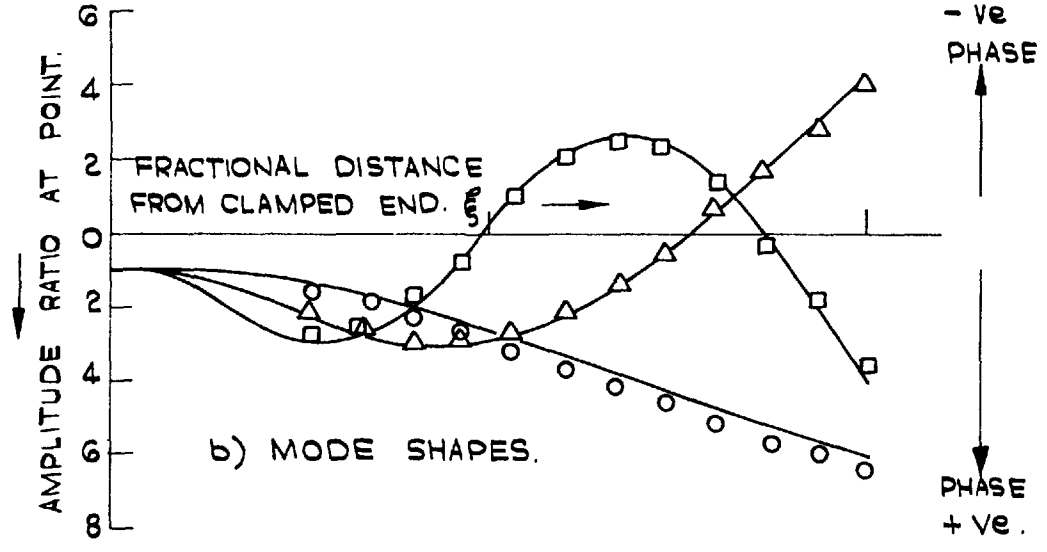

b) MODE SHAPES.

FIG. 5.9. THREE-LAYER BEAM 4.

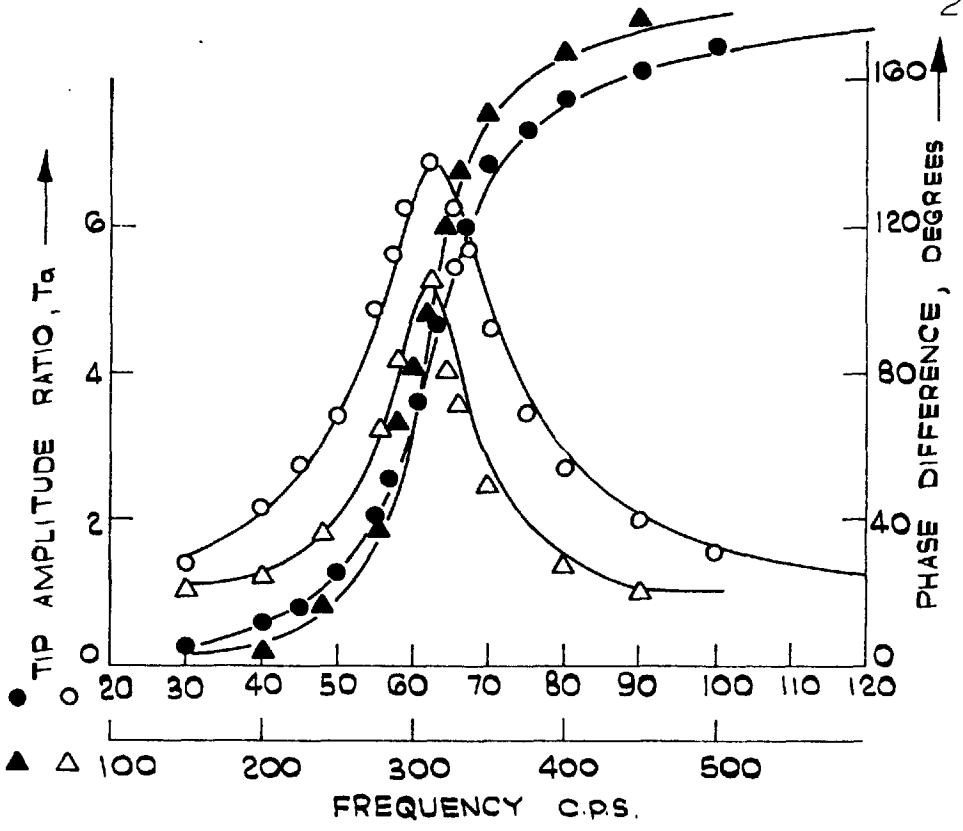

a) RESONANCE CURVES.

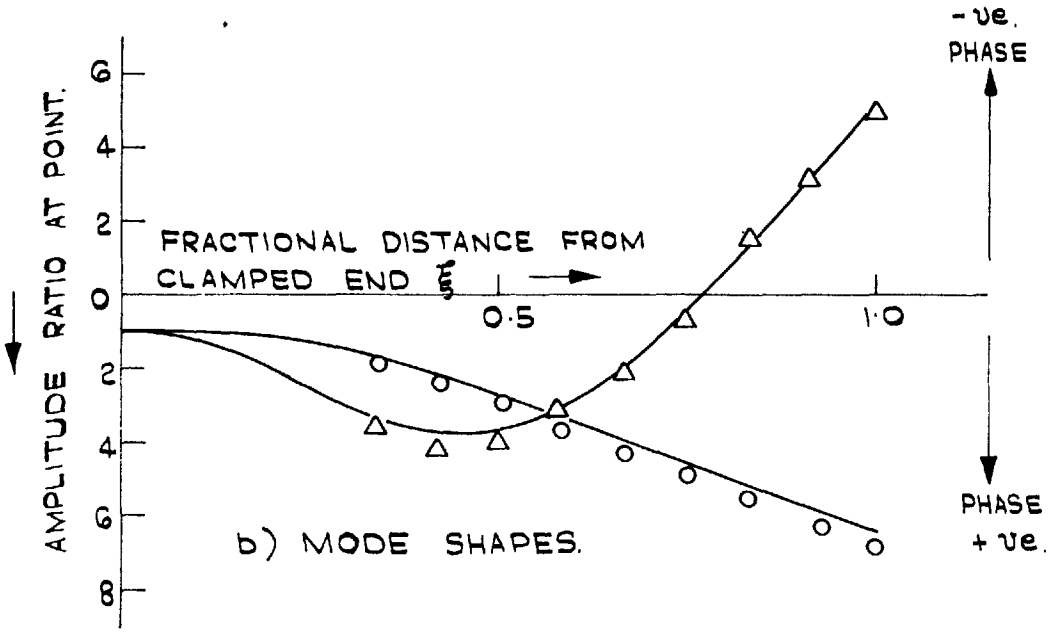

b) MODE SHAPES.

FIG. 5.10. THREE-LAYER BEAM 4A.

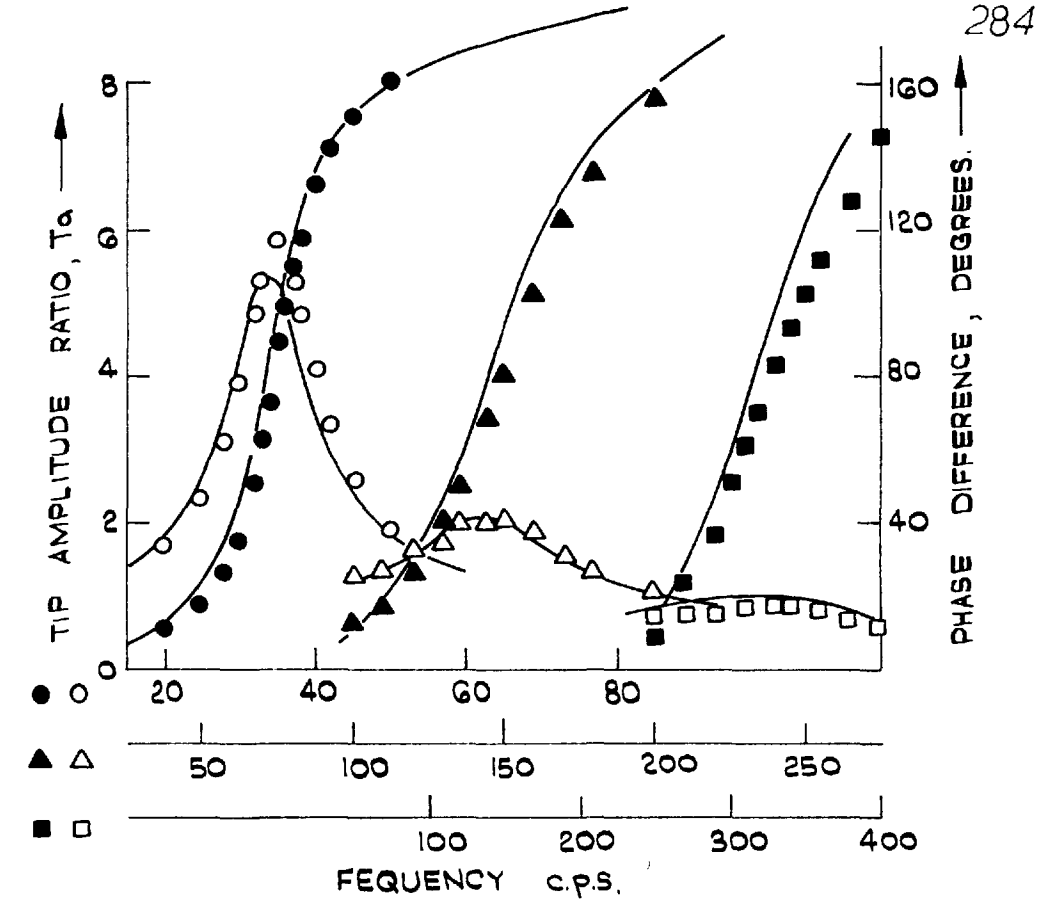

a) RESONANCE CURVES.

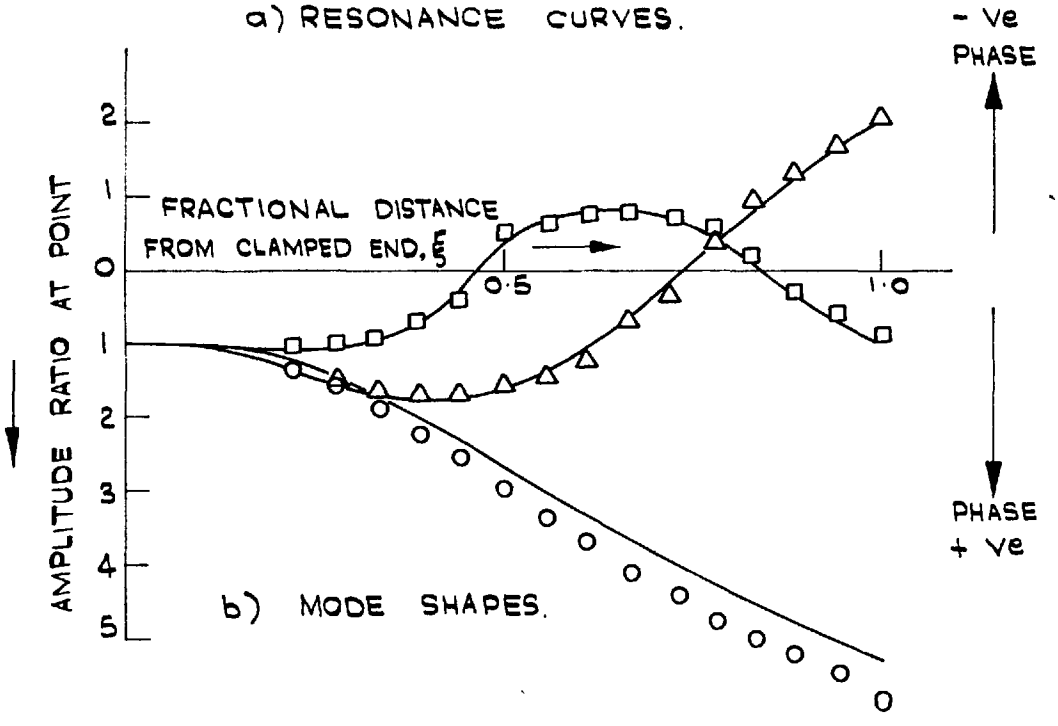

b) MODE SHAPES.

FIG. 5.11. FIVE-LAYER BEAM 5.

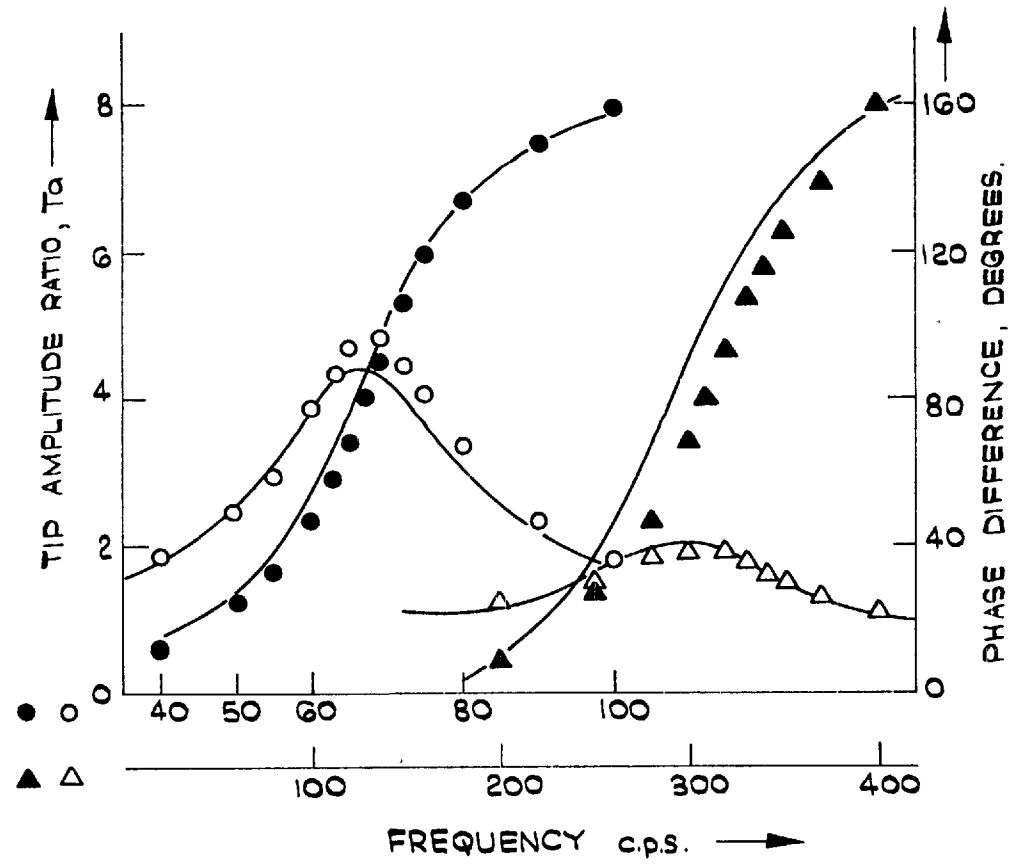

a) RESONANCE CURVES.

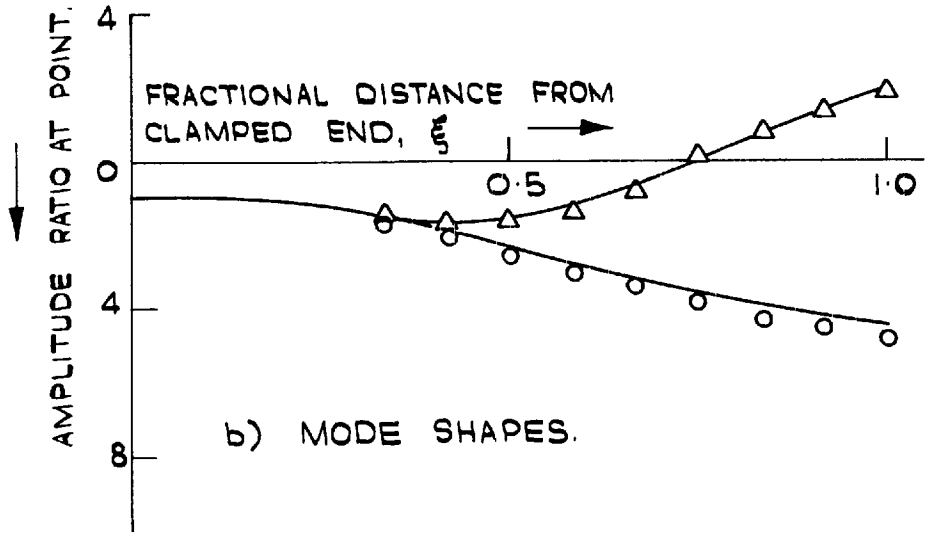

b) MODE SHAPES.

FIG. 5. 12. FIVE - LAYER BEAM 5 A.

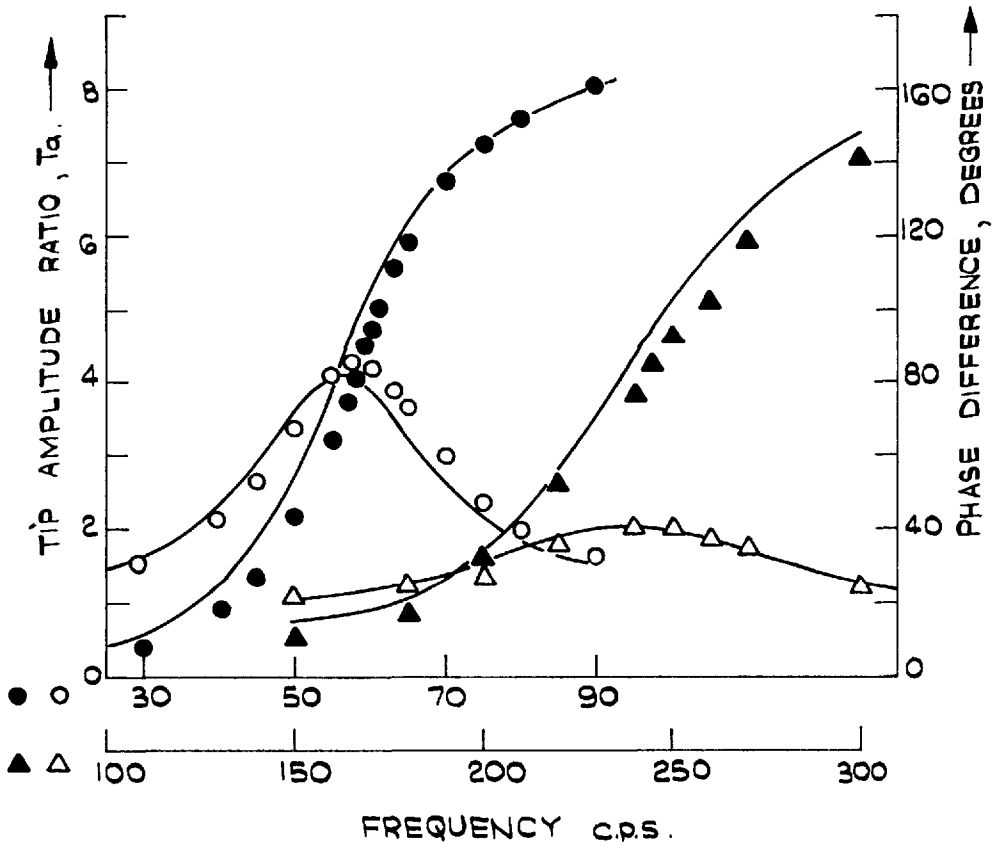

a) RESONANCE CURVES.

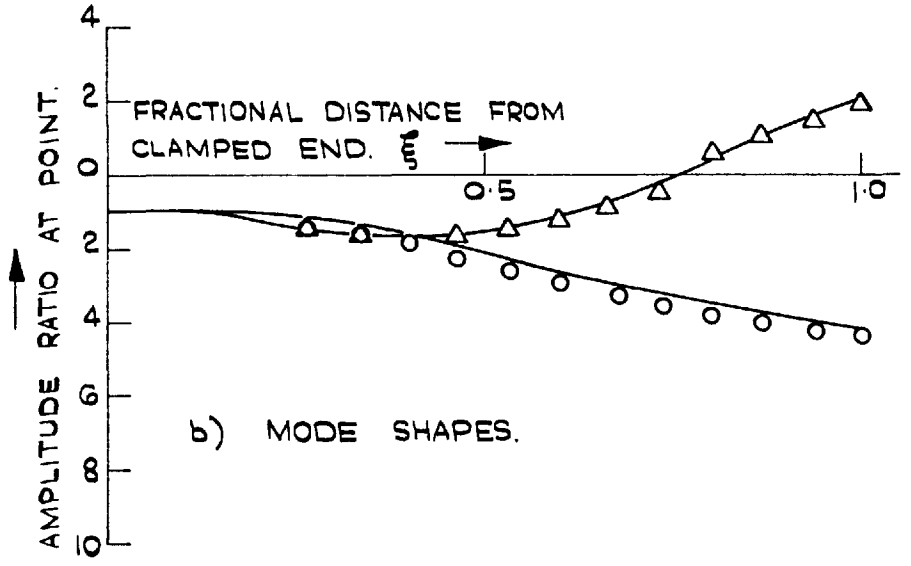

b) MODE SHAPES.

FIG. 5.13. FIVE- LAYER BEAM G.

layers was obtained by subtracting the total metal thickness from the beam overall thickness. As the bonding layers were much stiffer than the viscoelastic layers, their contribution to the beam effective stiffness would be more than that of a viscoelastic material of the same thickness. This contribution would be more significant in the five-layer beams which had more bonding layers.

The measured tip amplitude ratios agree well with the calculated values, especially in the second and third modes. The worst agreement occurs very close to the first resonant frequencies, where maximum errors of up to 8 per cent are seen to exist in a few cases. The longer beams (e.g. beams 3, 3A, and 5) give worse results than the shorter ones.

Several factors could be responsible for this discrepancy. Any error in the material loss factor, for instance, was bound to reflect itself most at resonance. It has already been stated in section 3.7.a that the loss factor for P.V.C. could be as much as 5 per cent in error. Such an error would lead to an error of about 5 per cent in the measured amplitude ratio. Another factor might be the elasticity of the araldite bonding layers. The theory assumes an infinitely shear-stiff bonding layer of negligible thickness. If this layer is not sufficiently stiff, the actual shear deformation in the viscoelastic layers (and hence, the cyclic energy loss) will be less than that

predicted theoretically. The actual tip amplitude ratio will, therefore, be more than the calculated value. It may be remarked that the above factors would also affect the higher modes. However, their overall effect on the amplitude ratios would be more easily detectable in the first mode than in the higher modes where the amplitudes, for any given amount of damping, are invariably less. It was originally thought that the lack of exact agreement in the amplitude ratios could be partly due to possible rocking of the vibrator table owing to slight differences in the dynamic loading from both sides of the double cantilever beam. This was checked by measuring the displacement amplitudes at various points on the clamping device. No rocking could be detected, and it was concluded that errors from this source were very unlikely.

The experimental and theoretical phase differences compare very favourably in all the cases. Any disagreement is due to either lack of exact agreement in the resonant frequencies or temperature effects.

The measured mode shapes are compared with the theoretical ones in figs 5.6b to 5.13b. In the graphs, the amplitude ratio of the motion at any point to the input motion is plotted at each point. It is seen that the nature of the agreement is the same as for the tip amplitude ratios, namely, the first mode experimental values are slightly

higher than the theoretical values, while the second and third mode values show very close agreement. These results show that the agreement in the displacement response is not just restricted to the tip displacements, but,in fact, holds for each point on the beam.

5.5.c. Beams with evoseal viscoelastic layers

The results for the specimens with evoseal viscoelastic layers are given in comparison with the theoretical values in figs 5.14 and 5.15. The results correspond to a time of cure of three months.

It is seen that for the two beams, the agreement between the measured and the calculated resonant frequencies is comparatively poor, the maximum error being as high as 10 per cent. The measured frequencies were consistently lower than the theoretical values. This is due to the fact, already mentioned, that the viscoelastic material of the beam was curing at a much slower rate, and hence, was much softer than the shear specimen. Since the theoretical values were calculated using the properties obtained from tests on the shear specimen, they were bound to give higher values for the resonant frequencies.

As for the tip displacement amplitude ratios, agreement between the experimental and the theoretically calculated values is fairly good for beam 7, but clearly poor for

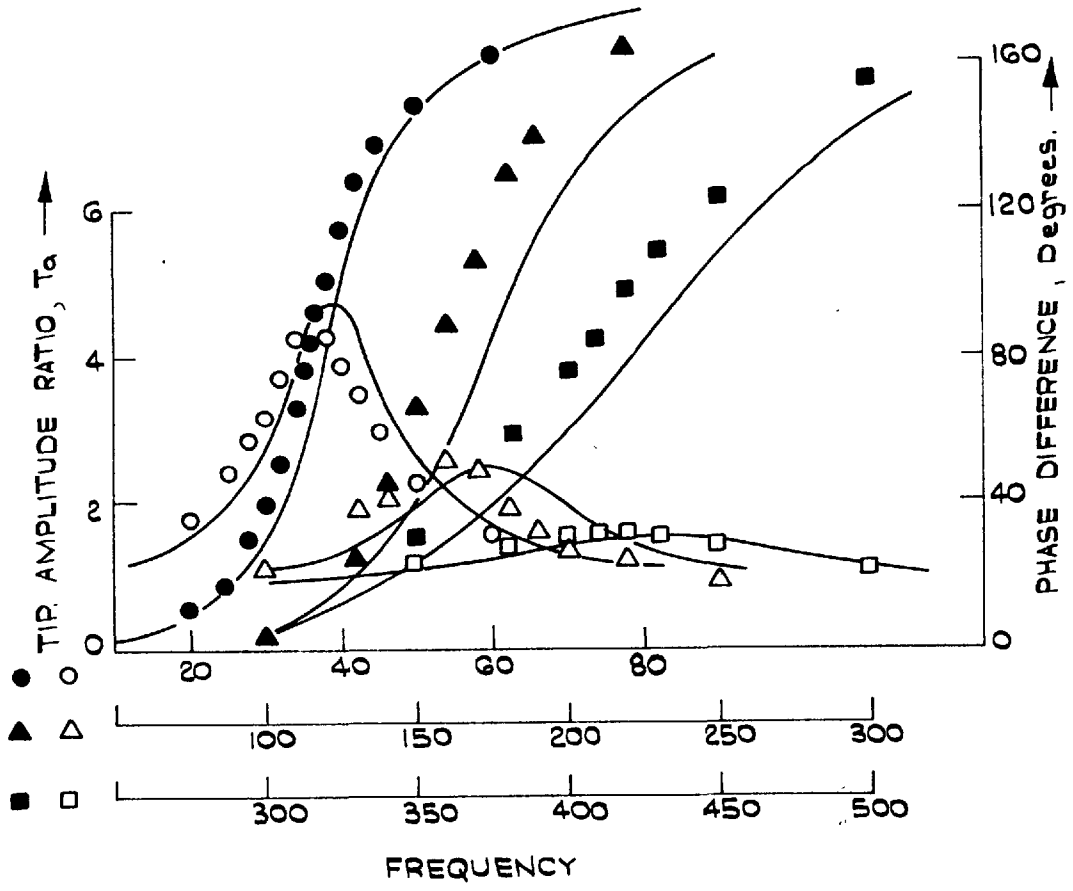

a) RESONANCE CURVES.

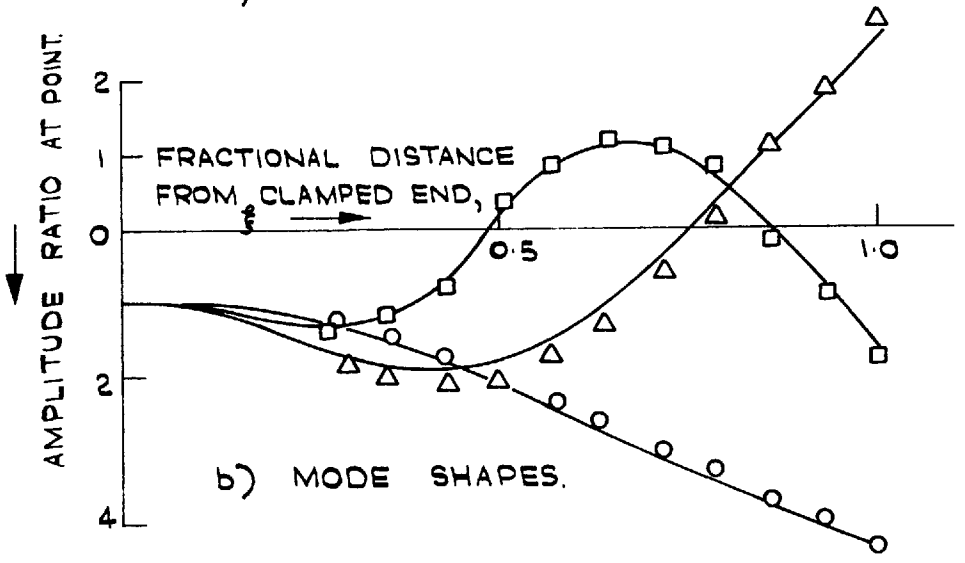

b) MODE SHAPES.

FIG. 5.14. THREE - LAYER BEAM 7.

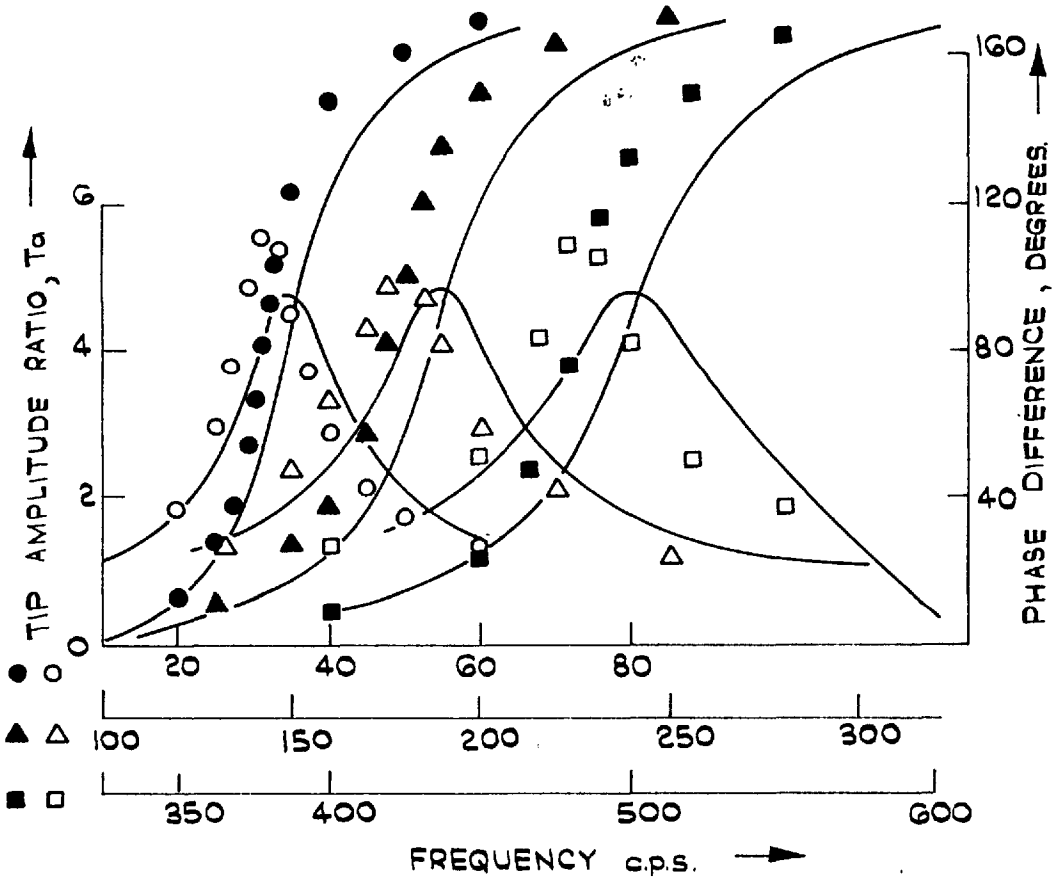

a) RESONANCE CURVES.

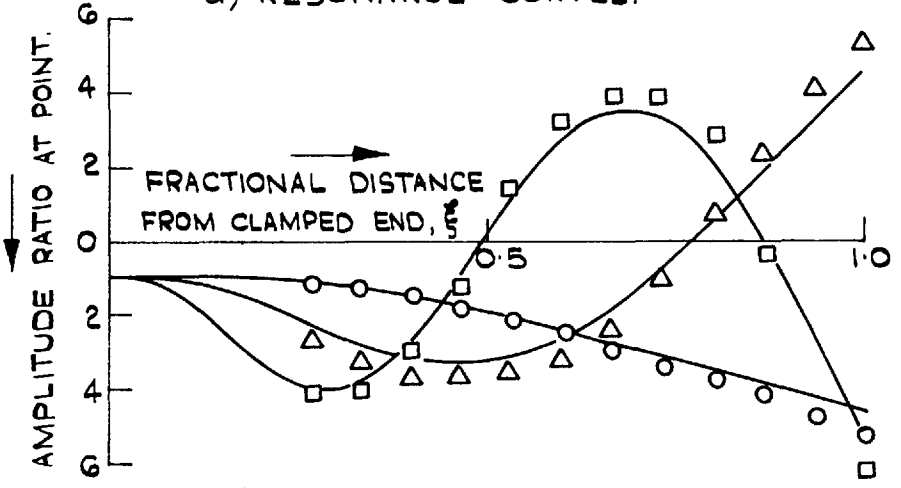

b) MODE SHAPES.

FIG. 5.15. THREE-LAYER BEAM 8.

beam 8. This might at first sight appear surprising, especially in view of the fact that the error trends in the two cases are dissimilar. In the first mode, for instance, the measured resonant tip amplitude is less for beam 7, but more for beam 8, than the corresponding theoretical value.

This apparent inconsistency is, however, readily explained using the "optimisation curves" presented in chapter 6. Considering only the first mode, the thickness ratio, H, and the theoretical shear parameter* at resonance, V_1, for each beam are given in the table below. Also given is the shear parameter, V_{1opt}, corresponding to the maximum overall loss factor for the given beam thickness ratio. The material loss factor is assumed to be 1.0 (for ease of interpolation), a value very close to the values obtained from tests on the shear specimen.

	BEAM 7	BEAM 8
H	0.5	0.375
V_1	1.9	0.35
$V_{1\,opt}(\eta_1=1.0)$	0.72	0.78

The above values, together with the optimisation curves, show that while beam 7 is on the portion of the T_a-versus-V_1

*This shear parameter is calculated using the properties of the shear specimen, hence the qualifying term, "theoretical".

curve beyond the damping peak, beam 8 is on the rather sensitive portion of the curve before the peak.

To illustrate the significance of this, suppose that the in-phase shear modulus of the viscoelastic material of the beams was 30 per cent less than that of the shear specimen. (The value, 30 per cent, was actually arrived at by "working backwards" to determine, from the optimisation curves, the change in the shear modulus, G_1', which would give rise to the observed error in the first mode resonant frequency for beam 7). Then, since the shear parameter is directly proportional to the in-phase shear modulus, the actual values of ν_1 for beams 7 and 8 would be 1.33 and 0.245 respectively. From the curing curves for evoseal (fig. 3.30), it is observed that the material loss factor shows very little change with the curing time, so that, in the argument to follow, it will be assumed to have the same value for the beams as for the shear specimen.

From the optimisation curves for H = 0.5 (fig. 6.1, chapter 6), it is seen that a change in ν_1 from 1.9 to 1.33 would result in a drop in the tip amplitude ratio from 4.9 to 4.6, or a percentage <u>decrease</u> of about 6. This change in ν_1 would also cause a decrease in the resonant frequency factor from 6.5 to 5.6, or a decrease in the resonant frequency of about 7 per cent. Similarly, by interpolation from the optimisation curves for H = 0.1 and

0.5 (figs 6.3 and 6.1), it is seen that, for beam 8, the change in γ_1 would give rise to a decrease in the resonant frequency of 8.5 per cent, and an <u>increase</u> in the tip amplitude ratio of 14.5 per cent. These values (column A) are shown side by side with the actual percentage differences between the experimental and theoretical values (column B) in the table below.

	BEAM 7		BEAM 8	
	A	B	A	B
% increase in amplitude ratio	-6.1	-5.3	14.5	16.0
% decrease in frequency	7.0	7.0	8.5	9.5

The close and consistent agreement between the figures, apart from explaining the observed behaviour in the tip amplitude ratios, also implies that the true difference between the in-phase shear moduli of the shear specimen and the beam evoseal must have been around 30 per cent. It also confirms the assertion that the disparity in the results was due to the difference in the curing rates of the beam and shear specimens.

It might be thought that, in view of the fact that evoseal is a relatively soft viscoelastic material, there was a possibility of the various layers having independent flexural motions, especially at the higher modes. This would, of course, violate one of the assumptions of the

theory (see section 2.1.b, chapter 2), and would lead to incorrect results. However, this was checked, for each mode, by measuring the displacement amplitudes in each layer at any cross-section. These were found to be the same in each case, implying that all the layers of the beams had the same flexural motions up to at least the third mode.

The theoretical phase difference-versus-frequency curves shown in figs 5.14a and 5.15a are seen to be displaced (horizontally towards the right) from the experimental points. This is due to the difference in the experimental and theoretical resonant frequencies. Once more, the agreement between the mode shapes (figs 5.14b and 5.15b) is seen to be a reflection of the agreement in the resonant tip amplitude ratios.

The difficulty encountered with the evoseal sandwich beams might raise the question whether it would not have been possible to obtain the exact properties of the beam evoseal from a shear test on a portion cut off from the beams. This approach was examined thoroughly and discarded for several reasons. Firstly, it would be extremely difficult to cut a small portion off the beam, to the size of a shear specimen, without squashing the soft viscoelastic layer appreciably. Secondly, the specimen would have to be tested in the sandwich form; that is, with the metal facing layers in tact. The facing layers would then be bonded to the fixed supports and the centre-piece of the

shear-test apparatus (fig. 3.5), as in the case of the hycadamp shear specimen. This would considerably increase the total effective moving mass. Since evoseal is a relatively soft viscoelastic material, the contribution of the inertia forces to the total measured force would be so large that the accuracy of the determination of the material properties would be extremely poor. Moreover, with such an arrangement, there would be four araldite bonding layers (instead of two, as for the beam) to each half of the shear specimen. Any bonding imperfections would, therefore, cause a different level of error. Finally, the shear specimen cut off from the beam would have a smaller "effective curing thickness" (see section 5.4.b) than the beam itself, and would thus tend to cure faster than the beam. As the process of preparation of the specimen for a shear test would take at least three days to complete, the material properties obtained in this way would invariably be different from those of the beam evoseal, thus defeating the purpose of the test.

5.6. Concluding remarks

The tests carried out cover a wide range of material properties and beam geometry. Consider, for instance, the three-layer configuration. Table 5.c gives the shear parameter, ν_1, and the material loss factor, η_1, at the first resonant frequency, as well as the thickness ratio, H,

Beam no.	Material loss factor η_1	Thickness ratio H	Shear parameter at first mode ν_1	Shear parameter at maximum loss factor $\nu_{1\,opt}$
3	0.50	0.54	2.04	0.88
3A	0.54	0.54	1.65	0.87
3B	0.61	0.54	0.96	0.84
4	0.58	0.73	0.68	0.79
4A	0.53	0.73	0.41	0.80
7	1.09	0.50	1.90	0.78
8	1.12	0.37	0.35	0.72

TABLE 5.c

Three-layer beams tested. Details of the thickness ratio, first mode shear parameter, material loss factor, and optimum shear parameter.

for each of the beams tested. The shear parameter corresponding to the maximum beam loss factor (for each set of values of η and H) is also given in each case, this being obtained from the optimisation curves in chapter 6. The table shows that the beams tested spread over regions before, close to, and beyond the peaks of the damping-versus-shear parameter curves for various values of the thickness ratio and the material loss factor (see chapter 6). Materials with widely differing properties have been used, as for instance, a relatively soft viscoelastic material, evoseal, and a fairly hard one, velbex P.V.C. Also, for the five-layer beams, various combinations of materials and geometry were tested.

The generally good agreement obtained can thus be regarded as a satisfactory check, over a wide range of properties and geometry, on the theory developed for symmetrical three-layer and five-layer beams, and, in general, for symmetrical multi-layer beams.

CHAPTER 6

AN INTRODUCTION TO THE DESIGN STUDY OF SYMMETRICAL MULTI-LAYER BEAMS

Introduction

It will now be shown how the foregoing analysis can be applied in the design study of multi-layer beams. Systems with harmonic excitation will be considered, and the general treatment will be illustrated with the specific case of cantilever beams subjected to displacement forcing at the root. For simplicity, strain amplitude dependence will be neglected.

The parameters for the study of the resonant responses of multi-layer beams are first established, and the general nature of the dependence of the damping and the stiffness on these variables is predicted from the differential equations. Illustrations are then given with a detailed study of the stiffness, damping, and resonant amplitude responses of three-layer cantilever beams. Results of studies carried out on five-layer beams are also presented, chiefly to demonstrate how they can be used as an improvement on three-layer beams. Various applications of the results of this study are illustrated.

6.1. Theoretical considerations

6.1.a. Relevant parameters

Consider first the three-layer beam. On neglecting strain dependence, the differential equations for the beam are as given in equations 4.1.xv. In this preliminary discussion, the extensional damping terms (already shown to make little contribution to the system damping for most practical cases) are ignored. Also, the contribution of the viscoelastic extensional terms (i.e. the terms containing the in-phase Young's modulus of the viscoelastic material as a factor) to the coefficients of the differential equations is assumed neglible. The consequences of these assumptions and their accuracy are examined at a later stage.

Assume, to begin with, that the thickness ratio, H, and the material loss factor, η_1, are kept constant. Then, from equations 4.1.xv, it is seen that as the forcing frequency, the material properties, and the beam length are varied, every other coefficient of the differential equations remains unchanged except ν_1, $\sigma_1 (= \eta_1 \nu_1)$, and β_1*. For any given values of β_1, ν_1, and the modified forcing function, $p_m = \frac{\ell^3}{EI} p(\ell\xi)$, there is only one solution to the equations, no matter the actual values of the material properties, the beam geometry (for a given H), and

*For the definitions of these symbols, see equations 4.1.xvi, 4.1.xvii, and 4.1.xviii.

the forcing frequency. It follows, therefore, that the dynamic state of the beam is uniquely determined by the quantities, H, η_1 , ν_1 , β_1 , and p_m. Any response of the beam can thus be expressed as a function of these five variables. In particular, a "typical" displacement amplitude of the beam (e.g. the tip displacement amplitude in the case of a cantilever beam) can be expressed as,

$a_T = f_a(\eta_1, H, \nu_1, \beta_1, p_m)$ .....6.1.i.

The general functional notation, $w_i = f_w(u_1, u_2, u_3, \ldots)$, used throughout this chapter, is meant to designate that w_i can be expressed, implicitly or explicitly, as a function of the variables, u_1, u_2, u_3, ...etc.

If resonance* is defined as the state at which this displacement is a maximum in the immediate neighbourhood on the frequency axis (which, for any given geometry and material properties, is parallel to the β_1 axis), then, the resonant state is given by

$f'_a(\eta_1, H, \nu_1, \beta_{on}, p_m) = \frac{\partial f_a}{\partial \beta_1} = 0$ .....6.1.ii, where β_{on}, the value of β_1 at resonance, defines the resonant frequency at the n-th mode being considered. Using the functional notation defined above, equation 6.1.ii can be put in the form, $\beta_{on} = f_\beta(\eta_1, H, \nu_1, p_m)$ .....6.1.iii.

From the above reasoning, the beam loss factor, which

*Other methods of defining resonance can be employed without prejudicing the argument presented in this section.

has been defined in terms of energy ratios at a resonant frequency (see section 4.6.b), can also be expressed as

$\eta_{on} = f_{\eta_o}(\eta_1, H, \nu_1, \beta_{on}, p_m)$ .....6.1.iv.

It is possible to eliminate β_{on} from equation 6.1.iv, using equation 6.1.iii. This gives $\eta_{on} = f_{\eta}(\nu_1, H, \eta_1, p_m)$ ..6.1.v. In other words, the beam loss factor is uniquely determined by the four parameters, ν_1 , H, η_1 , p_m.

These four quantities, along with β_{on}, constitute the relevant parameters in the general study of the resonant responses of three-layer beams. ν_1 has already been called the "shear parameter". β_{on} is called the "resonant frequency factor", or simply the "frequency factor", there being very little risk here of confusing it with β_1 (the non-resonant frequency factor). The inclusion of β_{on} as one of the parameters may appear superfluous in view of equation 6.1.iii. However, it will be seen later that under certain conditions, it is very convenient to use it as one of the independent variables for characterising the damping response. The presence of the modified forcing function, p_m, as a basic parameter is significant. It shows that, in general, the damping (in fact, any response) of the structure is a function of the forcing function. The nature and significance of these parameters will be examined in more detail later.

In its general form, the argument presented above

is applicable to beams with more than three layers. The only additional complication is that the number of parameters increases with the number of layers. For instance, for the symmetrical five-layer beam, the frequency factor, β_{on}, and the beam loss factor, η_{on}, can each be expressed as a function of the six quantities, H_1, H_2, e_1, ν_2, η_2, and p_m. Hence these variables, together with β_{on}, form the seven parameters associated with the design study of five-layer beams.

6.1.b. Parameters for systems with constant forcing function.

From the argument presented in section 6.1.a, it is seen that the parameters on which β_{on} and η_{on} depend can be classified into two groups: parameters external to the vibrating system; namely, p_m; and parameters which are inherent to the system, for example, η_1, H, and ν_1, for the three-layer configuration.

In general, for any given configuration, it is not easy to seperate the effects of these two groups of parameters. When, however, the forcing function is independent of the position along the beam, this separation is readily achieved. For instance, with a uniformly distributed force (of constant amplitude), the modified forcing function is a constant for any given system, and so can be easily eliminated from the equations (e.g. by

division). Also, for systems subjected to displacement forcing, the modified forcing function is directly proportional to β_1 (see section 4.2.c). Hence, at resonance, it will also be proportional to β_{on}, and can, therefore, be eliminated by replacing it with β_{on}. For systems such as these, the frequency factor and the beam loss factor can, from equations 6.1.iii and 6.1.v, be expressed as,

$\beta_{on} = f_{\beta_{on}}(\eta_1, H, \nu_1)$ .....6.1.vi, and

$\eta_{on} = f_{\eta_{on}}(\eta_1, H, \nu_1)$ .....6.1.vii, for the three-layer configuration. In other words, the system damping, and any resonant response, can now be expressed in terms of only the parameters inherent to the system; it is thus possible to study the effects of these parameters on their own. The rest of the general theoretical considerations will be restricted to such systems.

6.1.c. Variation of the beam loss factor and the frequency factor with the system parameters.

In the design study of multi-layer beams, two quantities are of special interest; namely, the damping and the dynamic stiffness. In this work, η_{on} and β_{on} are taken as measures of these quantities for any mode, n. It is possible to obtain some idea of the nature of the dependence of η_{on} and β_{on} on the system parameters, purely from examination of the differential equations. Once again,

for simplicity of illustration, the arguments presented are centred on the three-layer configuration.

The shear parameter, ν_1.

Consider first the shear parameter, ν_1. Assume that η_1 and H are held constant. Then, at very low values of ν_1 (i.e. as $\nu_1 \to 0$), the damping terms of the differential equations become very small, and equations 4.1.xv tend to

$$\left.\begin{aligned} (D^4 - \beta_1)u_o + \alpha_1 D^3 X_{o1} &= p_{mc} \quad ; \quad \mu_1 D^3 u_o + D^2 X_{o1} = 0 \\ (D^4 - \beta_1)v_o + \alpha_1 D^3 Y_{o1} &= 0 \quad ; \quad \mu_1 D^3 v_o + D^2 Y_{o1} = 0 \end{aligned}\right\} \ldots.6.1.viii,$$

p_{mc}, being the now constant modified forcing function. The disappearance of the damping terms implies that no energy dissipation occurs, and hence, that the loss factor is zero.

The solution of equations 6.1.viii, for any boundary condition, gives

(a) $v_o = Y_{o1} = 0$; in other words, the quadrature components of the displacement and the shear deformation disappear; and

(b) u_o and X_{o1}, the in-phase components of the displacement and the shear, become infinitely large at the resonant frequency defined by $\beta_{on} = k_n^4(1 - \alpha_1\mu_1)$ ....6.1.ix, where k_n^4 is the frequency factor for a plain undamped Euler beam. Thus, for simply supported beams,

$k_n = n\pi$, n = 1,2,3,... ; for cantilever beams,

k_n = 1.875, 4.694, ...; and so on.

Interpreted physically, the above result shows that

for very short beams or beams with very soft viscoelastic layers, the shear deformation and the displacement become very large at resonance; but they are both in phase (or anti-phase) with each other and with the exciting force, so that no energy loss occurs. Equation 6.1.ix defines the resonant frequency for the limiting case of a sandwich beam made up of two similar elastic layers, spaced apart as hitherto, and vibrating in phase. Incidentally, equation 6.1.ix also gives the lower limit of the frequency factor, β_{on}, for any three-layer beam of the given thickness ratio, H.

Again, as γ_1 tends to infinity, it is seen from equations 4.1.xv, that X_{o1} and Y_{o1} (and hence their derivatives) tend to zero, with the equations reducing to

$(D^4 - \beta_1)u_o = p_{mc}$; and $D^4 v_o = 0$ .....6.1.x.

This is clearly the Euler bi-harmonic equation for a plain undamped beam, and the solution gives the displacement as infinitely large at the resonant frequency defined by

$\beta_{on} = k_n^4$ ....6.1.xi.

The above result can also be interpreted physically. For very long beams or beams with very stiff viscoelastic layers, very little shear deformation occurs in the viscoelastic layer, and hence the damping is small. The beam behaves more like a plain solid beam. Equation 6.1.xi gives the upper limit of the frequency factor for sandwich

beams.

As γ_i increases from zero to infinity, the beam loss factor must pass through a maximum (or maxima) at some intermediate value of γ_i. It will in fact be seen from the specific cases considered later, that only one peak occurs in the damping-versus-shear parameter curve for the given mode; a fact which intuition would have led one to anticipate. Also as γ_i varies from the state of "infinite shear" ($\gamma_i = 0$) to the "shear-free" state ($\gamma_i = \infty$) it is reasonable to expect the frequency factor, β_{on}, to increase continuously from its lower to its upper limit.

The material loss factor, η_i

It is best to consider the effect of the material loss factor η_i by first examining what happens when the shear parameter γ_i is varied, keeping η_i and H constant, as in the above discussion. Another look at the differential equations 4.1.xv will show that the only coefficient that is affected by a variation in γ_i is σ_i ($= \eta_i \gamma_i$). β_i may also be affected, but it is an arbitrary coefficient, since it contains the forcing frequency, ω. In any case, for any value of γ_i, it has to be varied until the resonant condition is reached before the beam loss factor (and the resonant frequency factor) can be obtained.

As γ_i is increased from zero, σ_i increases, and so does the beam loss factor. η_{on}; and at some values of σ_i and γ_i,

η_{on} attains its maximum value. Further increase in ν_1 and σ_1 leads to a drop in η_{on}. Now, the rate at which σ_1 increases as ν_1 increases is evidently determined by η_1. When $\eta_1 = 0$, the system damping is zero, and the η_{on}-versus-ν_1 curve coincides with the ν_1 axis. For very small values of η_1, the energy loss in the system is small, so that the overall damping is small. Also, as ν_1 increases, σ_1 increases rather slowly; consequently, the value of ν_1 at which the maximum η_{on} occurs is relatively high. On the other hand, as ν_1 becomes larger and larger, σ_1 approaches infinity rather slowly, so that the damping tends to zero rather gradually. For high values of η_1, σ_1 increases rapidly with ν_1; hence the peaks of the damping curves would be expected to occur at smaller values of ν_1. Besides, for a given value of ν_1, σ_1 tends to infinity at a much faster rate, so that the damping decreases to zero more rapidly.

It follows, therefore, that for a given thickness ratio, the η_{on}-versus-ν_1 curves, for various values of the material loss factor, will get peakier as η_1 increases, the peaks being at the same time displaced towards the axis, $\nu_1 = 0$. Also, at sufficiently large values of the shear parameter, the curves will intersect giving rise to regions where it is possible to obtain a higher η_{on} with a smaller η_1.

The effect of the material loss factor on the frequency factor, β_{on}, can also be similarly argued. It has already been postulated that the frequency factor increases

as ν_1 (and hence, σ_1) increases. Since, for any ν_1, σ_1 increases with increase in η_1, it follows that the frequency factor will also increase with η_1. Hence, the graphs of the frequency factor against the shear parameter (at a constant thickness ratio) will all start and end at the limits already determined, in equations 6.1.ix and 6.1.xi but the curves for higher values of η_1 will tend to the upper limit much more rapidly.

Thickness ratio, H

It is rather difficult to deduce from the differential equations how the thickness ratio, H, affects the beam loss factor and the frequency parameter, since all the coefficients of the equations (including ν_1 and β_1) depend on H. From purely physical considerations, however, it will be expected that for given values of ν_1 and η_1, the beam damping will increase as the thickness ratio (which is a measure of the volume of viscoelastic material in a given volume of the beam) increases.

6.1.d Variation of the beam loss factor with the frequency factor

In equation 6.1.vii the beam loss factor η_{on} has been expressed as a function of η_1, H, and ν_1. It is, however, possible using equations 6.1.vi, to express it in terms η_1, H, and β_{on}: thus using β_{on} as a basic parameter in place of ν_1. When this is done, it is easy to deduce the

shape of the resulting η_{on}-versus-β_{on} curves (at constant η_i and H) from the predictions above. For instance, it has been stated that as ν_i varies, the frequency factor increases from $k_n^4(1-\alpha_i\mu_i)$ to k_n^4, while the beam loss factor increases from zero to a maximum and drops gradually to zero once more. Hence, curves of η_{on}-versus-β_{on} will start at $\beta_{on} = k_n^4(1-\alpha_i\mu_i)$, increase to a maximum at some value of β_{on}, and then terminate at $\beta_{on} = k_n^4$.

Although the above discussion has, for simplicity, been particularised to three-layer beams, much of the reasoning applies equally to higher order beams. For five-layer beams, for instance, the nature of the dependence of the beam loss factor and the frequency factor on the shear parameter and the material loss factor, for given values of H_1, H_2, and e_1, is the same as discussed above. The effects of the other parameters can be examined on similar lines.

Some of the general trends predicted above were arrived at by Mead, by considering the solutions obtained from analysis of three-layer simply-supported plates [62,63]. However, the treatment given here is quite general, and the deductions have been made straight from the differential equations. Hence they apply to beams of <u>all</u> boundary conditions.

6.1.e The nature of the parameters - three-layer beam.

The parameters established above for the design study of three-layer beams are η_1, H, ν_1 and β_{on}. Of these, the thickness ratio, H, and the material loss factor, η_1, need no further introduction.

The shear parameter, ν_1, apart from depending on the thickness ratio, is proportional to the ratio, $\frac{G_1'}{E_2}$, and the square of the ratio, $p_1 = \frac{\ell}{h_2}$. It is thus entirely dependent on the beam geometry and material properties. Its importance lies in the fact that for given values of H and η_1, it uniquely determines the system resonant response no matter the values of the material properties or the beam dimensions.

The frequency factor, β_{on}, has already been regarded as a measure of the dynamic stiffness of the beam. This is because, for given beam geometry and properties, a higher value of β_{on} means a higher resonant frequency. β_{on} can also be looked upon as a measure of the "state of shear deformation" of the beam. It has been shown in equations 6.1.ix and 6.1.xi that, for sandwich beams, β_{on} varies between the limits, $k_n^4(1-\alpha_1\mu_1)$ and k_n^4, corresponding to states of infinite shear and zero shear respectively, in the viscoelastic layer. For any given η_1 and H, therefore, a high value of β_{on} implies small shear deformation in the viscoelastic material. In other words, the greater the shear deformation in the viscoelastic material, the

more is the reduction in the stiffness of the beam. It is emphasised that β_{on} is not a 'basic' parameter, since it depends not only on the material property and geometry, but also on the resonant frequency which is not usually known a priori. Its inclusion as a design parameter stems from the fact that, quite often, it serves as a convenient base for analysing the damping response. Besides, if the shear parameter is not known or easily determined, β_{on} can be easily obtained experimentally and used as a means of evaluating ν_1 (see section 6.2.c).

It is significant that the only material property which appears explicitly as a parameter is η_1. The other properties appear in the parameters ν_1 and β_{on} as ratios. It is thus possible to vary them, without affecting the system resonant response. For instance, for a given thickness ratio H, the in-phase shear modulus, G_1', and the Young's modulus, E_2, can be increased by the same ratio without causing any change in ν_1, and hence, in the system damping and frequency factor. Besides, since these material properties appear in parameters which also depend on the beam geometry, it is possible to eliminate the effect of a change in properties with a suitable alteration of the beam geometry. Thus, for a given H, if the in-phase shear modulus, G_1', is increased to four times its value, and the beam length is halved, the shear parameter, ν_1 (and hence, any resonant response of the system for a given η_1)

will remain unaffected.

It may be noted that the dependence of the shear modulus, G_1', on temperature and frequency does not affect the considerations above. A variation in the temperature (or frequency) merely alters the value of ν_1, leading to a corresponding change in the system resonant response.

Damping efficiency

The beam loss factor, η_{on}, has been shown to be a function of the material loss factor, η_1. To be able to assess the usefulness of a given material loss factor, in increasing the damping response, a "damping efficiency"* is defined as the ratio of the beam loss factor, η_{on}, to the material loss factor, η_1.

6.2. Design study of three-layer cantilever beams with displacement forcing at the root.

6.2.a. Optimisation curves for the first mode

The general considerations given in section 6.1. will now be illustrated with the study of the resonant responses of three-layer cantilever beams subjected to displacement forcing at the root.

Fig. 6.1. shows the variation of the beam loss factor, η_{o1}, the frequency factor, β_{o1}, and the tip displacement amplitude ratio, T_a, with the shear parameter, ν_1, at a

*This ratio is referred to as "the relative loss factor" by Ross, Ungar, and Kerwin [47].

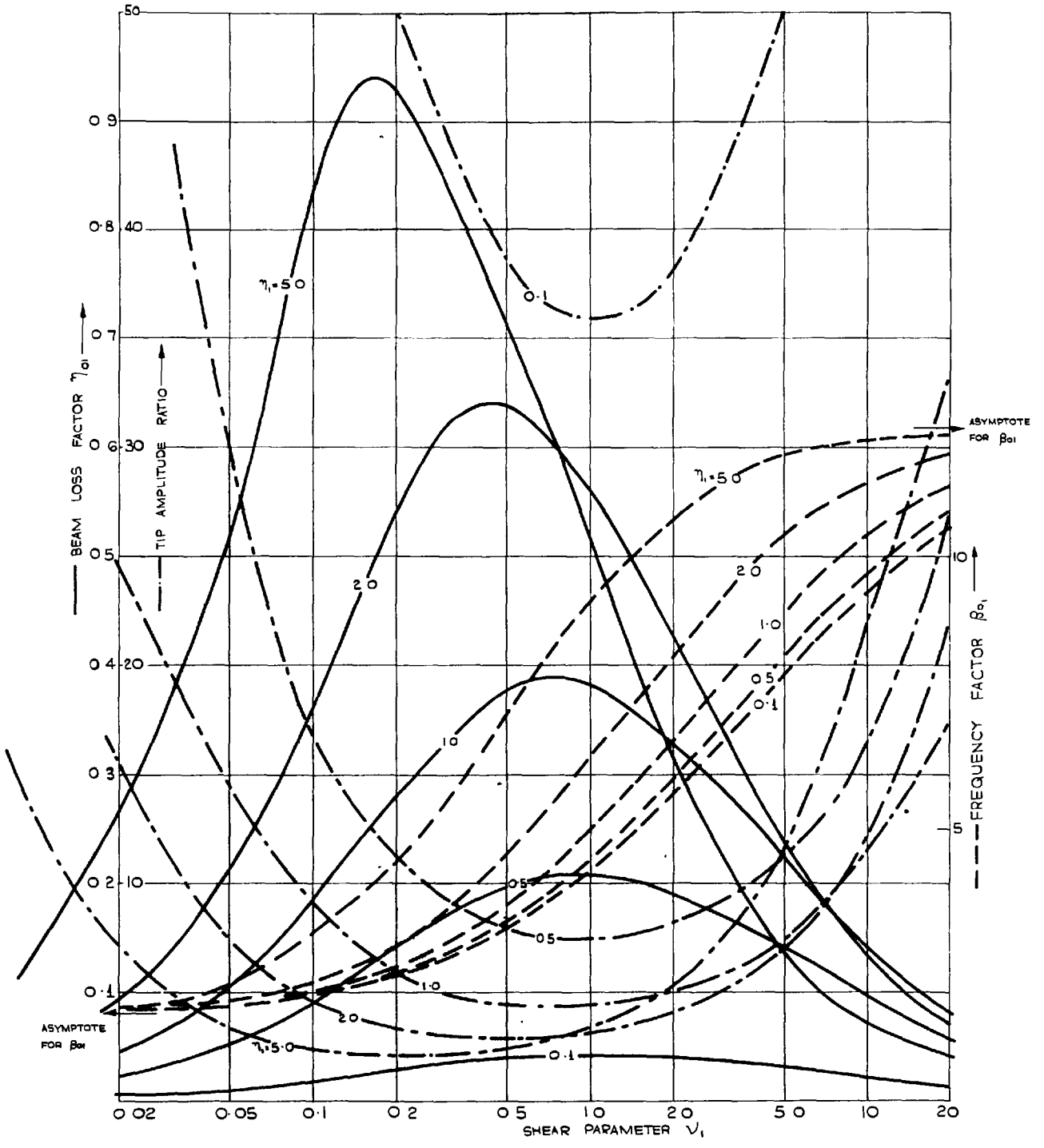

FIG 6 1 THREE LAYER BEAM VARIATION OF BEAM LOSS FACTOR η_{01}, FREQUENCY FACTOR β_{01}, AND TIP AMPLITUDE RATIO T_a, WITH SHEAR PARAMETER ν_1 FOR THICKNESS RATIO $H = 0.5$

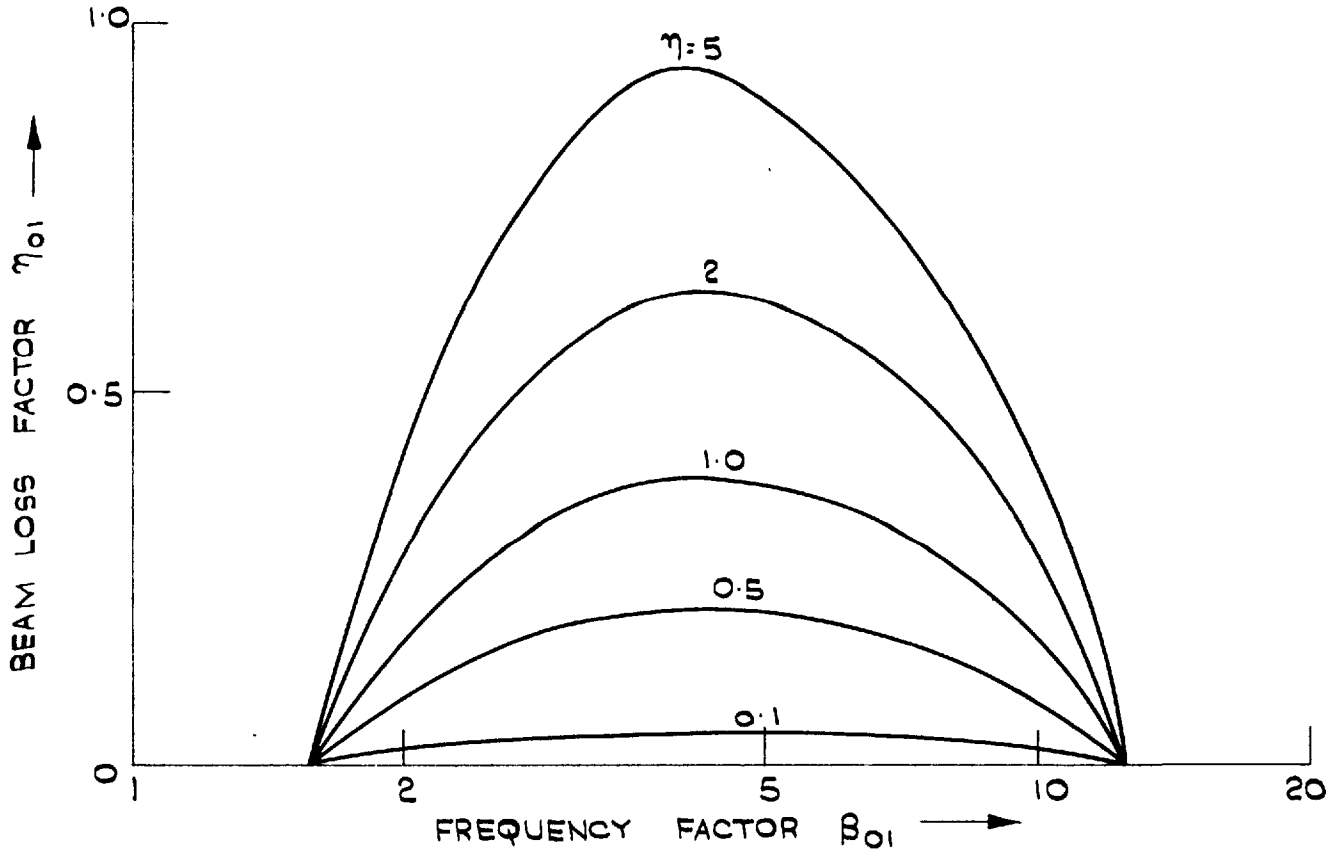

FIG. G. 2. THREE LAYER BEAM : VARIATION OF BEAM LOSS FACTOR η_{01} WITH FREQUENCY FACTOR β_{01} FOR THICKNESS RATIO H = 0·5.

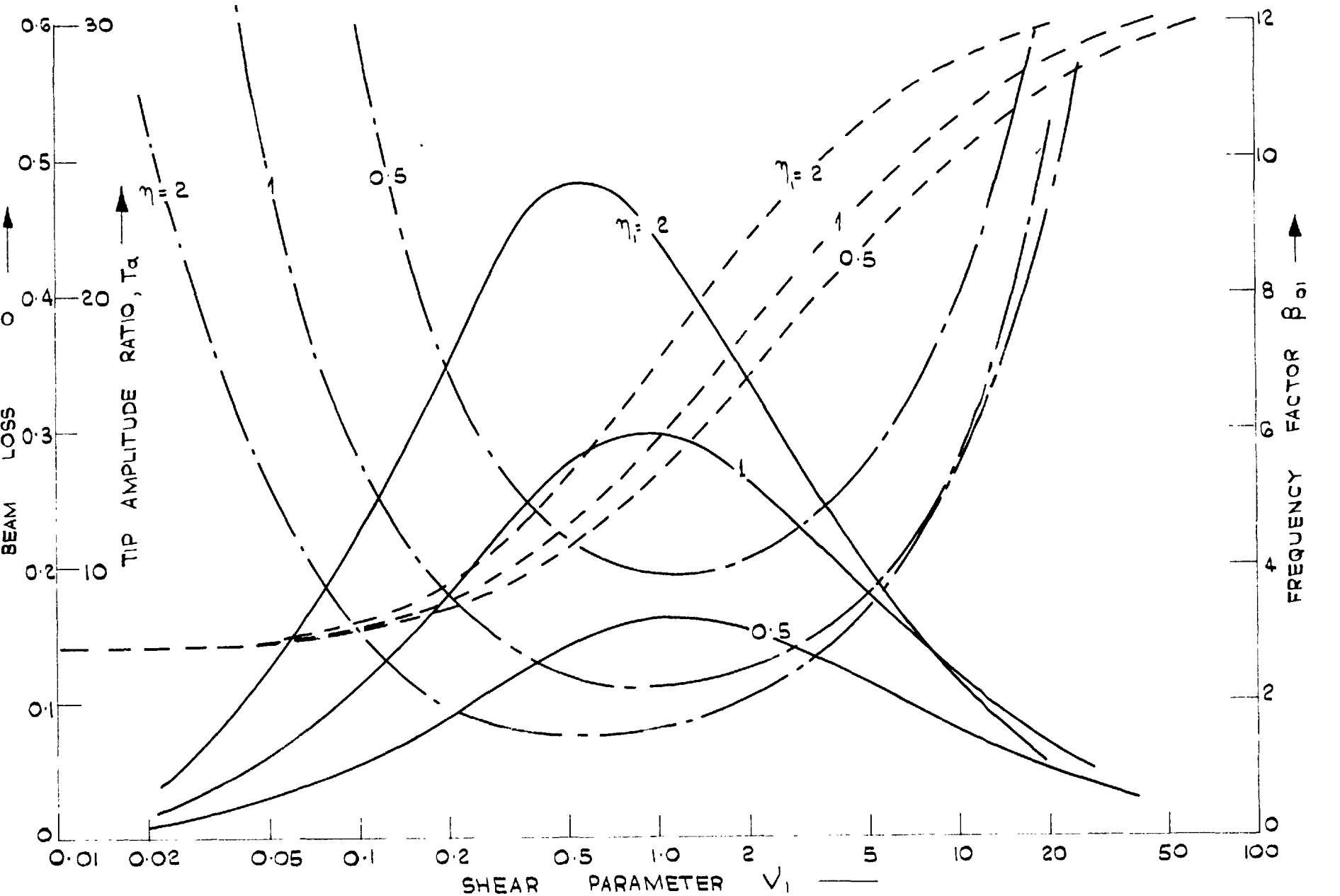

FIG. 6.3. THREE - LAYER BEAM VARIATION OF BEAM LOSS FACTOR η_{01}, AMPLITUDE RATIO Ta, AND FREQUENCY FACTOR β_{01}, WITH THE SHEAR PARAMETER V_1 H = 0·1

— — — FREQUENCY FACTOR β_{01}

—— BEAM LOSS FACTOR η_{01}

-·——·- TIP AMPLITUDE RATIO Ta

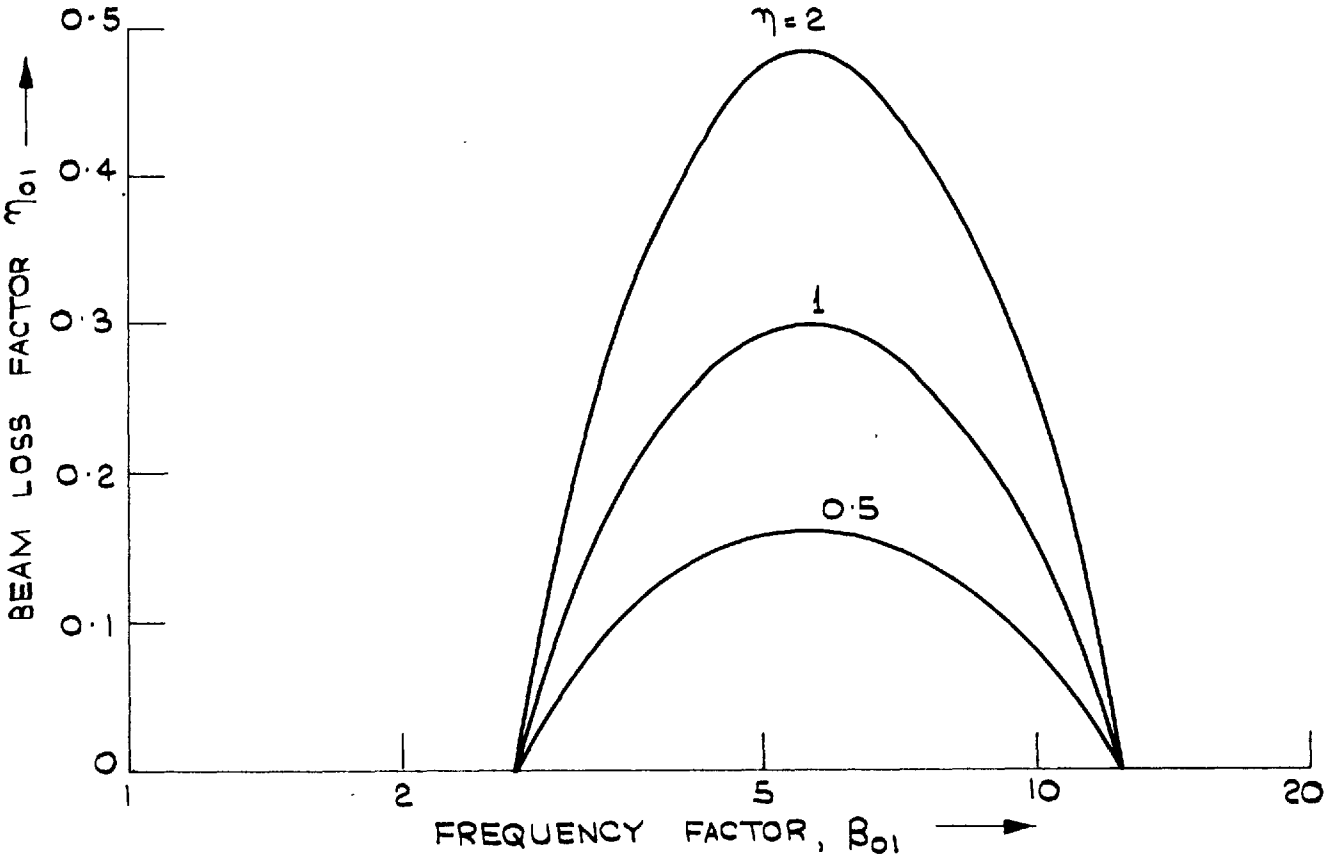

FIG 6.4. THREE LAYER BEAM: VARIATION OF BEAM LOSS FACTOR η_{01} WITH FREQUENCY FACTOR β_{01} FOR A THICKNESS RATIO $H = 0{\cdot}1$.

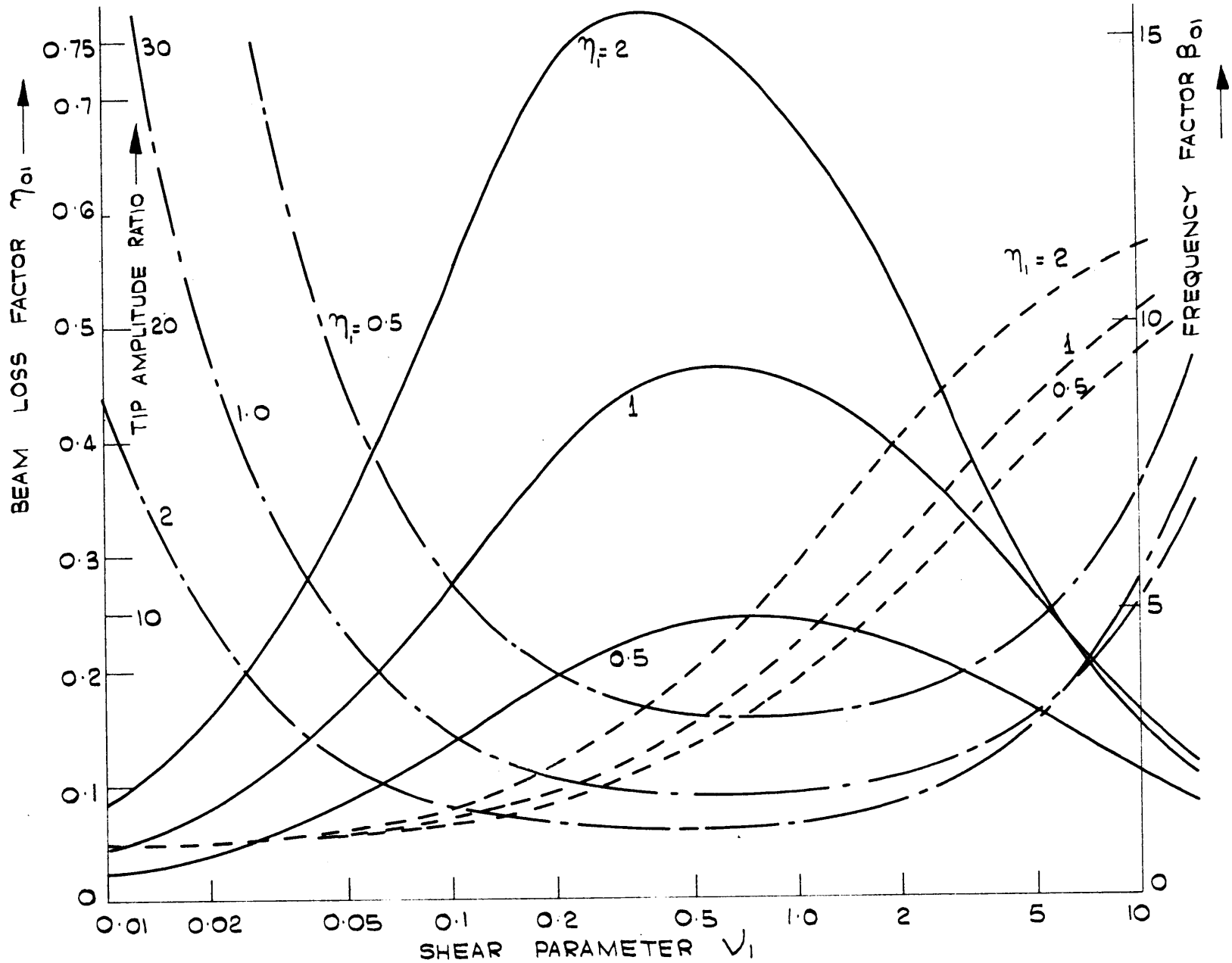

FIG. 6.5. THREE - LAYER BEAM : VARIATION OF BEAM LOSS FACTOR η_{01}, TIP AMPLITUDE RATIO, Ta AND FREQUENCY FACTOR B_{01}, WITH SHEAR PARAMETER ν_1 FOR THICKNESS RATIO H = 1·0

– – – – FREQUENCY FACTOR B_{01} ·——· TIP AMPLITUDE RATIO, Ta.

——— BEAM LOSS FACTOR η_{01}

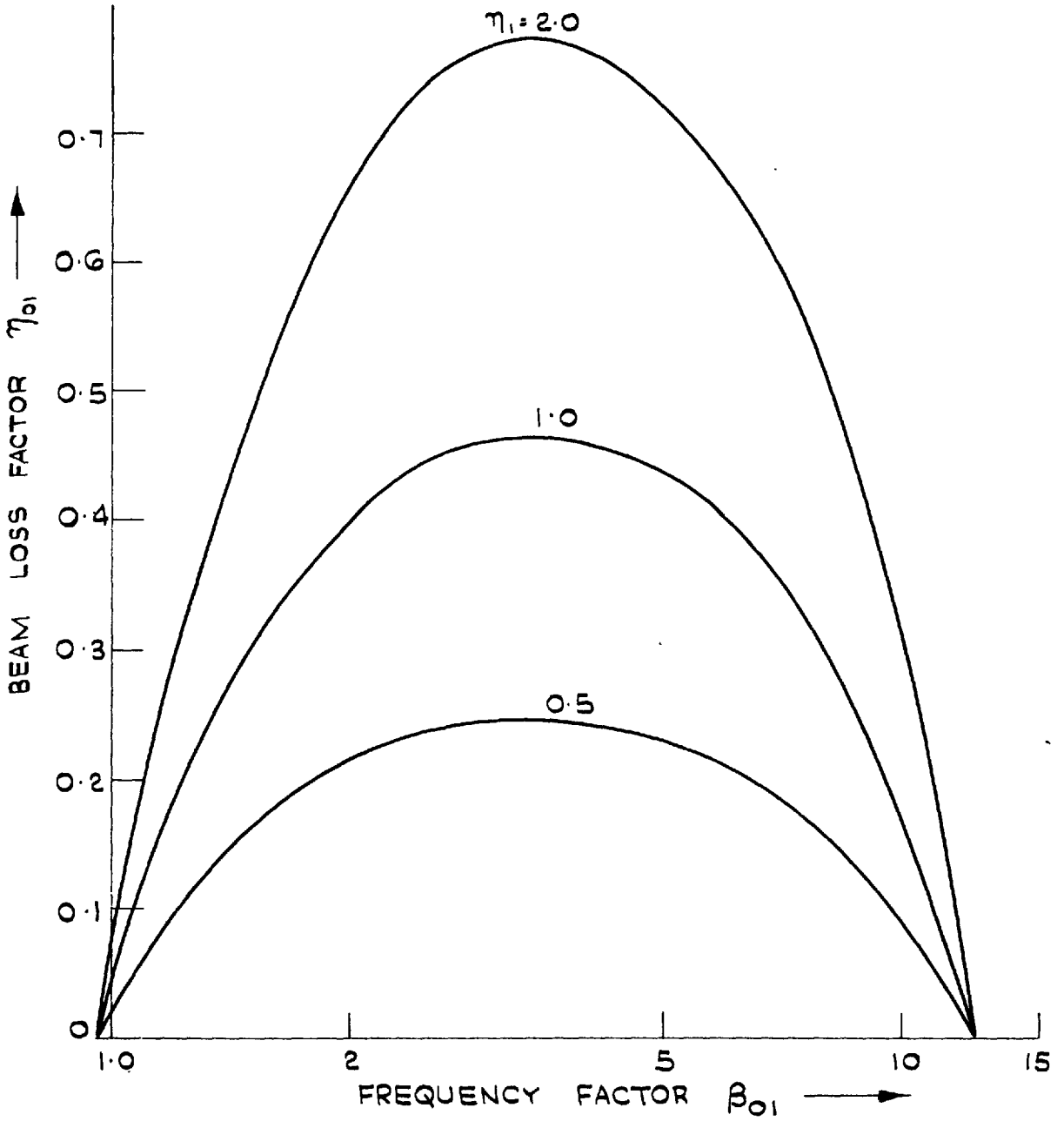

FIG. 6.6. THREE - LAYER BEAM : VARIATION OF BEAM LOSS FACTOR η_{01} WITH THE FREQUENCY FACTOR β_{01} FOR THICKNESS RATIO H = 1.

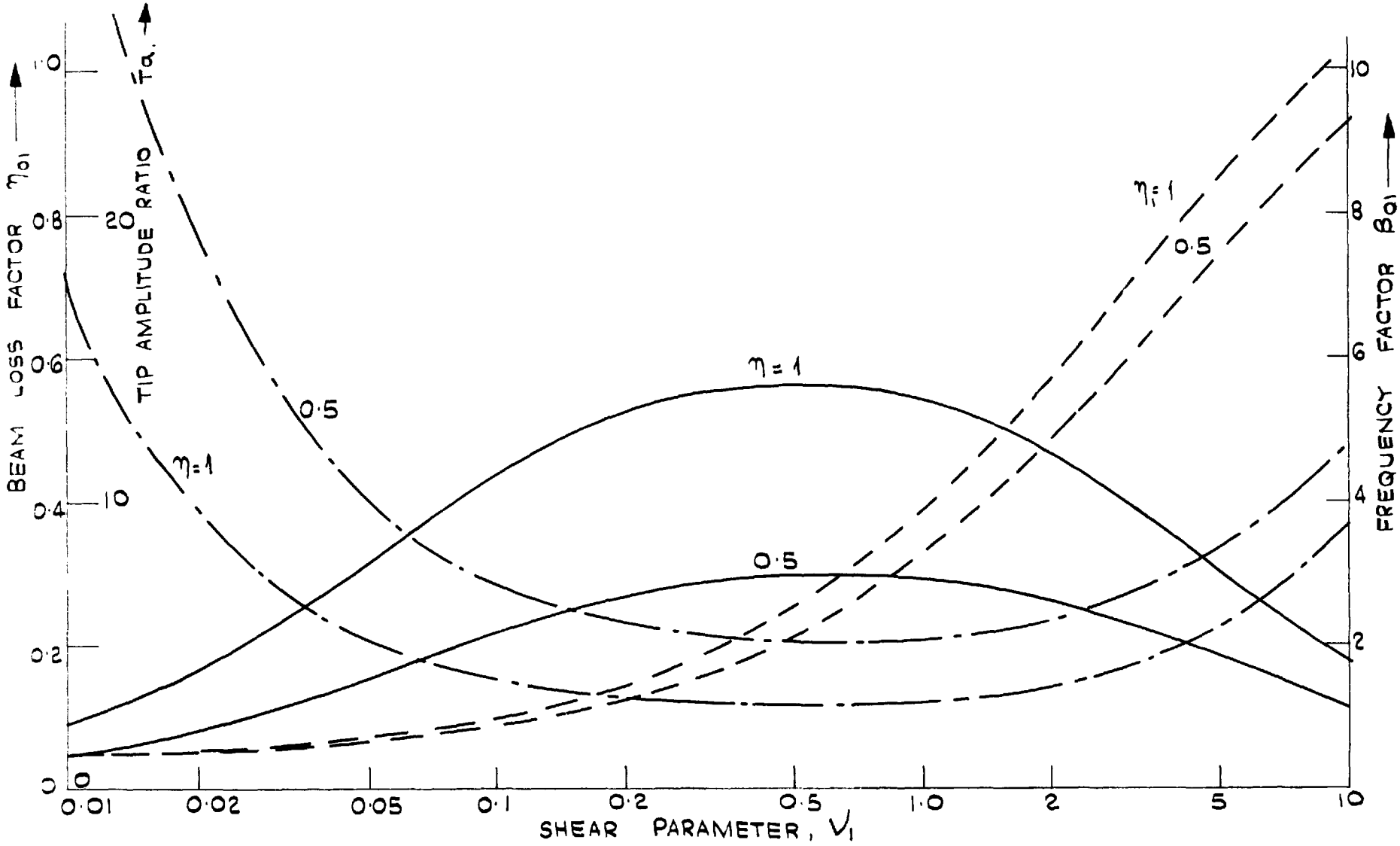

FIG. G.7. THREE-LAYER BEAM: VARIATION OF BEAM LOSS FACTOR η_{01}, FREQUENCY FACTOR β_{01}, AND TIP AMPLITUDE RATIO Ta, WITH THE SHEAR PARAMETER V_1, FOR THICKNESS RATIO H = 2.

——— BEAM LOSS FACTOR η_{01} — — — FREQUENCY FACTOR, β_{01}

·—·—· TIP AMPLITUDE RATIO Ta

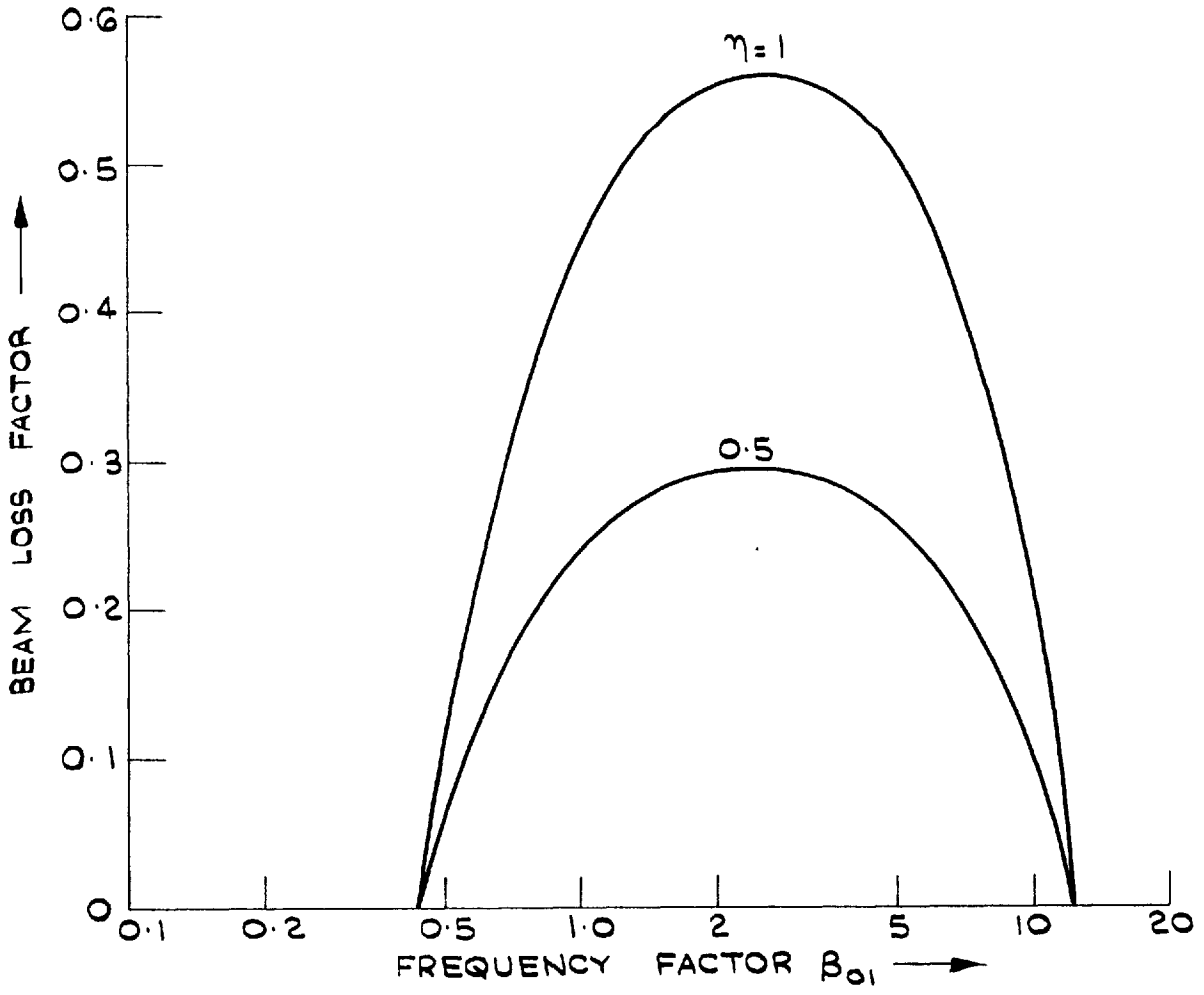

FIG. 6.8. THREE LAYER BEAM : VARIATION OF BEAM LOSS FACTOR η_{01} WITH FREQUENCY FACTOR β_{01}; FOR THICKNESS RATIO H = 2.

constant thickness ratio, $H = 0.5$, and for various values of the material loss factor, η_1. The graphs are for the first mode*.

As already anticipated, each damping curve passes through a maximum at a value of ν_1 which decreases as the material loss factor, η_1, increases. It is also seen that the higher the material loss factor, the greater the maximum value of the beam loss factor. The curves for higher values of η_1 are seen to drop more rapidly beyond the peak, intersecting with the curves for lower values of η_1. Hence, there exist regions of the curves where a high material loss factor is, in fact, a disadvantage as regards the beam damping response. For instance, at $\nu_1 = 1.0$, it is seen that a material loss factor of 2 gives more beam damping than a value of 5; at $\nu_1 = 6$, more beam loss factor is obtained with a material loss factor of 0.5, than with a value ten times as large (5.0).

The β_{01}-curves are seen to rise gradually at first, and then more rapidly in the region of the peaks of the damping curves, and to gradually approach the upper limit (=12.36). For any given value of the shear parameter, the frequency

*The values plotted in all the graphs presented in this section were obtained by solving the differential equations (the viscoelastic extensional terms being included) as described in section 4.2, and calculating the beam loss factor in the manner indicated in section 4.6.b.

factor increases with the material loss factor, η_1, the rate of increase being greatest in the region of the damping peaks.

It may be remarked that the damping and stiffness curves remind one of the displacement and phase resonance curves for damped beams. The trends are, of course, opposite, the curves for high values of η_1 behaving like the response curves for lightly damped systems, and vice versa.

As would be expected, the tip amplitude curves behave in the opposite manner to the damping curves, having their minimum values at about the same values of γ_1 as for the peaks of the corresponding damping curves. This, incidentally, shows that the beam loss factor, as defined here, is a fair reflection of the tip amplitude, a point which will be considered in more detail later.

Fig. 6.2 shows the beam loss factor, η_{o1}, plotted against the frequency factor for the same thickness ratio H = 0.5. An interesting feature of the curves is that, for a given H, the maximum loss factor occurs at the same value of β_{o1}, no matter the value of the material loss factor. It has already been stated that the frequency factor can be regarded as characterising the state of shear deformation in the beam. The above observation, therefore, implies that, for any given thickness ratio, there is a unique state of shear at which the maximum damping

obtainable with that configuration, occurs; and that this state is unaffected by the material loss factor. It is also seen that the curves for various values of η_1 do not intersect each other, which implies that, judged on the basis of equal stiffness (i.e. β_{o1}), a beam with a higher material loss factor, η_1, will also necessarily have a higher beam loss factor, η_{o1}. These facts would not have been very obvious from fig. 6.1 - a justification for including β_{o1} as a design parameter.

Curves similar to those given in figs 6.1 and 6.2 can be obtained for various values of the thickness ratio, H. This has, in fact, been done for three other thickness ratios: H = 0.1, 1.0, and 2.0, as shown in figs 6.3 to 6.8. From these graphs, it is possible to plot the maximised beam loss factor, $\eta_{o1\,opt}$, against the thickness ratio, H, for various values of the material loss factor, η_1. Such a graph is shown in fig. 6.9. The graph shows that the maximum beam loss factor increases as the thickness ratio increases, a trend which has already been anticipated. Also shown in fig. 6.9 is the variation of the shear parameter, $\gamma_{1\,opt}$, and the frequency factor, $\beta_{o1\,opt}$, corresponding to the maximum beam loss factor, with the thickness ratio. Both quantities are seen to decrease with increase in H.

The maximum beam loss factor is also plotted against the material loss factor, η_1, for various values of H, in

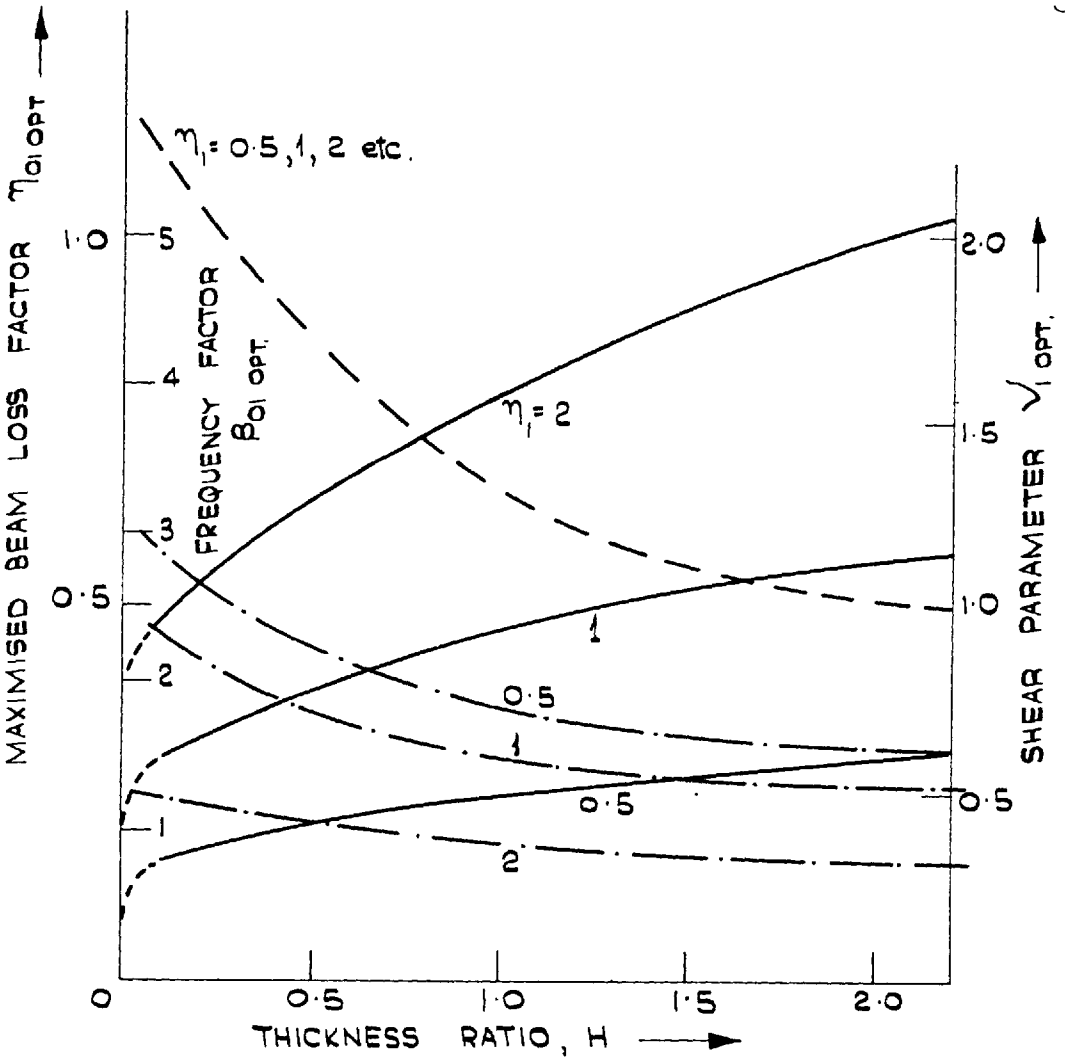

FIG. 6.9. THREE-LAYER BEAM. MAXIMISED BEAM LOSS FACTOR, $\eta_{01\,OPT}$; CORRESPONDING SHEAR PARAMETER $V_{1\,OPT}$. AND FREQUENCY FACTOR $\beta_{01\,OPT}$ AGAINST THICKNESS RATIO H.

—— $\eta_{01\,OPT}$

– – – $\beta_{01\,OPT}$

—·— $V_{1\,OPT}$.

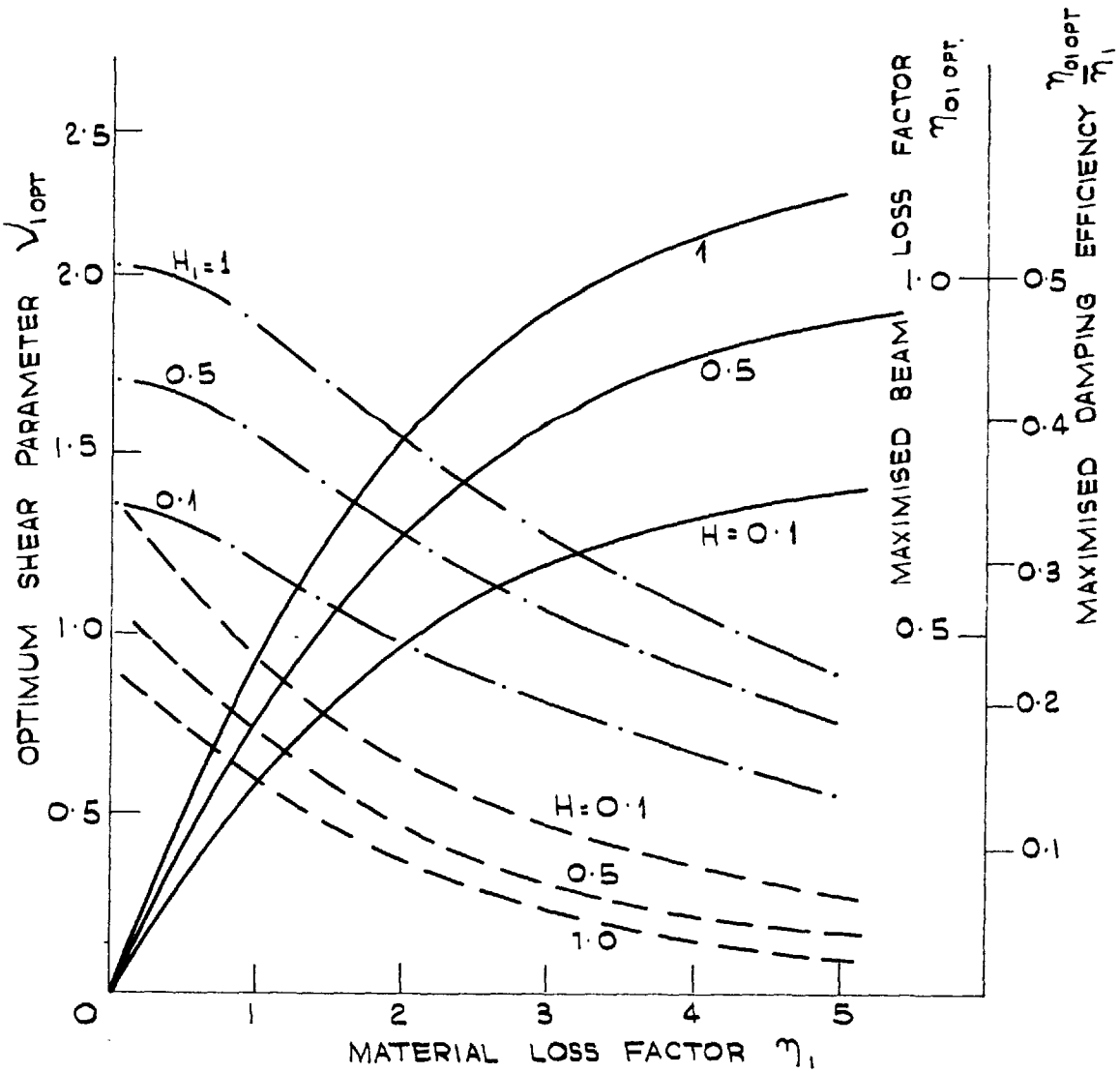

FIG. 6.10. THREE-LAYER BEAM. MAXIMISED BEAM LOSS FACTOR $\eta_{01\,OPT}$, DAMPING EFFICIENCY $\frac{\eta_{01\,OPT}}{\eta_1}$, AND CORRESPONDING SHEAR PARAMETER $\nu_{1\,OPT}$ AGAINST THE MATERIAL LOSS FACTOR.

——— $\eta_{01\,OPT}$ MAXIMISED BEAM LOSS FACTOR.

– – – $\nu_{1\,OPT}$. CORRESPONDING SHEAR PARAMETER.

·——· $\frac{\eta_{01\,OPT}}{\eta_1}$ MAXIMISED DAMPING EFFICIENCY.

fig. 6.10. The figure also contains curves showing the variation of the maximised damping efficiency, $\frac{\eta_{01opt}}{\eta_1}$, and the shear parameter, ν_{1opt}, at maximum loss factor, with η_1. As the material loss factor increases from zero, the beam loss factor also increases. An interesting feature of the curves is that whilst the maximum beam loss factor increases with the material loss factor, the maximised damping efficiency shows an opposite trend. Thus, although more damping is obtained with a higher material loss factor, better use is, in fact, made of the material loss factor at its smaller rather than its higher values; in other words, the law of diminishing returns holds. The maximised damping efficiency curves tend towards finite values at $\eta_1 = 0$, for each thickness ratio. These limits are difficult to establish for the general case; but their presence implies that the maximum efficiency obtainable with a given damping treatment is limited by the beam geometry. The greater the value of H,(i.e. the thicker the damping layer compared with metal layers), the greater is the damping efficiency obtainable.

The shear parameter at maximum beam loss factor is seen to decrease as η_1 increases, as was predicted earlier in section 6.1.c.

6.2.b Investigation of the higher modes

Graphs similar to those given in section 6.2.a for the first mode, can also be obtained for the higher modes. The natural question to ask is: is there any simple relation between them? To investigate this, it is noted that two of the parameters, namely, β_{on} and γ_1, contain the beam length, ℓ. It seems logical, therefore, to attempt to replace this with a 'characteristic' length for each mode, and to examine whether the resulting parameters uniquely determine the system resonant response.

One method of approach immediately suggests itself. For the n-th mode, $\beta_{on} = \frac{m\omega_{on}^2 \ell^4}{EI}$ (from equations 4.1.xvi), where ω_{on} is the n-th mode resonant frequency. This can be written in the form, $\frac{m\omega_{on}^2}{EI}\left(\frac{\ell}{\beta_{on}^{1/4}}\right)^4 = 1$ ..... 6.2.i; from which it can be seen that it is possible to define a "characteristic length", ℓ_c, for each mode, such that the frequency factor is the same at all modes. This characteristic length is thus given by $\ell_c = \frac{\ell}{\beta_{on}^{1/4}}$ ..... 6.2.ii. If ℓ_c is used, instead of ℓ, in the definition of the shear parameter, a "characteristic shear parameter", $\gamma_c = \frac{\gamma_1}{\beta_{on}^{1/2}}$ .....6.2.iii, results. The beam loss factor, η_{on}, can now be expressed as a function of γ_c (instead of γ_1), H and η_1. Is this relation independent of the mode? In other words, for fixed values of H, and η_1, is there a unique relationship between η_{on} and γ_c ?

For a beam whose absolute displacement and shear deformation amplitudes are sinusoidally distributed along its length at the resonant frequency, it can be shown (see Appendix III) that the beam loss factor as defined here is, in fact, a unique function of the characteristic shear parameter, γ_c. This is in agreement with the analysis of Kerwin et al [41,44,47] **, and of Mead [62,63].

This is, however, not so for the general case. Fig. 6.11 for instance, shows the beam loss factor for the first three modes, plotted against γ_c; η_1 and H being kept constant at 0.5. The graphs are for a cantilever beam subjected to displacement forcing at the root. A similar set of graphs is also given in fig. 6.12 for the first two modes, H, and η_1 being held constant at 0.5 and 2.0 respectively. It is seen that these curves do not overlap; and that the maximum beam loss factor is slightly different for each mode. In other words, the beam loss factor is not a unique function of the characteristic shear parameter, γ_c, in this case.

The reason for this is not difficult to appreciate. The beam loss factor as defined, depends on the mode shape of the beam at resonance. For a cantilever beam, and indeed for most other damped beams, the mode shapes, especially at the lower modes, are distinctly dissimilar. It is, therefore, not easy to choose a characteristic

**See foot note next page (i.e. page 332)

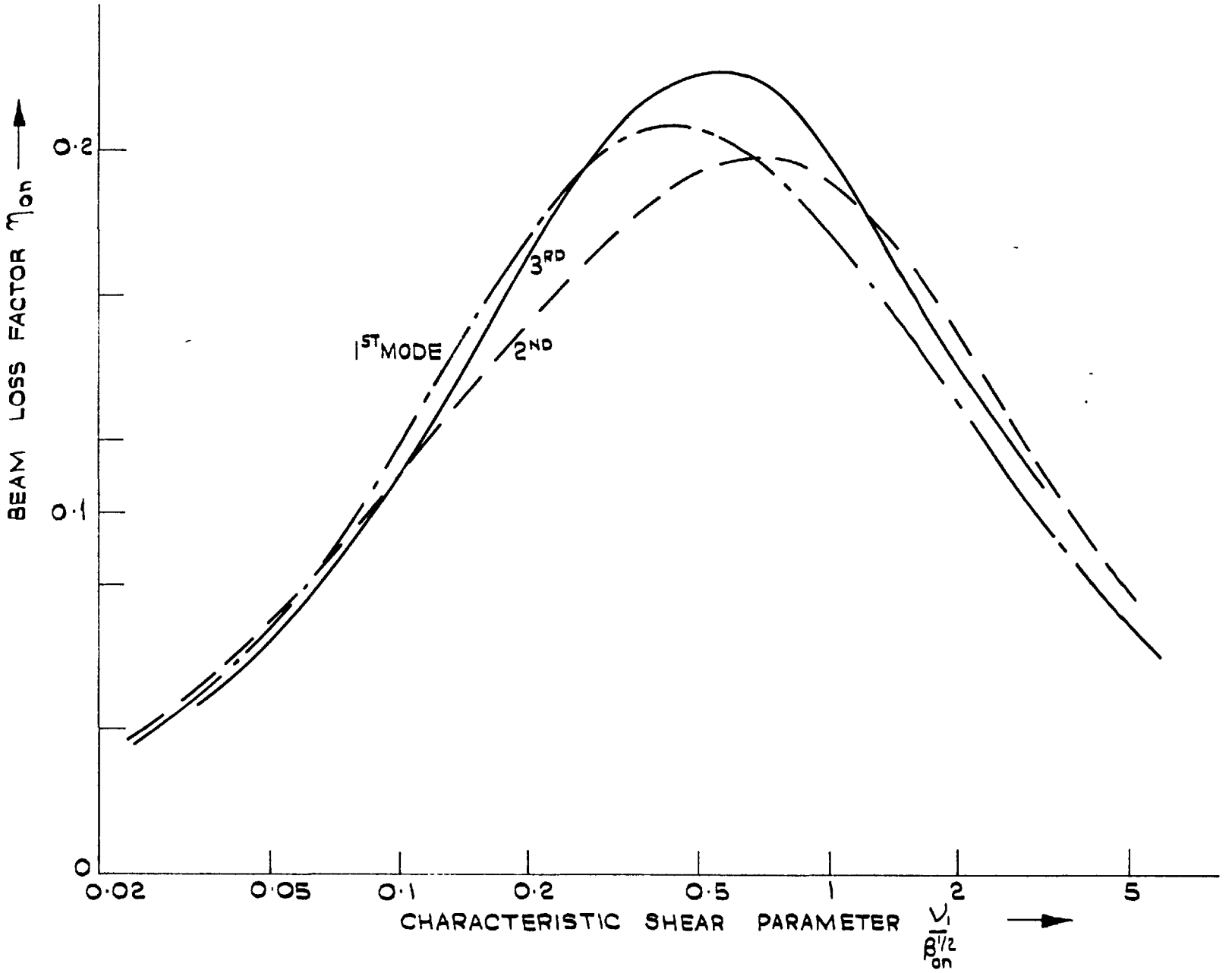

FIG. 6.11. THREE-LAYER BEAM : VARIATION OF BEAM LOSS FACTOR η_{on} WITH THE CHARACTERISTIC SHEAR PARAMETER $\frac{\nu_1}{\beta_{on}^{1/2}}$ FOR THREE MODES. THICKNESS RATIO H = 0·5 . MATERIAL LOSS FACTOR $\eta_1 = 0.5$.

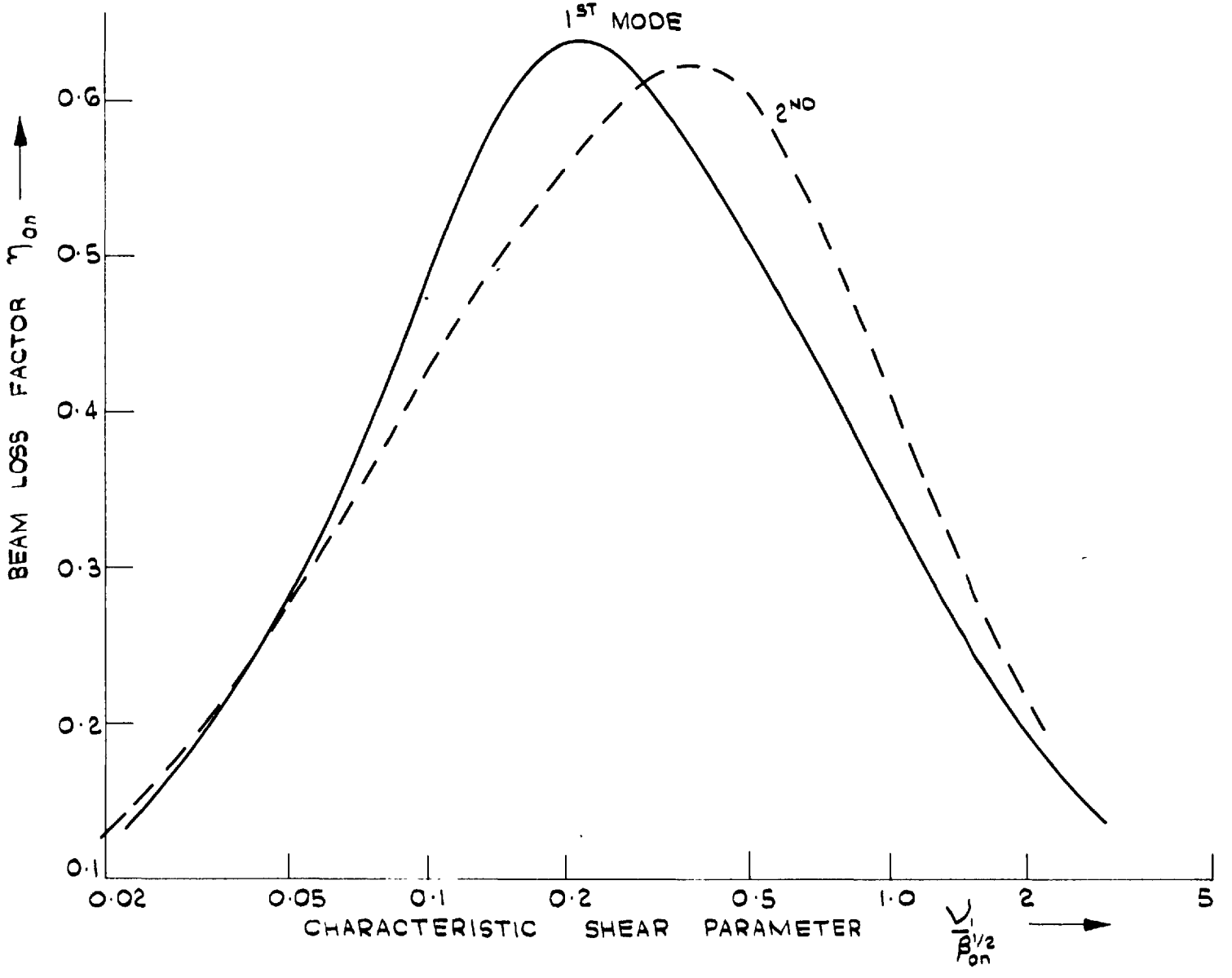

FIG. G.12. THREE-LAYER BEAM. VARIATION OF BEAM LOSS FACTOR η_{on} WITH THE CHARACTERISTIC SHEAR PARAMETER, $\frac{\nu_1}{\beta_{on}^{1/2}}$, FOR THE 1ST TWO MODES. THICKNESS RATIO $H = 0{\cdot}5$ MATERIAL LOSS FACTOR $\eta_1 = 2$.

length which will be a true reflection of the beam shape for all modes. The characteristic length is defined here from consideration of the resonant frequency factor. It will thus not necessarily be truly "characteristic" of the mode shapes. It would be truly characteristic in the special case mentioned earlier where the true mode shape of the beam was a number of identical sine waves. This is the basic assumption underlying the analysis of Ross, Ungar and Kerwin (and the "normal mode" approach of Mead), and hence explains why they obtain a unique damping relation for all the modes**. In this regard, it is clear that their analysis cannot be applied to the lower modes of cantilever beams with good accuracy.

Although the damping curves do not overlap, it is seen that for values of γ_c far from the peaks, they are fairly close to each other. The differences are more pronounced in the region of the peaks. For instance, from fig. 6.11, the maximum error in the damping, in assuming that the second mode curve is coincident with the first mode curve is about 16 per cent (at $\gamma_c = 0.3$). Similarly, for the third mode, the error is about 12 per cent (at $\gamma_c = 0.6$). Where a large error may result is in the

**The 'Kerwin shear parameter' (which is a half of the reciprocal of the 'Mead shear parameter' for a beam) is different from the characteristic shear parameter defined here. Both definitions are, however, simply related; and the above condition holds good in each case (see Appendix III).

exact location of the damping peaks. For instance, still referring to fig. 6.11, the assumption of coincidence of all the curves with that for the first mode, would lead to errors of about 80 and 25 per cent in the location of the second mode and third mode damping peaks respectively. Luckily, however, the damping curves (at any rate, for moderately low values of the material loss factor) have fairly broad peaks, so that a large error in the values of ν_c involves a much smaller error in the beam loss factor.

The near-equal values of η_{on} (at a given ν_c) for these modes permit some general observations to be made. For any given beam, $\nu_c (= \frac{\nu_1}{\beta_{on}^{1/2}})$ will normally decrease as the mode number increases. This is because $\beta_{on}^{1/2}$ is directly proportional to the resonant frequency; and although ν_1 may increase with frequency (owing to the frequency-dependence of the shear modulus, G_1') its rate of increase will usually not be as rapid. It follows that if a beam is designed so that, at the first mode, it is at the peak of the damping curve, then the higher modes will have progressively less damping than this mode, unless the material loss factor increases sufficiently rapidly with frequency to counter the effect of the decrease in ν_c. Similarly, if it is desired to design a beam so that the higher modes are highly damped, it would be necessary to

ensure that at the first mode, the shear parameter is much greater than that for maximum damping.

These observations are borne out by the experimental results presented in section 5.5 (chapter 5). Reference to table 5.c will show that beam 3, for instance, has at the first mode, a shear parameter of 2.09 which is much greater than the optimum (0.88). From the tip amplitude response curves for the beam (fig. 5.6a), it is clear that the higher modes (second and third, at any rate) are more damped. (The material loss factor for P.V.C. varies very little with frequency, - see the section on material properties, chapter 3 - , so that its dependence on frequency has negligible effect here). On the other hand, beam 4 has a shear parameter close to the value for maximum damping. From its resonance curves (fig. 5.9a), it is seen that the resonant tip amplitude ratios for the 2nd and 3rd modes are of the same order of magnitude, and not much different from that for the first mode, implying that these higher modes are progressively less damped.

Figs 6.13 and 6.14 show the resonant tip amplitude ratios (corresponding to figs 6.11 and 6.12 respectively) plotted against the characteristic shear parameter. As would perhaps be expected, the curves lie one above the other, in spite of the fact that the corresponding damping curves intersect. This is due to the fact, already mentioned, that

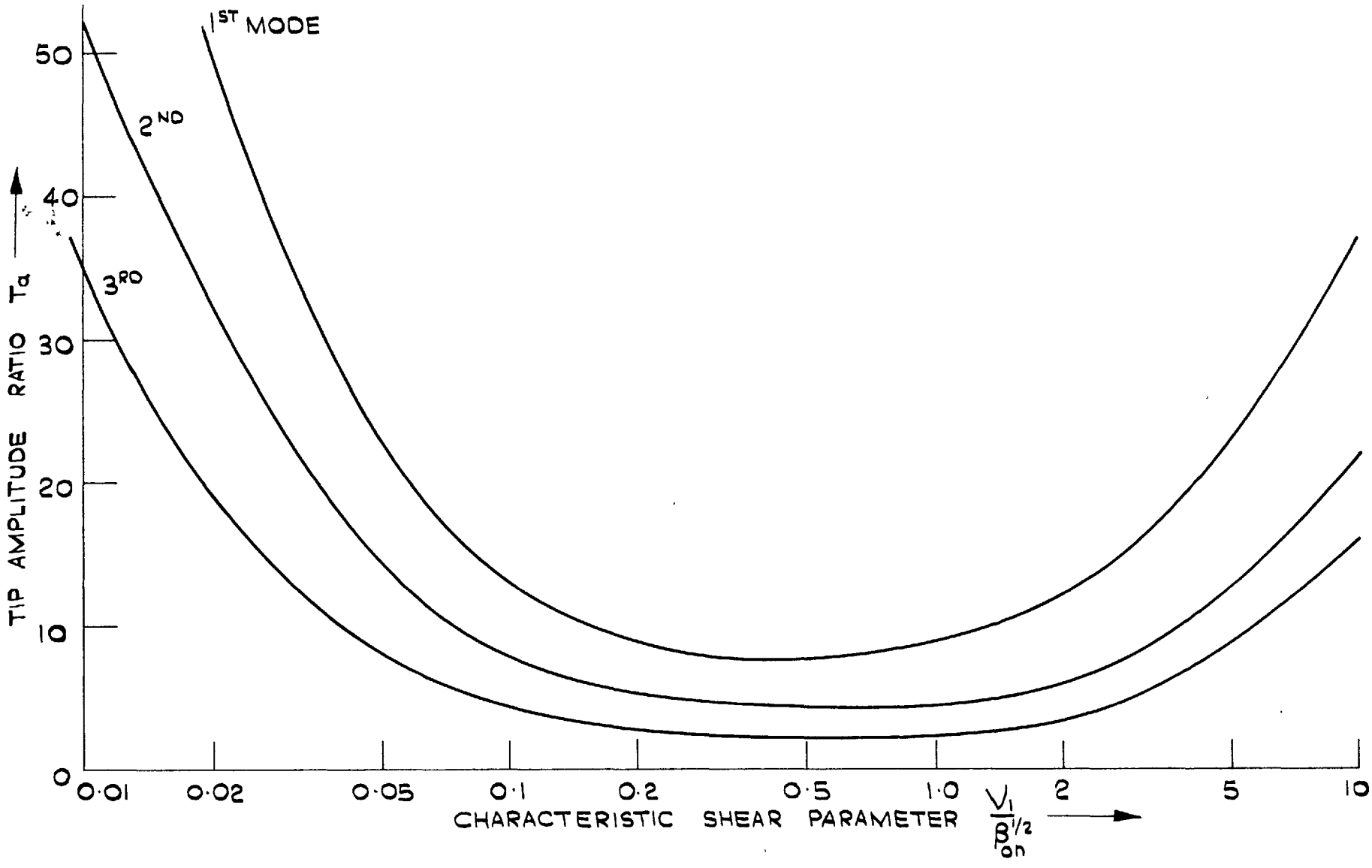

FIG. G.13. : THREE-LAYER BEAM : VARIATION OF TIP AMPLITUDE RATIO, T_a WITH THE CHARACTERISTIC SHEAR PARAMETER $\frac{V_1}{\beta_{on}^{1/2}}$ FOR THREE MODES.

MATERIAL LOSS FACTOR $\eta_1 = 0{\cdot}5$. THICKNESS RATIO $H = 0{\cdot}5$.

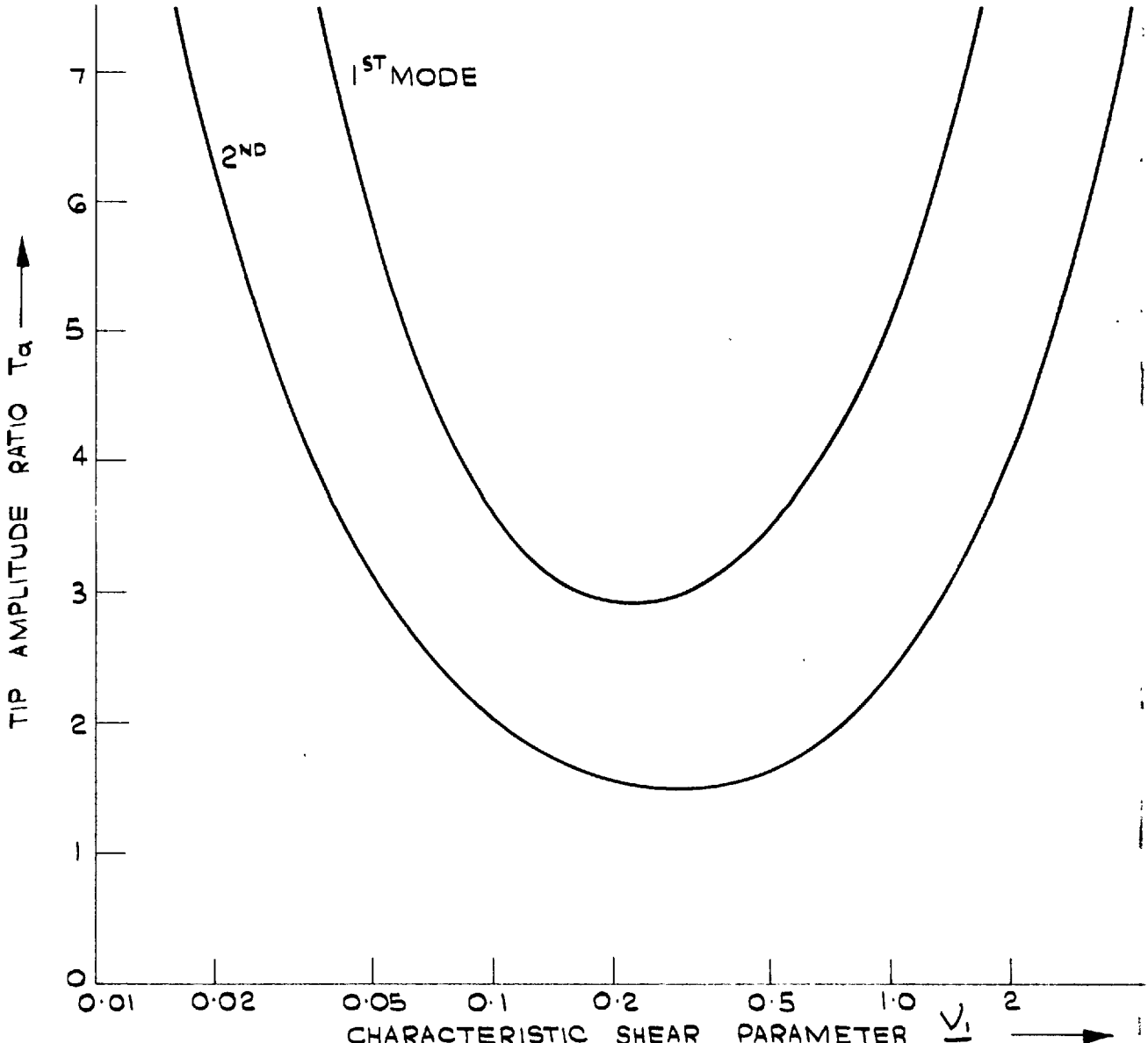

FIG. G. 14. THREE LAYER BEAM. VARIATION OF THE TIP AMPLITUDE RATIO, Ta WITH THE CHARACTERISTIC SHEAR PARAMETER, $\frac{V_1}{\beta_{on}^{1/2}}$, FOR 2 MODES.

THICKNESS RATIO H = 0·5.

MATERIAL LOSS FACTOR $\eta_1 = 2{\cdot}0$.

for any given beam loss factor, the tip amplitude ratio becomes less as the mode number increases.

6.2.c. Application of the graphs

There are many ways in which the optimisation curves of the last section can be applied. An obvious one is in the design of beams to satisfy some damping and stiffness requirements. The problem can take several forms, such as:
(a) the choice of a suitable geometry, for given material properties;
(b) the choice of a suitable material, for a given geometry;
(c) the choice of both material and geometry, but with some restriction on, say, weight, length, etc.
The procedure adopted in most cases is usually straightforward. Besides, this aspect of the design study has received fairly wide treatment from previous investigators (e.g. Kerwin et al [47] and Mead [62]). It will, therefore, not be dealt with in detail here.

One point, however, needs some mention. If the viscoelastic material properties are frequency-dependent (as they invariably are), a "trial and error" procedure has to be adopted if the resonant frequency is not initially specified. To illustrate how this can be done, consider the following problem: The cross-sectional dimensions and the material properties of a three-layer beam are given; and it is further specified that the beam loss

factor at the n-th mode should not be less than a prescribed value. It is desired to find a suitable length, and the corresponding resonant frequency.

The problem can be tackled in the following manner. Choose a trial value for the resonant frequency, and from the information on the viscoelastic material properties given, obtain the corresponding shear modulus, G_1', and the material loss factor, η_1. Use this value of η_1, and the given thickness ratio of the beam, as well as the optimisation curves for the n-th mode (assumed available), to determine the shear parameter, ν_1, and the frequency factor, β_{on}, corresponding to the given value of the beam loss factor. From this shear parameter, ν_1, and the above shear modulus, G_1', calculate the corresponding length of the beam. Use this length and β_{on} to calculate the corresponding resonant frequency, ω_{on}. If this is different from that assumed initially, use it as a better approximation and repeat the process until an initially assumed frequency and the calculated one are approximately the same. Convergence will usually be rapid since the variation of the material properties with frequency is normally slow.

The optimisation graphs can also be employed in the estimation of the viscoelastic material properties. All that is necessary is that the geometry of the system, the resonant frequency, and the tip amplitude ratio be known.

The last two can be determined very readily by testing a given length of the beam as a cantilever beam subjected to displacement forcing at the root. Suppose, for instance, that such a test on a three-layer beam, of thickness ratio H = 0.5, gave an amplitude ratio of 13.0 and a first mode resonant frequency such that $\beta_{o1} = 2.02$. Then, to determine the properties, it is only necessary to find, from the graphs for H = 0.5, (fig. 6.1) the loss factor, η_1, and the shear parameter corresponding to the given amplitude ratio and frequency factor. This is readily done by interpolation, as illustrated below.

As a first trial value, take a material loss factor, $\eta_1 = 0.5$. From the β_{o1}-versus-ν_1 curve corresponding to it, it is seen that when $\beta_{o1} = 2.02$, $\nu_1 = 0.15$. Also from the tip amplitude ratio curve, when $T_a = 13$, $\nu_1 = 0.12$. The difference between these two values of ν_1 is 0.03. Next, take a material loss factor, $\eta_1 = 1.0$. From its β_{o1} curve, when $\beta_{o1} = 2.02$, $\nu_1 = 0.09$; and from its T_a curve, when $T_a = 13$, $\nu_1 = 0.058$; giving a difference of -0.032 between the two values of ν_1. Interpolation between the two differences gives $\eta_1 \doteq 0.75$. It is, in fact, seen that $\eta_1 = 0.75$ and $\beta_{o1} = 2.02$ gives $T_a = 13$ and also $\nu_1 = 0.1$. Since the beam dimensions and other material properties are known, the shear modulus, G_1', can be calculated from ν_1. The shear modulus and the loss

factor of the viscoelastic material at the given resonant frequency are thus known.

It may be remarked that the best portion of the curves for this purpose is the region immediately before the peaks of the damping curves. At very high values of γ, the curves begin to intersect, and interpolation becomes rather difficult. In an actual practical case, it would be necessary to start off with a fairly long beam to locate the working position on the curves. The beam can then be shortened appropriately to get it to the region where interpolation is best. Moreover, frequency-dependence can be examined by suitably choosing thickness ratios, and then shortening the beam lengths progressively.

The obvious disadvantage in using this as a method of determining the material properties is that it does not take account of strain effects. It is thus not suitable for the accurate determination of the material properties of viscoelastic materials with very pronounced strain-dependence. On the other hand, it has the advantage that it can be used to determine the properties of viscoelastic materials as bonded, so that the properties of the bonding agent are taken into account. This is particularly important if these material properties are to be later used in predicting a given response of the beam accurately. Besides, the set-up for the test is very simple and requires

very little instrumentation.

The above design study has yet another important application. This comes in the prescription of laws of frequency-dependence for viscoelastic materials, an essential prerequisite in the process of the "tailoring" of these materials. The basic philosophy recognises the fact that frequency-dependence is inherent in viscoelastic materials; and that it is possible to influence the nature of this dependence quite considerably by chemical and physical processes well under the command of physicists and chemists. It then sets out to examine whether it is indeed possible to put frequency-dependence to advantage, and if so, in what ways. Two examples will be considered, as an illustration of the approach.

Suppose it is required to design a three-layer beam of a given thickness ratio, H, mass per unit length, m, elastic layer thickness, h_2, and Young's modulus, E_2; such that the damping at any given mode is independent of the beam length. What law of frequency-dependence should the viscoelastic material have?

To start with, assume that the material loss factor is frequency-independent. Of the system parameters, only γ_1 and β_{on} contain the beam length, ℓ. From the optimisation curves for fixed values of H and η_1, it is seen that for any value of the shear parameter, γ_1, there is only one value of the beam loss factor, η_{on}. If the beam length, ℓ,

varies, γ_1 also varies being proportional to ℓ^2 ; and hence the beam loss factor, η_{on}, changes. If η_{on} is, therefore, to remain constant as ℓ varies, it follows that γ_1 must also remain fixed for all values of ℓ : which implies that $\ell^2 G_1'$ = constant .....6.2.iv, since E_2, H, h_2, are all constant. Again, for any γ_1, there is only one value of β_{on}, so that if γ_1 is to remain constant, β_{on} must also remain constant as ℓ varies, i.e. $\beta_{on} = \frac{m\omega_{on}^2 \ell^4}{EI}$ = constant, for all ℓ ; and since $\frac{EI}{m}$ is constant, it follows that $\omega_{on}^2 \ell^4$ = constant .....6.2.v. The variable, ℓ, can be eliminated from equations 6.2.iv and 6.2.v to give the condition $G_1' = K_g \omega_{on}$ .....6.2.vi, K_g being a constant. Hence, to achieve the desired condition, the shear modulus must be directly proportional to the frequency and the material loss factor has to be frequency-independent. For such a beam, the resonant frequency will be inversely proportional to the square of the length (equation 6.2.v) as in the case of a plain undamped beam.

As a second example,(example 2, for short), consider an even more practical problem. Suppose it is required to design a beam (of given dimensions and elastic layer properties) which is such that its beam loss factor is the same for all modes. What law of frequency-dependence should the viscoelastic properties obey?

Assume once more that the material loss factor does not vary with frequency. Then, the method for obtaining

the exact solution involves the following steps. For the given beam thickness ratio and the assumed material loss factor, obtain for each mode, the graphs of the beam loss factor, η_{on}, and the frequency factor, β_{on}, against the shear parameter, γ_1. For the given constant η_{on}, obtain from each set of curves the corresponding values of γ_1 and β_{on}. Using the given beam dimensions, calculate G_1' from γ_1, and ω_{on} from β_{on}. Do this for all the modes. A graph of G_1' against ω_{on} gives the required law.

It is, however, possible to obtain an approximate and simpler solution, by assuming that the curves of the beam loss factor against the characteristic shear parameter, γ_c, are the same for all the modes. It has already been shown that although this is not true, the error is not very appreciable. If this is done, then the only requirement for a constant beam loss factor for all modes is that $\gamma_c = \frac{\gamma_1}{\beta_{on}^{1/2}}$ = constant .....6.2.vii; and since, for a given beam, EI, m, ℓ, H and h_2 are constant, equation 6.2.vii reduces to $G_1' = K_w \omega_{on}$ .....6.2.viii. In other words, the in-phase shear modulus must be proportional to the resonant frequency, a condition which is definitely satisfied when the shear modulus, G_1', is directly proportional to the frequency.

It is thus seen that a three-layer beam whose viscoelastic layer has a shear modulus varying in direct

proportion with the frequency, will have, not only a 'modal' beam loss factor that is independent of the length, but also, for a given length, a beam loss factor that is approximately independent of the mode; provided the material loss factor, η_1, is constant with frequency. It is possible to think of similar problems, and to work out the laws to satisfy the design requirements; but the above cases serve to illustrate the method of approach.

In the two cases considered, it has been assumed that the material loss factor is frequency-independent. It has been mentioned earlier that the material loss factors for many viscoelastic materials vary only slightly with frequency. Such an effect would, therefore, only cause a slight variation in the design condition being sought. In any case, if it is required to take account of the frequency-dependence of the loss factor, this can be done using the optimisation curves. To obtain a unique solution, it would be necessary to first prescribe one of the following:

(a) the frequency-dependence of the loss factor, η_1,

(b) the frequency-dependence of the shear modulus, G_1';

(c) some relation between the shear modulus, G_1', and the material loss factor, η_1.

As an illustration of the method of approach, suppose that in example 2 considered earlier, instead of a

constant η_1, a relation between G_1' and η_1 is specified. Then the procedure for plotting the frequency-dependence curves is as follows: Choose a value of η_1, and calculate the corresponding G_1'. Go to the damping curve corresponding to this value of η_1 and the given thickness ratio. For the prescribed value of the beam loss factor, find the corresponding characteristic shear parameter, ν_c. Using the beam dimensions given, and the value of G_1' calculated above, calculate, from ν_c the corresponding frequency, ω_{on}. This is now the frequency corresponding to η_1 and G_1'. Choose another value of η_1 and repeat the process. Continue until enough points are obtained for plotting the G_1'-versus-ω and η_1-versus-ω curves.

6.2.d. Effect of the viscoelastic extensional terms

In the theoretical considerations leading to the establishment of the design parameters (section 6.1.a), it was assumed that the viscoelastic extensional terms made negligible contribution to the system response. If, for instance, this were not so, a variation in the shear parameter, ν_1, due to a change in the shear modulus, G_1', would also cause a change in all the other coefficients of the differential equations. The resonant response of the system would, therefore, depend not only on ν_1, H, and η_1, but also on $g_1 = G_1'/E_2$. Under what conditions, if any,

does the parameter, g_1, have appreciable effect on the system response?

To examine this, it is best to consider the worst possible case. It has been shown in section 4.2.f, that the extensional terms become relatively important at (a) large values of $\frac{G_1'}{E_2}$ (or $\frac{E_1'}{E_2}$); (b) large values of H; and (c) small values of ν_1 (short lengths of beam). The stiffest viscoelastic material reported in the literature has $\eta_1 E_1' = 5.8 \times 10^4$ lb/sq. in. [23,24]. Remembering that $E_1' = 3G_1'$, it follows that the value of $g_1 = 10^{-2}$ ($\eta_1 = 1$) can be regarded as a truly upper limit for practically all present day engineering materials. (For concrete, for instance, assuming a Young's modulus of 4×10^6 lb/sq. in., $g_1 \doteq 5 \times 10^{-3}$, for $\eta_1 = 1.0$). With this value of g_1, and the largest thickness ratio considered in the optimisation graphs, namely, H = 2; graphs of the various resonant responses can be obtained as in the previous section. This has been done for $\eta_1 = 1.0$. Table 6.a gives a comparison of these results with those obtained for $g_1 = 5 \times 10^{-4}$ (and the same values of H and η_1). The latter set is completely indistinguishable with the values for $g_1 = 2 \times 10^{-5}$, both of which were plotted together in all the graphs given in section 6.2.a. The percentage differences between the two sets of values for the beam loss factor, the frequency factor, and the tip amplitude ratio, are given underneath the figures

SHEAR PARAMETER	TIP AMPLITUDE RATIO, T_a		BEAM LOSS FACTOR, η_{o1}		FREQUENCY FACTOR, β_{o1}	
ν_1	$\frac{G_1'}{E_2} = 5\times10^{-4}$	$\frac{G_1'}{E_2} = 10^{-2}$	$\frac{G_1'}{E_2} = 5\times10^{-4}$	$\frac{G_1'}{E_2} = 10^{-2}$	$\frac{G_1'}{E_2} = 5\times10^{-4}$	$\frac{G_1'}{E_2} = 10^{-2}$
0.0125	13.94646	9.75394 (-30.0)	0.11083	0.13095 (18.15)	0.50204	0.53536 (6.63)
0.05	5.18416	4.80080 (-7.40)	0.30899	0.31897 (3.24)	0.69617	0.73172 (5.10)
0.1125	3.64992	3.54961 (-2.74)	0.45231	0.45713 (1.07)	1.01809	1.05271 (3.40)
0.2	3.18233	3.13393 (-1.52)	0.52367	0.52754 (0.74)	1.42354	1.45660 (2.32)
0.45	2.93506	2.91946 (-0.53)	0.55968	0.56344 (0.67)	2.35927	2.40092 (1.77)
0.8	2.96541	2.96989 (0.15)	0.55272	0.55385 (0.20)	3.38904	3.42905 (1.18)
1.25	3.15489	3.16721 (0.39)	0.52640	0.52544 (-0.18)	4.44238	4.48055 (0.86)
3.2	4.40132	4.40818 (0.18)	0.38874	0.38810 (-0.16)	7.13138	7.18575 (0.06)

TABLE 6.a

Three-layer beam: Solutions showing the effect of the viscoelastic extensional terms. H = 2.0 , η_1 = 1.0

for $g_1 = 10^{-2}$.

It is seen from the tables that the values agree closely except for very small values of the shear parameter, ν_1; that is, for short beams. The peaks of the damping curves occur at the same value of the shear parameter, and agreement is best in this region for the damping and the tip amplitude responses. Thus, even for this extreme case, the error involved in ignoring the effect of the viscoelastic extensional terms is seen to be small for most of the range of values of ν_1.

It is even more revealing to consider a specific example. Assume that the beam overall thickness is 0.6 in., and that the beam is being designed to have the maximum damping for H = 2 and $\eta_1 = 1.0$. If the metal layers are made of aluminium ($E_2 = 10^7$ lb/in^2.), then for $g_1 = 10^{-2}$, the beam length would have to be 1.34 in.. If steel had been used instead, the length would be 2.3 in.. Such a beam would be too short to be of any practical use. Besides, for such short lengths, some of the assumptions of the theory (e.g. no shear deformation in the elastic layers etc.) would no longer hold (see limitations of the theory, section 7.1). This illustration emphasises the truly limiting nature of the assumed value of g_1, and the close agreement between the values obtained for this value of g_1,

and those for lower values, confirms that extensional effects can, in most practical cases, be ignored.

6.3. Five-layer beam: Effect of the distribution of the elastic layers on the stiffness and damping response — constant viscoelastic-layer to elastic-layer thickness ratio.

The relevant parameters in the study of the resonant responses of five-layer beams have been obtained in section 6.1.a and b as H_1, H_2, e_1, η_2, ν_2, and β_{on} for systems with constant modified forcing function. The effect of these parameters can be studied in the same way as for the three-layer beam. Thus, by keeping H_1, H_2 and e_1 constant, it is possible to obtain, for various values of the material loss factor, η_2, the familiar curves of the beam loss factor and the frequency factor against the shear parameter ν_2. Then, by varying each of the quantities H_1, H_2 and e_1 in turn, and repeating the process each time, a whole family of graphs can be obtained, as in the three-layer case.

In the present work, however, it is intended to investigate only an aspect of these graphs; one which has an important place in the design application of multi-layer beams. It is best presented as a problem. For a given ratio of $\frac{\text{total viscoelastic layer thickness}}{\text{total elastic layer thickness}}$, how does the distribution of the elastic layers affect the system stiffness and damping?

The significance of this problem can be illustrated with the following example. Suppose it is intended to make a damped symmetrical sandwich structure out of two available layers of viscoelastic material (of equal thickness), and some elastic material, available in any desired thickness. The structure is to have a fixed overall thickness. Two methods of approach can be adopted. A three-layer beam can be constructed, by bonding the two viscoelastic layers together, and using this as the central layer, the thickness of the elastic facing layers being so chosen as to give the desired overall thickness. Alternatively, a five-layer beam can be made. A problem immediately arises as to how the elastic layers have to be distributed. The central layer could be made relatively thick, with the facing layers extremely thin; or vice versa. Or, the three elastic layers could be made of equal thickness. What should guide one in deciding how these layers should be distributed? The present study is aimed at illustrating how such a problem can be tackled.

Suppose the given thickness ratio of $\frac{\text{total viscoelastic layer thickness}}{\text{total elastic layer thickness}}$ is k_T. It follows, therefore, that $\frac{2h_2}{2h_3 + h_1} = k_T$; or $2H_2 = k_T(2 + H_1)$ ...6.3.i. H_2, is thus expressible as a function of H_1, and is known when H_1 is known. Also, since the facing layers and the central layer are of the same material, $e_1 = 1$. The

independent variables now reduce to three, namely, η_2 , H_1 , and ν_2 , similar to the three-layer case. The computational procedure thus involves varying H_1 in steps; and at each step, obtaining the beam loss factor and the frequency factor-versus-shear parameter curves.

Such a set of graphs is given in fig. 6.15 for a thickness ratio $k_T = \frac{1}{2}$, and a material loss factor, $\eta_2 = 1.0$. The graphs are for a cantilever beam subjected to displacement forcing at the root and vibrating in the first mode. Fig. 6.16 also gives the variation of the beam loss factor with the frequency factor.

Fig. 6.15 shows that as the thickness ratio, H_1 , is gradually increased from zero (i.e. the three-layer case), the beam loss factor, for any given value of the shear parameter, increases; while the frequency factor, β_{o_1}, decreases. A maximum value is soon reached for the damping response, at a thickness ratio of around 1.0, beyond which value the damping decreases with increase in H_1 . The frequency factor also shows a turning point - a minimum - at about $H_1 = 1.0$, and thence increases as H_1 increases.

This variation is brought out more clearly by fig. 6.17, which shows the variation of the maximum beam loss factor, and the corresponding frequency factor and shear parameter with the thickness ratio, H_1 . Some important features of these graphs need mention.

(1) The graph of the maximised beam loss factor against

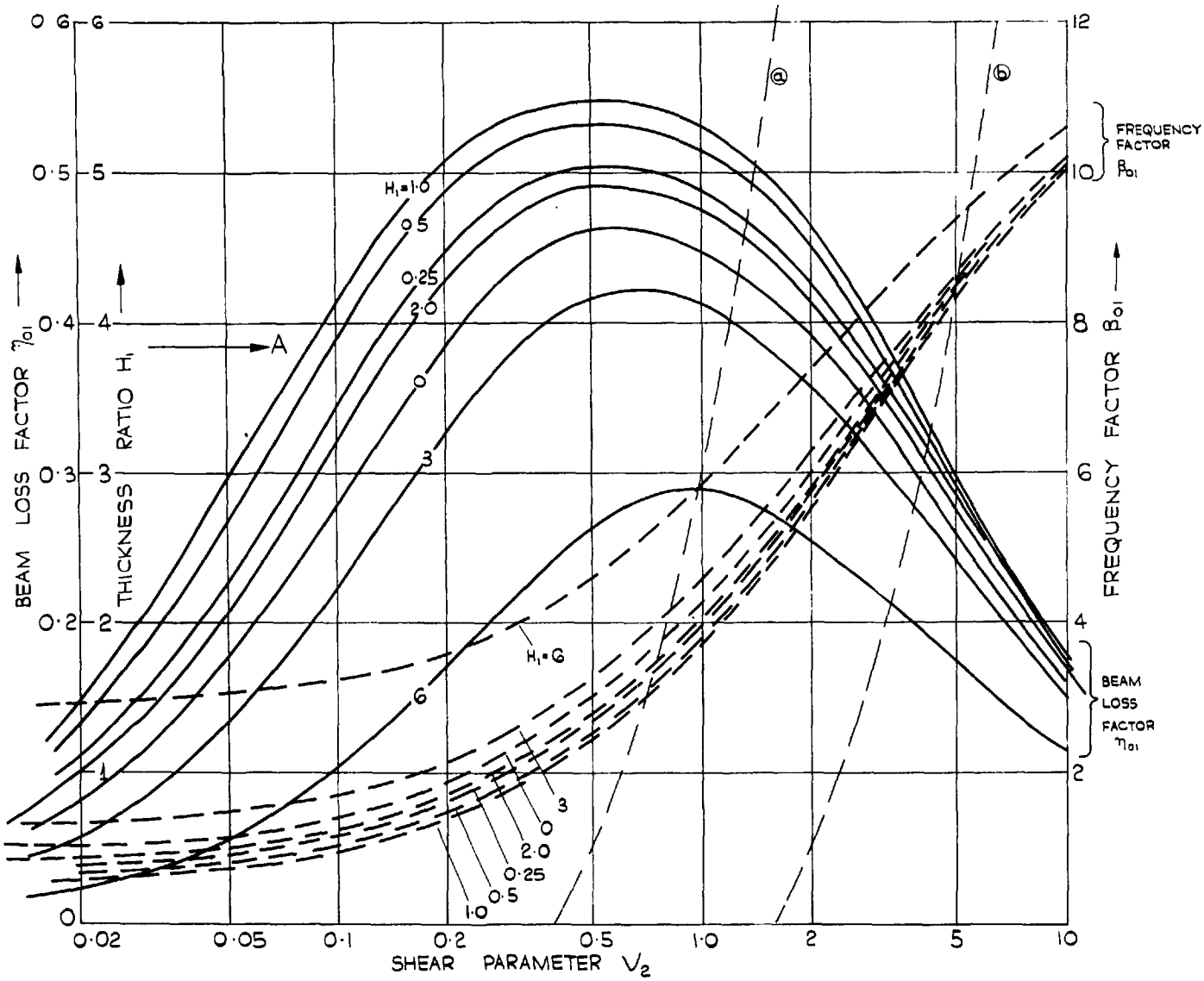

FIG 6.15 FIVE LAYER BEAM: BEAM LOSS FACTOR η_{01}, AND FREQUENCY FACTOR β_{01} AGAINST SHEAR PARAMETER V_2. MATERIAL LOSS FACTOR $\eta_2 = 1.0$

$\frac{\text{TOTAL VISCOELASTIC THICKNESS}}{\text{TOTAL ELASTIC THICKNESS}} = \frac{1}{2}$

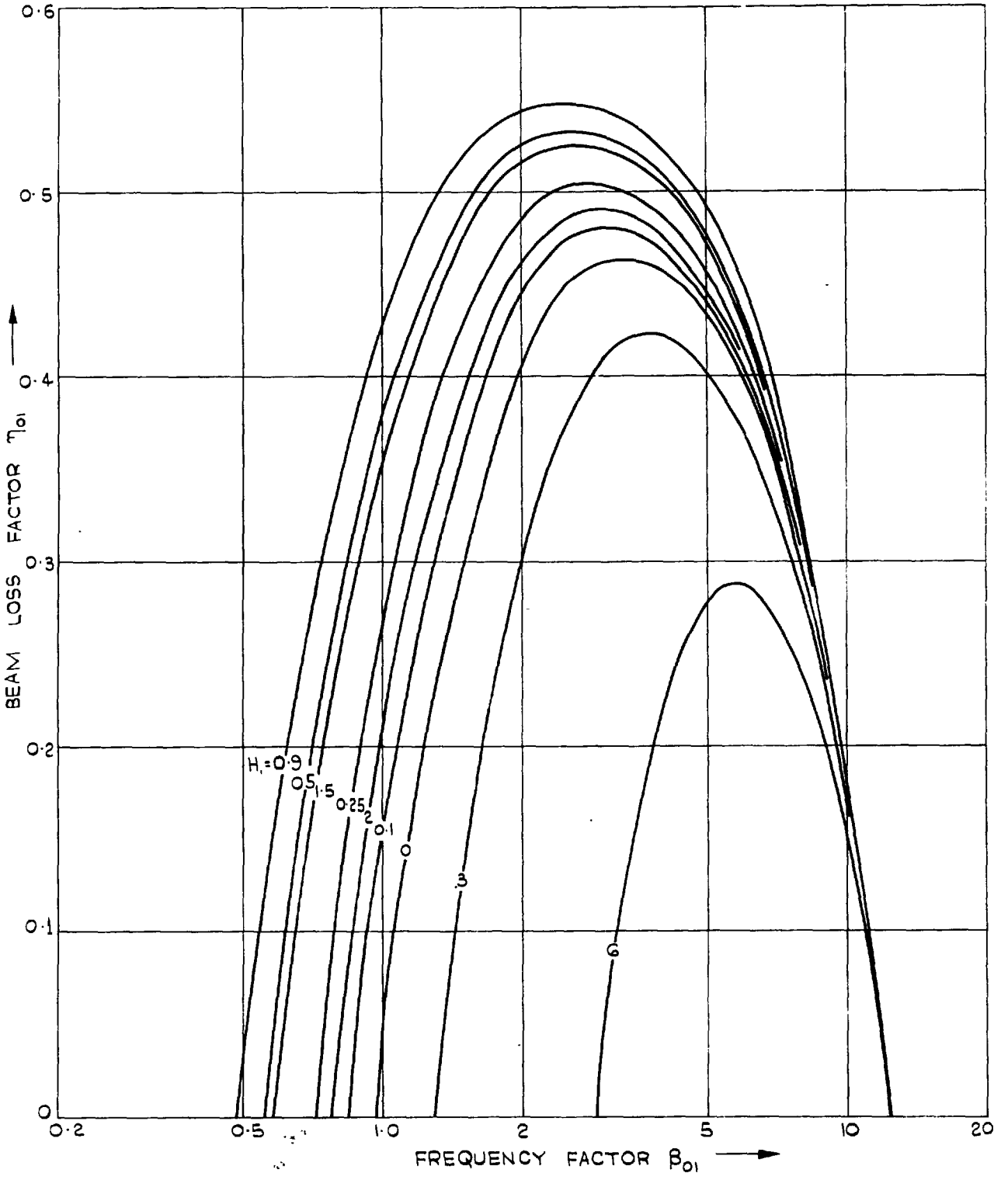

FIG 6.16. FIVE LAYER BEAM: BEAM LOSS FACTOR η_{01} AGAINST FREQUENCY FACTOR β_{01} FOR MATERIAL LOSS FACTOR $\eta_2 = 1{\cdot}0$

$\frac{\text{TOTAL VISCOELASTIC LAYER THICKNESS}}{\text{TOTAL ELASTIC LAYER THICKNESS}} = \frac{1}{2}$.

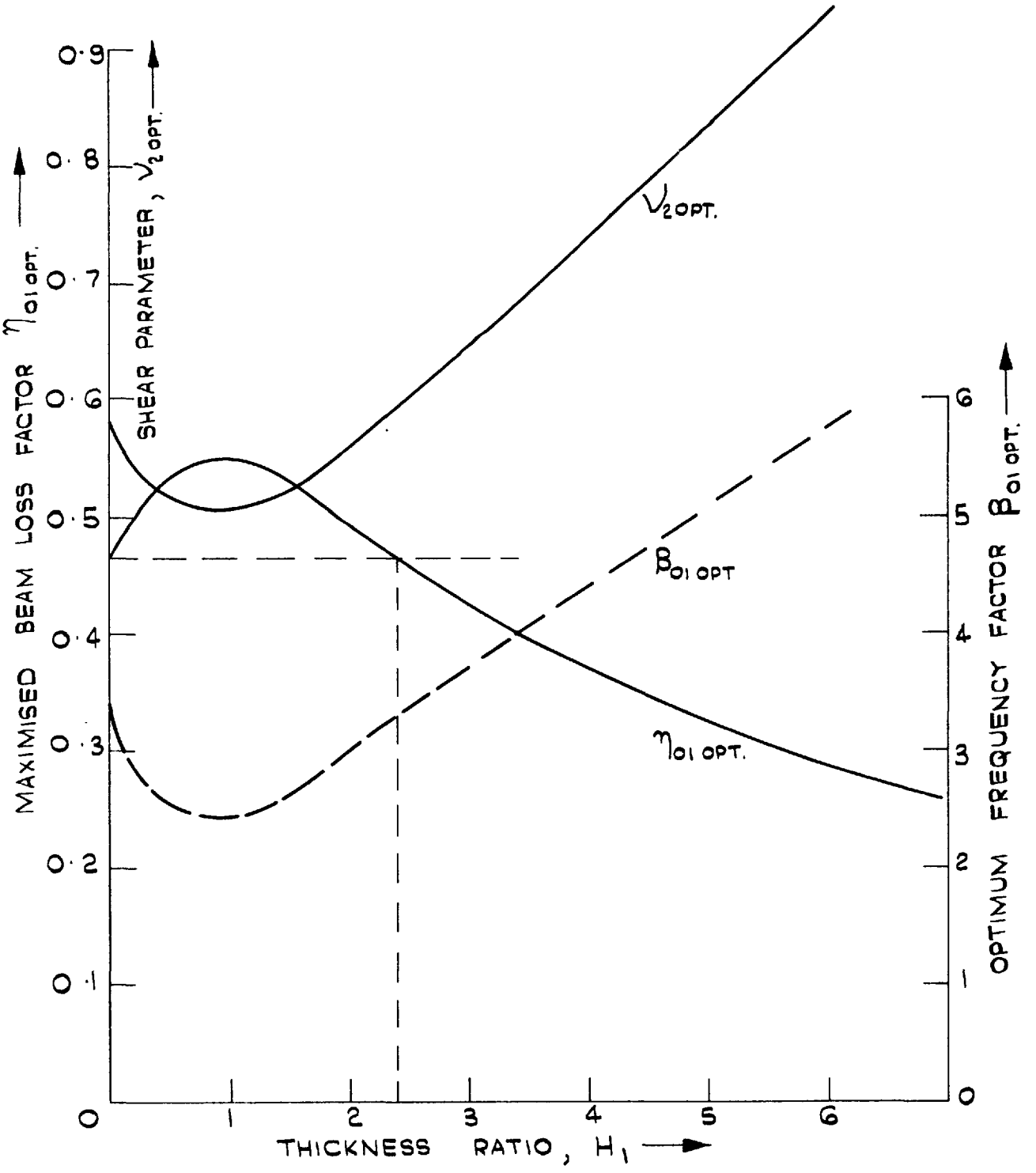

FIG. 6.17. FIVE LAYER BEAM : MAXIMISED BEAM LOSS FACTOR, $\eta_{01\,OPT.}$; CORRESPONDING FREQUENCY PARAMETER, $\beta_{01\,OPT.}$ AND SHEAR PARAMETER, $\nu_{2\,OPT}$ AGAINST METAL THICKNESS RATIO, H_1. MATERIAL LOSS FACTOR $\eta_2 = 1{\cdot}0$.

H_1 shows a maximum at about $H_1 = 1.0$ (in fact, $H_1 = 0.95$ from the graph). This maximum value, 0.55, represents the largest possible beam loss factor obtainable from a five-layer beam with $k_T = \frac{1}{2}$ ($\eta_2 = e_1 = 1.0$). It is seen that this corresponds to a configuration in which the elastic layers are of about equal thickness.

(2) As H_1 is increased beyond 1.0, the damping decreases and becomes equal to that of a three-layer beam (of the same thickness ratio, k_T) at a value of $H_1 = 2.4$. Beyond this value, the five-layer configuration gives less maximum beam loss factor than the corresponding three-layer beam.

(3) As the maximised beam loss factor increases to a maximum, the corresponding frequency factor, $\beta_{o_1 opt}$, decreases to a minimum at the same value of H_1. As H_1 is further increased, $\beta_{o_1 opt}$ now increases, reaching the value for the corresponding three-layer beam at the same value of $H_1 = 2.4$. Thus, it may be said, of the behaviour of $\eta_{o_1 opt}$ and $\beta_{o_1 opt}$, that "what is gained in damping is lost in stiffness, and vice versa".

(4) From the graphs of figs 6.16 and 6.17, it is seen that for any given beam loss factor, the frequency factor for the five-layer configuration is greater than, equal to, or less than that for the corresponding three-layer configuration, according as H_1 is greater than, equal to, or less

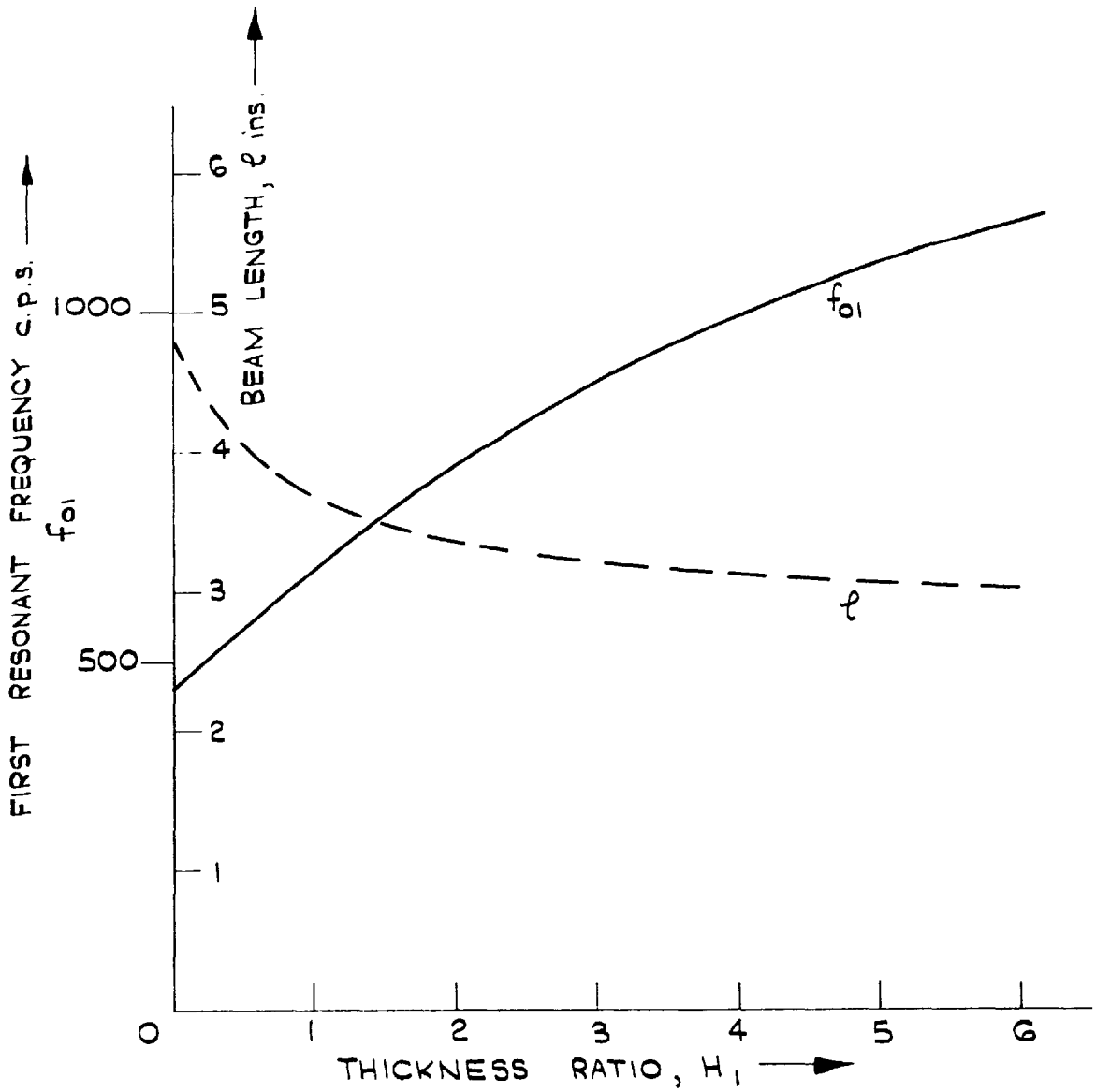

FIG. 6.18. FIVE LAYER BEAM: 1ST RESONANT FREQUENCY, f_{01}; AND BEAM LENGTH, ℓ ins. AT MAXIMUM BEAM LOSS FACTOR AGAINST THICKNESS RATIO, H_1.

[$E_3 = 10^7$ lb/in^2, $G'_2 = 5000$ lb/in^2, $\rho_3 = 0{\cdot}1$ lb/in^3, $\rho_2 = 0{\cdot}05$ lb/in^3

TOTAL METAL THICKNESS = TWICE TOTAL VISCOELASTIC LAYER THICKNESS = 0·4"]

than 2.4. This is true for all values of the beam loss factor attainable using both configurations. A similar statement can also be made about the beam loss factor. Thus, for any given frequency factor obtainable using both configurations, the five-layer beam will yield a beam loss factor which is greater than, equal to, or less than that of the corresponding three-layer beam, according as H_1 is less than, equal to, or greater than 2.4.

(5) The shear parameter at the maximum beam loss factor varies in much the same way as the corresponding frequency factor, showing a minimum at the same value of H_1.

It must be emphasised that a high value of the frequency factor, β_{01}, does not necessarily imply a high resonant frequency. Fig. 6.18, for instance, shows graphs of the resonant frequency and beam length at the maximum beam loss factor, plotted against H_1, assuming a constant in-phase shear modulus of 5,000 lb/in^2., as well as $E_3 = 10^7$ lb/in^2., $\rho_3 = 0.1$ lb/in^3., $\rho_2 = 0.05$ lb/in^3., and total metal thickness = 0.5 in. ($k_T = \frac{1}{2}$). It is seen that, although from fig. 6.17 the β_{01opt} curve has a minimum value, the corresponding resonant frequency increases with H_1, since the beam length, ℓ, decreases with increase in H_1.

The optimisation curves obtained above can now be employed in answering questions such as this: For any

given length of beam, and material properties, what thickness ratio gives the best damping performance? Assume that the shear modulus G_2' is frequency-independent. Then, if the total viscoelastic layer thickness is k_V, then the total elastic layer thickness is $\frac{k_V}{k_T}$; and it is easily shown from the expression for the shear parameter, γ_2, (equation 4.7.ix.f), that $\gamma_2 = \frac{2\ell^2 G_2' k_T}{E_3 k_V}(2 + H_1)$, extensional viscoelastic terms being neglected. This gives $\gamma_2 = C_L(2 + H_1)$ ..... 6.3.ii, where C_L is some constant, known for the given system. Thus γ_2 and H_1 are linearly related. For each H_1, the corresponding γ_2 can be calculated, and with this, the corresponding η_{o1} and β_{o1} can be obtained from the curves.

More conveniently, the graph of H_1 against γ_2 can be plotted on the same sheet as the optimisation curves, the axis of H_1 being vertical. Two such graphs, (a) and (b), are shown in fig. 6.15. (a) is for a length of 4 in., while (b) is for an 8-inch length. The shear modulus is assumed to be 5,000 lb/in^2. in each case. The other material properties, and beam dimensions are taken as $E_3 = 10^7$ lb/in^2. , $\rho_3 = 0.1$ lb/in^3., $\rho_2 = 0.05$ lb/in^3., total metal thickness = 0.4 in..

To illustrate how to obtain the desired values from these graphs, consider the beam of length, 4 inches. Take any value of H_1 . The corresponding value of γ_2 is

obtained by moving horizontally across (along that value of H_1) until curve (a) is reached. Move vertically along this value of ν_2, and read off the values of η_{o1} and β_{o1} corresponding to the chosen value of H_1. The resonant frequency is calculated from β_{o1} using the beam dimensions. Repeat this procedure until the desired range of values of H_1 has been covered.

It is seen from the graphs, and from the above procedure, that for values of H_1 between 0 and 6, the values for the beam loss factor and the frequency factor for ℓ = 4 in. lie in the portion of the curves between ν_2 = 0.4 and 1.6; while for ℓ = 8 in., they lie in the region between ν_2 = 1.6 and 6.4. It will thus be obvious that the variation of the damping and the frequency with H_1 in each case would depend on the regions where the curves of H_1-versus-ν_2 cut the damping and frequency factor curves. For instance, fig. 6.19 gives the beam loss factor and frequency curves for (a) and (b). The two sets of curves are by no means similar. Thus, while the natural frequency curve for ℓ = 4 in. shows a marked variation with H_1, the corresponding curve for ℓ =8 in. is almost insensitive to H_1. This is because curve (b) cuts the graphs at the portion where the β_{o1} curves are crowded together. Also the damping curve for ℓ = 4 in. has a peak close to H_1 = 1.0, while for ℓ = 8 in., the peak occurs at a lower

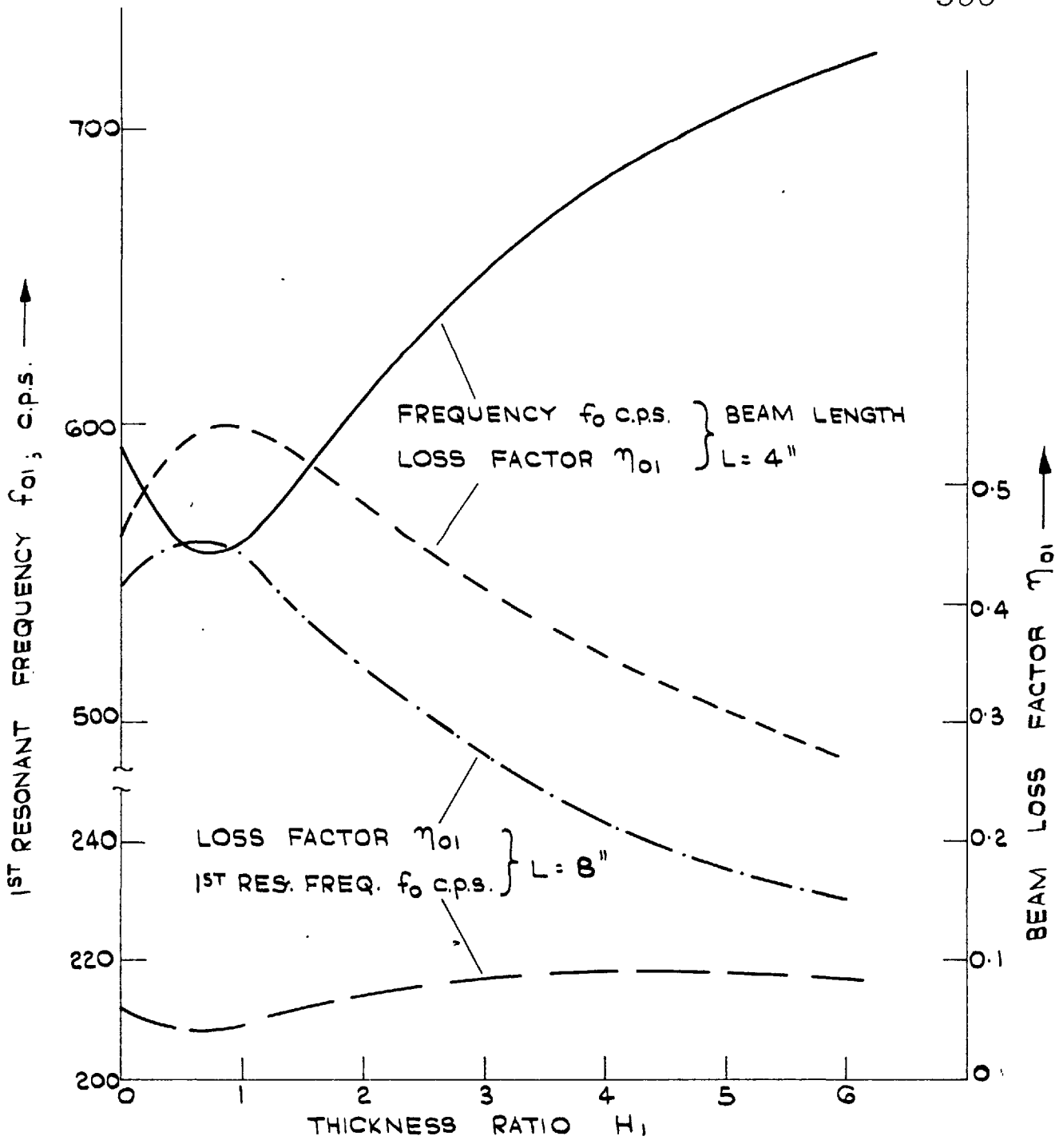

FIG. G.19. FIVE-LAYER BEAM : VARIATION OF BEAM LOSS FACTOR AND RESONANT FREQUENCY WITH METAL THICKNESS RATIO H_1, FOR GIVEN LENGTHS OF BEAM

$$\frac{\text{VISCOELASTIC LAYER THICKNESS}}{\text{TOTAL METAL THICKNESS.}} = \frac{1}{2}$$

MATERIAL LOSS FACTOR $\eta_2 = 1{\cdot}0$

value of $H_1(0.7)$.

From equations 6.3.ii, and a careful study of the graphs of fig. 6.15, it will be seen that the frequency and damping curves (plotted against H_1) for any given length of beam, will take the same form of variation as the maximised beam loss factor and the corresponding frequency factor curves of fig. 6.17, if the H_1-versus-ν_2 curve intersects the graphs in regions where the separation between the η_{o1} or β_{o1} curves is such that

$$\frac{\nu_{H_1''}(Z_1)}{\nu_{H_1'}(Z_1)} > \frac{2 + H_1''}{2 + H_1'} \quad \ldots\ldots\ldots 6.3.iii.$$

In equation 6.3.iii, $\nu_{H_1''}(Z_1)\{\text{or } \nu_{H_1'}(Z_1)\}$ designates the shear parameter corresponding to any value $Z = Z_1$, on the Z-versus-ν_2 curve for any $H_1 = H_1''\{\text{or } H_1'\}$. Z, here, stands for either η_{o1} or β_{o1}. Also, it is assumed that the Z-versus-ν_2 curve corresponding to $H_1 = H_1'$, occurs before that for $H_1 = H_1''$, as one moves across the graphs (within the region of intersection), in the direction of ν_2 increasing. This direction is indicated by the arrow head A in fig. 6.15.

6.4. Relation between the beam loss factor and the tip amplitude ratio.

In section 4.6.b, the beam loss factor was defined as an energy ratio. The definition was, however, related to a given response - the tip displacement amplitude response - since the frequency at which this loss factor

was determined corresponded to the maximum tip displacement amplitude. It is thus natural to ask: Is this loss factor a true reflection of the tip displacement amplitude response? In other words, for any given mode, is there a unique relationship between them, in the sense that to any beam loss factor, there corresponds one and only one tip amplitude ratio, no matter the beam geometry?

It is perhaps easy to see that such a unique relation is unlikely , as the beam loss factor depends, not only on the displacement amplitudes, but also on their phase relations, and , in fact, on the actual beam mode shape, which, in turn, depends on the beam geometry. But how far off is it?

Fig. 6.20 gives a graph of the beam loss factor for the first mode, plotted against the tip amplitude ratio at resonance. Points for this graph were indiscriminately taken from the responses of three-layer and five-layer beams of differing geometry. Although only a few points are shown for clarity, many more points had been plotted, and the scatter in the points were the same. It is seen from the graph that for beam loss factors of up to 0.2, the points lie practically on a smooth curve. Beyond this value, slight discrepancies occur between points from the various configurations. The close agreement of the points is, however, remarkable, and except for extremely accurate

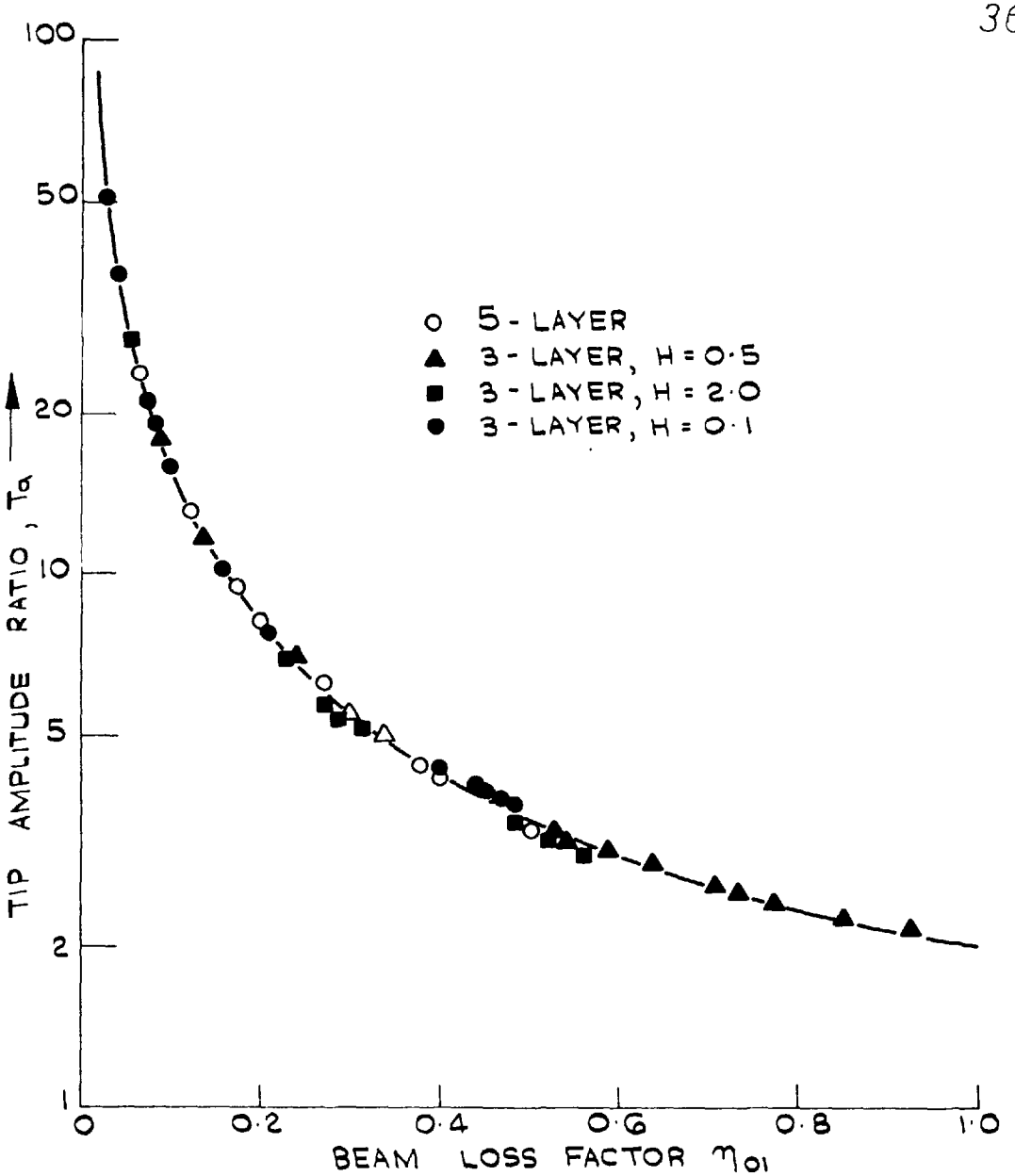

FIG. 6.20. BEAM LOSS FACTOR η_{01} AGAINST TIP AMPLITUDE RATIO T_a FOR 3-LAYER AND 5-LAYER BEAMS.

work, the beam loss factor can be regarded as uniquely related to the tip displacement amplitude ratio.

An important significance of this is that if it is required to design a cantilever beam to have a given resonant tip amplitude ratio when subjected to displacement forcing at the root, all that is necessary is to design the beam to have a given loss factor. The geometry or configuration chosen is rather unimportant.

6.5. Concluding remarks

In addition to the conclusions already arrived at in the various sections of this chapter, some general concluding remarks can be made.

(a) A clear understanding of the parameters essential in the design study of multi-layer beams is important for efficient design. This chapter has been aimed at showing how the effects of these parameters can be carefully and systematically investigated. Once they have been understood, the choice of materials and geometry becomes easy and straightforward.

(b) With careful choice of materials, and optimisation of the geometry, high beam loss factors can be readily achieved. For instance, from fig. 6.9, it is seen that for a three-layer cantilever beam with a viscoelastic layer having a material loss factor of 2, and only twice as thick as each of the elastic layers, it is possible

to obtain a beam loss factor of 1.0.

(c) Owing to the nature of the dependence of the beam loss factor on the shear parameter, it can be said that, as a general rule, stiff viscoelastic materials are suitable for short lengths of beam and for relatively stiff elastic layers, while soft viscoelastic materials are suited to long beams and to elastic layers with low Young's modulus.

(d) Temperature effects can be readily taken account of by careful design. For instance, suppose a three-layer cantilever beam of thickness ratio, H = 0.1, is designed to have a beam loss factor of 0.2 in its first mode; and that its viscoelastic layer has a material loss factor, of about 1.0, which either increases or remains constant with decrease in temperature. From fig. 6.3 it is seen that the minimum value of the shear parameter necessary is 0.24. If this value is used in carrying out this design in the summer, it is clear from the optimisation graphs that the shear parameter can increase to 4.0 during the winter, with the beam loss factor always being greater than , or at least equal to the prescribed value of 0.2. This implies a possible increase of the in-phase shear modulus to about 16 times its summer value. For evoseal, the most temperature sensitive viscoelastic material investigated in chapter 3, such an increase in the shear modulus would require a drop in temperature, from summer to winter, of 40°C - a more-than-

adequate allowance for a normal winter.

If a higher beam loss factor is desired for the same temperature drop, this can be readily achieved by using a higher thickness ratio, since, for any given material loss factor, the graph of the beam loss factor against the shear parameter becomes 'broader' as the thickness ratio increases. Thus, with a thickness ratio of 1.0, the beam loss factor could be kept to a minimum of 0.35, for the same material loss factor and the same temperature range as above. However, a higher thickness ratio implies a lower stiffness (i.e. frequency factor) for any given shear parameter; and in certain cases, it might be necessary to strike a compromise between the damping and stiffness requirements.

(e) Frequency-dependence can be utilised to advantage by seeking for laws of dependence that favour some desired responses. For instance, it has been shown that a three-layer beam with a viscoelastic layer the in-phase shear modulus of which is directly proportional to the frequency, will, for any given mode, have a beam loss factor independent of the beam length; and for any given length, the overall loss factor of such a beam will be approximately independent of the mode. This is true no matter the end conditions of the beam, provided the material loss factor exhibits negligible frequency-dependence.

It is useful to examine how the material properties

given in section 3.7 approximate this "straight line" law. Reference to the graphs will show that at room temperatures, and between 50 and 200 c.p.s., the deviation from the straight line law may vary within ±35 per cent for evoseal, and within ±45 per cent for P.V.C. Hycadamp shows a much less marked deviation within the frequency range, 200 to 400 c.p.s., and at room temperatures - the departure from the law being within ±5 per cent.

The above comparisons may not be very encouraging. However, the straight line law can certainly be a target at which chemists and physicists engaged in the tailoring of viscoelastic materials should aim.

(f) The optimisation curves can be employed in the determination of the viscoelastic material properties. The method, apart from its simpicity, has the particular advantage that the properties are determined under conditions of bonding, so that the properties of the bonding material are taken into account.

(g) For a given ratio of total viscoelastic layer thickness to total metal layer thickness, the five-layer configuration can yield more damping than the three-layer, provided that the correct geometry is used. Such an improvement in the damping may entail a loss in stiffness, depending entirely on the geometry and the material properties chosen.

C H A P T E R 7

CONCLUSION

Detailed conclusions on the experimental verification of the theory developed, and on the application of this theory in the design study of multi-layer beams are given in sections 5.6 (page 296) and 6.5 (page 364) respectively.

7.1. The theory, its scope and limitations

The differential equations developed in the general form in chapter 2, were solved and verified for beams with viscoelastic materials whose non-linear behaviour was such that it did not cause any appreciable deviation from the (linear) elliptical stress - strain law. However, the equations are equally applicable to systems with viscoelastic materials having any kind of non-linear stress - strain law. All that is necessary is that this law be prescribed in the general form given in equation 2.1.i (page 40). Once this is done, it is possible to seek a solution of the resulting non-linear equations by either numerical methods similar to those employed here or other standard methods (see for instance [126, 127]). Besides, the analysis can be extended to take account of the hysteresis damping in the elastic materials, by replacing the simple straight-line stress - strain law used here by the general stress - strain law of equation 2.1.i.

Some of the assumptions made in the development of the theory, however, impose some limitations to its range of applicability. For instance, shear deformation in the elastic layers was neglected in the analysis. This would become important for very short beams, and at the higher modes of vibration. Rotatory inertia effects, also ignored in the development of the theory, will be significant at the higher frequencies. Mead has shown [62] that for symmetrical three-layer plates (with a linear viscoelastic core), rotatory inertia effects may be neglected so long as $\omega^2 \ll \frac{2G_1'}{\rho_2 h_1 h_2}$ .....7.1.i, where ρ_2 ,and h_2 are the density and the thickness, respectively, of the facing layers; G_1' and h_1 are the shear modulus and the thickness, respectively, of the core; and ω is the forcing frequency.

It was also assumed that all the layers had the same vertical displacement, y, at each cross-section; in other words, that there was no thickness-wise deformation in the layers. The implication of this has already been stated in section 2.1. It is easy to see that this assumption neglects the necessary reduction in thickness which results when the viscoelastic layers are deformed in shear, and which imposes an additional vertical motion on the layers. This effect is bound to be more significant for very thick viscoelastic layers, and at very high forcing frequencies.

It follows, from the above discussion, that the present

theory can be classed as a 'low frequency' analysis of multi-layer beams.

7.2. Suggestions for further work

The analysis presented here opens a wide field of study in the dynamic response of symmetrical multi-layer beams. The design study introduced in chapter 6, clearly shows how much useful information can be gained by a systematic approach. This study should be extended to beams with more layers, to examine how the system responses are affected by the number of layers, the distribution of material within these layers, and their relative stiffnesses (i.e. the ratios of the Young's moduli of the elastic layers, or of the shear moduli of the viscoelastic layers). Also, the effects of boundary conditions on the beam responses should be investigated.

A detailed study of the effects of rotatory inertia in all the layers and of shear in the elastic layers, should be carried out with a view to establishing the errors incurred in neglecting these effects at the higher modes. This can be done by ascribing shear functions, ϕ_i, to the elastic layers (as for the viscoelastic layers), and by taking the lateral inertia terms into account in considering the longitudinal equilibrium of an element of the beam. It should be pointed out that the shear functions, ϕ_i, for the elastic layers may not be assumed constant across the

layer thickness (as in the case of the viscoelastic layers), unless a "shear correction factor" [56,128] is used. The assumption of a constant shear deformation across the layer thickness, is permissible (without any correction factor) for the viscoelastic layers , only because they are much softer in extension than the elastic layers which, as a result, provide most of the forces causing shear deformation.

The effects of the thickness-wise motions of the layers, resulting from the shear in the viscoelastic layers, should also be examined, by including the appropriate inertia terms in the equations.

Only systems subjected to harmonic excitation have been analysed in detail here. The present work can evidently be carried on to investigate the free and random vibrations of such systems.

The general unsymmetrical multi-layer beam should also be investigated. It was shown in section 2.2.d, that the analysis of such a beam by the method presented here, may prove extremely difficult owing to the variation of the neutral axis position with the applied load or deflection. However, it can be tackled by other methods. One such method is the use of the variational principles of mechanics [58,129,130]. This would involve assuming, for each layer, displacement functions which satisfy continuity requirements at the interfaces. The strains can then be obtained, and

from these the stresses, using general stress - strain laws similar to that of section 2.1. The equations of motion can now be obtained by applying the appropriate extremum principles.

A P P E N D I X II

TABLES GIVING THE INPUT MOTION AND THE TEST TEMPERATURES FOR THE BEAM TESTS

TABLE 5.d Input motion, a_o', and temperature (of the viscoelastic layers), T, for the resonance tests.

Beam no.		First mode	Second mode	Third mode
3	T, °C	27.0	27.5	27.2
	a_o', in.	0.00055	0.00055	0.00029
3A	T, °C	27.4	27.5	25.6
	a_o', in.	0.00038	0.00038	0.00016
3B	T, °C	26.6	27.3	—
	a_o', in.	0.00064	0.00030	
4	T, °C	23.5	26.0	26.0
	a_o', in.	0.00068	0.00048	0.00018
4A	T, °C	25.4	25.8	—
	a_o', in.	0.00060	0.00029	
5	T, °C	25.0	24.3	24.5
	a_o', in.	0.00069	0.00053	0.00040
5A	T, °C	24.1	21.4	—
	a_o', in.	0.00056	0.00044	
6	T, °C	24.4	23.6	—
	a_o', in.	0.00063	0.00039	
7	T, °C	22.6	24.6	25.8
	a_o', in.	0.00067	0.00054	0.00040
8	T, C	24.7	24.6	25.8
	a, in.	0.00064	0.00051	0.00027

TABLE 5.e Input motion amplitude, a'_o, and temperature (of the viscoelastic layers), T, for the "mode shape" tests.

Beam no.		First mode	Second mode	Third mode
3	T, °C	26.0	26.7	27.5
	a'_o, in.	0.00045	0.00034	0.00022
3A	T, °C	26.3	27.0	27.2
	a'_o, in.	0.00038	0.00038	0.00016
3B	T, °C	26.6	27.3	—
	a'_o, in.	0.00064	0.00030	
4	T, °C	23.5	25.1	25.3
	a'_o, in.	0.00067	0.00048	0.00017
4A	T, °C	26.4	26.7	—
	a'_o, in.	0.00062	0.00028	
5	T, °C	24.7	22.2	23.5
	a'_o, in.	0.00069	0.00054	0.00038
5A	T, °C	24.4	22.5	—
	a'_o, in.	0.00092	0.00044	
6	T, °C	26.0	24.0	—
	a'_o, in.	0.00060	0.00047	
7	T, °C	25.0	25.0	26.0
	a'_o, in.	0.00067	0.00054	0.00041
8	T, °C	24.0	24.8	25.7
	a'_o, in.	0.00064	0.00051	0.00027

A P P E N D I X III

THE RELATION BETWEEN THE BEAM LOSS FACTOR AND THE SHEAR PARAMETER FOR BEAMS WITH SINUSOIDAL MODE SHAPES

The analyses of Kerwin et al [41,44,47], and of Mead [62,63], show that for a beam having displacement and shear deformation amplitudes which are sinusoidally distributed along its length, the damping can be expressed as a unique function of a "shear parameter", for given values of H and η_1. Although their definition of the beam loss factor is different from the one given here (see section 4.6.b), it will now be shown that this condition is also true for the beam loss factor, η_{on}, as defined here. Also, it will soon be evident that the shear parameters defined by the above-mentioned investigators differ from the 'characteristic shear parameter' defined in section 6.2.b. It will, however, be shown that these parameters are all related, and that the beam loss factor, η_{on}, is a unique function of each of them.

For the given beam, the absolute displacement, y_a, and the shear deformation, ϕ_1, at any point can, for the n-th mode, be expressed as,

$$\left.\begin{aligned} y_a &= a_{1n} \sin k_n\xi \cos \omega t + a_{2n} \sin k_n\xi \sin \omega t \\ \phi_1 &= a_{3n} \cos k_n\xi \cos \omega t + a_{4n} \cos k_n\xi \sin \omega t \end{aligned}\right\} \quad \text{.....A3.i ,}$$

harmonic excitation being assumed. k_n^4 is the resonant frequency factor for a plain undamped beam with the same boundary conditions as the given beam. For instance, for a simply-supported beam, $k_n = n\pi$, $n = 1,2$, etc.

To excite the beam in the manner prescribed, the forcing function must have a predominant component of the form, $p_n \sin k_n\xi \cos \omega t$, at the n-th mode. Hence, on neglecting the viscoelastic extensional terms, the expressions for the coefficients, a_{1n}, a_{2n}, a_{3n}, and a_{4n} are obtained (by comparison with equations 4.4.vi) as,

$$a_{1n} = -\frac{p_n}{k_n^3}\left[\frac{(k_n^2 + \nu_1)\left\{\alpha_1\mu_1 k_n^3 - (k_n^2 + \nu_1)(k_n - \frac{\beta_1}{k_n^3})\right\} - \sigma_1^2(k_n - \frac{\beta_1}{k_n^3})}{D_n}\right]$$

$$a_{2n} = p_n\left[\frac{\alpha_1\mu_1\sigma_1}{D_n}\right]$$

$$a_{3n} = p_n\left[\frac{\mu_1\left\{\alpha_1\mu_1 k_n^3 - (k_n^2 + \nu_1)(k_n - \frac{\beta_1}{k_n^3})\right\}}{D_n}\right]$$

$$a_{4n} = -p_n\left[\frac{\mu_1\left\{\sigma_1(k_n - \frac{\beta_1}{k_n^3})\right\}}{D_n}\right] \qquad \text{.....A3.ii}$$

where,

$$D_n = \left\{\alpha_1\mu_1 k_n^3 - (k_n^2 + \nu_1)(k_n - \frac{\beta_1}{k_n^3})\right\}^2 + \left\{\sigma_1(k_n - \frac{\beta_1}{k_n^3})\right\}^2$$

Remembering that $\sigma_1 = \eta_1\nu_1$ (see equations 4.1.xviii), the expressions of equations A3.ii can be rewritten thus,

$$a_{1n} = -p_n k_n^2 \left[\frac{(1+\nu_k)\left\{\alpha_1\mu_1 - (1+\nu_k)(1-\frac{\beta_1}{k_n^4})\right\} - \eta_1^2\nu_k^2(1-\frac{\beta_1}{k_n^4})}{D_n} \right]$$

$$a_{2n} = p_n k_n^2 \left[\frac{\alpha_1\mu_1\eta_1\nu_k}{D_n} \right]$$

$$a_{3n} = p_n k_n^3 \frac{\mu_1\left\{\alpha_1\mu_1 - (1+\nu_k)(1-\frac{\beta_1}{k_n^4})\right\}}{D_n}$$

$$a_{4n} = -p_n k_n^3 \frac{\mu_1\eta_1\nu_k(1-\frac{\beta_1}{k_n^4})}{D_n}$$

and $$D_n = k_n^6 \left[\left\{\alpha_1\mu_1 - (1+\nu_k)(1-\frac{\beta_1}{k_n^4})\right\}^2 + \left\{\eta_1\nu_k(1-\frac{\beta_1}{k_n^4})\right\}^2 \right]$$

where $\nu_k = \frac{\nu_1}{k_n^2}$, is twice the shear parameter defined by Kerwin et al [41, 44, 47]*. α_1 and μ_1 are functions of the thickness ratio, H, only (since the viscoelastic extensional terms are being neglected); hence, the coefficients, a_{1n}; a_{2n}, etc. can be expressed in the forms,

$a_{1n} = W'_n \varsigma_1$; $a_{2n} = W'_n \varsigma_2$; $a_{3n} = W'_n k_n \varsigma_3$; and $a_{4n} = W'_n k_n \varsigma_4$ A3iii

where each of the ς_i is a function of the quantities, ν_k, $\frac{\beta_1}{k_n^4}$, η_1, and H; and is independent of the mode. On the other hand, W'_n which equals $\frac{p_n}{k_n^4}$, depends only on the mode.

Assume now that both η_1 and H are held constant.

*ν_k is also the reciprocal of the shear parameter as defined by Mead for the case of a simply supported beam [62,63].

The absolute displacement amplitude, y_a, at any point is given by $y_a = (a_{1n}^2 + a_{2n}^2)^{1/2} \sin k_n \xi$

$= W_n' \varsigma_5(\nu_k, \frac{\beta_1}{k_n^4}) \sin k_n \xi$, from equation A3.iii,

where ς_5 is a function of ν_k and $\frac{\beta_1}{k_n^4}$ only.

For any given mode, as the frequency varies, the displacement amplitude at any point becomes a maximum when $\varsigma_5'(\nu_k, \bar{\beta}) = 0$ .....A3.iv , where ς_5' is the first derivative of ς_5 with respect to $\frac{\beta_1}{k_n^4}$; and $\bar{\beta} = \frac{\beta_{0n}}{k_n^4}$, is the value of $\frac{\beta_1}{k_n^4}$ at the n-th mode resonant frequency. It follows from equation A3.iv that $\bar{\beta}$ is expressible, implicitly or explicitly, as a unique function of ν_k ; hence, on employing the functional notation defined in section 6.1.a it can be written as $\bar{\beta} = f_{\bar{\beta}}(\nu_k)$ .....A3.v.
It is important to note that this functional relation is <u>independent of the mode</u>.

The beam loss factor, η_{on}, is defined in section 4.6.b, at the n-th mode resonant frequency (i.e. when $\frac{\beta_1}{k_n^4} = \bar{\beta}$), by the relation,

$$\eta_{on} = \frac{D_1'}{\frac{1}{2}\left[A_1' + B_1' + \left\{(A_1' - B_1')^2 + 4C_1'^2\right\}^{1/2}\right]} \qquad \text{.....A3.vi,}$$

where A_1', B_1', C_1', and D_1' are as given in equations 4.6.ix.

Consider, for instance, A_1'. On substituting for the displacement and shear components, the following expression

results:

$$A_1' = \int_0^1 \left[k_n^4 a_{1n}^2 + 2\alpha_1 k_n^3 a_{1n} a_{3n} + \lambda_2 k_n^2 a_{3n}^2 + \lambda_1 a_{3n}^2 \right] \sin^2 k_n \xi \, d\xi$$

$$= \frac{1}{2}\left[k_n^4 a_{1n}^2 + 2\alpha_1 k_n^3 a_{1n} a_{3n} + \lambda_2 k_n^2 a_{3n}^2 + \lambda_1 a_{3n}^2 \right] \quad \text{....A3.vii.}$$

It is noted that λ_2 which, from equation 4.6.v, is given by $\lambda_2 = \frac{6H^2 + eH^3}{8 + 12H + 6H^2 + eH^3}$, is a function of H only, since the viscoelastic extensional terms are being neglected. However, $\lambda_1 = \frac{12 p_1^2 g_1 H}{8 + 12H + 6H^2 + eH^3}$, from equation 4.6.v;

$$= \left(\frac{8 p_1^2 g_1}{4H + eH^2} \right) \left(\frac{1}{k_n^2} \right) \left(\frac{1.5 H (4H + eH^2)}{8 + 12H + 6H^2 + eH^3} \right) k_n^2 .$$

But from equations 4.1.xviii, $\nu_1 = \frac{8 p_1^2 g_1}{4H + eH^2}$.

Hence, $\lambda_1 = \frac{\nu_1}{k_n^2} \left(\frac{1.5 H(4H + eH^2)}{8 + 12H + 6H^2 + eH^3} \right) k_n^2 = \nu_k f_\lambda(H) k_n^2$,

where $f_\lambda(H)$ is a function of H only (viscoelastic extensional terms being ignored). A_1' can now be put in the form,

$$A_1' = \frac{1}{2}(k_n a_{3n})^2 \left[\left(\frac{k_n a_{1n}}{a_{3n}} \right)^2 + 2\alpha_1 \left(\frac{k_n a_{1n}}{a_{3n}} \right) + \lambda_2 + \nu_k f_\lambda(H) \right] \quad \text{..A3.viii}$$

It follows from equation A3.viii, and from the expressions for the coefficients (equations A3.iii), that A_1' can be expressed as $A_1' = (k_n a_{3n})^2 \, \varphi_A(\nu_k, \bar{\beta})$, for fixed values of H and η_1; where φ_A is some function of ν_k and $\bar{\beta}$, this function being independent of the mode.

Proceeding in a similar manner, each of the other quantities, B_1', C_1', and D_1', can be expressed as the product

of $(k_n a_{3n})^2$ and some function of ν_k and $\bar{\beta}$. Since the expression for the beam loss factor, η_{on} (equation A3.vi), is a ratio of homogeneous functions of the quantities, A_i', B_i', C_i', and D_i', it follows that η_{on} can be expressed as a function of ν_k and $\bar{\beta}$, in the form,

$\eta_{on} = \varphi_\eta(\nu_k, \bar{\beta})$ .....A3.ix, where the functional relation φ_η is independent of the mode. But equation A3.v shows that there is a functional relation between $\bar{\beta}$ and ν_k, a relation which is also independent of the mode. It follows, therefore, that η_{on} is expressible as a function of ν_k. In other words, for fixed values of η_i and H, there exists, for all modes, a unique relation between the beam loss factor defined here, and the Kerwin shear parameter (and hence, the Mead shear parameter), for the beam considered.

It was mentioned earlier that ν_k is different from the characteristic shear parameter, ν_c. However, since $\nu_k = \frac{\nu_i}{k_n^2}$; and $\bar{\beta} = \frac{\beta_{on}}{k_n^4}$; it follows that ν_c, which equals $\frac{\nu_i}{\beta_{on}^{1/2}}$, is related to ν_k and $\bar{\beta}$ thus: $\nu_c = \frac{\nu_k}{\bar{\beta}^{1/2}}$ .....A3.x. It has already been shown that both η_{on} and $\bar{\beta}$ are unique functions of ν_k. It follows, therefore, that η_{on} is also a unique function of ν_c. In other words, the relation between the beam loss factor, η_{on}, and the characteristic shear parameter, ν_c, is also independent of the mode.

The above considerations show that the unique relationship (between the damping and the shear parameter) obtained by Kerwin et al, and by Mead, is not a peculiarity of their definitions of these quantities, but rather a consequence of the assumed distribution of the displacement and the shear deformation along the beam.

REFERENCES

1. Grootenhuis,P.

"Shock and Vibration Transmission"

Paper presented to INSULATION CONVENTION at Seymour Hall, LONDON W.1.1964

2. Ruzicka,J.E., Cavanaugh R.D.

"Vibration Isolation of non-rigid bodies"

Part 9 of "Mechanical impedance methods for mechanical vibrations" edited by Plunkett R., A.S.M.E., NEW YORK N.Y. 1958.

3. Ruzicka,J.E.,

"Damping structural resonances using viscoelastic shear damping mechanisms", Parts I and II.

Paper contributed by the MACHINE DESIGN division for presentation at the winter annual meeting, New York N.Y Nov. 27-Dec.22 1960 of the ASME.

4. Morrow,C.T.

"Techniques for design to shock and vibration conditions."

Journal Environmental Engineering Feb. 1959 3.

5. Marin,J., and Stulen,F.B.

"A new fatigue strength-damping criterion for the design of resonant members."

Journal of Applied Mechanics 12 ; Trans ASME 67 1947 A-209.

6. Podnieks E.R. and Lazan B.J.,
"Effect of material damping and stress distribution on the resonant fatigue strength of parts."
WADC TN 55-284 August 1955.

7. Marin J., and Sharma M.G.,
"Material Design for resonant members."
section 6 of "structural damping" edited by Ruzicka;
ASME., New York N.Y. 1959.

8. Pisarenko G.S.,
"Dissipation of Energy during mechanical vibration" I & II.
Akademiya Nauk Ukrainskoi S.S.R. 1962.
English translation by National Lending Library Boston Spa. Yorksnire 1964.

9. Pisarenko G.S.,
"Vibrations of elastic systems taking account of energy dissipation in the material."
Technical Documentary Report no WADD TR 60-582 Feb. 1962.

10. Kimball A.L., and Lovell D.E.,
"Internal friction in Solids."
Physical Review, 2nd series, 30; 1927 948.

11. Demer L.J.
Bibliography of the material damping field."
WADC TR 56-180 June 1956.

12 Forster F.
"Ein Neues Messverfahren Zur Bestimmung des Elästizats-

moduls und Der Dämpfung."
Zeitschrift Metallkunde 29, 1937 109.

13. Lazan B.J.,
"Effect of Damping constants and stress distribution on the resonance response of members."
Journal of Applied Mechanics 20; Trans ASME 75, 1953 201.

14. Lazan B.J.,
"Energy dissipation mechanisms in structures, with particular reference to material damping."
Section 1 of structural Damping "edited by Ruzicka,"
ASME New York N.Y. 1959.

15. Podnieks F.R., and Lazan B.J.,
"Analytical methods for determining specific damping energy considering stress distribution."
WADC TR 56-44 June 1957, ASTIA Document no. AD 130777.

16. Robertson J.M., and Yerziadis A.J.,
"Internal Friction in Engineering Materials."
Journal of Applied Mechanics 13; Trans ASME 68 1946 A173.

17. Frendenthal A.M.,
"The inelastic behaviour of Engineering Materials and structures."
John Wiley and Sons, Inc. New York N.Y. 1959, chapter 10.

18. Van Heydekampf G.S.
"Damping Capacity of materials."
Proceedings, ASTM 31, 1931 part 1 157.

19. Birchon D.
"High Damping Alloys for tne reduction of noise and vibration."
Engineering Materials and Design, Sept. and Oct. 1964.

20. Oberst, H.
"Ueber die Dämpfung der Biegeschwingungen dünner Bleche durch fest haftende Beläge."
Acustica 2, Akustische Beihefte No 4, 1952 181.

21. Oberst, H., and Becker G.W.
"Ueber die Dampfung der Biegeschwingungen dunner Bleche durch fest haftende Belage, II."
Acustica 4, 1954 433.

22. Oberst, H.
"Akustik und Kunststoffe."
Kunststoffe, 43 1953 446.

23. Oberst,H.
"Werkstoffe mit extrem hoher innerer Dämpfung."
Acustica 6 144.

24. Becker G.W., and Oberst, H.
"Ueber das dynamisch-elastische Verhalten linearer, vernetzter und gefüllter Kunststoffe."
Kolloid Zeitschrift, 148, 1956 6.

25. van Itterbeek A; and Myncke H.
"Vibration of plates covered with a damping layer."
Acustica 3, 1953 207.

26. Schwarzl, F.
"Forced bending and extensional vibrations of a two-layer compound linear viscoelastic beam."
Acustica 8, 1958 164.

27. Liernard, P.
"Etude dune Methode de Mesure du Frottement Interieur de Revetement Plastiques Travaillant en Flexion."
Recherche Aeronautique, 20, 1951 11.

28. Mead D.J.
"The effect of a damping compound on Jet-Efflux excited vibrations : Part 1, structural damping due to the compound."
Aircraft Engineering 32 no. 373 March 1960.

* 30. Mead, D.J.
An experimental investigation of the damping properties of Aquaplas under random and harmonic excitation."
University of Southampton, A.A.S.U. Report no. 173 June 1961.

31. Mead, D.J. and Pearce, T.G.
"The optimum use of unconstrained layer damping treatments."
University of Southampton A.A.S.U. Report no. 126 July 1961.

32. Hertelendy, P.
"Displacement and strain energy distribution in a longitudinally vibrating cylindrical rod with a viscoelastic coating."
Trans. ASME 84 E (Journal of Applied Mechanics) 1, Mar. 1962. 17.

* For reference 29, see pg 402

33. Henry, L.A. and Freudenthal, A.M.
"Forced Vibrations of a viscoelastic cylinder case-bonded to a thin elastic shell."
Columbia Univ. Dept of Civil Engineering and Engineering Mechanics TR no. 22 [contract NorR 266 (78)] Jan. 1964.

34. Morris, R.E.
"Rubber Materials for damping vibrations of metals structures."
Proceedings of the 6th Joint Army-Navy-Air force conference on Elastomer Research and Development.
(U.S. Quarter master Research and Engineering Command Boston Mass. 1960) 2, 443.

35. James, R.R.
"Progress Report no. 5:Development of Damping treatments for destroyer Hulls."
Mare Island Naval Shipyard Rubber Lab. Report no. 94-30,1961.

36. Ungar, E.E. and Kerwin, E.M. Jnr.
"Plate damping due to thickness deformations in attached viscoelastic layers."
Journal of the Acoustical Society of America 36, no. 2, 386. Feb. 1964.

37. Foss, J.I.
"For the space age, a bibliography of sandwich plates and shells."
Report SM-42883, Douglas Aircraft Co. Santa Monica California, 1962.

38. Habip, L.M.
"A survey of modern developments in the analysis of sandwich structures."
Applied Mechanics Review 18, no. 2, February 1965 98.

39, Henderson, J.P.
"Damping of Structures."
Machine Design 36, no. 18 July, 1964, 119.

40. Kerwin, E.M. Jnr, and Ross, D.
"A comparison of the effectiveness of homogenous layers and constrained layers of viscoelastic material in damping flexural waves in plates."
Paper presented to Third International Congress on Acoustics, Stuttgart, Germany 1959.

41. Kerwin, E.M. Jnr.
"Damping of flexural waves by a constrained viscoelastic layer."
Journal of the Acoustical Society of America 31, no.7 1959.

42. Kerwin, E.M. Jnr.
"Vibration damping of a constrained damping layer."
BBN Report no.547 29th April, 1958 (submitted to Convair, San Diego).

43. Kerwin, E.M. Jnr.
"Vibration damping by a stiffened damping layer."
Paper U-8, 55th Meeting of the Acoustical Society of America 10th May, 1958.

44. Ross, D., Kerwin, E.M. Jnr. and Dyer I.
"Flexural vibration damping of multiple-layer plates."
BBN Report no. 564, 26 June 1959 (submitted to the ONR mecnanics branch).

45. Ross, D., and Kerwin, E.M. Jnr.
"Damping of flexural vibrations in plates by free and constrained viscoelastic layers."
BBN Report no.632 May, 28, 1959 (submitted to U.S. Navy Bureau of snips).

46. Ungar, E.E.,and Ross, D.
"Damping of flexural vibrations by alternate viscoelastic and elastic layers."
Fourth Midwestern Conference on Fluid and Solid Mechanics, University of Texas, 1959.

47. Ross,D. Ungar, E.E., and Kerwin E.M. Jnr.
"Damping of plate flexural vibrations by means of viscoelastic laminae."
Section 3 of the Colloquium on "Structural Damping," edited by Ruzicka ASME. Dec. 1959.

48. Kerwin, E.M. Jnr.
"Ideal Spaced damping treatments for flexural waves."
Paper M10, Acoustical society of America May, 1959

49. Kerwin, E.M. Jnr.
"Damping of flexural waves in plates by spaced damping

treatments having spacers of finite stiffness."
Paper presented to the Third International Congress on Acoustics, Stuttgart, Germany, 1959.

50. Ungar, E.E, and Kerwin, E.M. Jnr.
"Loss factors of viscoelastic systems in terms of energy concepts."
Journal of the Acoustical Society of America 34, 954, July 1962.

51. Ungar, E.E.
"Loss factors of viscoelastically damped beam structures."
Journal of the Acoustical Society of America 34, no. 8. August, 1962, 1082.

52. Ungar, E.E.
"Damping tapes for vibration control."
Product Engineering 31, Jan. 25, 1961, 57.

53. Ungar, E.E.
"Highly damped structures."
Machine Design 35 no. 4 Feb. 14, 1963, 162.

54. Parfitt G.G., and Lambetn, D.
"Damping of structural vibrations."
Aeronautical Research Council Current Papers no. 596, 1962.

55. Yu, Y.Y.
"A new theory of elastic sandwich plates - one dimensional case."
Journal of Applied Mechanics 26 1959, 417.

56. Yu, Y.Y.
"Simple thickness-shear modes of vibration of infinite sandwich plates."
Journal of Applied Mechanics 26 1959 679.

57. Yu, Y.Y.
"Flexural vibration of elastic sandwich plates."
Journal of the Aerospace Sciences 27, no. 4, April 1960.

58. Yu, Y.Y.
"Simplified vibration analysis of elastic sandwich plates."
Journal of the Aerospace Sciences 27, no. 12, Dec. 1960.

59. Yu, Y.Y.
"Damping of flexural vibration of sandwich plates."
FJournal of the Aerospace Sciences 29, no. 7, July 1962.

60. Yu, Y.Y.
"Non-linear flexural vibrations of sandwich plates."
Journal of the Acoustical Society of America 34 1962 117.

61. Yu, Y.Y.
"Application of variational equations of motion to the non-linear vibration analysis of homogeneous and layered plates and shells." Journal of Applied Mechanics 30 1963 79.

62. Mead, D.J. "The double-skin damping configuration."
University of Southampton A.A.S.U. Report no. 160.

63. Mead, D.J.
"The effect of certain damping treatments on the response of idealised aeroplane structures excited by noise."
University of Southampton, Ph.D Thesis 1963.

64. Mead, D.J.
"Criteria for comparing the effectiveness of damping treatments."
Noise Control 7, no. 3 May, 1961, 27.

65. Mead, D.J.
"The practical problems of assessing damping treatments."
University of Southampton: Institute of Sound and Vibration Research Memorandum no.102 May, 1963.
(An invited paper presented at the Spring Meeting of the Acoustical Society of America in New York May, 1963).

66. Mead, D.J.
"Damped sandwich plates for vibration control."
Environmental Engineering Quarterly, no.9 March, 1964, 11.

67. Plass, H.J. Jnr.
"Damping vibrations in elastic rods and sandwich structures by incorporation of additional viscoelastic material."
Proceedings of the Third Midwestern Conference on Solid Mechanics, University of Michigan April,1957, 48.

68. Whittier, J.S.
"The effect of configurational additions using viscoelastic interfaces on the damping of simple cantilever beams."
University of Minnesota WADC Technical Report no.58-568 August, 1958.

69. Kurtze, G.
"Damping of bending waves in multi-layer plates."
BBN Report no.614 1959, ASTIA AD 214535.

70. Kurtze, G. and Watters, B.G.
"New Wall design for high transmission loss or damping."
Journal of the Acoustical Society of America 31 no.6
June, 1959, 739.

71. Ruzicka, J.E.
"Damping structural resonances using viscoelastic shear damping mechanisms: Part I Design Configurations and Part II Experimental results."
Paper presented at the Winter Annual meeting, New York N.Y., Nov. 27-Dec. 2 1960, of the American Society of Mechanical Engineers.
(Also published in Journal of Engineering for Industry 83 1961, 403.

72. Freudenthal, A.M. and Bieniek, M.P.
"Forced vibration of sandwich structures."
WADD Technical Report no. 60-307 (USAF).

73. Bieniek, M.P., and Freudenthal, A.M.
"Forced vibrations of cylindrical sandwich shells."
Journal of the Aerospace Sciences 29 no.2 Feb. 1962, 180.

74. Yildiz, A.
"On the damping of a multi-layer plate."
Journal Acoustical Society of America,
34 1962, 353.

75. Mentel, T.J.
"Damping energy dissipated by interfaces in beam and plate supports and in sandwich cores."
WADC TR 58-547 1958 ASTIA AD 206667.

76. Keer, L. and Lazan, B.J.
"Damping and fatigue properties of sandwich configurations in flexure."
ASD TR 61-646 1961 ASTIA AD 272016.

77. Oberst, H.
"Akustische Anwendung von Schaumstoffen."
Kunststoffe 46-5, 1956, 190.

78. Yu, Y.Y.
"Forced flexural vibration of sandwich plates in plane strain."
Journal of Applied Mechanics, 27, Sept. 1960, 535.

79. Piaggio, H.T.H.
"An elementary treatise on differential equations and their applications."
G. Bell and Sons Ltd London 1962.

80. Bashforth, F., and Adams, J.C.
"An attempt to test theories of capillary attraction."
Cambridge University press New York 1883 18.

81. Marcal, P.V. and Turner, C.E.
"Numerical analysis of the elastic-plastic behaviour of axi-symmetrically loaded shells of revolution."
Jour. Mech. Eng. Sc. 5, no. 3, 1963 232.

82. Richardson, L.F.
"The approximate arithmetical solution by finite differences of physical problems."
Trans. Roy. Soc. London A210 1927 299.

83. Richardson, L.F. and Gaunt, J.A.
"The deferred approach to the limit."
Trans. Roy. Soc. London A226 1927 299.

84. Crandall, S.H.
"Engineering Analysis." Mc Graw Hill, 1956.

85. Clenshaw, C.W.
"The numerical solution of linear differential equations in Chebyshev series." Proc. Camb. Phil. Soc. 53 1957 134.

86. Lanczos, C.C.
"Table of Chebyshev polynomials."
National Bureau of Standards Applied Maths Series no.9, (Washington: Government Printing Office 1952).

87. National Physical Laboratory.
"Modern computing methods."
Notes on Applied Science no.16 (Second edition) 1961.

88. Fox, L.
"The numerical solution of two point boundary problems in ordinary differential equations." O.U.P? 1957.

89. Kurtze, G.
"Bending wave propagation in multi-layer plates."
Journal of the Acoustical Society of America, 31 Sept., 1959 1183.

90. Nielsen, L.
"Mechanical Properties of Polymers."
Reinhold Publishing Corporation, 1962.

91. Gui, Wilkinson, and Gehman.
"Vibration characteristics of tread stocks."
Ind. Eng. Chem. 44 1952 720.

92. Cramer, W.S. "Propagation of stress waves in rubber rods."
Journal of Polymer Science 26 1957, 57.

93. Gehman, S.D.
"Dynamic properties of elastomers."
Rubber Chemistry and Technology, 30 1957, 1203.

94. Payne, and Scott.
"Engineering Design with Rubber."
Maclaren and Sons Ltd. 1960.

95. Ferry, J.D.
"Viscoelastic properties of Polymers."
John Wiley and Sons Inc., 1961.

96. Harris and Crede.
"Shock and vibration Handbook, vol.2"
Mc Graw-Hill Book Company Inc, 1961.

97. Ungar, and Hatch.
"Your selection guide to high damping materials."
Product Engineering, April 1961.

98. Payne, A.R.,
"Non-linearity in the dynamic properties of rubber."
Proc, Third Rubber Technological Conference, London, 1956
(also Rubber Chem. and Tech. 30, 1957.

99. Fitzgerald, E.R., and Ferry, J.D.
"Method for determining the dynamic mechanical behaviour of gels and solids at audio-frequencies; comparison of mechanical and electrical properties."
Journal of Colloid Science 8 1953.

100. Cook, E.J. Lee, J.A. and Fitzgerald, E.R.
"Dynamic mechanical properties of materials for noise and vibration control: vols I and 2 "
Chesapeake Instrument Corporation Technical Report no. 187
1962.

101. Woodward, A.E., and Saver, J.A.
"The physical properties of polymers."
Soc. Chem. Ind. Monograph no.5, (Macmillan co.) 1959 245.

102. Williams, Landel, and Ferry.
"The temperature dependence of relaxation mechanisms in amorphous polymers and other glass-forming liquids."
Journal Amer. Chem. Soc. 77, 1955, 3701.

103. Kainradl, and Handler.
"Messung der dynamischen Eigenschaften von Vulkanisaten."
Kautschuk and Gummi 11 1958 193.

104. Praefcke, R.
"Determination of the dynamic properties of rubber-like materials."
London University M.Sc. Thesis 1964.

105. Roelig.
"Dynamic evaluation of damping and durability of rubber compounds."
Proc. Rubber Tech. Conf. London, 1938 821 ; also Kautschuk 15, 1939 7.

106. Roelig.
"Dependence of damping and dynamic modulus on temperature as a means of evaluating elastic behaviour of raw and vulcanised rubber."
Rubber Chem. and Tech. 18 1945 62 ; also Kautschuk 19, 1943 47.

107. Payne, A.R.
"Dynamic properties of vulcanised rubber: 7. The RABRM low frequency dynamic test machine."
Research Memo. R411 Shawbury RABRM 1958.

108. Payne, A.R.,
"Dynamic properties of vulcanised rubber: 1. A non resonant sinusoidal-strain machine for dynamic testing of polymers."
Research Report no.76 Shawbury RABRM 1955.

109. Payne, A.R.,
"Sinusoidal-strain dynamic testing of rubber products."
Materials Research and Standards, 1 1961, 942.

110. Philippoff.
"Mechanical investigations in a wide range of frequencies."
J. Appl. Physics 24 1953 685.

111. Fletcher and Gent.
"Apparatus for the measurement of the dynamic shear modulus and hysteresis of rubber at low frequencies."
J. Sci. Instr. 29, 1952 186.

112. Painter "Dynamic characteristics of silicone rubber."
Rubber Age 74, 1954, 701.

113. Williams and Ferry.
"Dynamic mechanical properties of polyvinyl acetate."
Journal Colloid Sci. 9, 1954, 479.

114. Fitzgerald.
"Mechanical resonance dispersion in crystalline polymers at audio-frequencies."
Journ. Chem. Physics 27, 1957, 1180.

115. Fitzgerald.
"Mechanical Resonance Dispersion in metals at audio-frequencies."
Physical Review, 108, 1957, 690.

116. de Mej. and van Amerongen.
"Dynamisch-mechanische Eigenschaften von Kauts chuk-Mischungen."
Kautschuk and Gummi 9, 1956, 56, also
Rubber Chem. and Techn. 29, 1956, 1215.

117. Gehman, Woodford and Stambaugh.
"Dynamic properties of rubber (Dependence in Pigment loading)."
Ind. Eng. Chem. 33, 1941, 1032.

118. Fletcher and Gent.
"Non-linearity in the dynamic properties of vulcanised rubber compounds."
Trans. Inst. Rub. Ind. 29, 1953 266.

119. Gessler and Payne.
"Dynamic properties of butyl containing Attrited Black."
J. Appl. Polymer Sci. 4, 1960, 127.

120. Payne, A.R.
"Dynamic properties of heat-treated butyl vulcanites."
Jour. Appl. Polymer Sci. 7, 1963, 873.

121. Payne, A.R.
"Dynamic mechanical properties of filler loaded vulcunites."
Rubber and plastic Age 42, 1961, 963.

122. Nolle.
"Methods for measuring dynamic mechanical properties of rubber-like materials."
Jour. Appl. Phys. 19 1948 753.

123. Koppllmann.
"Uber das dynamisch elastische Verhalten hoch polymerer Stoffe."
Kolloid Z. 144 1955 12.

124. Witte, Mrowca, and Guth.
"Propagation of audio-frequency sound in high polymers."
Jour. Appl. Phys. 20 1949 481

125. Becker.
"Mechanische Relaxionserscheinungen in nicht weichgematchten hoch polymeren Kunststoffen."
Kolloid Z. 140 1955 1.

126. Minorsky, N.
"Non-linear Oscillations."
Van Nostrand Co Inc. 1962.

127. Newland, D.E.
"Non-linear vibrations: A comparative study with applications to centrifugal pendulum vibration absorbers."
Thesis submitted in partial fulfilment of the requirements for the degree of Doctor of Science. M.I.T. May 1963.

128. Timoshenko, S. and Young, D.
"Vibration problems in Engineering."
Van Nostrand Co Inc. Third edition 1955.

129. Mindlin, R.D.
"An introduction to the mathematical theory of vibration of elastic plates."
U.S. Army Signal Corps Engineering Laboratories Fort Monmouth N.J. 1955.

130. Lanczos, C.
"The Variational Principles of Mechanics."
University of Toronto Press, Toronto Canada 1949.

29. D. J. Mead
"The effect of a damping compound on jet-efflux excited vibrations: Part II. The reduction of vibration and stress level due to the compound."
Aircraft Engineering 32, no 374, April 1960.